Molecular control of stem cell self-renewal by niche signaling targets

by

Heaji Shin

A dissertation submitted in partial fulfillment of the requirements for the degree of

Doctor of Philosophy
(Biochemistry)

at the
University of Wisconsin–Madison
2017

Date of final oral examination: Oct 26, 2017
The dissertation is approved by the following members of the committee:

Judith E. Kimble, Professor, Biochemistry
David A. Wassarman, Professor, Genetics
Grace E. Boekhoff-Falk, Associate Professor, Cell and Regenerative Biology
Michael D. Sheets, Professor, Biomolecular Chemistry
Thomas F.J. Martin, Professor, Biochemistry

To my parents

Abstract

Stem cell self-renewal lies at the heart of metazoan development and regeneration. Stem cells self-renew and give rise to differentiated progenitor cells, a fundamental regulatory process that underlies tissue homeostasis. The paradigm is that proximity to the stem cell niche, or a microenvironment in which the stem cells reside, determines the location and size of the stem cell pool; movement away from the niche triggers differentiation. However, the molecular basis of niche regulation of stem cells is poorly understood.

In this thesis, I investigate this question by examining direct niche signaling targets in the nematode *Caenorhabditis elegans* germline, an exceptional model of stem cells maintained in a stochastically dividing pool. In this system, a single-celled mesenchymal niche uses Notch signaling to maintain the germline stem cell (GSC) pool in a naïve state. Downstream, PUF family RNA binding proteins, FBF-1 and FBF-2 (collectively FBF), maintain stem cells at the expense of differentiation, but how Notch signaling controls FBF activity was not known. Here I describe the discovery and characterization of two direct Notch target genes, *sygl-1* and *lst-1,* and show that they are key niche signaling effectors that molecularly link Notch signaling to downstream post-regulatory RNA network.

sygl-1 and lst-1 are essential for stem cell maintenance: both are redundantly required to maintain GSCs, and either is sufficient to promote stem cell self-renewal. Both genes encode novel proteins that are spatially-restricted to the distal-most pool of cells corresponding to GSCs. Modulation of their spatial extents demonstrates that SYGL-1 and LST-1 govern the size of the stem cell pool, and this spatial restriction is critical to prevent tumorigenesis. Mechanistically, SYGL-1 and LST-1 likely control FBF activity within stem cells to repress FBF target mRNA expression. Collectively, SYGL-1 and LST-1 represent an exemplary model of niche maintenance of a stem cell pool: niche signaling activates direct effector genes to control downstream post-transcriptional RNA regulator; spatial regulation of SYGL-1/FBF or LST-1/FBF underlies progression from a stem cell state to a differentiated state.

Acknowledgements

Completing this thesis was challenging in many ways, but was a rewarding experience at the same time. The most satisfactory part was to witness how my thinking evolves over time — I learned how to think critically, teach myself, and work independently in close collaboration with others. My intellectual and personal growth would not have been possible without the help of many people I met during this course of my life.

I am indebted to my advisor, Judith Kimble, for taking me under her wings to work on fundamental biological problems and for sharing the excitement of doing discovery science. I am thankful for her generous support, countless encouragements, and patience, not to mention all the intellectual inputs over the years. Her mentoring style helped me develop independence and the ability to transform fundamental questions into tractable and testable models. From her I learned that the best mentors care about people, and the greatest scientists dedicate their life-long passion to do rigorous work. I wish I could pay it forward someday.

I also thank my committee, Grace Boekhoff-Falk, David Wassarman, Thomas Martin, and Michael Sheets for their helpful guidance and discussions throughout the years. I also thank Marvin Wickens for critically reading my work and giving me unique perspectives, as an honorary committee member. In addition, I appreciate Colleen Hayes for sharing her teaching philosophy, which helped me develop my own.

The best part of being in Judith's lab was to work in a collegial environment with a talented group of people. I thank the past and the present Kimble and Wickens lab members for their contribution to my work, either directly or indirectly. Aaron Kershner deserves a special recognition: This thesis would not have been possible without his pioneering discovery, and his generous mentoring at the bench during my initial years in the laboratory. I also thank Kimberly Haupt for years of collaboration, enthusiasm, and friendship. Sarah Crittenden, Hannah Seidel, Erika Sorensen, Kyle Friend, ChangHwan Lee, Scott Aoki, Elena Sorokin, Kyung Won Kim, Tina Lynch, and Johan Jeong were tremendous role models. Anne Helsley-Marchbanks offered generous advice on my written work, Peggy Kroll-Conner and Jadwiga Forster provided reliable technical supports, and Laura Vanderploeg in the Media lab helped with beautiful illustrations that advanced my thinking, which all I am grateful for.

Lastly, I thank my family and friends for supporting me over the years. My parents deserve the full credit for helping me being who and where I am. They also remind me that life is more about having passion than counting mere achievements. I dedicate my thesis to them.

Table of contents

Abbreviations

Brat: Brain Tumor

BMP: Bone Morphogenic Protein

CRISPR: Clustered Regularly Interspaced Short Palindromic Repeats

EMS: Ethyl methanesulfonate

EMSA: Electrophoretic Mobility Shift Assays

ESC: Embryonic Stem Cell

FBF: Fem-3 Binding Factor

FBE: FBF Binding Elements

FOG-1: Feminization of Germline 1

GFP: Green Fluorescent Protein

GLD: Germline Development Defective

GSC: Germline Stem Cells

iPSC: Induced Pluripotent Stem Cell

Insc: Inscuteable

JAK-STAT: Janus Kinase – Signal Transducer and Activator of Transcription

LST-1: Lateral Signaling Target 1

MAPK: Mitogen Activated Protein Kinase

MCP: Bacteriophage MS2 Coating Protein

Mira: Miranda

mRNA: messenger RNA

Mud: Mushroom Body Defect

Pins: Partner of Insc

Pon: Partner of Numb

Pros: Prospero

PUF: Pumilio and FBF

RNAi: RNA interference

sfGFP: Superfolder Green Fluorescent Protein

STAR: Signal Transduction and Activation of RNA

SYGL-1: Synthetic Germline Proliferation Defective 1

UTR: Untranslated Region

Wnt: Wingless and integration 1

List of figures and tables

Chapter 1.

Chapter 2.

Chapter 3.

Chapter 1

Introduction to stem cell self-renewal

1.1 Significance of the study

Stem cells are critical for proper organ formation, tissue maintenance, and repair. Essentially, all multi-cellular organisms start from a single totipotent zygote which has the potential to differentiate into all other cell lineages. Post-development, adult stem cells persist throughout the lifetime of an organism to replenish tissues in response to proliferative needs [1]. Key properties of stem cells include the ability to self-renew, while retaining the capacity to generate multiple cell types [2]. Understanding this crucial process promises insights into fundamental principles of development and offers future prospects for therapeutics, as the imbalance between self-renewal and differentiation can cause degenerative diseases and cancer [3].

Despite the importance of stem cell self-renewal in development and regeneration, molecular understanding of self-renewal is still in its infancy. In this thesis, I investigate the molecular control of stem cell self-renewal using *C. elegans* germline stem cells (GSCs) as a model. I begin this chapter by reviewing mechanisms of self-renewal identified to date, with a focus on various model systems that led to the current understanding of stem cell self-renewal. Next, I review key anatomical and molecular characteristics of *C. elegans* GSCs to serve as a background for the proceeding chapters. Finally, I review outstanding questions and pose my research questions.

1.2. Extrinsic and intrinsic regulators of stem cell self-renewal

A. Niche as a paradigm for extrinsic regulator of stem cell self-renewal

The stem cell niche, an anatomical location in which stem cells reside, is essential for stem cell self-renewal [4]. First proposed as a mechanism for controlling hematopoietic stem cells, the original idea postulated that the niche drives the stem cell state by providing

environmental cues that sustain long-term proliferative potential (**Figure 1A**) [5]. Experimentally, this hypothesis was verified by the identification of somatic cells that support GSCs in invertebrate model organisms such as *C. elegans* and *D. melanogaster* [6, 7], followed by the discovery of epithelial or mesenchymal niches that support various adult stem cells [4]. The niche has been a model: Although identifying niche domains unequivocally *in vivo* stills remains a challenge in complex tissues, this framework led to the investigation of the dynamic nature of niche and stem cell interactions at the molecular, cellular, and anatomical levels.

The stem cell niche uses conserved signaling pathways to relay physiological and environmental information to stem cells [4, 8]. To this end, distinct cellular architectures and adherent junctions mediate niche-stem cell interactions [9-11]. For example, *D. melanogaster* testes GSCs are maintained by two major pathways: JAK-STAT signaling from the hub cell niche results in niche adherence of stem cells [12, 13], and BMP signaling from hub and cyst stem cell niches maintain GSCs by transcriptionally repressing a differentiation-promoting regulator, Bam [14]. Although the importance of niche in stem cell maintenance is demonstrated *in vivo*, how niche is developmentally specified and interact with stem cells remains to be understood. The niche could originate as a stem cell independent lineage during development [e.g. 6], or as a result of stem cell differentiation [e.g. 15]; Stem cells of one lineage can provide niches for other stem cells [e.g. 16], or stem cell progenitors can also constitute the niche to promote stem cell retention and proliferation rates [17]. As such, niche and stem cell interactions are multi-faceted and dynamic. Thus, the remaining challenge is to understand the molecular mechanisms by which niche maintains stem cells.

B. Intrinsic regulation of stem cell self-renewal

In addition to extrinsic signals from the niche, intrinsic regulators also control stem cell self-renewal. Historically, cell cycle quiescence and cell division modes were thought to influence the stem cell state [18]. Recent evidence, however, reveals that these characteristics

reflect diverse modes of stem cell proliferation, rather than being strict requirements of the stem cell state *per se* [19]. Regardless, this framework has been useful in identifying cell-autonomous regulators that promote the stem cell state in multiple tissue types with different proliferation kinetics.

One classification relies on the pattern of cell division. Stem cell divisions are classified as either asymmetric or symmetric [20] with respect to daughter cell fates (**Figure 1B**). Asymmetric cell division refers to a strategy that follows an invariant pattern, in which each cell division results in one self-renewing daughter cell and one differentiating daughter [21]. In contrast, fate asymmetry can also be determined at the population level, such that the number of self-renewing daughter or differentiating daughter remains constant as a population [22, 23]. Typically, neuroblasts divide asymmetrically [24], whereas mammalian intestinal and epidermal stem cells divide symmetrically and are maintained as a pool [25, 26]. However, essentially all stem cells use symmetric division to expand the pool size during development and regeneration [20], suggesting that different modes of cell division are utilized to maintain stem cells as appropriate. One emerging view is that these two different strategies both reflect mechanisms by which stem cells compete for the niche space [27].

Another classification relies on features of the cell cycle (**Figure 1C**). Stem cells can exhibit distinct cell cycle characteristics: Some tissue stem cells such as mammalian hematopoietic and hair follicle stem cells are maintained as a quiescent stem cell pool [28, 29], whereas others have a constantly-cycling stem cell pool such as mammalian GSCs [30]. Many stem cell populations, including embryonic stem cells and Drosophila and *C. elegans* GSCs, are characterized by having a short G1 phase [31-35]. Although cell cycle characteristics alone are not a prerequisite for the stem cell state, emerging evidence suggests that these two are closely linked [18]. For example, short G1 or G0 quiescence is thought to be a strategy to bypass the G1 commitment window [36]; G2 quiescence is thought to maintain potency during stress or regeneration [37, 38]; mutations in cell cycle regulators can cause premature differentiation in

some tissue stem cells [39-41]. Thus, different stem cells can have distinct cell cycle characteristics that promote the stem cell state.

1.3. Key model systems

The stem cell state is accomplished by both cell-extrinsic and cell-intrinsic molecular regulators. Niche signaling provides extracellular cues, and cell-autonomous regulators modulate the balance between self-renewal and differentiation. Nevertheless, our understanding of stem cells is incomplete without knowing how extrinsic signaling is coordinated with cell-intrinsic regulators. Addressing this key question requires a tractable stem cell model in which niche and stem cell positions are well defined, and key molecular regulators that promote self-renewal and differentiation are well understood. Here I review a number of representative model systems that led to the current understanding of stem cells, focusing on the question of how extrinsic regulators are connected to cell autonomous regulators.

A. *Drosophila melanogaster* neuroblasts

Neuroblasts are neural stem cells, which generate terminally differentiated neurons and glial cells. *Drosophila* neuroblasts highlight the role of cell-intrinsic regulators of stem cell maintenance. Neuroblasts are maintained by asymmetric cell division: each division results in one self-renewing stem cell daughter and one progenitor that will give rise to glial or neuronal cells (**Figure 2A**) [24]. In this system, self-renewal is closely associated with asymmetrically segregating cell polarity regulators that control cell fate decisions.

Neuroblasts divide along an apical-basal polarity: This polarity is first established by Baz/Par6/aPKC complex that localizes to the apical cortex, which recruits Insc, followed by Pin/Gi/Mud cell polarity regulators to orientate mitotic spindles [42-47]. Phosphorylation by aPKC results in basal segregation of differentiation-promoting cell-fate regulators such as

Brat/Pros/Mira and Numb/Pon complex [48-53] (**Figure 2A**). Thus, cell polarity regulators asymmetrically segregate cell fate regulators to drive the stem cell state. While molecular mechanisms that lead to fate asymmetry are under intense investigation, extrinsic cues that promote self-renewal are not yet elucidated. For example, the existence of epithelial or glial cell niches is implicated, whereas the signaling mechanism or their contributions to asymmetric cell division are not understood [54].

B. *Drosophila melanogaster* germline stem cells

Drosophila GSCs are an exemplary model in which niche and cell-autonomous regulators are coordinated to govern fate asymmetry. Stem cells divide asymmetrically to compete for the niche space, and niche signaling and RNA fate regulators work together to repress differentiation at both the transcriptional and post-transcriptional levels. This model also demonstrates how stem cells of one lineage can influence stem cells of another, as both germline and somatic stem cells co-exist within the anatomical space (**Figure 2B**) [55].

In this system, an anatomically distinct niche harbors and maintains both germline and somatic stem cells at the apical tip of the tissue [55]. Somatic stem cells encase GSCs and provide additional support for self-renewal [56, 57]. In testes, JAK-STAT signaling from the hub cell cluster promotes GSC anchoring to niche and maintains somatic cyst stem cells, but JAK-STAT is largely dispensable for GSC maintenance [12, 13, 56]. Instead, BMP signaling from the hub and somatic cyst cells maintains GSCs [14, 58, 59] (**Figure 2B**). Specialized cellular structures such as microtubule-based nanotubules in the germ cells mediate short-range BMP signaling from the hub [11]. Similarly, cap cells maintain ovarian GSCs through BMP signaling [60]. Cell-adhesion molecules such as E-cadherin anchor GSCs to the niche to promote niche-stem cell interaction and to tightly restrict BMP expression [61-64]. In GSCs, BMP signaling triggers phosphorylation of Mad, which can complex with Med, to transcriptionally repress differentiation-promoting genes such as Bam, in both testis and ovary [65-67].

In both sexes, mechanisms of asymmetric stem cell division have been examined in depth to understand how developmentally-programmed mechanisms govern oriented cell division [21]. In testes, differential mother and daughter centrosome movements fix the position of mitotic spindles to orient the plane of cell division perpendicular to the hub cells [68]. In ovaries, a germ-cell specific organelle called spectrosome anchors the mitotic spindle to assist asymmetric division [69]. As a result, one daughter is retained within the niche while another daughter is displaced from the niche, causing invariant daughter asymmetry. Yet, whether niche signaling contributes to cell division asymmetry remains unknown.

Autonomously in the germline stem cells, a conserved family of RNA and translation regulators maintain the stem cell state by repressing differentiation-promoting genes and cell cycle regulators [70, 71]. RNA binding proteins Pumilio and Nanos cooperatively repress differentiation-promoting transcripts such as *brat* or *mei P-26* by recruiting CCR-4/NOT deadenylase complex [72-76]; Various microRNA processing proteins such as Argonuate and Dicer, and the piRNA processing protein Aubergine drive the stem cell state [77-81]; general translation regulators such as translation release factor Peolta or translation initiation factor eIF4A promote self-renewal [82, 83]. These regulators work largely in parallel to niche signaling to maintain the stem cell state. Nevertheless, it remains to be determined whether niche signaling directly regulates these cell-autonomous regulators. Thus, *Drosophila* GSCs are maintained by conserved signaling from niches of multiple origin, asymmetric cell division, and post-transcriptional and translational regulators.

C. Mammalian intestinal stem cells

Mammalian intestinal stem cells represent an exceptional model of stem cells maintained in a stochastically dividing population. Stem cells exist in two distinct populations: either a rapid-cycling pool or a slow-cycling, quiescent pool can regenerate the entire epithelium that turns over every 3-5 days [84, 85]. Studies focusing on this model highlight the importance

of stochastic cell division and the diverse states of stem cells during regeneration. Experimental approaches are also strengthened by the ability to culture *in vitro* reconstituted epithelium as so-called organoids [86].

Rapid-cycling stem cells are located at the crypt base and marked by *Lgr5*, an R-spondin receptor of the Wnt signaling pathway, or *Prominin-1,* a transmembrane glycoprotein, or *Olfm4*, an Olfactomedin family gene of unknown function (**Figure 3A**). [84, 87, 88]. *Lgr5* marked cells can regenerate the entire epithelium both *in vivo* and *in vitro*, and stem cells in this pool are developmentally equipotent exhibiting characteristics of neutral competition [25, 84]. A second, slow-cycling, quiescent stem cell pool is located at the +4 position and is identified by multiple molecular markers such as Bmi1, a polycomb repressor, Tert, a catalytic component of telomerase, and Lrig1, a transmembrane protein that is an ErbB signaling antagonist [89-92]. This quiescent pool is composed of secretory cells that appear differentiated [93, 94], but can repopulate the *Lgr5*-positive stem cell pool upon injury, as a stem cell pool reserve [85].

In this system, multiple signaling pathways such as Wnt, Notch, and Ephrin maintain the stem cell state, using Wnt as a primary signaling mechanism [95]. The Paneth cell niche, which intercalates between the crypt stem cells, expresses EGF, Wnt (*Wnt3*) and Notch ligand (*Dll4*) to maintain stem cells [15]. In addition, mesenchymal cells surrounding the crypt also support proliferation via the extra-cellular matrix [95].

Downstream, several niche signaling targets and cell-intrinsic regulators promote the stem cell state [96]. Major signaling targets include *Ascl2, c-myc, cyclin D1,* and *Snai1* transcription factors as Wnt target genes [97-102], and *Olfm4 and Prominin-1* as Notch target genes [103, 104]. In addition, multiple cell-intrinsic regulators, such as Musashi RNA binding protein, promote the stem cell state [88, 105].

Combined with lineage-tracing data, the identity of these niche signaling targets provides a unique perspective of stem cells maintained within a pool. Niche signaling targets show a diverse expression pattern within the crypt, and work in distinctive ways to promote the stem cell

state. For example, *Ascl2* is a Wnt target transcription factor that is spatially restricted to the crypt base. The spatial expression of Ascl2 can control the stem cell pool size by synergistically working with Wnt to activate target gene transcription [97, 106]. In contrast, other targets such as c-Myc or Prominin-1 show broad expression within crypt progenitors [88, 99]. c-Myc promotes proliferation and inhibits apoptosis downstream of Wnt signaling [107] but this does not explain all aspects of Wnt signaling in stem cell self-renewal [108]. Therefore, Wnt maintenance of stem cells likely involves other Wnt target genes. Interestingly, these various effectors of niche signaling respond differently during regeneration and aging, suggesting that they have diverse roles in different physiological contexts [109]. In sum, intestinal stem cells represent a highly plastic stem cell population, maintained by direct niche signaling targets and cell-autonomous regulators.

D. Embryonic stem cells, induced pluripotent stem cells

Embryonic stem cells (ESC) are pluripotent stem cells that can give rise to all embryonic lineages including the germline [110]. ESC cells are derived from the inner cell mass (ICM) of the blastocyst and can be cultured for an extended period without losing their potency [111, 112]. Induced pluripotent stem cells (iPSCs) are stem cells that have been reprogrammed from differenced cells [113]. Studies in ESCs and IPSCs demonstrate key transcriptional and epigenetic changes governing diverse pluripotent states, and highlight therapeutic potentials.

An embryo starts from a fertilized egg that later generates extra-embryonic and embryonic tissues after multiple divisions. At the blastocyst stage, the trophoblast and the ICM are distinctly specified: The trophoblast becomes the extra-embryonic lineage that can generate placenta, and the ICM develops into the epiblast that can make all embryonic lineages, and the hypoblast, a second source of extra-embryonic lineages [114]. *In vivo*, extra-embryonic lineages induce the pre-implantation epiblast to exist in the ground pluripotent state [115]. *In vitro*, the ICM is the source for ESC cultures that can contribute to all lineages when transplanted [111,

112]. Furthermore, pre and post-implantation epiblasts can be cultured to generate epiblast stem cells (EpiSCs) but exhibit limited potential when grafted in mice [116-118].

The key signal that maintains murine ESC cultures is LIF (Leukemia Inducing Factor), which activates JAK-STAT signaling [119, 120]. Inhibition of two differentiation promoting signals, MAP kinase Erk1/2 [121] and GSK-3 (Glycogen Synthase Kinase 3) [122] further enhances the pluripotent state. Identification of these key signaling pathways enabled a chemical method to maintain murine ESC cultures called the 2 inhibitor (2i) system, which includes two ERK and GSK inhibitors in addition to LIF [123]. Of note, human ESCs are not responsive to LIF and show molecular signatures similar to murine EpiSCs [124, 125], demonstrating species differences between ESC models.

iPSCs are reprogrammed from terminally-differentiated somatic cells by introducing defined transcription factors such as Oct4, Sox2, Klf4 and c-Myc [113]. iPSCs represent a unique state of pluripotency similar but not identical to ESCs, potentially due to cell type of origin [126, 127]; Despite these differences, iPSCs can give rise to all embryonic lineages and form germline teratomas, a hallmark of pluripotency [113]. Oct4, Sox2, and Klf4 are pioneer transcription factors that bind at the enhancers of the self-renewal promoting genes; they also work in part by displacing lineage-specific transcription factors from somatic enhancers by recruiting Hdac1 [128, 129] In contrast, c-Myc functions to facilitate the binding of Oct4, Sox2, and Klf4 to chromatin [129]. In addition, recent advances in culture methods allow small molecule-based reprogramming in lieu of transcription factors to generate embryonic and extra-embryonic lineages [130, 131] holding great potential for therapeutic approaches.

Studies focusing on ESCs and iPSCs have generated useful concepts related to pluripotency. Stem cells exist in a naïve state or in a state primed for differentiation, which can be delineated by the degree of commitment, metabolic state, morphology, and molecular signatures associated with each state [115]. Notably, naïve and primed states can be reversed in murine ES culture upon addition of Klf4, suggesting that these two fates are distinct but

nevertheless plastic [132]. Furthermore, an intermediate “formative state” of cells that have exited the naïve phase, but have not entered the primed state for commitment, has been proposed as a distinct state [133]. To summarize, studies in ESCs and iPSCs have greatly contributed to our understanding of pluripotency and cellular plasticity. Pluripotent states can exist in the naïve, formative, and primed states, with distinct molecular signatures and cellular plasticity defining each state [133]. Future challenges include understanding the molecular mechanisms governing each state and their transitions, and the development of culture methods that can mimic *in vivo* tissue development.

E. *Caenorhabditis elegans* germline stem cells

C. elegans GSCs provide a simple paradigm of stem cells being maintained in a stochastically-dividing population [134]. In this system, a stem cell pool is maintained by Notch signaling from the niche and by a conserved family of post-transcriptional RNA regulators. Studies in this model demonstrate the robust regulatory network driving the naïve and primed states of stem cell self-renewal. Also highlighted are the cross-regulation between the network hubs, a combinatorial control, and the redundancies that drive biological robustness within the network [135].

The gonad is a polarized tissue that contains mitotically-cycling cells at the distal end (**Figure 3B**). A single cell niche of mesenchymal origin is located at the tip of the gonad and embraces the distal-most pool of cells, which maintains them in the naïve state [6, 10, 136]. More proximally, stem cell progenitors are in the primed state, prior to overt differentiation (entry into meiotic cell cycle) and ultimately gametogenesis at the proximal end (**Figure 3B**) [134]. GSCs are maintained throughout development and can regenerate the tissue after severe stress such as starvation [137, 138].

The niche utilizes Notch signaling to maintain the stem cell pool [139, 140]. The niche expresses Notch ligands LAG-2 and APX-1 [141-143] and germ cells express GLP-1/Notch

receptor to receive the signal from the niche [144]. Receptor activation triggers the Notch intracellular domain (NICD) to translocate to the nucleus, to form a CSL/Mastermind/NICD ternary complex, which can activate the transcription of target genes [145]. The *C. elegans* counterparts of the ternary complex LAG-1/LAG-3/GLP-1 NICD were identified decades ago [146-148], but the identity and function of target genes that drive self-renewal were largely unknown prior to this thesis work.

Downstream of GLP-1/Notch signaling, a post-transcriptional RNA network acts intrinsically to control the transition between self-renewal and differentiation (**Figure 3C**) [134]. One major hub that drives the stem cell state is composed of PUF family RNA binding proteins FBF-1 and FBF-2 (collectively FBF) [150, 151]. PUF proteins are conserved RNA regulators that recognize a distinct 7-9 nucleotide elements, often found in the 3' untranslated regions (UTR) within the mRNA [152]. In particular, FBF is a broad-spectrum regulator that can associate with >1000 RNAs [153, 154]. Most relevant to self-renewal is its repression of *gld-1, gld-2,* and *gld-3* mRNAs that drive differentiation [150, 155, 156], and the repression of the meiotic cell cycle program to inhibit differentiation [157].

The second hub is composed of GLD and NOS proteins, which drive differentiation as two branches of translational regulation (**Figure 3C**) [134, 158]. One branch is GLD-1, a signal transduction and activation of RNA (STAR)/Quaking family protein that can associate with > 400 mRNAs to repress translation [159, 160]; NOS-3, a Nanos homolog, is also in this branch and promotes meiosis by activating *gld-1* mRNA [161]. The other branch includes GLD-2/3/4 proteins that encode cytoplasmic poly A polymerases and their regulatory subunit, which together activate differentiation-promoting mRNAs [155, 162-164]. Most relevant are GLD-1 repression of *glp-1/*Notch mRNA to inhibit self-renewal [165], and GLD-2/3 activation of *gld-1/*STAR mRNA to reinforce entry into meiosis [164]. Therefore, nodes of the RNA regulatory network cross-regulate each other to balance stem cell self-renewal and differentiation.

This regulatory network highlights two key concepts. The first is combinatorial control of mRNA regulation, which is used broadly in development [166] but also applicable to stem cells. Two examples stand out in the context of *C. elegans* stem cell self-renewal. One is FBF, which not only represses *gld-1* mRNA to promote self-renewal [150], but also activates *gld-1* mRNA to promote differentiation [167, 168]. This dual role likely results from recruiting different protein complexes, such as CCR-4/Not deadenylase to destabilize mRNA in stem cells or cytoplamic poly A polymerase to stabilize mRNA in primed cells [168]. Regardless, the molecular switch that triggers the transition remains unknown. Another example is the GLS-1/GLD-4 complex, another cytoplasmic poly A polymerase that drives differentiation by activating *gld-1*/STAR mRNA [156, 163] but also promote self-renewal by activating *glp-1*/Notch mRNA [156]. In this case, a regulatory protein, GLD-3, is thought to mediate the transition between the two different modes, but the molecular details remain unknown. Such examples argue for the importance of identifying regulatory components that mediate combinatorial control.

Another concept is the robustness of the network. Redundant genes promote self-renewal and differentiation such that removal of a single regulator does not result in a complete loss or gain of cell fates. Instead, phenotypically-subtle changes are observed [135]. For example, FBF-1 and FBF-2 are paralogs that redundantly maintain adult GSCs; Furthermore, another CPEB protein FOG-1 is redundant with FBF to maintain larval GSCs [151]. Removal of either FBF-1, FBF-2 or FOG-1 does not greatly compromise GSC self-renewal [151, 169]. Similarly, two major branches of meiosis have to be simultaneously removed to completely block differentiation [134]. Therefore, *C. elegans* GSCs present a stem cell model maintained by Notch signaling from the niche, and an elaborate post-transcriptional RNA network in GSCs.

1.4. Major unanswered questions

Studies in several model systems have revealed key features and shared molecular mechanisms of stem cell maintenance. Key foundational concepts include niche maintenance of stem cells and conserved molecular regulators that repress differentiation at multiple levels. Also highlighted are the concepts of naïve and primed stem cell states and their molecular signatures. Finally, strategies to maintain a robust regulatory network that balances naïve and primed states were discussed.

Regardless, several questions remain unanswered. First, how does niche signaling promote the stem cell state? Despite significant progress in identifying niche signaling and its components, the mechanism by which niche maintains stem cells remains poorly understood. Only a handful of niche signaling targets have been identified to date, and how they govern downstream cell-autonomous regulators are largely not understood. Second, what controls the transition between naïve and primed states? While the discovery of key molecular regulators has significantly advanced our understanding, the regulated transition between self-renewal and differentiation is poorly understood. This question of how the transition is regulated has important implications for stem cell homeostasis.

This thesis addresses two aforementioned questions. Using *C. elegans* GSCs as a model, the next two chapters describe the discovery and characterization of two direct Notch signaling targets that account for niche maintenance of stem cells. These novel genes, called *sygl-1* and *lst-1*, are redundantly required for stem cell self-renewal, are sufficient for stem cell maintenance, and their spatial expression patterns govern the stem cell pool size. Both proteins likely work with FBF to maintain the stem cell state, as trans-acting regulatory proteins to maintain FBF in the repressive mode. Collectively, SYGL-1 and LST-1 link niche signaling to the downstream post-transcriptional RNA network and demonstrate niche maintenance of stem cell pool by spatially regulated niche signaling targets.

References

1. Hsu YC, Pasolli HA, Fuchs E. Dynamics between stem cells, niche, and progeny in the hair follicle. Cell. 2011;144(1):92-105. Epub 2011/01/11. doi: 10.1016/j.cell.2010.11.049. PubMed PMID: 21215372; PubMed Central PMCID: PMC3050564.

2. Siminovitch L, McCulloch EA, Till JE. The Distribution of Colony-Forming Cells among Spleen Colonies. J Cell Comp Physiol. 1963;62:327-36. Epub 1963/12/01. PubMed PMID: 14086156.

3. He S, Nakada D, Morrison SJ. Mechanisms of stem cell self-renewal. Annu Rev Cell Dev Biol. 2009;25:377-406. doi: 10.1146/annurev.cellbio.042308.113248. PubMed PMID: 19575646.

4. Voog J, Jones DL. Stem cells and the niche: a dynamic duo. Cell Stem Cell. 2010;6(2):103-15. Epub 2010/02/11. doi: 10.1016/j.stem.2010.01.011. PubMed PMID: 20144784; PubMed Central PMCID: PMC3012646.

5. Schofield R. The relationship between the spleen colony-forming cell and the haemopoietic stem cell. Blood Cells. 1978;4(1-2):7-25. Epub 1978/01/01. PubMed PMID: 747780.

6. Kimble JE, White JG. On the control of germ cell development in *Caenorhabditis elegans*. Dev Biol. 1981;81(2):208-19. PubMed PMID: 7202837.

7. Xie T, Spradling AC. A niche maintaining germ line stem cells in the *Drosophila* ovary. Science. 2000;290(5490):328-30. Epub 2000/10/13. PubMed PMID: 11030649.

8. Scadden DT. Nice neighborhood: emerging concepts of the stem cell niche. Cell. 2014;157(1):41-50. Epub 2014/04/01. doi: 10.1016/j.cell.2014.02.013. PubMed PMID: 24679525; PubMed Central PMCID: PMC4161226.

9. Gattazzo F, Urciuolo A, Bonaldo P. Extracellular matrix: a dynamic microenvironment for stem cell niche. Biochim Biophys Acta. 2014;1840(8):2506-19. Epub 2014/01/15. doi:

10.1016/j.bbagen.2014.01.010. PubMed PMID: 24418517; PubMed Central PMCID: PMC4081568.

10. Hall DH, Winfrey VP, Blaeuer G, Hoffman LH, Furuta T, Rose KL, *et al*. Ultrastructural features of the adult hermaphrodite gonad of *Caenorhabditis elegans*: relations between the germ line and soma. Dev Biol. 1999;212(1):101-23. Epub 1999/07/27. doi: 10.1006/dbio.1999.9356. PubMed PMID: 10419689.

11. Inaba M, Buszczak M, Yamashita YM. Nanotubes mediate niche-stem-cell signalling in the *Drosophila* testis. Nature. 2015;523(7560):329-32. Epub 2015/07/02. doi: 10.1038/nature14602. PubMed PMID: 26131929; PubMed Central PMCID: PMC4586072.

12. Kiger AA, Jones DL, Schulz C, Rogers MB, Fuller MT. Stem cell self-renewal specified by JAK-STAT activation in response to a support cell cue. Science. 2001;294(5551):2542-5. Epub 2001/12/26. doi: 10.1126/science.1066707. PubMed PMID: 11752574.

13. Tulina N, Matunis E. Control of stem cell self-renewal in *Drosophila* spermatogenesis by JAK-STAT signaling. Science. 2001;294(5551):2546-9. Epub 2001/12/26. doi: 10.1126/science.1066700. PubMed PMID: 11752575.

14. Kawase E, Wong MD, Ding BC, Xie T. Gbb/Bmp signaling is essential for maintaining germline stem cells and for repressing bam transcription in the *Drosophila* testis. Development. 2004;131(6):1365-75. Epub 2004/02/20. doi: 10.1242/dev.01025. PubMed PMID: 14973292.

15. Sato T, van Es JH, Snippert HJ, Stange DE, Vries RG, van den Born M, *et al*. Paneth cells constitute the niche for Lgr5 stem cells in intestinal crypts. Nature. 2011;469(7330):415-8. Epub 2010/11/30. doi: 10.1038/nature09637. PubMed PMID: 21113151; PubMed Central PMCID: PMC3547360.

16. Leatherman JL, Dinardo S. Zfh-1 controls somatic stem cell self-renewal in the *Drosophila* testis and nonautonomously influences germline stem cell self-renewal. Cell Stem Cell. 2008;3(1):44-54. doi: 10.1016/j.stem.2008.05.001. PubMed PMID: 18593558; PubMed Central PMCID: PMC2601693.

17. Hsu YC, Fuchs E. A family business: stem cell progeny join the niche to regulate homeostasis. Nat Rev Mol Cell Biol. 2012;13(2):103-14. Epub 2012/01/24. doi: 10.1038/nrm3272. PubMed PMID: 22266760; PubMed Central PMCID: PMC3280338.

18. Orford KW, Scadden DT. Deconstructing stem cell self-renewal: genetic insights into cell-cycle regulation. Nat Rev Genet. 2008;9(2):115-28. Epub 2008/01/19. doi: 10.1038/nrg2269. PubMed PMID: 18202695.

19. Hime GR, Abud HE. The stem cell state. Adv Exp Med Biol. 2013;786:1-4. Epub 2013/05/23. doi: 10.1007/978-94-007-6621-1_1. PubMed PMID: 23696348.

20. Morrison SJ, Kimble J. Asymmetric and symmetric stem-cell divisions in development and cancer. Nature. 2006;441(7097):1068-74. doi: 10.1038/nature04956. PubMed PMID: 16810241.

21. Chen C, Fingerhut JM, Yamashita YM. The ins(ide) and outs(ide) of asymmetric stem cell division. Curr Opin Cell Biol. 2016;43:1-6. doi: 10.1016/j.ceb.2016.06.001. PubMed PMID: 27318429; PubMed Central PMCID: PMC5154912.

22. Watt FM, Hogan BL. Out of Eden: stem cells and their niches. Science. 2000;287(5457):1427-30. Epub 2000/02/26. PubMed PMID: 10688781.

23. Potten CS, Loeffler M. Stem cells: attributes, cycles, spirals, pitfalls and uncertainties. Lessons for and from the crypt. Development. 1990;110(4):1001-20. Epub 1990/12/01. PubMed PMID: 2100251.

24. Doe CQ. Neural stem cells: balancing self-renewal with differentiation. Development. 2008;135(9):1575-87. doi: 10.1242/dev.014977. PubMed PMID: 18356248.

25. Snippert HJ, van der Flier LG, Sato T, van Es JH, van den Born M, Kroon-Veenboer C, *et al*. Intestinal crypt homeostasis results from neutral competition between symmetrically dividing Lgr5 stem cells. Cell. 2010;143(1):134-44. doi: 10.1016/j.cell.2010.09.016. PubMed PMID: 20887898.

26. Clayton E, Doupe DP, Klein AM, Winton DJ, Simons BD, Jones PH. A single type of progenitor cell maintains normal epidermis. Nature. 2007;446(7132):185-9. Epub 2007/03/03. doi: 10.1038/nature05574. PubMed PMID: 17330052.

27. Simons BD, Clevers H. Strategies for homeostatic stem cell self-renewal in adult tissues. Cell. 2011;145(6):851-62. Epub 2011/06/15. doi: 10.1016/j.cell.2011.05.033. PubMed PMID: 21663791.

28. Tumbar T, Guasch G, Greco V, Blanpain C, Lowry WE, Rendl M, *et al*. Defining the epithelial stem cell niche in skin. Science. 2004;303(5656):359-63. Epub 2003/12/13. doi: 10.1126/science.1092436. PubMed PMID: 14671312; PubMed Central PMCID: PMC2405920.

29. Wilson A, Laurenti E, Oser G, van der Wath RC, Blanco-Bose W, Jaworski M, *et al*. Hematopoietic stem cells reversibly switch from dormancy to self-renewal during homeostasis and repair. Cell. 2008;135(6):1118-29. Epub 2008/12/09. doi: 10.1016/j.cell.2008.10.048. PubMed PMID: 19062086.

30. Spradling A, Fuller MT, Braun RE, Yoshida S. Germline stem cells. Cold Spring Harb Perspect Biol. 2011;3(11):a002642. Epub 2011/07/28. doi: 10.1101/cshperspect.a002642. PubMed PMID: 21791699; PubMed Central PMCID: PMC3220357.

31. Becker KA, Ghule PN, Therrien JA, Lian JB, Stein JL, van Wijnen AJ, *et al*. Self-renewal of human embryonic stem cells is supported by a shortened G1 cell cycle phase. J Cell Physiol. 2006;209(3):883-93. Epub 2006/09/15. doi: 10.1002/jcp.20776. PubMed PMID: 16972248.

32. Grimmler M, Wang Y, Mund T, Cilensek Z, Keidel EM, Waddell MB, *et al*. Cdk-inhibitory activity and stability of p27Kip1 are directly regulated by oncogenic tyrosine kinases. Cell. 2007;128(2):269-80. doi: 10.1016/j.cell.2006.11.047. PubMed PMID: 17254966.

33. Savatier P, Huang S, Szekely L, Wiman KG, Samarut J. Contrasting patterns of retinoblastoma protein expression in mouse embryonic stem cells and embryonic fibroblasts. Oncogene. 1994;9(3):809-18. Epub 1994/03/01. PubMed PMID: 8108123.

34. Fox PM, Vought VE, Hanazawa M, Lee MH, Maine EM, Schedl T. Cyclin E and CDK-2 regulate proliferative cell fate and cell cycle progression in the *C. elegans* germline. Development. 2011;138(11):2223-34. Epub 2011/05/12. doi: 10.1242/dev.059535. PubMed PMID: 21558371; PubMed Central PMCID: PMC3091494.

35. Hsu HJ, LaFever L, Drummond-Barbosa D. Diet controls normal and tumorous germline stem cells via insulin-dependent and -independent mechanisms in *Drosophila.* Dev Biol. 2008;313(2):700-12. Epub 2007/12/11. doi: 10.1016/j.ydbio.2007.11.006. PubMed PMID: 18068153; PubMed Central PMCID: PMC2254938.

36. Massague J. G1 cell-cycle control and cancer. Nature. 2004;432(7015):298-306. Epub 2004/11/19. doi: 10.1038/nature03094. PubMed PMID: 15549091.

37. Nguyen PD, Gurevich DB, Sonntag C, Hersey L, Alaei S, Nim HT, *et al*. Muscle Stem Cells Undergo Extensive Clonal Drift during Tissue Growth via Meox1-Mediated Induction of G2 Cell-Cycle Arrest. Cell Stem Cell. 2017;21(1):107-19 e6. Epub 2017/07/08. doi: 10.1016/j.stem.2017.06.003. PubMed PMID: 28686860.

38. Seidel HS, Kimble J. Cell-cycle quiescence maintains *Caenorhabditis elegans* germline stem cells independent of GLP-1/Notch. Elife. 2015;4. doi: 10.7554/eLife.10832. PubMed PMID: 26551561; PubMed Central PMCID: PMC4718729.

39. Wang Z, Lin H. The division of *Drosophila* germline stem cells and their precursors requires a specific cyclin. Curr Biol. 2005;15(4):328-33. Epub 2005/02/23. doi: 10.1016/j.cub.2005.02.016. PubMed PMID: 15723793.

40. Chen D, Wang Q, Huang H, Xia L, Jiang X, Kan L, *et al*. Effete-mediated degradation of Cyclin A is essential for the maintenance of germline stem cells in *Drosophila*. Development. 2009;136(24):4133-42. Epub 2009/11/13. doi: 10.1242/dev.039032. PubMed PMID: 19906849.

41. Ables ET, Drummond-Barbosa D. Cyclin E controls *Drosophila* female germline stem cell maintenance independently of its role in proliferation by modulating responsiveness to niche

signals. Development. 2013;140(3):530-40. Epub 2013/01/08. doi: 10.1242/dev.088583. PubMed PMID: 23293285; PubMed Central PMCID: PMC3561789.

42. Schober M, Schaefer M, Knoblich JA. Bazooka recruits *Inscuteable* to orient asymmetric cell divisions in *Drosophila* neuroblasts. Nature. 1999;402(6761):548-51. Epub 1999/12/11. doi: 10.1038/990135. PubMed PMID: 10591217.

43. Li P, Yang X, Wasser M, Cai Y, Chia W. Inscuteable and Staufen mediate asymmetric localization and segregation of prospero RNA during *Drosophila* neuroblast cell divisions. Cell. 1997;90(3):437-47. Epub 1997/08/08. PubMed PMID: 9267024.

44. Wodarz A, Ramrath A, Kuchinke U, Knust E. Bazooka provides an apical cue for Inscuteable localization in *Drosophila* neuroblasts. Nature. 1999;402(6761):544-7. Epub 1999/12/11. doi: 10.1038/990128. PubMed PMID: 10591216.

45. Yu F, Ong CT, Chia W, Yang X. Membrane targeting and asymmetric localization of *Drosophila* partner of inscuteable are discrete steps controlled by distinct regions of the protein. Mol Cell Biol. 2002;22(12):4230-40. Epub 2002/05/25. PubMed PMID: 12024035; PubMed Central PMCID: PMC133846.

46. Schaefer M, Shevchenko A, Shevchenko A, Knoblich JA. A protein complex containing Inscuteable and the Galpha-binding protein Pins orients asymmetric cell divisions in *Drosophila*. Curr Biol. 2000;10(7):353-62. Epub 2001/02/07. PubMed PMID: 10753746.

47. Schaefer M, Petronczki M, Dorner D, Forte M, Knoblich JA. Heterotrimeric G proteins direct two modes of asymmetric cell division in the *Drosophila* nervous system. Cell. 2001;107(2):183-94. Epub 2001/10/24. PubMed PMID: 11672526.

48. Knoblich JA, Jan LY, Jan YN. The N terminus of the *Drosophila* Numb protein directs membrane association and actin-dependent asymmetric localization. Proc Natl Acad Sci U S A. 1997;94(24):13005-10. Epub 1997/12/16. PubMed PMID: 9371790; PubMed Central PMCID: PMC24253.

49. Shen CP, Jan LY, Jan YN. Miranda is required for the asymmetric localization of Prospero during mitosis in *Drosophila*. Cell. 1997;90(3):449-58. Epub 1997/08/08. PubMed PMID: 9267025.

50. Doe CQ, Chu-LaGraff Q, Wright DM, Scott MP. The *prospero* gene specifies cell fates in the *Drosophila* central nervous system. Cell. 1991;65(3):451-64. Epub 1991/05/03. PubMed PMID: 1673362.

51. Bello B, Reichert H, Hirth F. The *brain tumor* gene negatively regulates neural progenitor cell proliferation in the larval central brain of *Drosophila*. Development. 2006;133(14):2639-48. Epub 2006/06/16. doi: 10.1242/dev.02429. PubMed PMID: 16774999.

52. Betschinger J, Mechtler K, Knoblich JA. Asymmetric segregation of the tumor suppressor brat regulates self-renewal in *Drosophila* neural stem cells. Cell. 2006;124(6):1241-53. Epub 2006/03/28. doi: 10.1016/j.cell.2006.01.038. PubMed PMID: 16564014.

53. Wang H, Ouyang Y, Somers WG, Chia W, Lu B. Polo inhibits progenitor self-renewal and regulates Numb asymmetry by phosphorylating Pon. Nature. 2007;449(7158):96-100. Epub 2007/09/07. doi: 10.1038/nature06056. PubMed PMID: 17805297; PubMed Central PMCID: PMC3047501.

54. Sousa-Nunes R, Somers WG. Mechanisms of asymmetric progenitor divisions in the *Drosophila* central nervous system. Adv Exp Med Biol. 2013;786:79-102. Epub 2013/05/23. doi: 10.1007/978-94-007-6621-1_6. PubMed PMID: 23696353.

55. Spradling AC, Nystul T, Lighthouse D, Morris L, Fox D, Cox R, *et al*. Stem cells and their niches: integrated units that maintain *Drosophila* tissues. Cold Spring Harb Symp Quant Biol. 2008;73:49-57. Epub 2008/11/22. doi: 10.1101/sqb.2008.73.023. PubMed PMID: 19022764.

56. Leatherman JL, Dinardo S. Germline self-renewal requires cyst stem cells and stat regulates niche adhesion in *Drosophila* testes. Nat Cell Biol. 2010;12(8):806-11. Epub 2010/07/14. doi: 10.1038/ncb2086. PubMed PMID: 20622868; PubMed Central PMCID: PMC2917891.

57. Wang X, Pan L, Wang S, Zhou J, McDowell W, Park J, *et al*. Histone H3K9 trimethylase Eggless controls germline stem cell maintenance and differentiation. PLoS Genet. 2011;7(12):e1002426. Epub 2012/01/05. doi: 10.1371/journal.pgen.1002426. PubMed PMID: 22216012; PubMed Central PMCID: PMC3245301.

58. Casanueva MO, Ferguson EL. Germline stem cell number in the *Drosophila* ovary is regulated by redundant mechanisms that control Dpp signaling. Development. 2004;131(9):1881-90. Epub 2004/04/24. doi: 10.1242/dev.01076. PubMed PMID: 15105369.

59. Issigonis M, Tulina N, de Cuevas M, Brawley C, Sandler L, Matunis E. JAK-STAT signal inhibition regulates competition in the *Drosophila* testis stem cell niche. Science. 2009;326(5949):153-6. Epub 2009/10/03. doi: 10.1126/science.1176817. PubMed PMID: 19797664; PubMed Central PMCID: PMC3073347.

60. Xie T, Spradling AC. *decapentaplegic* is essential for the maintenance and division of germline stem cells in the *Drosophila* ovary. Cell. 1998;94(2):251-60. Epub 1998/08/08. PubMed PMID: 9695953.

61. Song X, Zhu CH, Doan C, Xie T. Germline stem cells anchored by adherens junctions in the *Drosophila* ovary niches. Science. 2002;296(5574):1855-7. Epub 2002/06/08. doi: 10.1126/science.1069871. PubMed PMID: 12052957.

62. Yan D, Wu Y, Yang Y, Belenkaya TY, Tang X, Lin X. The cell-surface proteins Dally-like and Ihog differentially regulate Hedgehog signaling strength and range during development. Development. 2010;137(12):2033-44. Epub 2010/05/27. doi: 10.1242/dev.045740. PubMed PMID: 20501592; PubMed Central PMCID: PMC2875843.

63. Hayashi Y, Kobayashi S, Nakato H. *Drosophila* glypicans regulate the germline stem cell niche. J Cell Biol. 2009;187(4):473-80. Epub 2009/12/02. doi: 10.1083/jcb.200904118. PubMed PMID: 19948496; PubMed Central PMCID: PMC2779228.

64. Wang X, Harris RE, Bayston LJ, Ashe HL. Type IV collagens regulate BMP signalling in *Drosophila*. Nature. 2008;455(7209):72-7. Epub 2008/08/15. doi: 10.1038/nature07214. PubMed PMID: 18701888.

65. Chen D, McKearin DM. A discrete transcriptional silencer in the *bam* gene determines asymmetric division of the *Drosophila* germline stem cell. Development. 2003;130(6):1159-70. Epub 2003/02/07. PubMed PMID: 12571107.

66. Chen D, McKearin D. Dpp signaling silences *bam* transcription directly to establish asymmetric divisions of germline stem cells. Curr Biol. 2003;13(20):1786-91. Epub 2003/10/17. PubMed PMID: 14561403.

67. Song X, Wong MD, Kawase E, Xi R, Ding BC, McCarthy JJ, *et al*. Bmp signals from niche cells directly repress transcription of a differentiation-promoting gene, *bag of marbles*, in germline stem cells in the *Drosophila* ovary. Development. 2004;131(6):1353-64. Epub 2004/02/20. doi: 10.1242/dev.01026. PubMed PMID: 14973291.

68. Yamashita YM, Jones DL, Fuller MT. Orientation of asymmetric stem cell division by the APC tumor suppressor and centrosome. Science. 2003;301(5639):1547-50. doi: 10.1126/science.1087795. PubMed PMID: 12970569.

69. Deng W, Lin H. Spectrosomes and fusomes anchor mitotic spindles during asymmetric germ cell divisions and facilitate the formation of a polarized microtubule array for oocyte specification in *Drosophila*. Dev Biol. 1997;189(1):79-94. Epub 1997/09/01. doi: 10.1006/dbio.1997.8669. PubMed PMID: 9281339.

70. Slaidina M, Lehmann R. Translational control in germline stem cell development. J Cell Biol. 2014;207(1):13-21. Epub 2014/10/15. doi: 10.1083/jcb.201407102. PubMed PMID: 25313405; PubMed Central PMCID: PMC4195835.

71. Xie T. Control of germline stem cell self-renewal and differentiation in the *Drosophila* ovary: concerted actions of niche signals and intrinsic factors. Wiley Interdiscip Rev Dev Biol. 2013;2(2):261-73. Epub 2013/09/07. doi: 10.1002/wdev.60. PubMed PMID: 24009036.

72. Forbes A, Lehmann R. Nanos and Pumilio have critical roles in the development and function of *Drosophila* germline stem cells. Development. 1998;125(4):679-90. PubMed PMID: 9435288.

73. Gilboa L, Lehmann R. Repression of primordial germ cell differentiation parallels germ line stem cell maintenance. Curr Biol. 2004;14(11):981-6. Epub 2004/06/09. doi: 10.1016/j.cub.2004.05.049. PubMed PMID: 15182671.

74. Joly W, Chartier A, Rojas-Rios P, Busseau I, Simonelig M. The CCR4 deadenylase acts with Nanos and Pumilio in the fine-tuning of Mei-P26 expression to promote germline stem cell self-renewal. Stem Cell Reports. 2013;1(5):411-24. doi: 10.1016/j.stemcr.2013.09.007. PubMed PMID: 24286029; PubMed Central PMCID: PMC3841267.

75. Neumuller RA, Betschinger J, Fischer A, Bushati N, Poernbacher I, Mechtler K, *et al*. Mei-P26 regulates microRNAs and cell growth in the *Drosophila* ovarian stem cell lineage. Nature. 2008;454(7201):241-5. Epub 2008/06/06. doi: 10.1038/nature07014. PubMed PMID: 18528333; PubMed Central PMCID: PMC2988194.

76. Harris RE, Pargett M, Sutcliffe C, Umulis D, Ashe HL. Brat promotes stem cell differentiation via control of a bistable switch that restricts BMP signaling. Dev Cell. 2011;20(1):72-83. Epub 2011/01/18. doi: 10.1016/j.devcel.2010.11.019. PubMed PMID: 21238926; PubMed Central PMCID: PMC3178012.

77. Jin Z, Xie T. Dcr-1 maintains *Drosophila* ovarian stem cells. Curr Biol. 2007;17(6):539-44. Epub 2007/02/20. doi: 10.1016/j.cub.2007.01.050. PubMed PMID: 17306537.

78. Park JK, Liu X, Strauss TJ, McKearin DM, Liu Q. The miRNA pathway intrinsically controls self-renewal of *Drosophila* germline stem cells. Curr Biol. 2007;17(6):533-8. Epub 2007/02/27. doi: 10.1016/j.cub.2007.01.060. PubMed PMID: 17320391.

79. Ma X, Zhu X, Han Y, Story B, Do T, Song X, *et al*. Aubergine Controls Germline Stem Cell Self-Renewal and Progeny Differentiation via Distinct Mechanisms. Dev Cell.

2017;41(2):157-69 e5. Epub 2017/04/26. doi: 10.1016/j.devcel.2017.03.023. PubMed PMID: 28441530.

80. Edwards LJ, Goodship AE, Birch HL, Patterson-Kane JC. Effect of exercise on age-related changes in collagen fibril diameter distributions in the common digital extensor tendons of young horses. Am J Vet Res. 2005;66(4):564-8. Epub 2005/05/20. PubMed PMID: 15900933.

81. Hatfield SD, Shcherbata HR, Fischer KA, Nakahara K, Carthew RW, Ruohola-Baker H. Stem cell division is regulated by the microRNA pathway. Nature. 2005;435(7044):974-8. Epub 2005/06/10. doi: 10.1038/nature03816. PubMed PMID: 15944714.

82. Xi R, Doan C, Liu D, Xie T. Pelota controls self-renewal of germline stem cells by repressing a Bam-independent differentiation pathway. Development. 2005;132(24):5365-74. Epub 2005/11/11. doi: 10.1242/dev.02151. PubMed PMID: 16280348.

83. Shen R, Weng C, Yu J, Xie T. eIF4A controls germline stem cell self-renewal by directly inhibiting BAM function in the *Drosophila* ovary. Proc Natl Acad Sci U S A. 2009;106(28):11623-8. Epub 2009/06/27. doi: 10.1073/pnas.0903325106. PubMed PMID: 19556547; PubMed Central PMCID: PMC2710669.

84. Barker N, van Es JH, Kuipers J, Kujala P, van den Born M, Cozijnsen M, *et al*. Identification of stem cells in small intestine and colon by marker gene Lgr5. Nature. 2007;449(7165):1003-7. doi: 10.1038/nature06196. PubMed PMID: 17934449.

85. Tian H, Biehs B, Warming S, Leong KG, Rangell L, Klein OD, *et al*. A reserve stem cell population in small intestine renders Lgr5-positive cells dispensable. Nature. 2011;478(7368):255-9. Epub 2011/09/20. doi: 10.1038/nature10408. PubMed PMID: 21927002; PubMed Central PMCID: PMC4251967.

86. Sato T, Vries RG, Snippert HJ, van de Wetering M, Barker N, Stange DE, *et al*. Single Lgr5 stem cells build crypt-villus structures *in vitro* without a mesenchymal niche. Nature. 2009;459(7244):262-5. Epub 2009/03/31. doi: 10.1038/nature07935. PubMed PMID: 19329995.

87. Schuijers J, van der Flier LG, van Es J, Clevers H. Robust cre-mediated recombination in small intestinal stem cells utilizing the *olfm4* locus. Stem Cell Reports. 2014;3(2):234-41. Epub 2014/09/26. doi: 10.1016/j.stemcr.2014.05.018. PubMed PMID: 25254337; PubMed Central PMCID: PMC4175542.

88. Zhu L, Gibson P, Currle DS, Tong Y, Richardson RJ, Bayazitov IT, *et al*. Prominin 1 marks intestinal stem cells that are susceptible to neoplastic transformation. Nature. 2009;457(7229):603-7. Epub 2008/12/19. doi: 10.1038/nature07589. PubMed PMID: 19092805; PubMed Central PMCID: PMC2633030.

89. Sangiorgi E, Capecchi MR. Bmi1 is expressed *in vivo* in intestinal stem cells. Nat Genet. 2008;40(7):915-20. doi: 10.1038/ng.165. PubMed PMID: 18536716; PubMed Central PMCID: PMC2906135.

90. Breault DT, Min IM, Carlone DL, Farilla LG, Ambruzs DM, Henderson DE, *et al*. Generation of mTert-GFP mice as a model to identify and study tissue progenitor cells. Proc Natl Acad Sci U S A. 2008;105(30):10420-5. Epub 2008/07/25. doi: 10.1073/pnas.0804800105. PubMed PMID: 18650388; PubMed Central PMCID: PMC2492454.

91. Potten CS, Kovacs L, Hamilton E. Continuous labelling studies on mouse skin and intestine. Cell Tissue Kinet. 1974;7(3):271-83. Epub 1974/05/01. PubMed PMID: 4837676.

92. Potten CS. Extreme sensitivity of some intestinal crypt cells to X and gamma irradiation. Nature. 1977;269(5628):518-21. Epub 1977/10/06. PubMed PMID: 909602.

93. Buczacki SJ, Zecchini HI, Nicholson AM, Russell R, Vermeulen L, Kemp R, *et al*. Intestinal label-retaining cells are secretory precursors expressing Lgr5. Nature. 2013;495(7439):65-9. Epub 2013/03/01. doi: 10.1038/nature11965. PubMed PMID: 23446353.

94. van Es JH, Sato T, van de Wetering M, Lyubimova A, Gregorieff A, Zeinstra L, *et al*. Dll1+ secretory progenitor cells revert to stem cells upon crypt damage. Nat Cell Biol. 2012;14(10):1099-104. Epub 2012/09/25. doi: 10.1038/ncb2581. PubMed PMID: 23000963; PubMed Central PMCID: PMC3789123.

95. Meran L, Baulies A, Li VSW. Intestinal Stem Cell Niche: The Extracellular Matrix and Cellular Components. Stem Cells Int. 2017;2017:7970385. Epub 2017/08/25. doi: 10.1155/2017/7970385. PubMed PMID: 28835755; PubMed Central PMCID: PMC5556610.

96. Horvay K, Abud HE. Regulation of intestinal stem cells by Wnt and Notch signalling. Adv Exp Med Biol. 2013;786:175-86. Epub 2013/05/23. doi: 10.1007/978-94-007-6621-1_10. PubMed PMID: 23696357.

97. Schuijers J, Junker JP, Mokry M, Hatzis P, Koo BK, Sasselli V, *et al*. Ascl2 acts as an R-spondin/Wnt-responsive switch to control stemness in intestinal crypts. Cell Stem Cell. 2015;16(2):158-70. doi: 10.1016/j.stem.2014.12.006. PubMed PMID: 25620640.

98. Horvay K, Casagranda F, Gany A, Hime GR, Abud HE. Wnt signaling regulates Snai1 expression and cellular localization in the mouse intestinal epithelial stem cell niche. Stem Cells Dev. 2011;20(4):737-45. doi: 10.1089/scd.2010.0188. PubMed PMID: 20670162.

99. Sansom OJ, Meniel VS, Muncan V, Phesse TJ, Wilkins JA, Reed KR, *et al*. Myc deletion rescues Apc deficiency in the small intestine. Nature. 2007;446(7136):676-9. Epub 2007/03/23. doi: 10.1038/nature05674. PubMed PMID: 17377531.

100. He TC, Sparks AB, Rago C, Hermeking H, Zawel L, da Costa LT, *et al*. Identification of c-MYC as a target of the APC pathway. Science. 1998;281(5382):1509-12. Epub 1998/09/04. PubMed PMID: 9727977.

101. Tetsu O, McCormick F. Beta-catenin regulates expression of cyclin D1 in colon carcinoma cells. Nature. 1999;398(6726):422-6. Epub 1999/04/14. doi: 10.1038/18884. PubMed PMID: 10201372.

102. Shtutman M, Zhurinsky J, Simcha I, Albanese C, D'Amico M, Pestell R, *et al*. The cyclin D1 gene is a target of the beta-catenin/LEF-1 pathway. Proc Natl Acad Sci U S A. 1999;96(10):5522-7. Epub 1999/05/13. PubMed PMID: 10318916; PubMed Central PMCID: PMC21892.

103. VanDussen KL, Carulli AJ, Keeley TM, Patel SR, Puthoff BJ, Magness ST, *et al*. Notch signaling modulates proliferation and differentiation of intestinal crypt base columnar stem cells. Development. 2012;139(3):488-97. Epub 2011/12/23. doi: 10.1242/dev.070763. PubMed PMID: 22190634; PubMed Central PMCID: PMC3252352.

104. Konishi H, Asano N, Imatani A, Kimura O, Kondo Y, Jin X, *et al*. Notch1 directly induced CD133 expression in human diffuse type gastric cancers. Oncotarget. 2016;7(35):56598-607. Epub 2016/08/05. doi: 10.18632/oncotarget.10967. PubMed PMID: 27489358; PubMed Central PMCID: PMC5302937.

105. Kayahara T, Sawada M, Takaishi S, Fukui H, Seno H, Fukuzawa H, *et al*. Candidate markers for stem and early progenitor cells, Musashi-1 and Hes1, are expressed in crypt base columnar cells of mouse small intestine. FEBS Lett. 2003;535(1-3):131-5. Epub 2003/02/01. PubMed PMID: 12560091.

106. van der Flier LG, van Gijn ME, Hatzis P, Kujala P, Haegebarth A, Stange DE, *et al*. Transcription factor *achaete scute-like* 2 controls intestinal stem cell fate. Cell. 2009;136(5):903-12. doi: 10.1016/j.cell.2009.01.031. PubMed PMID: 19269367.

107. Dang CV, O'Donnell KA, Zeller KI, Nguyen T, Osthus RC, Li F. The c-Myc target gene network. Semin Cancer Biol. 2006;16(4):253-64. Epub 2006/08/15. doi: 10.1016/j.semcancer.2006.07.014. PubMed PMID: 16904903.

108. Finch AJ, Soucek L, Junttila MR, Swigart LB, Evan GI. Acute overexpression of Myc in intestinal epithelium recapitulates some but not all the changes elicited by Wnt/beta-catenin pathway activation. Mol Cell Biol. 2009;29(19):5306-15. Epub 2009/07/29. doi: 10.1128/MCB.01745-08. PubMed PMID: 19635809; PubMed Central PMCID: PMC2747972.

109. Itzkovitz S, Lyubimova A, Blat IC, Maynard M, van Es J, Lees J, *et al*. Single-molecule transcript counting of stem-cell markers in the mouse intestine. Nat Cell Biol. 2011;14(1):106-14. Epub 2011/11/29. doi: 10.1038/ncb2384. PubMed PMID: 22119784; PubMed Central PMCID: PMC3292866.

110. Bradley A, Evans M, Kaufman MH, Robertson E. Formation of germ-line chimaeras from embryo-derived teratocarcinoma cell lines. Nature. 1984;309(5965):255-6. Epub 1984/05/17. PubMed PMID: 6717601.

111. Evans MJ, Kaufman MH. Establishment in culture of pluripotential cells from mouse embryos. Nature. 1981;292(5819):154-6. Epub 1981/07/09. PubMed PMID: 7242681.

112. Martin GR. Isolation of a pluripotent cell line from early mouse embryos cultured in medium conditioned by teratocarcinoma stem cells. Proc Natl Acad Sci U S A. 1981;78(12):7634-8. Epub 1981/12/01. PubMed PMID: 6950406; PubMed Central PMCID: PMC349323.

113. Takahashi K, Yamanaka S. Induction of pluripotent stem cells from mouse embryonic and adult fibroblast cultures by defined factors. Cell. 2006;126(4):663-76. Epub 2006/08/15. doi: 10.1016/j.cell.2006.07.024. PubMed PMID: 16904174.

114. Gardner RL, Beddington RS. Multi-lineage 'stem' cells in the mammalian embryo. J Cell Sci Suppl. 1988;10:11-27. Epub 1988/01/01. PubMed PMID: 3077932.

115. Nichols J, Smith A. Naive and primed pluripotent states. Cell Stem Cell. 2009;4(6):487-92. Epub 2009/06/06. doi: 10.1016/j.stem.2009.05.015. PubMed PMID: 19497275.

116. Brons IG, Smithers LE, Trotter MW, Rugg-Gunn P, Sun B, Chuva de Sousa Lopes SM, *et al*. Derivation of pluripotent epiblast stem cells from mammalian embryos. Nature. 2007;448(7150):191-5. Epub 2007/06/29. doi: 10.1038/nature05950. PubMed PMID: 17597762.

117. Tesar PJ, Chenoweth JG, Brook FA, Davies TJ, Evans EP, Mack DL, *et al*. New cell lines from mouse epiblast share defining features with human embryonic stem cells. Nature. 2007;448(7150):196-9. Epub 2007/06/29. doi: 10.1038/nature05972. PubMed PMID: 17597760.

118. Osorno R, Tsakiridis A, Wong F, Cambray N, Economou C, Wilkie R, *et al*. The developmental dismantling of pluripotency is reversed by ectopic Oct4 expression. Development. 2012;139(13):2288-98. Epub 2012/06/07. doi: 10.1242/dev.078071. PubMed PMID: 22669820; PubMed Central PMCID: PMC3367440.

119. Smith AG, Heath JK, Donaldson DD, Wong GG, Moreau J, Stahl M, *et al*. Inhibition of pluripotential embryonic stem cell differentiation by purified polypeptides. Nature. 1988;336(6200):688-90. Epub 1988/12/15. doi: 10.1038/336688a0. PubMed PMID: 3143917.

120. Niwa H, Burdon T, Chambers I, Smith A. Self-renewal of pluripotent embryonic stem cells is mediated via activation of STAT3. Genes Dev. 1998;12(13):2048-60. Epub 1998/07/03. PubMed PMID: 9649508; PubMed Central PMCID: PMC316954.

121. Burdon T, Stracey C, Chambers I, Nichols J, Smith A. Suppression of SHP-2 and ERK signalling promotes self-renewal of mouse embryonic stem cells. Dev Biol. 1999;210(1):30-43. Epub 1999/06/12. doi: 10.1006/dbio.1999.9265. PubMed PMID: 10364425.

122. Wray J, Kalkan T, Gomez-Lopez S, Eckardt D, Cook A, Kemler R, *et al*. Inhibition of glycogen synthase kinase-3 alleviates Tcf3 repression of the pluripotency network and increases embryonic stem cell resistance to differentiation. Nat Cell Biol. 2011;13(7):838-45. Epub 2011/06/21. doi: 10.1038/ncb2267. PubMed PMID: 21685889; PubMed Central PMCID: PMC3160487.

123. Ying QL, Wray J, Nichols J, Batlle-Morera L, Doble B, Woodgett J, *et al*. The ground state of embryonic stem cell self-renewal. Nature. 2008;453(7194):519-23. Epub 2008/05/24. doi: 10.1038/nature06968. PubMed PMID: 18497825; PubMed Central PMCID: PMC5328678.

124. Takahashi K, Tanabe K, Ohnuki M, Narita M, Ichisaka T, Tomoda K, *et al*. Induction of pluripotent stem cells from adult human fibroblasts by defined factors. Cell. 2007;131(5):861-72. Epub 2007/11/24. doi: 10.1016/j.cell.2007.11.019. PubMed PMID: 18035408.

125. Yu J, Vodyanik MA, Smuga-Otto K, Antosiewicz-Bourget J, Frane JL, Tian S, *et al*. Induced pluripotent stem cell lines derived from human somatic cells. Science. 2007;318(5858):1917-20. Epub 2007/11/22. doi: 10.1126/science.1151526. PubMed PMID: 18029452.

126. Chin MH, Mason MJ, Xie W, Volinia S, Singer M, Peterson C, *et al*. Induced pluripotent stem cells and embryonic stem cells are distinguished by gene expression signatures. Cell

Stem Cell. 2009;5(1):111-23. Epub 2009/07/03. doi: 10.1016/j.stem.2009.06.008. PubMed PMID: 19570518; PubMed Central PMCID: PMC3448781.

127. Polo JM, Liu S, Figueroa ME, Kulalert W, Eminli S, Tan KY, *et al*. Cell type of origin influences the molecular and functional properties of mouse induced pluripotent stem cells. Nat Biotechnol. 2010;28(8):848-55. Epub 2010/07/21. doi: 10.1038/nbt.1667. PubMed PMID: 20644536; PubMed Central PMCID: PMC3148605.

128. Chronis C, Fiziev P, Papp B, Butz S, Bonora G, Sabri S, *et al*. Cooperative Binding of Transcription Factors Orchestrates Reprogramming. Cell. 2017;168(3):442-59 e20. Epub 2017/01/24. doi: 10.1016/j.cell.2016.12.016. PubMed PMID: 28111071; PubMed Central PMCID: PMC5302508.

129. Soufi A, Donahue G, Zaret KS. Facilitators and impediments of the pluripotency reprogramming factors' initial engagement with the genome. Cell. 2012;151(5):994-1004. Epub 2012/11/20. doi: 10.1016/j.cell.2012.09.045. PubMed PMID: 23159369; PubMed Central PMCID: PMC3508134.

130. Yang Y, Liu B, Xu J, Wang J, Wu J, Shi C, *et al*. Derivation of Pluripotent Stem Cells with *In Vivo* Embryonic and Extraembryonic Potency. Cell. 2017;169(2):243-57 e25. Epub 2017/04/08. doi: 10.1016/j.cell.2017.02.005. PubMed PMID: 28388409.

131. Li X, Liu D, Ma Y, Du X, Jing J, Wang L, *et al*. Direct Reprogramming of Fibroblasts via a Chemically Induced XEN-like State. Cell Stem Cell. 2017;21(2):264-73 e7. Epub 2017/06/27. doi: 10.1016/j.stem.2017.05.019. PubMed PMID: 28648365.

132. Guo G, Yang J, Nichols J, Hall JS, Eyres I, Mansfield W, *et al*. Klf4 reverts developmentally programmed restriction of ground state pluripotency. Development. 2009;136(7):1063-9. Epub 2009/02/20. doi: 10.1242/dev.030957. PubMed PMID: 19224983; PubMed Central PMCID: PMC2685927.

133. Smith A. Formative pluripotency: the executive phase in a developmental continuum. Development. 2017;144(3):365-73. Epub 2017/02/02. doi: 10.1242/dev.142679. PubMed PMID: 28143843; PubMed Central PMCID: PMC5430734.

134. Kimble J, Crittenden SL. Controls of germline stem cells, entry into meiosis, and the sperm/oocyte decision in *Caenorhabditis elegans*. Annu Rev Cell Dev Biol. 2007;23:405-33. Epub 2007/05/18. doi: 10.1146/annurev.cellbio.23.090506.123326. PubMed PMID: 17506698.

135. Kershner A, Crittenden SL, Friend K, Sorensen EB, Porter DF, Kimble J. Germline stem cells and their regulation in the nematode *Caenorhabditis elegans*. Adv Exp Med Biol. 2013;786:29-46. doi: 10.1007/978-94-007-6621-1_3. PubMed PMID: 23696350.

136. Cinquin O, Crittenden SL, Morgan DE, Kimble J. Progression from a stem cell-like state to early differentiation in the *C. elegans* germ line. Proc Natl Acad Sci U S A. 2010;107(5):2048-53. doi: 10.1073/pnas.0912704107. PubMed PMID: 20080700; PubMed Central PMCID: PMC2836686.

137. Angelo G, Van Gilst MR. Starvation protects germline stem cells and extends reproductive longevity in *C. elegans*. Science. 2009;326(5955):954-8. doi: 10.1126/science.1178343. PubMed PMID: 19713489.

138. Seidel HS, Kimble J. The oogenic germline starvation response in *C. elegans*. PLoS One. 2011;6(12):e28074. doi: 10.1371/journal.pone.0028074. PubMed PMID: 22164230; PubMed Central PMCID: PMC3229504.

139. Austin J, Kimble J. glp-1 is required in the germ line for regulation of the decision between mitosis and meiosis in *C. elegans*. Cell. 1987;51(4):589-99. PubMed PMID: 3677168.

140. Berry LW, Westlund B, Schedl T. Germ-line tumor formation caused by activation of glp-1, a *Caenorhabditis elegans* member of the Notch family of receptors. Development. 1997;124(4):925-36. PubMed PMID: 9043073.

141. Gao D, Kimble J. APX-1 can substitute for its homolog LAG-2 to direct cell interactions throughout *Caenorhabditis elegans* development. Proc Natl Acad Sci U S A. 1995;92(21):9839-42. PubMed PMID: 7568229; PubMed Central PMCID: PMC40898.

142. Henderson ST, Gao D, Christensen S, Kimble J. Functional domains of LAG-2, a putative signaling ligand for LIN-12 and GLP-1 receptors in *Caenorhabditis elegans*. Mol Biol Cell. 1997;8(9):1751-62. Epub 1997/10/06. PubMed PMID: 9307971; PubMed Central PMCID: PMC305734.

143. Henderson ST, Gao D, Lambie EJ, Kimble J. lag-2 may encode a signaling ligand for the GLP-1 and LIN-12 receptors of *C. elegans*. Development. 1994;120(10):2913-24. PubMed PMID: 7607081.

144. Crittenden SL, Troemel ER, Evans TC, Kimble J. GLP-1 is localized to the mitotic region of the *C. elegans* germ line. Development. 1994;120(10):2901-11. PubMed PMID: 7607080.

145. Bray SJ. Notch signalling in context. Nat Rev Mol Cell Biol. 2016;17(11):722-35. doi: 10.1038/nrm.2016.94. PubMed PMID: 27507209.

146. Petcherski AG, Kimble J. LAG-3 is a putative transcriptional activator in the *C. elegans* Notch pathway. Nature. 2000;405(6784):364-8. Epub 2000/06/01. doi: 10.1038/35012645. PubMed PMID: 10830967.

147. Christensen S, Kodoyianni V, Bosenberg M, Friedman L, Kimble J. *lag-1*, a gene required for *lin-12* and *glp-1* signaling in *Caenorhabditis elegans*, is homologous to human CBF1 and *Drosophila* Su(H). Development. 1996;122(5):1373-83. Epub 1996/05/01. PubMed PMID: 8625826.

148. Roehl H, Kimble J. Control of cell fate in *C. elegans* by a GLP-1 peptide consisting primarily of ankyrin repeats. Nature. 1993;364(6438):632-5. Epub 1993/08/12. doi: 10.1038/364632a0. PubMed PMID: 8350921.

149. Kershner AM, Shin H, Hansen TJ, Kimble J. Discovery of two GLP-1/Notch target genes that account for the role of GLP-1/Notch signaling in stem cell maintenance. Proc Natl Acad Sci

U S A. 2014;111(10):3739-44. doi: 10.1073/pnas.1401861111. PubMed PMID: 24567412; PubMed Central PMCID: PMC3956202.

150. Crittenden SL, Bernstein DS, Bachorik JL, Thompson BE, Gallegos M, Petcherski AG, *et al*. A conserved RNA-binding protein controls germline stem cells in *Caenorhabditis elegans*. Nature. 2002;417(6889):660-3. doi: 10.1038/nature754. PubMed PMID: 12050669.

151. Thompson BE, Bernstein DS, Bachorik JL, Petcherski AG, Wickens M, Kimble J. Dose-dependent control of proliferation and sperm specification by FOG-1/CPEB. Development. 2005;132(15):3471-81. doi: 10.1242/dev.01921. PubMed PMID: 16000383; PubMed Central PMCID: PMC1350643.

152. Wickens M, Bernstein DS, Kimble J, Parker R. A PUF family portrait: 3'UTR regulation as a way of life. Trends Genet. 2002;18(3):150-7. PubMed PMID: 11858839.

153. Kershner AM, Kimble J. Genome-wide analysis of mRNA targets for *Caenorhabditis elegans* FBF, a conserved stem cell regulator. Proc Natl Acad Sci U S A. 2010;107(8):3936-41. doi: 10.1073/pnas.1000495107. PubMed PMID: 20142496; PubMed Central PMCID: PMC2840422.

154. Prasad A, Porter DF, Kroll-Conner PL, Mohanty I, Ryan AR, Crittenden SL, *et al*. The PUF binding landscape in metazoan germ cells. RNA. 2016. doi: 10.1261/rna.055871.116. PubMed PMID: 27165521.

155. Eckmann CR, Crittenden SL, Suh N, Kimble J. GLD-3 and control of the mitosis/meiosis decision in the germline of *Caenorhabditis elegans*. Genetics. 2004;168(1):147-60. doi: 10.1534/genetics.104.029264. PubMed PMID: 15454534; PubMed Central PMCID: PMC1448115.

156. Millonigg S, Minasaki R, Nousch M, Novak J, Eckmann CR. GLD-4-mediated translational activation regulates the size of the proliferative germ cell pool in the adult *C. elegans* germ line. PLoS Genet. 2014;10(9):e1004647. doi: 10.1371/journal.pgen.1004647. PubMed PMID: 25254367; PubMed Central PMCID: PMC4177745.

157. Merritt C, Seydoux G. The Puf RNA-binding proteins FBF-1 and FBF-2 inhibit the expression of synaptonemal complex proteins in germline stem cells. Development. 2010;137(11):1787-98. doi: 10.1242/dev.050799. PubMed PMID: 20431119; PubMed Central PMCID: PMC2867315.

158. Hansen D, Schedl T. Stem cell proliferation versus meiotic fate decision in *Caenorhabditis elegans*. Adv Exp Med Biol. 2013;757:71-99. Epub 2012/08/09. doi: 10.1007/978-1-4614-4015-4_4. PubMed PMID: 22872475; PubMed Central PMCID: PMC3786863.

159. Jungkamp AC, Stoeckius M, Mecenas D, Grun D, Mastrobuoni G, Kempa S, *et al*. *In vivo* and transcriptome-wide identification of RNA binding protein target sites. Mol Cell. 2011;44(5):828-40. doi: 10.1016/j.molcel.2011.11.009. PubMed PMID: 22152485; PubMed Central PMCID: PMC3253457.

160. Wright JE, Gaidatzis D, Senften M, Farley BM, Westhof E, Ryder SP, *et al*. A quantitative RNA code for mRNA target selection by the germline fate determinant GLD-1. EMBO J. 2011;30(3):533-45. Epub 2010/12/21. doi: 10.1038/emboj.2010.334. PubMed PMID: 21169991; PubMed Central PMCID: PMC3034010.

161. Hansen D, Hubbard EJ, Schedl T. Multi-pathway control of the proliferation versus meiotic development decision in the *Caenorhabditis elegans* germline. Dev Biol. 2004;268(2):342-57. doi: 10.1016/j.ydbio.2003.12.023. PubMed PMID: 15063172.

162. Wang L, Eckmann CR, Kadyk LC, Wickens M, Kimble J. A regulatory cytoplasmic poly(A) polymerase in *Caenorhabditis elegans*. Nature. 2002;419(6904):312-6. doi: 10.1038/nature01039. PubMed PMID: 12239571.

163. Schmid M, Kuchler B, Eckmann CR. Two conserved regulatory cytoplasmic poly(A) polymerases, GLD-4 and GLD-2, regulate meiotic progression in *C. elegans*. Genes Dev. 2009;23(7):824-36. doi: 10.1101/gad.494009. PubMed PMID: 19339688; PubMed Central PMCID: PMC2666339.

164. Suh N, Jedamzik B, Eckmann CR, Wickens M, Kimble J. The GLD-2 poly(A) polymerase activates *gld-1* mRNA in the *Caenorhabditis elegans* germ line. Proc Natl Acad Sci U S A. 2006;103(41):15108-12. doi: 10.1073/pnas.0607050103. PubMed PMID: 17012378; PubMed Central PMCID: PMC1622784.

165. Marin VA, Evans TC. Translational repression of a *C. elegans* Notch mRNA by the STAR/KH domain protein GLD-1. Development. 2003;130(12):2623-32. Epub 2003/05/09. PubMed PMID: 12736207.

166. Wolpert L. Positional Information and Pattern Formation. Curr Top Dev Biol. 2016;117:597-608. doi: 10.1016/bs.ctdb.2015.11.008. PubMed PMID: 26970003.

167. Kaye JA, Rose NC, Goldsworthy B, Goga A, L'Etoile ND. A 3'UTR pumilio-binding element directs translational activation in olfactory sensory neurons. Neuron. 2009;61(1):57-70. doi: 10.1016/j.neuron.2008.11.012. PubMed PMID: 19146813; PubMed Central PMCID: PMC4274156.

168. Suh N, Crittenden SL, Goldstrohm A, Hook B, Thompson B, Wickens M, *et al*. FBF and its dual control of *gld-1* expression in the *Caenorhabditis elegans* germline. Genetics. 2009;181(4):1249-60. doi: 10.1534/genetics.108.099440. PubMed PMID: 19221201; PubMed Central PMCID: PMC2666496.

169. Lamont LB, Crittenden SL, Bernstein D, Wickens M, Kimble J. FBF-1 and FBF-2 regulate the size of the mitotic region in the *C. elegans* germline. Dev Cell. 2004;7(5):697-707. doi: 10.1016/j.devcel.2004.09.013. PubMed PMID: 15525531.

170. Homem CC, Knoblich JA. *Drosophila* neuroblasts: a model for stem cell biology. Development. 2012;139(23):4297-310. Epub 2012/11/08. doi: 10.1242/dev.080515. PubMed PMID: 23132240.

Fig 1
Chapter 1

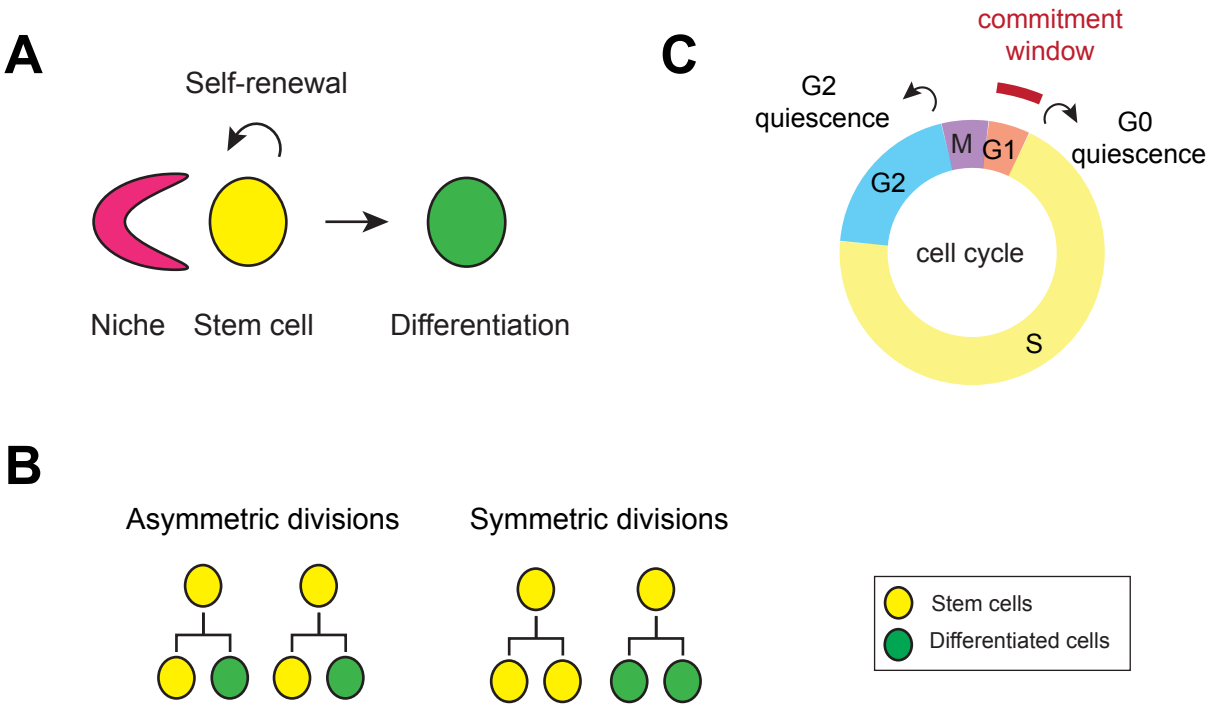

Figure 1. Introduction to stem cell self-renewal.

(A) The niche hypothesis [5]. Stem cell niche is a microenvironment in which stem cells reside and receive signals to self-renew. Displacement from the niche triggers differentiation. Yellow, a stem cell. Green, a differentiated cell. **(B)** Schematic of the stem cell cycle. Stem cells typically have a short G1 phase of the cell cycle to bypass the commitment window (Red). Stem cells can also exit cell cycle and enter G1 or G2 quiescence. Adapted from [38]. **(C)** Stem cell division modes. Stem cells can either divide asymmetrically or symmetrically. In an asymmetric cell division (Left), a stem cell daughter and a differentiating daughter are produced after cell division. In a symmetric cell division (right), the fate outcome is variant but the number of stem cells are maintained as a population. Yellow, stem cells. Green, differentiated cells. Adapted from [20].

Fig 2
Chapter 1

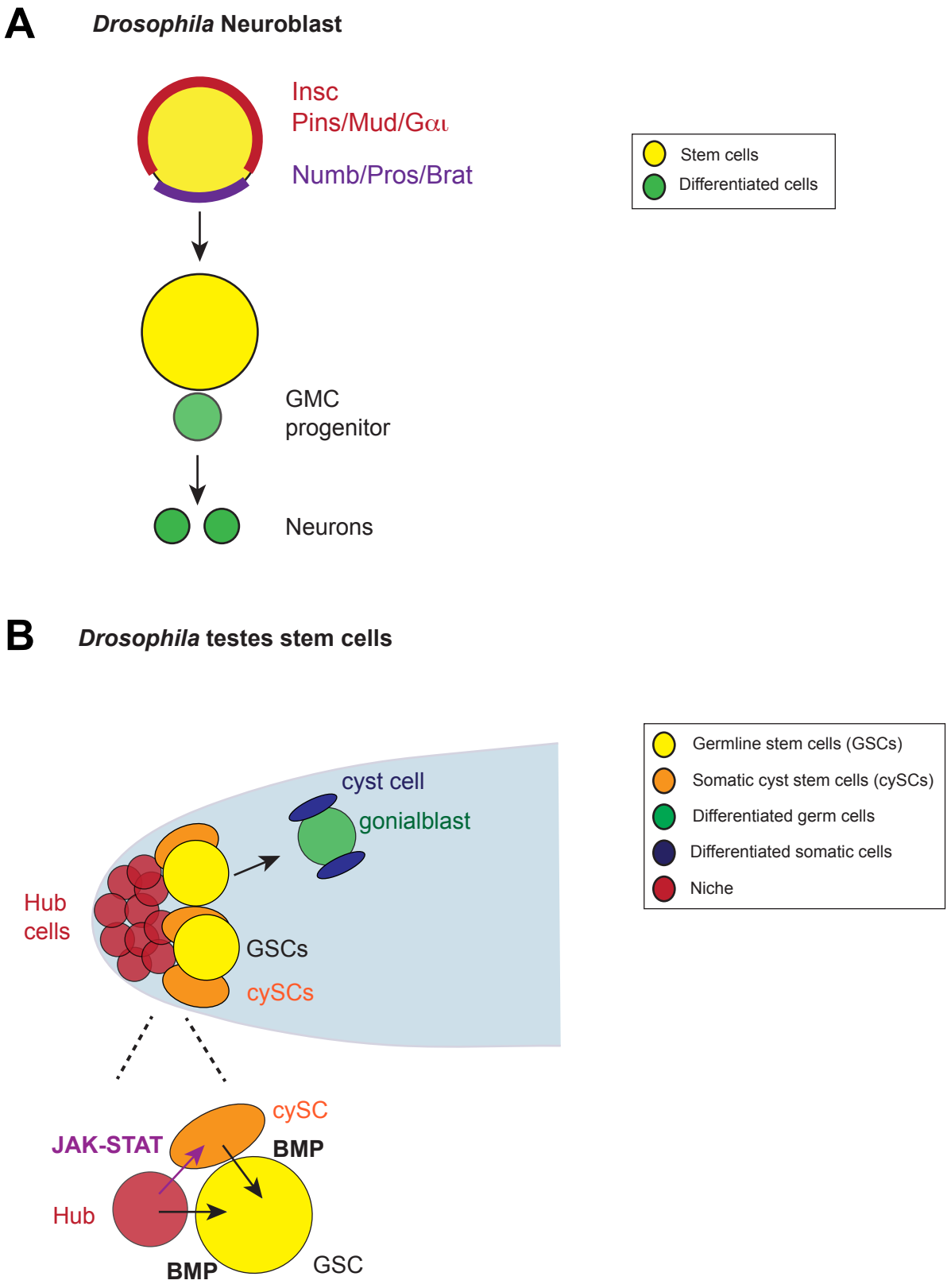

Figure 2. Stem cells maintained by asymmetric stem cell divisions.

(A) Schematic of *Drosophila* neuroblast stem cell division. Cell polarity regulators asymmetrically segregate cell fate regulators: The Insc, Pins/Mud/Gai complex localizes to apical polarity, and the Num/Pros/Brat complex localizes to basal polarity. Asymmetric segregation of fate determinants results in fate asymmetry and trigger differentiation. GMC, Ganglion Mother Cell. See text for details. Adapted from [170]. **(B)** Schematic of *Drosophila* testis. (Top) The hub cell niche maintains both germline stem cells (GSCs) and somatic cyst stem cells (CySCs). Oriented cell divisions displace daughter cells from the niche, which cause differentiation. GSCs and CySCs are closely associated during development. (Bottom) The hub cell niche maintains GSCs through BMP signaling, and CySCs through JAK-STAT signaling. CySCs provide additional support to maintain GSCs through BMP signaling. See text for details. Adapted from [17].

Fig 3
Chapter 1

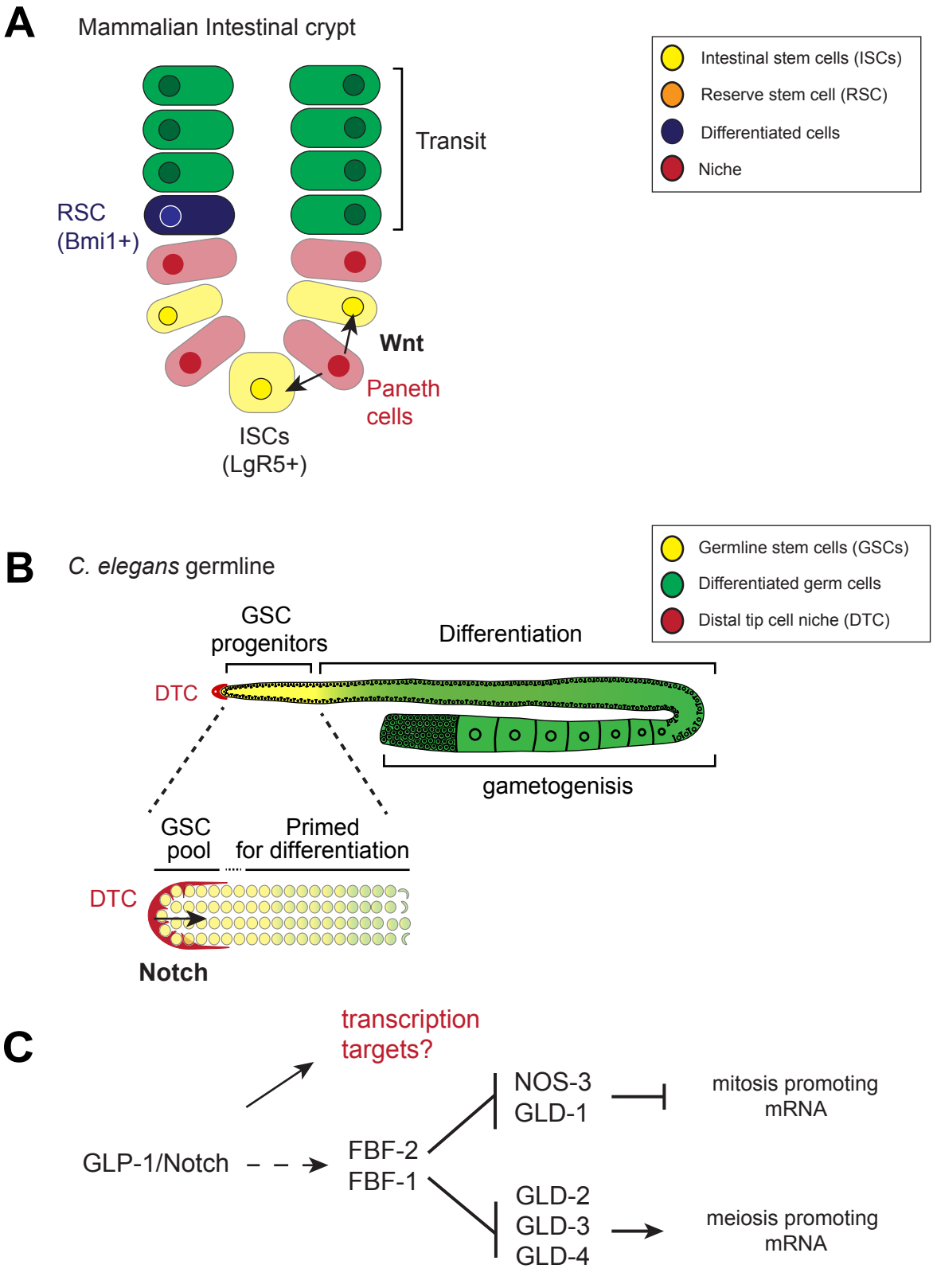

Figure 3. Stem cells maintained by stochastic cell divisions.

(A) Schematic of the mammalian intestine. Intestinal stem cells are located at the crypt base, and move upward as they differentiate. The Paneth cell niche intercalates between stem cells and maintains them, primarily using Wnt signaling. Additional reserve stem cell pool is found in +4 position, marked by a polycomb protein Bmi1. See text for details. Adapted from [27]. **(B)** Schematic of the *C. elegans* gonad. (Top) Mitotically dividing stem cell progenitors are located at the distal end of the gonad. A single cell niche at the distal end embraces the distal-most germ cells and maintain in the naïve state. As cells move proximally, cells are primed for differentiation. (Bottom) The niche utilizes Notch signaling to maintain germline stem cells. Adapted from [134]. **(C)** A regulatory gene network governing self-renewal vs. differentiation of *C. elegans* germline stem cells. Notch signaling from the niche, and the post-transcriptional RNA network governs stem cell self-renewal. PUF family of RNA binding proteins FBF-1 and FBF-2 act as molecular hub for self-renewal. Downstream, GLD-1, GLD-2, GLD-3, GLD-4 (collectively GLD) and NOS-1 proteins constitute two redundant branches governing differentiation. Arrows, direct activation. Dotted arrows, indirect activation. Bars, repression. Adapted from [134].

Chapter 2

Discovery of two GLP-1/Notch target genes

that account for the role of GLP-1/Notch signaling in stem cell maintenance

---

This chapter is published as:
Kershner AM, Shin H, Hansen TJ, Kimble J. Discovery of two GLP-1/Notch target genes that account for the role of GLP-1/Notch signaling in stem cell maintenance. Proc Natl Acad Sci U S A. 2014;111(10):3739-44.

I generated Figure 3C-D, Figure S2B, Figure S6D-F, and contributed reagents to generate Figure 2 and Figure S3. A. Kershner generated all other figures and wrote the paper, together with J. Kimble.

Discovery of two GLP-1/Notch target genes that account for the role of GLP-1/Notch signaling in stem cell maintenance

Aaron Kershner,[a] Heaji Shin,[b] Tyler J. Hansen,[b] Judith Kimble[a,b*]

[a]Howard Hughes Medical Institute and [b]Department of Biochemistry, University of Wisconsin-Madison, Madison, WI 53706 USA

[*]Corresponding author: Judith Kimble
Department of Biochemistry
University of Wisconsin-Madison
433 Babcock Drive
Madison, WI 53706 USA
608-262-6188
608-265-5820 (fax)
jekimble@wisc.edu

Keywords: stem cells, niche, Notch signaling

Short title: Two Notch target genes control stem cells

Abstract

A stem cell's immediate microenvironment creates an essential "niche" to maintain stem cell self-renewal. Many niches and their intercellular signaling pathways are known, but for the most part, the key downstream targets of niche signaling remain elusive. Here we report the discovery of two GLP-1/Notch target genes, *lst-1* (lateral signaling target) and *sygl-1* (synthetic Glp), that function redundantly to maintain germline stem cells (GSCs) in the nematode *Caenorhabditis elegans*. Whereas *lst-1* and *sygl-1* single mutants appear normal, *lst-1 sygl-1* double mutants are phenotypically indistinguishable from *glp-1/Notch* mutants. Multiple lines of evidence demonstrate that GLP-1/Notch signaling activates *lst-1* and *sygl-1* expression in GSCs within the niche. Therefore, these two genes fully account for the role of GLP-1/Notch signaling in GSC maintenance. Importantly, *lst-1* and *sygl-1* are not required for GLP-1/Notch signaling *per se*. We conclude that *lst-1* and *sygl-1* forge a critical link between Notch signaling and GSC maintenance.

Significance Statement

Stem cells generate tissues, and they can be hijacked in cancer. A fundamental mechanism of stem cell regulation is signaling from their immediate microenvironment, or niche. Although many niches and signaling pathways have been identified, much less is known about how stem cells respond. Here we report the discovery of two key niche signaling effector genes. These genes are activated in stem cells by Notch signaling, a conserved and clinically significant pathway, and together are essential for the stem cell state. Surprisingly, neither was previously implicated in stem cell regulation and their sequences yield few clues to their functions. We suggest that these newly discovered genes may be pioneers for a new class of stem cell regulators.

Introduction

Stem cell self-renewal requires signaling from a specialized microenvironment, or stem cell niche (1, 2). Well-defined stem cell niches include the distal tip cell (DTC) for *Caenorhabditis elegans* germline stem cells (GSCs) (3), the cap and hub cells for *Drosophila* GSCs (e.g., 4, 5) and Paneth cells for murine intestinal stem cells (6). These niches employ a variety of intercellular signaling pathways (e.g. Notch, BMP, JAK/Stat, Wnt), all of which have been implicated broadly in stem cell regulation throughout the animal kingdom (1). The identification of direct molecular links between niche signaling and downstream targets driving stem cell self-renewal is crucial for understanding niche function. Yet few such links have been established.

Here we focus on how Notch signaling controls stem cell self-renewal. Notch signaling typically occurs between adjacent cells, one signaling and the other receiving, and activates target genes using a transcription factor complex that includes the DNA binding protein CSL (human CBF1/RBPJ□, *Drosophila* Su(H), and *C. elegans* LAG-1) (7). Although Notch signaling regulates stem cells in vertebrates, including those in the mammalian muscle, brain, and intestine (reviewed in 8), its use in the nematode *C. elegans* to maintain GSCs provides the best defined and most tractable paradigm (Fig. 1*A*). In this case, a single mesenchymal cell, the distal tip cell (DTC), forms the niche for GSCs. The DTC uses GLP-1/Notch signaling to maintain GSCs, and when GSCs leave their DTC niche they are triggered to enter the meiotic cell cycle and begin differentiation (3, 9). Regardless of sex or developmental stage, laser ablation of the DTC or genetic ablation of GLP-1/Notch signaling causes all GSCs to cease self-renewal and differentiate, the so-called Glp (germline proliferation defective) phenotype (3, 9, 10). No other signaling pathway has the same profound effect on *C. elegans* GSC maintenance. Therefore, *C. elegans* GLP-1/Notch provides an unequalled entrée into understanding Notch regulation of stem cells.

The key direct targets of GLP-1/Notch signaling that promote GSC self-renewal remain an open question. A partial answer is that GLP-1/Notch signaling activates *fbf-2* transcription (11).

FBF-2, a PUF family mRNA binding protein, is a broad-spectrum inhibitor of differentiation and a regulator of GSC self-renewal together with its nearly identical paralog FBF-1 (see 12 for review). FBF-1 and FBF-2 function redundantly to maintain GSCs in late larvae and adults (13). GLP-1/Notch signaling also activates *lip-1,* which encodes a dual specificity phosphatase and ERK/MAPK inhibitor (14). LIP-1 promotes robust germline proliferation, but has not been implicated in GSC self-renewal *per se* (15). Therefore, two GLP-1/Notch target genes are known, but neither accounts for GLP-1/Notch regulation of GSC self-renewal.

Additional GLP-1/Notch targets must exist to drive GSC self-renewal but such genes have been elusive. Thirty years of genetics have not found them, either by screening for mutants with a Glp phenotype or by isolating suppressors and enhancers of genes in the GSC control pathway. Here we report that *lst-1* and *sygl-1* function redundantly as pivotal GSC regulators with a double mutant GSC phenotype indistinguishable from that of *glp-1/Notch* mutants. We also provide evidence that both genes are GLP-1/Notch targets but not components of GLP-1/Notch signaling *per se*. The *lst-1* and *sygl-1* genes establish a previously unidentified and important link between niche signaling and stem cell maintenance.

Results

GLP-1/Notch targets essential for larval GSC self-renewal not yet known. Wild-type adults possess a total of ~2000 germ cells, with ~1000 in each of two gonadal arms (Fig. 2*A*; S1*A* and *E*) (e.g. 16), whereas *glp-1* null mutants make a total of only ~4-8 germ cells that all differentiate precociously (Fig. S1*B* and *E*) (9). Previous studies identified *fbf-2* and *lip-1* as germline targets of GLP-1/Notch signaling, but neither on its own was essential for GSC self-renewal (see Introduction). One possibility might have been that *fbf-2* and *lip-1* function redundantly to maintain GSCs. To test this idea, we examined *fbf-2; lip-1* double mutants, but they were self-fertile with essentially normal germlines (Fig. S1*E*). Another possibility might have been that *lip-*

1 functions redundantly with the two nearly identical *fbf-1* and *fbf-2* genes, but *fbf-1 fbf-2; lip-1* triple mutant germlines were similar to *fbf-1 fbf-2* double mutant germlines (Fig. S1*C*-*E*). Therefore, we reasoned that one or more additional GLP-1/Notch target genes must await discovery.

Identification of *lst-1* and *sygl-1* as functionally redundant stem cell regulators. Our strategy to identify the key GLP-1/Notch targets essential for GSC maintenance was as follows. We hypothesized that (1) such genes are targets of both GLP-1/Notch signaling and the FBF RNA-binding protein, (2) they are expressed in GSCs, and (3) their functions in GSC self-renewal is masked by redundancy or pleiotropy. The idea that such genes might be targets of FBF regulation was entirely speculative and based simply on *fbf-2* and *lip-1* being FBF targets (11, 15); the idea that they might function redundantly or have pleiotropic effects was based on the failure to find them previously despite many genetic screens.

We compared lists of putative Notch and FBF-1 targets. The Notch target list of 163 genes was derived bioinformatically with all harboring clusters of at least four LAG-1 binding sites (LBSs) (17); the FBF-1 target list of 1350 mRNAs was obtained experimentally using immunoprecipitation of FBF-1 with associated mRNAs followed by microarray analysis (18). Fifteen genes were common to both lists (Fig. 1*B* and Table S1*A*). We depleted each of the 15 using RNAi, but none caused a Glp phenotype (Table S1*B*). Among those 15 genes, T27F6.4 was expressed within the GSC niche, according to a database of mRNA *in situ* hybridizations to ~10,000 *C. elegans* genes (Nematode Expression Pattern DataBase; http://nematode.lab.nig.ac.jp); the other 14 were either not in the database or did not stain detectably in the niche. With the idea that T27F6.4 might function redundantly with one of the other 14 genes, we performed double RNAi against T27F6.4 and other genes in the common pool. The double RNAi knockdown of T27F6.4 plus *lst-1* caused a Glp phenotype but others did not (Table S2 and Table S3); the double RNAi of T27F6.4 plus *lst-1* gave similar results in either

a wild-type strain or the *rrf-1* mutant, which is sensitive to RNAi in only some tissues, including the germline (19) (Table S2). We therefore named T27F6.4 *sygl-1* (synthetic Glp).

Molecularly, the *lst-1* gene is predicted to produce two mRNAs and polypeptides (Fig. 1*C* and *D*, top), while *sygl-1* is predicted to produce a single mRNA and polypeptide (Fig. 1*C* and *D*, bottom). BLAST analysis of *lst-1* and *sygl-1* sequences revealed homologs in closely related nematodes, including *Caenorhabditis briggsae* and *Caenorhabditis remanei*, but not in more distantly related organisms. We queried LST-1 and SYGL-1 amino acid sequences using a variety of algorithms. A structure prediction program (Phyre2; 20) predicted a single Nanos-like zinc finger in LST-1 (Fig. 1*D*), but no motifs or folded domains in SYGL-1; a signal sequence prediction program (SignalP; 21) predicted a signal sequence at the N-terminus of LST-1L (Fig. 1*D*), but not in LST-1S or SYGL-1; algorithms designed to identify low complexity (SEG; 22) or intrinsically disordered sequences (MFDp2; 23) predict that both proteins harbor multiple low complexity sequences and are largely disordered (Fig. 1*D*). We conclude that *lst-1* and *sygl-1* encode novel proteins with a central role in stem cell regulation.

***lst-1* and *sygl-1* function redundantly to promote GSC self-renewal**. To investigate more rigorously the effects of *lst-1* and *sygl-1* on GSC self-renewal, we obtained two deletion mutants: *lst-1(ok814)* and *sygl-1(tm5040)* (Fig. 1*C* and Fig. S2). The *lst-1* deletion removes most exons and introns unique to the longer *lst-1* isoform; the *sygl-1* deletion removes the first exon, including the ATG translational start codon. These two mutants are likely loss-of-function alleles, since they reproducibly mimic the strongest defect observed with RNAi (see below).

Both *lst-1* and *sygl-1* single deletion mutants possessed germlines comparable in size and organization to wild-type (Fig. 2*A*-*C* and *F*), and they were both self-fertile as hermaphrodites and cross-fertile as males. By contrast, all *lst-1 sygl-1* double deletion mutants displayed a dramatic Glp defect, regardless of sex (Fig. 2*D*-*F* and Fig. S3*A*-*J*). When *lst-1* or *sygl-1* single mutants were targeted with RNAi against the other [e.g. *lst-1(ok814) sygl-1(RNAi)*], the resultant

germlines were also Glp (Table S2). We conclude that *lst-1* and *sygl-1* function redundantly to promote GSC self-renewal in larvae of both sexes.

We observed no obvious somatic defect in either single mutant or the double mutant. For example, all were viable with normal body shape. Nonetheless, we note that *lst-1* plays roles in neurons and the developing vulva, indicating that at least *lst-1* likely functions in tissues other than the germline (17, 24).

***lst-1 sygl-1* Glp defect comparable to *glp-1* Glp defect**. Mutants lacking the GLP-1/Notch receptor make only 4-8 germ cells, which differentiate precociously to produce 16-32 sperm (each germ cell makes four sperm) (9). To ask if *lst-1 sygl-1* Glp sterility mimicked that of a *glp-1* mutant, we used a germline marker (PGL-1) to count germ cell number (Fig. 2*F* and Fig. S3*K-N*) and also asked if germ cells differentiated precociously during development. Newly hatched *lst-1 sygl-1* L1 larvae contained two germ cells, as did wild-type controls; late *lst-1 sygl-1* L1s had made a total of five germ cells on average (n=10, range 4-7) and that number was essentially unchanged in early L3s, which contained only six germ cells on average (n=9, range=4-8). By contrast, wild-type early L3 larvae contained ~35 germ cells on average, as did *lst-1* and *sygl-1* single mutants (Fig. 2*F*). Moreover, *lst-1 sygl-1* germ cells differentiated as sperm during the third larval stage (L3), which is one stage earlier than normal and therefore precocious (Fig. S4). Importantly, sperm number in double mutants was consistent with the number of PGL-1–positive undifferentiated germ cells, and no evidence for cell death was seen. We conclude that the *lst-1 sygl-1* GSC defect is indistinguishable from that of a *glp-1* null mutant (9).

GLP-1/Notch signaling is also required to maintain GSCs throughout larval development and in adults (9). To ask if *lst-1* and *sygl-1* were similarly required in later development, we treated wild-type L4 larvae with RNAi and then scored their germlines as adults (two days later) (Fig. S5*A*). Features diagnostic of GSCs were scored: (i) presence of a Mitotic Zone (25), (ii)

presence of mitotic marker REC-8 (26) in distal germ cells (Fig. 2*G* and *H*), and (iii) absence of meiotic marker HIM-3 (27) in the same germ cells (Fig. S5*C* and *D*). When treated with either control RNAi (empty vector), *lst-1* RNAi, or *sygl-1* RNAi (each mixed 1:1 with empty vector), all adult distal germlines maintained a Mitotic Zone (Fig. 2*G* and Fig. S5*B* and *C*). However, when treated with *lst-1 sygl-1* double RNAi, adult germlines lost their Mitotic Zone and instead contained only differentiating germ cells in the meiotic cell cycle (Fig. 2*H* and Fig. S5*B*). In addition, these *lst-1 sygl-1* double RNAi adult germlines lost REC-8 staining and gained HIM-3 staining to the distal end (Fig. 2*H* and Fig. S5*D*). We conclude that *lst-1* and *sygl-1* function in adults to promote GSC self-renewal. Therefore, like GLP-1/Notch signaling, *lst-1* and *sygl-1* are essential for GSC self-renewal and function in larvae, adults, and both sexes.

***lst-1 sygl-1* is epistatic to *glp-1(gf)* but not *gld-2 gld-1* germline tumors**. If *lst-1* and *sygl-1* are critical GLP-1/Notch targets for GSC self-renewal, they should act downstream of GLP-1/Notch signaling and upstream of GLD regulators promoting meiotic differentiation (Fig. S6*A*). We first explored these predictions genetically, asking if the *lst-1 sygl-1* Glp phenotype was epistatic to the germline tumorous phenotype of two key mutants. First was the constitutively active gain-of-function allele *glp-1(oz112gf),* which encodes an unregulated GLP-1/Notch receptor and drives germline tumors independently of signaling ligand (28). All *glp-1(gf)* mutants made germline tumors when treated with control RNAi (Fig. S6*B* and *F*), but >90% of *glp-1(gf); lst-1(RNAi) sygl-1(RNAi)* animals produced tiny germlines with only sperm (Fig. S6*C* and F). Because *lst-1* and *sygl-1* are required for *glp-1(gf)* to drive tumor formation, they likely do not act upstream, but instead act either downstream or in parallel to GLP-1/Notch signaling. Second was the *gld-2 gld-1* double null mutant, which makes germline tumors because of a failure to enter the meiotic cell cycle and differentiate (29). Like the *gld-2 gld-1* double mutant, all *gld-2 gld-1 lst-1 sygl-1* quadruple mutants formed germ cell tumors (Fig. S6*D-F*). Therefore,

lst-1 and *sygl-1* likely work upstream of *gld-1* and *gld-2*. These epistasis results are consistent with the idea that *lst-1* and *sygl-1* are critical GLP-1/Notch targets for GSC self-renewal.

GLP-1/Notch signaling activates *lst-1* and *sygl-1* expression within the niche. To test the idea that *lst-1* and *sygl-1* function downstream of GLP-1/Notch signaling, we asked if GLP-1/Notch signaling activates their expression. When assayed by mRNA *in situ* hybridization, both *lst-1* and *sygl-1* mRNAs localized to the distal-most germline, within the GSC niche (Fig. 3*A* and *B*, arrows); both genes are also expressed more proximally in developing oocytes (Fig. 3*A* and *B*), which became useful as a control in later experiments. To ask whether their niche expression relies on GLP-1/Notch signaling, we took advantage of the *gld-2 gld-1* double mutant, which generates a tumorous germline independently of GLP-1/Notch signaling (29) and also independently of *lst-1* and *sygl-1* (Fig. S6*D-F*). When GLP-1/Notch signaling was normal and active, *lst-1* and *sygl-1* mRNAs were both expressed in germ cells within the niche of *gld-2 gld-1* double mutants, but when GLP-1/Notch signaling was eliminated, both mRNAs became undetectable (Fig. 3*C* and *D*). Therefore, *lst-1* and *sygl-1* expression in the GSC niche depends on GLP-1/Notch signaling.

LAG-1 binding sequences in *sygl-1* promoter required for expression within niche. GLP-1/Notch signaling activates transcription via the LAG-1/CSL DNA-binding protein and its binding to the LAG-1 binding sequence (LBS) (30). The *lst-1* LBSs were previously shown to mediate Notch activation in the soma (17), and, given the reliance of *lst-1* expression on GLP-1/Notch signaling in the distal germline (Fig. 3*C*), it seemed likely that the *lst-1* LBSs would also be critical for Notch activation in the distal germline. We therefore turned to *sygl-1* and asked if its LBSs were critical for expression within the niche. For this experiment, we generated a *Mos1*-mediated single copy insertion of a Histone 2B::GFP reporter transgene driven by the *sygl-1* promoter, which harbors a cluster of four LBSs (Fig. 1*C* and Fig. 3*E*) (see Materials and

Methods). The wild-type *sygl-1* promoter drove expression of Histone 2B::GFP in the distal-most germ cells (Fig. 3*E*), but that expression was eliminated when all four LBSs were mutated from the consensus RTGGGAA to RACGGAA, a sequence that LAG-1 cannot bind *in vitro* (30) (Fig. 3*E*). The lack of distal expression was not due to gene silencing, as the LBS mutant reporter supported proximal expression (Fig. S7). Therefore, the *sygl-1* LBSs are responsible for expression distally in the niche but not proximally in oocytes.

***lst-1* and *sygl-1* are not required for GLP-1/Notch signaling *per se*.** One potential caveat to the model that *lst-1* and *sygl-1* function downstream of GLP-1/Notch to regulate GSCs might have been that they encode essential components of Notch signaling rather than encoding key downstream stem cell regulators. To explore this concern, we asked if GLP-1/Notch signaling remains functional in the *lst-1 sygl-1* double mutant.

Our assay took advantage of the *gld-2 gld-1 lst-1 sygl-1* germline tumor (Fig. S6*E*), which carries an ideal reporter of GLP-1/Notch signaling: the *sygl-1(tm5040)* deletion mutant retains its LBS cluster and generates a truncated *sygl-1(tm5040)* mRNA that lacks its translational start codon and lacks wild-type SYGL-1 activity (Fig. 1*C*, Fig. 4*A* and Fig. S2*B*). The *gld-2 gld-1 lst-1 sygl-1* quadruple mutant expressed this GLP-1/Notch reporter in germ cells within the niche as expected (Fig. 4*B*). More importantly, that reporter expression required GLP-1/Notch signaling: when signaling was eliminated, reporter expression was no longer detected in the niche (Fig. 4*C*). Therefore, GLP-1/Notch signaling is active and functional in animals harboring both *lst-1* and *sygl-1* deletions. We conclude that *lst-1* and *sygl-1* deletions do not affect GLP-1/Notch signaling *per se* even though their double mutant phenotype mimics a complete loss GLP-1/Notch signaling. Therefore, these two pivotal stem cell regulators are targets of GLP-1/Notch signaling and function downstream of GLP-1/Notch signaling to promote GSC self-renewal (Fig. 4*D*).

Discussion

A central question in stem cell biology is how niche signaling maintains stem cells. Here we identify two genes, *lst-1* and *sygl-1,* which are activated by GLP-1/Notch signaling and function redundantly to maintain the stem cell state. Remarkably, these two genes fully account for the stem cell function of GLP-1/Notch niche signaling. Both *lst-1* and *sygl-1* encode novel proteins and therefore may represent a new class of stem cell regulators. Here we place this discovery in context and discuss its implications.

The DTC niche and GLP-1/Notch signaling maintain GSCs by activation of two redundant genes, *lst-1* and *sygl-1*. The DTC niche was discovered decades ago and its use of GLP-1/Notch signaling to maintain GSCs was found soon thereafter (see Introduction). A longstanding question has been how the DTC niche and GLP-1/Notch signaling promote GSC self-renewal. A partial answer is *fbf-2* activation (11), but FBF only maintains GSCs in adults whereas the DTC niche and GLP-1/Notch signaling maintain them in both larvae and adults (9, 13). Therefore, a larval GSC-promoting activity was predicted to exist – an activity that would complement the previously found adult GSC-promoting activity of FBF. Our search for this additional GSC-promoting activity was guided by several predictions.

Two straightforward predictions were that this gene would be a direct target of GLP-1/Notch signaling and that its RNA would be expressed in the distal-most GSCs within their niche. Another prediction, which was based on the striking failure to find this gene despite extensive mutant screens, was that it likely functioned redundantly with at least one other gene. A final and more risky prediction was that it might be an FBF target, a highly speculative prediction that turned out to be crucial. A comparison of candidate Notch and FBF targets identified 15 in common, one of which was expressed in germ cells within the niche according to an extensive *in situ* hybridization database; RNAi directed against that one gene plus the 14 others led to identification of *lst-1* and *sygl-1*, two genes required for GSC self-renewal in larvae. Follow-up

experiments demonstrated that a double mutant harboring deletions of both *lst-1* and *sygl-1* abolished GSC self-renewal in a manner indistinguishable from a *glp-1* null mutant. However, removal of either gene alone, using either RNAi or a deletion mutant, did not affect GSCs, confirming the prediction of redundancy for genes driving the larval GSC-promoting activity.

Surprisingly, *lst-1* and *sygl-1* are not larval-specific but instead are essential for the GSC state in both larvae and adults. Thus, in addition to the dramatic GSC loss found upon deletion of the two genes, adult GSCs fail to self-renew when treated later in development with RNAi against both *lst-1* and *sygl-1*. The *lst-1* gene was previously identified as a target of Notch signaling in the soma (17). Here we show that *lst-1* and *sygl-1* are also regulated by GLP-1/Notch signaling in GSCs within the niche and that *lst-1* and *sygl-1* function downstream of GLP-1/Notch signaling rather than as an integral component of signaling *per se*. Together these findings demonstrate that the niche and GLP-1/Notch signaling maintain GSCs by activation of *lst-1* and *sygl-1*, and that these two genes are essential effectors of niche signaling for GSC self-renewal. We do not yet know whether overexpression of *lst-1* or *sygl-1* is sufficient for GSC self-renewal, because transgenes driving them in an unregulated fashion could not be generated. Nonetheless, their dramatic loss-of-function phenotype demonstrates unambiguously that *lst-1* and *sygl-1* are critical downstream targets of niche signaling that are essential for all GSC self-renewal.

How might LST-1 and SYGL-1 promote GSC maintenance? A major question emerging from this work is how LST-1 and SYGL-1 proteins promote GSC self-renewal. Few clues come from their amino acid sequences. LST-1 harbors a single C-terminal Nanos-like zinc finger, suggesting RNA binding activity. However, LST-1 is not a canonical Nanos protein, which possesses two zinc fingers in tandem (31); moreover, zinc fingers can perform many molecular functions in addition to RNA binding (32). The LST-1L protein also harbors a predicted signal sequence, implying a possible membrane association or secretion of this isoform. The only

other features of note are low complexity sequences (LCS) in both LST-1 and SYGL-1. In other proteins, LCSs can promote assembly of RNA-protein granules (33), consistent with the possibility of a role in RNA regulation. However, ideas for LST-1 and SYGL-1 molecular activities remain highly speculative at the current time.

The *lst-1* and *sygl-1* amino acid sequences are not conserved outside of nematodes. As such, these two key stem cell regulators may have evolved recently and represent a new mechanism for stem cell regulation. Or they may represent a broadly conserved mechanism of stem cell regulation that relies on proteins whose amino acid sequences are not recognizable across evolution. Instructive cases of proteins not recognizable by amino acid sequence similarity have been found in other pathways. For example, *C. elegans* SYS-1 encodes a □-catenin whose amino acid sequence bears little resemblance to canonical homologs; its discovery therefore relied on genetic phenotype rather than amino acid similarity (34). Here discovery of LST-1 and SYGL-1 required a well-defined niche/stem cell system in a genetically tractable organism, sophisticated knowledge of Notch and FBF targets and the motivation to probe for redundant functions. To our knowledge, similar searches have not been applied broadly. Although not yet definitive, we favor the idea that LST-1 and SYGL-1 are pioneers for a previously unidentified class of stem cell regulators.

Notch target genes and stem cell self-renewal. In addition to *C. elegans* GSCs, other types of stem cells also depend on Notch signaling for self-renewal (see Introduction) (reviewed in 8). Critical downstream targets have also been identified, the most well-studied being genes encoding the Hes/Hey family of bHLH transcription factors. For example, mouse embryos with a conditional brain-specific CSL knockout lose virtually all neural stem cells (NSCs) (35) and *Hes1; Hes3; Hes5* triple mutant embryos similarly lose NSCs in many parts of the developing brain (36), consistent with the idea that these transcription factors are key targets of niche signaling. Yet a brain-specific CSL knockout has a broader effect on NSCs than found in the

Hes1; Hes3; Hes5 triple mutant (35, 37), and a muscle-specific CSL knockout similarly has a more dramatic defect than a mutant lacking key *Hes* genes (38, 39). Therefore, removal of known downstream Notch targets in brain and muscle stem cells does not fully recapitulate the effect of removing the DNA-binding protein responsible for most Notch signaling. This discrepancy may be explained by additional targets or by a lack of congruence between Notch signaling and CSL activity (reviewed in 40). Regardless, our work reports two GLP-1/Notch targets that do in fact fully recapitulate the effect of this canonical signaling pathway on stem cell maintenance. Indeed, *lst-1* and *sygl-1* provide a previously unidentified example of Notch target genes that fully explains the effects of Notch signaling on stem cells of a particular tissue. A fascinating possibility is that similarly pivotal targets of niche signaling exist in other stem cell systems.

Materials and Methods

Nematode culture and RNA interference. Strains were maintained at 20°C following standard protocols (41), except for H2B::GFP reporter transgenic lines which were maintained at 25°C. Wild-type was the N2 Bristol strain. See Supplemental Materials and Methods for full list of strains and alleles used in this study. RNAi feeding experiments were carried out following established protocols (42). For multiple gene knockdowns, HT115 bacteria containing *lst-1*, *sygl-1*, and empty (pL4440) RNAi vectors were grown separately in overnight cultures and then seeded to RNAi plates in equal volumes.

Immunocytochemistry and mRNA *in situ* hybridization. Antibody staining of dissected gonads was carried out as described (15), and staining of whole animals was carried out as described (44). See Supplemental Materials and Methods for protocols. mRNA *in situ* hybridization was performed on dissected gonads from either adults grown to 24 hours post L4

stage or L4 larvae, using digoxigenin labeled DNA probes (45). See Supplemental Materials and Methods for protocols.

Transgenic *C. elegans*. Transgenes were inserted into the genome using the *Mos1*-mediated single copy insertion method (45). See Supplemental Materials and Methods. The presence of H2B::GFP was scored in unfixed dissected gonads in PBS + 0.1% Tween-20, 0.25 mM Levamisole, and Hoechst 33342 (Invitrogen) diluted 1:10,000, and visualized using the Zeiss Axioimager microscope.

Acknowledgments

We thank *C. elegans* knockout consortia for deletions, the *Caenorhabditis* Genetics Center [funded by National Institutes of Health - Office of Research Infrastructure Programs (P40 OD010440)] for strains, Susan Strome for PGL-1 and SP56 antibodies, Developmental Studies Hybridoma Bank for the anti-DAO-5 antibody, and Monica Zetka for anti-HIM-3 antibodies. We thank members of the J. K and Wickens laboratories for insightful comments. JK was supported by NIH (GM069454) and is an investigator of the Howard Hughes Medical Institute.

References

1. Morrison SJ & Spradling AC (2008) Stem cells and niches: mechanisms that promote stem cell maintenance throughout life. *Cell* 132(4):598-611.

2. Lander AD*, et al.* (2012) What does the concept of the stem cell niche really mean today? *BMC Biology* 10:19.

3. Kimble JE & White JG (1981) On the control of germ cell development in *Caenorhabditis elegans*. *Dev. Biol.* 81:208-219.

4. Xie T & Spradling AC (2000) A niche maintaining germ line stem cells in the *Drosophila* ovary. *Science* 290(5490):328-330.

5. Kiger AA, Jones DL, Schulz C, Rogers MB, & Fuller MT (2001) Stem cell self-renewal specified by JAK-STAT activation in response to a support cell cue. *Science* 294(5551):2542-2545.

6. Sato T*, et al.* (2011) Paneth cells constitute the niche for Lgr5 stem cells in intestinal crypts. *Nature* 469(7330):415-418.

7. Kopan R (2012) Notch signaling. *Cold Spring Harbor perspectives in biology* 4(10).

8. Koch U, Lehal R, & Radtke F (2013) Stem cells living with a Notch. *Development* 140(4):689-704.

9. Austin J & Kimble J (1987) *glp-1* is required in the germ line for regulation of the decision between mitosis and meiosis in C. elegans. *Cell* 51:589-599.

10. Morgan DE, Crittenden SL, & Kimble J (2010) The *C. elegans* adult male germline: Stem cells and sexual dimorphism. *Dev. Biol.* 346(2):204-214.

11. Lamont LB, Crittenden SL, Bernstein D, Wickens M, & Kimble J (2004) FBF-1 and FBF-2 regulate the size of the mitotic region in the *C. elegans* germline. *Dev. Cell* 7(5):697-707.

12. Kershner A*, et al.* (2013) Germline stem cells and their regulation in the nematode *Caenorhabditis elegans*. *Adv. Exp. Med. Biol.* 786:29-46.

13. Crittenden SL*, et al.* (2002) A conserved RNA-binding protein controls germline stem cells in *Caenorhabditis elegans*. *Nature* 417:660-663.

14. Berset T, Fröhli Hoier E, Battu G, Canevascini S, & Hajnal A (2001) Notch inhibition of RAS signaling through MAP kinase phosphatase LIP-1 during *C. elegans* vulval development. *Science* 291(5506):1055-1058.

15. Lee M-H, Hook B, Lamont LB, Wickens M, & Kimble J (2006) LIP-1 phosphatase controls the extent of germline proliferation in *Caenorhabditis elegans*. *EMBO J.* 25(1):88-96.

16. Crittenden SL, Leonhard KA, Byrd DT, & Kimble J (2006) Cellular analyses of the mitotic region in the *Caenorhabditis elegans* adult germ line. *Mol. Biol. Cell* 17(7):3051-3061.

17. Yoo AS, Bais C, & Greenwald I (2004) Crosstalk between the EGFR and LIN-12/Notch pathways in *C. elegans* vulval development. *Science* 303(5658):663-666.

18. Kershner AM & Kimble J (2010) Genome-wide analysis of mRNA targets for *Caenorhabditis elegans* FBF, a conserved stem cell regulator. *Proc. Natl. Acad. Sci. USA* 107(8):3936-3941.

19. Kumsta C & Hansen M (2012) *C. elegans rrf-1* mutations maintain RNAi efficiency in the soma in addition to the germline. *PLoS ONE* 7(5):e35428.

20. Kelley LA & Sternberg MJ (2009) Protein structure prediction on the Web: a case study using the Phyre server. *Nat. Protoc.* 4(3):363-371.

21. Petersen TN, Brunak S, von Heijne G, & Nielsen H (2011) SignalP 4.0: discriminating signal peptides from transmembrane regions. *Nat. Methods* 8(10):785-786.

22. Wootton JC & Federhen S (1993) Statistics of local complexity in amino acid sequences and sequence databases. *Comput Chem* 17(2):149-163.

23. Mizianty MJ, Peng Z, & Kurgan L (2013) MFDp2: Accurate predictor of disorder in proteins by fusion of disorder probabilities, content and profiles. *Intrinsically Disordered Proteins* 1(1):e24428.

24. Singh K*, et al.* (2011) *C. elegans* Notch signaling regulates adult chemosensory response and larval molting quiescence. *Curr. Biol.* 21(10):825-834.

25. Crittenden SL, Troemel ER, Evans TC, & Kimble J (1994) GLP-1 is localized to the mitotic region of the *C. elegans* germ line. *Development* 120:2901-2911.

26. Hansen D, Hubbard EJA, & Schedl T (2004) Multi-pathway control of the proliferation versus meiotic development decision in the *Caenorhabditis elegans* germline. *Dev. Biol.* 268(2):342-357.

27. Zetka MC, Kawasaki I, Strome S, & Müller F (1999) Synapsis and chiasma formation in *Caenorhabditis elegans* require HIM-3, a meiotic chromosome core component that functions in chromosome segregation. *Genes Dev.* 13(17):2258-2270.

28. Berry LW, Westlund B, & Schedl T (1997) Germ-line tumor formation caused by activation of *glp-1*, a *Caenorhabditis elegans* member of the *Notch* family of receptors. *Development* 124(4):925-936.

29. Kadyk LC & Kimble J (1998) Genetic regulation of entry into meiosis in *Caenorhabditis elegans*. *Development* 125(10):1803-1813.

30. Christensen S, Kodoyianni V, Bosenberg M, Friedman L, & Kimble J (1996) *lag-1*, a gene required for *lin-12* and *glp-1* signaling in *Caenorhabditis elegans*, is homologous to human CBF1 and *Drosophila* Su(H). *Development* 122:1373-1383.

31. Curtis D*, et al.* (1997) A CCHC metal-binding domain in Nanos is essential for translational regulation. *EMBO J.* 16(4):834-843.

32. Laity JH, Lee BM, & Wright PE (2001) Zinc finger proteins: new insights into structural and functional diversity. *Curr Opin Struct Biol* 11(1):39-46.

33. Kato M*, et al.* (2012) Cell-free formation of RNA granules: low complexity sequence domains form dynamic fibers within hydrogels. *Cell* 149(4):753-767.

34. Phillips BT & Kimble J (2009) A new look at TCF and β-catenin through the lens of a divergent *C. elegans* Wnt pathway. *Dev. Cell* 17(1):27-34.

35. Imayoshi I, Sakamoto M, Yamaguchi M, Mori K, & Kageyama R (2010) Essential roles of Notch signaling in maintenance of neural stem cells in developing and adult brains. *J. Neurosci.* 30(9):3489-3498.

36. Hatakeyama J*, et al.* (2004) *Hes* genes regulate size, shape and histogenesis of the nervous system by control of the timing of neural stem cell differentiation. *Development* 131(22):5539-5550.

37. Imayoshi I, Shimogori T, Ohtsuka T, & Kageyama R (2008) Hes genes and neurogenin regulate non-neural versus neural fate specification in the dorsal telencephalic midline. *Development* 135(15):2531-2541.

38. Vasyutina E*, et al.* (2007) *RBP-J* (*Rbpsuh*) is essential to maintain muscle progenitor cells and to generate satellite cells. *Proc. Natl. Acad. Sci. USA* 104(11):4443-4448.

39. Fukada S*, et al.* (2011) Hesr1 and Hesr3 are essential to generate undifferentiated quiescent satellite cells and to maintain satellite cell numbers. *Development* 138(21):4609-4619.

40. Johnson JE & Macdonald RJ (2011) Notch-independent functions of CSL. *Curr. Top. Dev. Biol.* 97:55-74.

41. Brenner S (1974) The genetics of *Caenorhabditis elegans*. *Genetics* 77(1):71-94.

42. Ahringer Je (2006) Reverse genetics. *WormBook,* ed The *C. elegans* Research Community. Available at: http:http://www.wormbook.org, doi/10.1895/wormbook.1.47.1.

43. Duerr JS (2006) Immunohistochemistry. *WormBook,* ed The *C. elegans* Research Community. Available at: http://www.wormbook.org, 10.1895/wormbook.1.105.1.

44. Lee M-H & Schedl T (2006) RNA *in situ* hybridization of dissected gonads. *WormBook,* ed The *C. elegans* Research Community. Available at: http://www.wormbook.org, 10.1895/wormbook.1.107.1.

45. Frøkjær-Jensen C*, et al.* (2008) Single-copy insertion of transgenes in *Caenorhabditis elegans*. *Nat. Genet.* 40(11):1375-1383.

Supplemental Materials and Methods

Nematode culture and RNA interference. Strains were maintained at 20°C following standard protocols (1), except for H2B::GFP reporter transgenic lines which were maintained at 25°C. Wild-type was the N2 Bristol strain. Mutations were as follows: *LG I*: *gld-1(q485)* (2); *gld-2(q497)* (3); *lst-1(ok814)* (4); *sygl-1(tm5040)* (this work); *rrf-1(pk1417)* (5)*; LG II*: *fbf-1(ok91)* (6); *fbf-2(q704)* (6); *fbf-2(q738)* (7); *LG III*: *glp-1(q46)* (8); *glp-1(oz112 gf)* (9); *LG IV*: *lip-1(zh15)* (10); *eri-1(mg366)* (11). *lst-1(ok814)* and *sygl-1(tm5040)* single mutants were outcrossed against wild-type at least eight times prior to analysis. Balancers were as follows: *LG I*: *hT2[qIs48]* (12); *LG II*: *mIn1[mIs14 dpy-10(e128)]*; *LG III*: *hT2[qIs48]*; *qC1[qIs26]*. Transgenes were as follow: *LG II*: *qSi26[$P_{sygl\text{-}1(wt)}$::H2B::GFP::sygl-1 3'end; unc-119(+)]* (this work); *qSi29[$P_{sygl\text{-}1(4XLBS\ mut)}$::H2B::GFP::sygl-1 3'end; unc-119(+)]* (this work); *LG III*: *qIs153[$P_{lag\text{-}2}$::MYR::GFP; $P_{ttx\text{-}3}$::DsRED* (13); *LG IV*: *teIs1[oma-1::GFP; unc-119(+)]* (14); unknown *LG*: *qIs147[Psur-5::GFP]*.

Nematode strains used in this study

N2: wild-type

GR1373: *eri-1(mg366) IV*

NL2098: *rrf-1(pk1417) I*

EG4322: *ttTi5605 II; unc-119(ed3) III*

JK2879: *gld-2(q497) gld-1(q485) I/ hT2[qIs48](I;III)*

JK3308: *fbf-2(q738)/ mIn1[mIs14 dpy-10(e128)] II; lip-1(zh15) IV*

JK3520: *unc-32(e189) glp-1(oz112 gf)/ qC1[qIs26] III*

JK3545: *gld-2(q497) gld-1(q485) I/ hT2[qIs48](I;III); unc-32(e189) glp-1(q46) III/ hT2[qIs48](I;III)*

JK3635: *fbf-1(ok91) fbf-2(q704)/ mIn1[mIs14 dpy-10(e128)] II*

JK4008: *fbf-1(ok91) fbf-2(q704)/ mIn1[mIs14 dpy-10(e128)] II; lip-1(zh15) IV*

JK4356: *lst-1(ok814) I*

JK4475: *qIs153[P_{lag-2}::MYR::GFP; P_{ttx-3}::DsRED] III*

JK4774: *lst-1(ok814) sygl-1(tm5040) I/ hT2[qIs48](I;III)*

JK4795: *lst-1(ok814) sygl-1(tm5040) I/ hT2[qIs48](I;III); qIs147[P_{sur-5}::GFP] (LG?)*

JK4832: *gld-2(q497) gld-1(q485) lst-1(ok814) sygl-1(tm5040) I/ hT2[qIs48](I;III)*

JK4862: *glp-1(q46) III/ hT2[qIs48](I;III)*

JK4873: *gld-2(q497) gld-1(q485) I/ hT2[qIs48](I;III); unc-32(e189) III/ hT2[qIs48](I;III)*

JK4899: *sygl-1(tm5040) I*

JK5017: *gld-2(q497) gld-1(q485) lst-1(ok814) sygl-1(tm5040) I/ hT2[qIs48](I;III); glp-1(q46) III/ hT2[qIs48](I;III)*

JK5018: *qSi26[$P_{sygl-1(wt)}$::H2B::GFP::sygl-1 3'end; unc-119(+)] II ; unc-119(ed3) III; teIs1[oma-1::GFP, unc-119(+)]* IV *teIs1* was crossed out prior to scoring

JK5072: *qSi29[$P_{sygl-1(4XLBS\ mut)}$::H2B::GFP::sygl-1 3'end; unc-119(+)] II ; unc-119(ed3) III; teIs1[oma-1::GFP; unc-119(+)]* IV *teIs1* was crossed out prior to scoring

Immunocytochemistry

Antibody staining of dissected gonads was carried out essentially as described (15). Briefly, dissected gonads were fixed in 3% (wt/vol) paraformaldehyde, 100mM K_2HPO_4 (pH 7.2) for 0.5-1 hours at room temperature and then permeabilized in 100% methanol at -20°C for 10 minutes. Samples were washed three times in PBST (PBS + 0.1% Tween-20) and blocked in PBST + 0.5% BSA for 30 min at room temperature. Primary antibodies were incubated at 4°C overnight at the following dilutions in PBST + 0.5% BSA: the sperm marker mouse anti-SP56, 1:100 (16); the nucleolar marker mouse anti-DAO-5, 1:10 (17); the meiotic marker rabbit anti-HIM-3, 1:200 (18); the mitotic marker rabbit anti-REC-8, 1:5,000 (SDIX); and the germ cell marker rabbit anti-PGL-1, 1:100 (19). Cy5, Cy3, and FITC conjugated secondary antibodies (Jackson

ImmunoResearch) were used at 1:500 dilution in PBST + 0.5% BSA for 1-2 hours at room temperature. 4', 6-diamidino-2-phenylindole (DAPI, 0.5 ng/µl) was included to visualize DNA. Compound microscope images were taken using a Zeiss Axioimager microscope, and confocal images were taken using a Leica TCS SP8.

Antibody staining of whole animals was carried out essentially as described (20). Briefly, animals were subjected to three rounds of freeze-thaw cycles in FRB (80 mM KCl, 20 mM NaCl, 10 mM EGTA, 5 mM spermidine, 15 mM PIPES pH7.4, 25% (vol/vol) methanol, 0.8% paraformaldehyde) followed by a 30-minute fixation on ice. Fixed samples were washed twice in TT (100 mM Tris pH 7.4, 1% Triton X-100, 1 mM EDTA) and then reduced for 4 hours in TT + 1% beta-mercaptoethanol at 37°C. Samples were then washed once in BO_3T (50 mM H_3BO_3 pH 9.5, 25 mM NaOH, 0.01% Triton X-100) and incubated with BO_3T + 10 mM dithiothreitol at room temperature for 15 minutes. Next, samples were washed once with BO_3T and then oxidized with BO_3T + 0.3% H_20_2 for 15 minutes at room temperature followed by two washes with PBST. Samples were blocked in PBST + 0.5% BSA, and stained using rabbit anti-PGL-1 antibodies (19) at a 1:100 dilution in PBST + 0.5% BSA. FITC conjugated anti-rabbit secondary antibodies (Jackson ImmunoResearch) were used at 1:500 dilution in PBST + 0.5% BSA. DAPI (0.5 ng/µl) was included to visualize DNA. Samples were imaged using a Zeiss Axioimager microscope.

mRNA *in situ* Hybridization

mRNA *in situ* hybridizations were carried out on dissected gonads from either adult hermaphrodites grown to 24 hours post L4 stage or from L4 larva, as indicated in the figure legends for Fig 3 and Fig 4, following standard protocols (21). For probe generation, PCR fragments were amplified from cDNA using the following primers: *lst-1*, prAK102 (5'-ggcttcttcgtcggagaacatg-3') and prAK104 (5'-gaaccggcacgatcgagttg-3'); *sygl-1*, prAK329 (5'-atgccattccattatccaaaactc-3') and prAK330 (5'-atagctgttggagcccatcatc-3'). Fragments were

occasionally subject to two rounds of PCR to generate more concentrated probe. Next, single stranded digoxigenin (DIG)-dUTP labeled DNA probes were generated from the PCR fragments using DIG labeling mix (Roche) following the manufacturer's protocol with either antisense or sense primer as follows: *lst-1* sense, prAK105 (5'-gttgacgtggatcttgacat-3'), *lst-1* antisense prAK101 (5'-gttgagcaaaccacagtcgg-3'), *sygl-1* sense prAK331 (5'-ggaaacatgtccacctcatcgtc-3'), and *sygl-1* antisense prAK332 (5'-ggtaactgtggagaccaaatcgg-3'). Probes were ethanol precipitated, resuspended in hybridization buffer (HB; 5× SSC, 50% (vol/vol) deionized formamide, 100 µg/ml herring sperm DNA, 50 µg/ml heparin, 0.1% Tween 20), and boiled for one hour. To prepare worm samples, dissected gonads were fixed in 3% (wt/vol) paraformaldehyde, 0.25% (vol/vol) glutaraldehyde, 100 mM K_2HPO_4 (pH 7.2) at room temperature for two hours. Samples were then permeabilized in 100% methanol at -20°C and washed three times in PBST. Samples were then digested with 50 µg/ml Proteinase K in PBST for 30 minutes at room temperature and then fixed again using 3% (wt/vol) paraformaldehyde, 0.25% (vol/vol) glutaraldehyde, 100 mM K_2HPO_4 (pH 7.2) at room temperature for 15 minutes. After a 15-minute incubation with PBST + 2 mg/ml glycine, fixed samples were washed three times with PBST. Gonads were then treated with a 1:1 mixture of PBST and HB for 5 minutes at 48°C, followed by an incubation with 100% HB at 48°C for one hour. Boiled probes were then added to the samples and were incubated at 48°C for 24-36 hours. Next, samples were first washed 2-3 times in HB, then washed 2-3 times in a 1:1 mixture of PBST and HB, and then washed 2-3 times with PBST. For probe detection, samples were first blocked as above and then treated with anti-DIG antibody (Roche) diluted to 1:1000 in PBST + 0.5% BSA and incubated overnight at 4°C. Samples were then washed 2-3 times with PBST + 0.5% BSA and stained with BCIP/NBT substrate (Sigma) in 100 mM Tris (pH9.5), 100 mM NaCl, 5 mM $MgCl_2$, 0.1% Tween 20, 1 mM Levamisole. After staining appeared in the sample treated with anti-sense probe, samples were washed 2-3 times in PBST, and then viewed using a Zeiss Axioskop microscope.

Transgenic *C. elegans*

For H2B::GFP reporter transgenes, a construct (pJK1634) containing ~2.2 kb of sequence upstream of the *sygl-1* start driving expression of H2B::GFP coding sequence from pCM1.35 (Addgene plasmid 17248) (22) followed by the *sygl-1* 3'UTR and intergenic region was cloned into the *Spe I* site of pCFJ151 (23) (Addgene plasmid 19330). A separate clone (pJK1635) was generated identical to pJK1634 except that each of the four consensus LAG-1 binding sites was mutated from the wild-type consensus RTGGGAA to the mutant form RACGGAA using QuickChange Site Directed Mutagenesis Kit (Stratagene). pJK1634 and pJK1635 were then used to integrate the constructs into the *ttTi5605* site in *LGII* of strain EG4322 to make *qSi26* and *qSi29,* respectively, using *Mos1*-mediated single copy insertion (MosSCI) direct insertion method (23). Multiple transgenic lines generated for each construct showed similar expression patterns. Since *gfp* transgenes are often silenced in the germline, each reporter was crossed into an *oma-1::gfp* germline expressing strain that can desilence other germline *gfp* transgenes in *trans* (24). Reporters were maintained for at least 10 generations in the *oma-1::gfp* background, after which they were crossed out and maintained at 25°C. The presence of H2B::GFP was scored in unfixed tissues by dissecting gonads in PBST, 0.25 mM Levamisole, and Hoechst 33342 (Invitrogen) diluted 1:10,000, and visualized using the Zeiss Axioimager microscope. For both transgenic lines, H2B::GFP was observed in the proximal region of the germline. Distal H2B::GFP was scored only in germlines with loop expression. Distal expression was never observed in the absence of proximal expression.

Northern blots

Total RNA was extracted from staged N2, *lst-1(ok814)* (JK4356), and *sygl-1(tm5040)* (JK4899) adults grown to 24 hours past L4 stage using Trizol Reagent (Invitrogen). RNA was then poly(A) selected using the poly(A) Purist Kit (Ambion), and 5 µg of poly(A) RNA was run in each

lane on a 1% (wt/vol) or 1.2% (wt/vol) agarose gel under denaturing conditions using the NorthernMax-Gly kit (Ambion). RNA Millennium Markers (Ambion) were also run as a size marker. Separated RNA was transferred to a positively-charged nylon membrane (BrightStar-Plus, Ambion) using NorthernMax transfer buffer (Ambion), and transferred RNA was then crosslinked to the membrane using Stratalinker UV crosslinker (Stratagene). *In vitro*-transcribed ^{32}P-radiolabeled antisense RNA probes were prepared from cDNA templates using Strip-EZ RNA T7 kit (Ambion) or MAXIscript T7 kit (Ambion). Hybridization and washes were carried out at 68°C using NorthernMax wash buffers (Ambion). Hybridized membranes were exposed overnight to a phosphor screen (Molecular Dynamics) and detected using a Typhoon Scanner (GE Healthcare).

Primers used to make probes are as follows: *lst-1*, prAK102 (5'-ggcttcttcgtcggagaacatg-3') and prAK103 (5'-TAATACGACTCACTATAGGGAGAgaaccggcacgatcgagttg-3'); *sygl-1,* prHJS143 (5'-CCGCTGAGCAATAACTAGCatgccattccattatccaaaactc-3') and prHJS144 (5'-TAATACGACTCACTATAGGGctactgcaaataatagctgttgg-3'); *eft-3*, KRN195 (5'-caagtacgcttgggtctc-3') and KRN196 (5'-TAATACGACTCACTATAGGcctcagagaatggtggctc-3'). Capitals letters in prAK103, KRN196, and prHJS144 indicate the T7 promoter sequence used for *in vitro* transcription. Capital letters in prHJS143 indicate the T7 terminator sequence.

References

1. Brenner S (1974) The genetics of *Caenorhabditis elegans*. *Genetics* 77(1):71-94.

2. Francis R, Barton MK, Kimble J, & Schedl T (1995) *gld-1*, a tumor suppressor gene required for oocyte development in *Caenorhabditis elegans*. *Genetics* 139(2):579-606.

3. Kadyk LC & Kimble J (1998) Genetic regulation of entry into meiosis in *Caenorhabditis elegans*. *Development* 125(10):1803-1813.

4. Singh K*, et al.* (2011) *C. elegans* Notch signaling regulates adult chemosensory response and larval molting quiescence. *Curr Biol* 21(10):825-834.

5. Sijen T*, et al.* (2001) On the role of RNA amplification in dsRNA-triggered gene silencing. *Cell* 107:465-476.

6. Crittenden SL*, et al.* (2002) A conserved RNA-binding protein controls germline stem cells in *Caenorhabditis elegans*. *Nature* 417:660-663.

7. Lamont LB, Crittenden SL, Bernstein D, Wickens M, & Kimble J (2004) FBF-1 and FBF-2 regulate the size of the mitotic region in the *C. elegans* germline. *Dev Cell* 7(5):697-707.

8. Austin J & Kimble J (1987) *glp-1* is required in the germ line for regulation of the decision between mitosis and meiosis in C. elegans. *Cell* 51:589-599.

9. Berry LW, Westlund B, & Schedl T (1997) Germ-line tumor formation caused by activation of *glp-1*, a *Caenorhabditis elegans* member of the *Notch* family of receptors. *Development* 124(4):925-936.

10. Berset T, Fröhli Hoier E, Battu G, Canevascini S, & Hajnal A (2001) Notch inhibition of RAS signaling through MAP kinase phosphatase LIP-1 during *C. elegans* vulval development. *Science* 291(5506):1055-1058.

11. Kennedy S, Wang D, & Ruvkun G (2004) A conserved siRNA-degrading RNase negatively regulates RNA interference in *C. elegans*. *Nature* 427(6975):645-649.

12. Siegfried K & Kimble J (2002) POP-1 controls axis formation during early gonadogenesis in *C. elegans*. *Development* 129(2):443-453.

13. Byrd DT, Knobel K, Affeldt K, Crittenden SL, & Kimble J (2014) A DTC niche plexus surrounds the germline stem cell pool in *Caenorhabditis elegans*. *PLoS ONE* (in press).

14. Lin R (2003) A gain-of-function mutation in *oma-1*, a *C. elegans* gene required for oocyte maturation, results in delayed degradation of maternal proteins and embryonic lethality. *Dev Biol* 258(1):226-239.

15. Lee M-H, Hook B, Lamont LB, Wickens M, & Kimble J (2006) LIP-1 phosphatase controls the extent of germline proliferation in *Caenorhabditis elegans*. *EMBO J* 25(1):88-96.

16. Ward S, Roberts TM, Strome S, Pavalko FM, & Hogan E (1986) Monoclonal antibodies that recognize a polypeptide antigenic determinant shared by multiple *Caenorhabditis elegans* sperm-specific proteins. *J Cell Biol* 102(5):1778-1786.

17. Hadwiger G, Dour S, Arur S, Fox P, & Nonet ML (2010) A monoclonal antibody toolkit for *C. elegans*. *PLoS ONE* 5(4):e10161.

18. Zetka MC, Kawasaki I, Strome S, & Müller F (1999) Synapsis and chiasma formation in *Caenorhabditis elegans* require HIM-3, a meiotic chromosome core component that functions in chromosome segregation. *Genes Dev* 13(17):2258-2270.

19. Kawasaki I*, et al.* (1998) PGL-1, a predicted RNA-binding component of germ granules, is essential for fertility in *C. elegans*. *Cell* 94(5):635-645.

20. Duerr JS (2006) Immunohistochemistry. *WormBook,* ed The *C. elegans* Research Community. Available at: http://www.wormbook.org, 10.1895/wormbook.1.105.1.

21. Lee M-H & Schedl T (2006) RNA *in situ* hybridization of dissected gonads. *WormBook,* ed The *C. elegans* Research Community. Available at: http://www.wormbook.org, 10.1895/wormbook.1.107.1.

22. Merritt C, Rasoloson D, Ko D, & Seydoux G (2008) 3' UTRs are the primary regulators of gene expression in the *C. elegans* germline. *Curr Biol* 18(19):1476-1482.

23. Frøkjær-Jensen C*, et al.* (2008) Single-copy insertion of transgenes in *Caenorhabditis elegans*. *Nat Genet* 40(11):1375-1383.

24. Shirayama M*, et al.* (2012) piRNAs initiate an epigenetic memory of nonself RNA in the *C. elegans* germline. *Cell* 150(1):65-77.

25. Crittenden SL, Leonhard KA, Byrd DT, & Kimble J (2006) Cellular analyses of the mitotic region in the *Caenorhabditis elegans* adult germ line. *Mol Biol Cell* 17(7):3051-3061.

26. Gerstein MB*, et al.* (2010) Integrative analysis of the *Caenorhabditis elegans* genome by the modENCODE project. *Science* 330(6012):1775-1787.

27. Hansen D, Hubbard EJA, & Schedl T (2004) Multi-pathway control of the proliferation versus meiotic development decision in the *Caenorhabditis elegans* germline. *Dev Biol* 268(2):342-357.

28. Dernburg AF*, et al.* (1998) Meiotic recombination in *C. elegans* initiates by a conserved mechanism and is dispensable for homologous chromosome synapsis. *Cell* 94(3):387-398.

Fig 1
Chapter 2

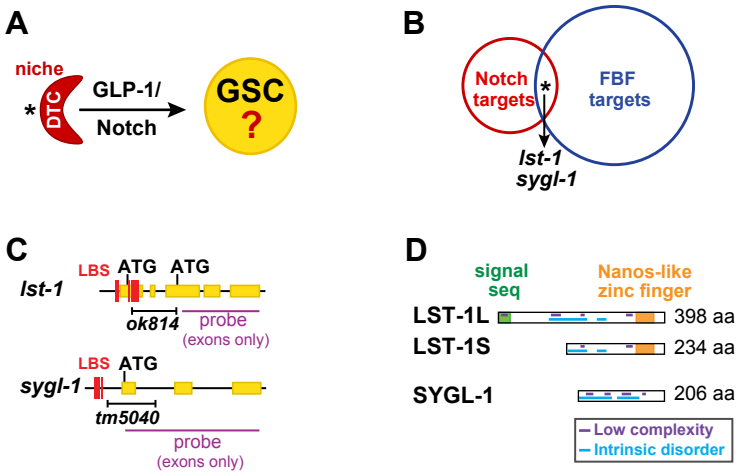

Figure legends

Fig. 1. Identification of *lst-1* and *sygl-1* as candidate GSC regulators. (***A***) DTC (red) uses GLP-1/Notch signaling to maintain GSCs within the niche. (***B***) Fifteen genes (asterisk) are shared between lists of putative Notch and FBF targets. Double RNAi of two common genes, *lst-1* and *sygl-1*, caused a Glp phenotype. Also see Table S1 and Table S2. (***C***) *lst-1* and *sygl-1* genes. Yellow, exons; red lines, LAG-1 binding sites (LBS); black bar, deletions; purple line, probe for *in situ* hybridizations (exons only). (***D***) LST-1 and SYGL-1 proteins and their predicted motifs.

Fig 2
Chapter 2

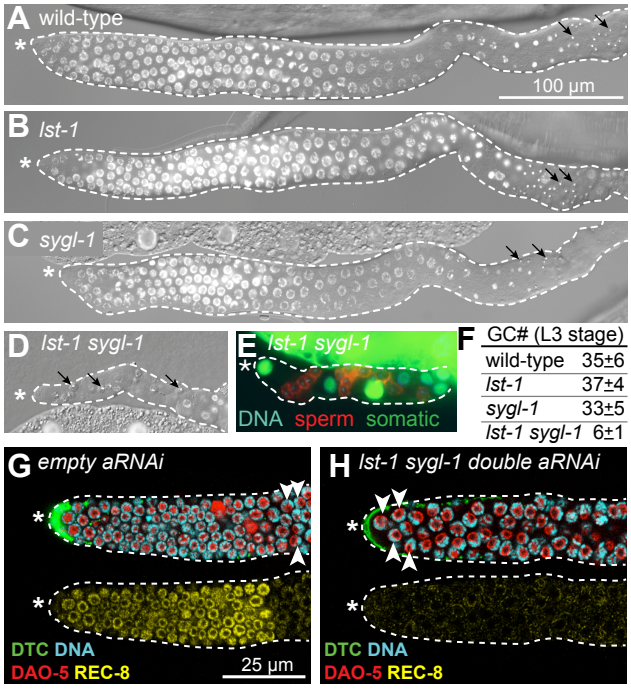

Fig. 2. *lst-1* and *sygl-1* function redundantly to promote GSC self-renewal in larvae and adults. (***A-D***) DIC and DAPI-stained images of gonads dissected from L4 hermaphrodites. Asterisk marks distal end; dotted line outlines germline plus somatic gonadal cells; arrows mark mature sperm. (*A-C*) Wild-type (100% non-Glp, n>100), *lst-1(ok814)* (100% non-Glp, n=146), and *sygl-1(tm5040)* (100% non-Glp, n=159) all produce normal germlines. (*D*) *lst-1 sygl-1* double mutants produce Glp germlines with only a few differentiated sperm (100% Glp, n=76). (***E***) Gonad from *lst-1 sygl-1* L4 with a somatic GFP marker (green), a sperm marker (red) and DNA staining (blue). All non-sperm cells expressed somatic GFP. Each gonadal arm contained 14 ± 3 sperm (n=9) on average (from 3-4 pre-meiotic germ cells). (***F***) Total pre-meiotic germ cells (GC#) in entire L3 gonad, scored with PGL-1 germ cell marker. For wild-type and each single mutant, n=5; for *lst-1 sygl-1* double mutant, n=9. (***G-H)*** Representative confocal images of wild-type late L4 larval germlines treated with RNAi for 48 hours; DTC expresses GFP (green). Same conventions as in (*A-D*); Mitotic Zone scored by presence of mitotic marker REC-8 (yellow) and absence of crescent-shaped DAPI staining typical of early meiotic prophase nuclei (white arrowheads). Anti-DAO-5 (red, nucleolar marker) counter-stain facilitates scoring of DAPI crescents. (*G*) Germline treated with empty RNAi vector possesses a Mitotic Zone. (*H*) Germline treated with *lst-1 sygl-1* double RNAi lacks a Mitotic Zone and hence lacks GSCs.

Fig 3
Chapter 2

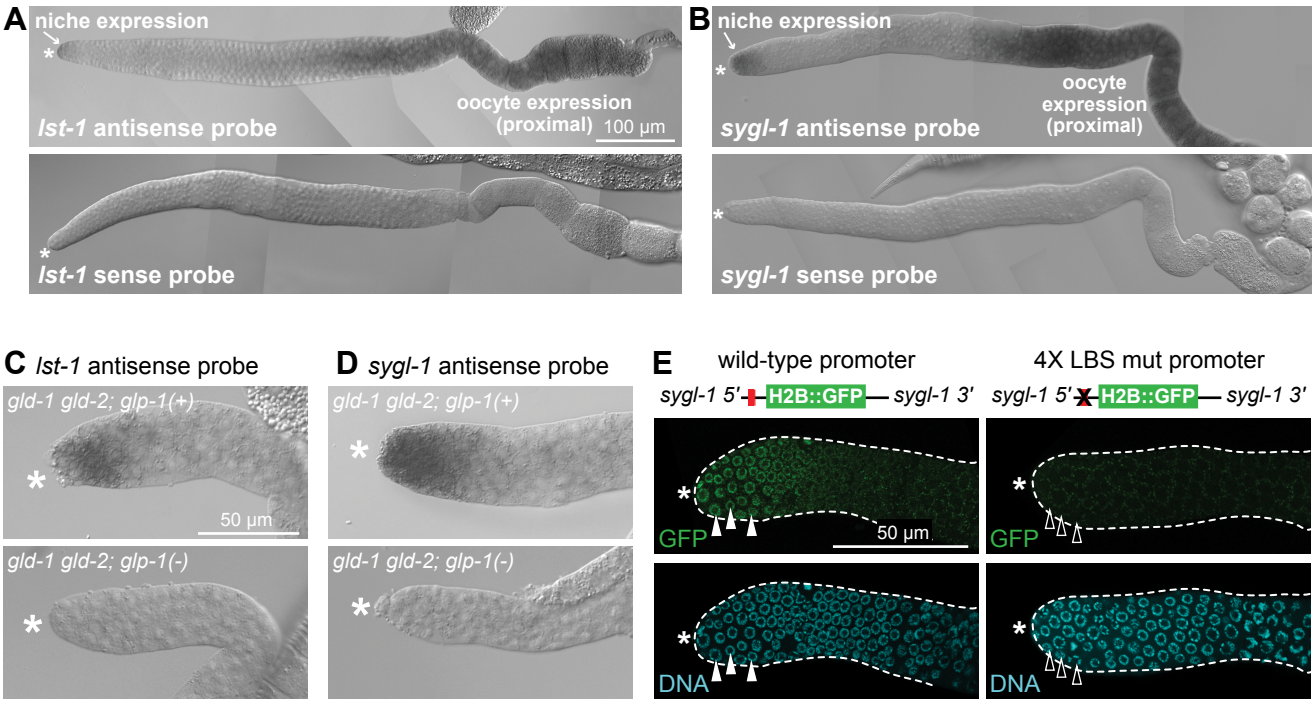

Fig. 3. *lst-1* and *sygl-1* are targets of GLP-1/Notch activation. (***A-B***) *lst-1* and *sygl-1* mRNA expression in wild-type young adult gonads. (***C-D***) Expression of *lst-1* and *sygl-1* in GSCs within the niche requires GLP-1/Notch. Shown are L4 gonads. GLP-1(+): *lst-1*: 97% positive, n=37; *sygl-1*: 97% positive n=36. GLP-1(-): *lst-1*: 0% positive, n=28; *sygl-1*: 0% positive, n=33. (***E***) Wild-type *sygl-1* promoter drives reporter expression in germ cells within the niche (100% GFP-positive, n=45), while 4X LBS mut *sygl-1* promoter does not (0% distal positive, n=46). Filled white triangles mark nuclei positive for H2B::GFP; empty white triangles mark nuclei negative for H2B::GFP. Since reporters were occasionally silenced, only germlines expressing GFP proximally were scored (see Supplementary Methods). (A-E) Asterisk marks distal end.

Fig 4
Chapter 2

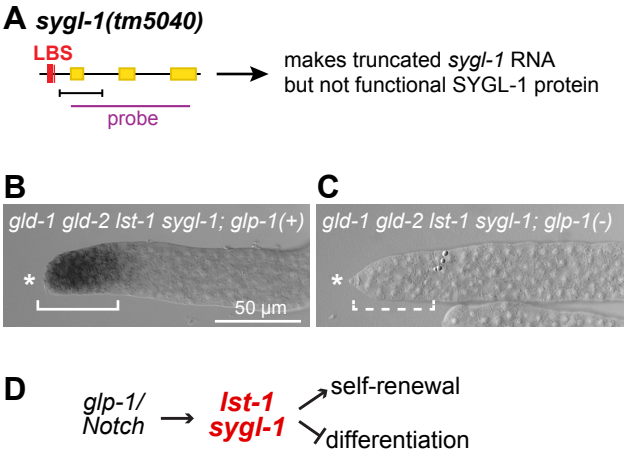

Fig. 4. *lst-1* and *sygl-1* do not affect GLP-1/Notch signaling. (***A***) GLP-1/Notch reporter assay exploits *sygl-1(tm5040)* deletion mutant (see Results). Conventions same as Fig. 1*C*. (***B***, ***C***) L4 hermaphrodite gonads were probed for GLP-1/Notch reporter by *in situ* hybridization. Shown are representative images of distal gonads. Both mutants have tumorous germlines that appear the same. (*B*) The *gld-2 gld-1 lst-1 sygl-1* quadruple mutant stains positively for the GLP-1/Notch reporter (solid bracket; 91% positive, n=35). (*C*) The *gld-2 gld-1 lst-1 sygl-1; glp-1* quintuple mutant does not stain positively for the GLP-1/Notch reporter (dashed bracket; 0% positive, n=27). (***D***) Model for *lst-1* and *sygl-1* function in the GSC self-renewal pathway.

S1 Fig
Chapter 2

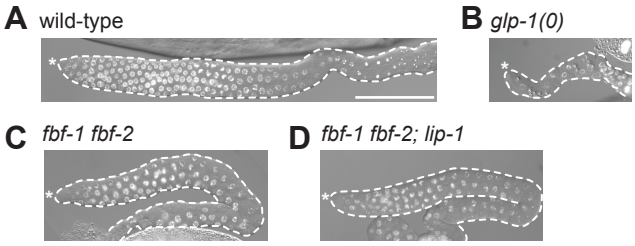

E

Genotype	Total # GCs in adult	Mitotic Zone?	Sperm only?	Reference
wild-type	~2000	+	-	(58)
glp-1(null)	4-8	-	+	(8)
glp-1(ts) L1 shift	4-8	-	+	(8)
glp-1(ts) L4/A shift	>100	-	+	(8)
fbf-1 fbf-2	>100	-	+	(6)
fbf-2; lip-1	>100	+	-	(this work)
fbf-1 fbf-2; lip-1	>100	-	+	(this work)

Fig. S1. Known GLP-1/Notch target genes do not mimic *glp-1*. (***A-D***) Gonads dissected from L4 hermaphrodites (overlay of DIC and DAPI stained images). Asterisk marks distal end, where the GSC niche resides; dotted line demarcates germline tissue. Scale bar in (*A*) applies to all panels and equals 100 µm. (*A*) Wild-type GSCs generate normal germ cell number. (*B*) *glp-1* null mutant GSCs generate only 4-8 germ cells, which differentiate as sperm (8). (*C*) *fbf-1 fbf-2* double mutant GSCs generate germ cells normally during larval development, but lose their capacity for self-renewal in late L4 larvae and adults (6). (*D*) *fbf-1 fbf-2; lip-1* triple mutants lack the only two previously known GLP-1/Notch target genes affecting germline proliferation (*fbf-2* and *lip-1*); their GSC self-renewal capacity is restricted to larval development as in *fbf-1 fbf-2* double mutants (this work). (***E***) Table summarizing mutant effects on GSC self-renewal.

S2 Fig
Chapter 2

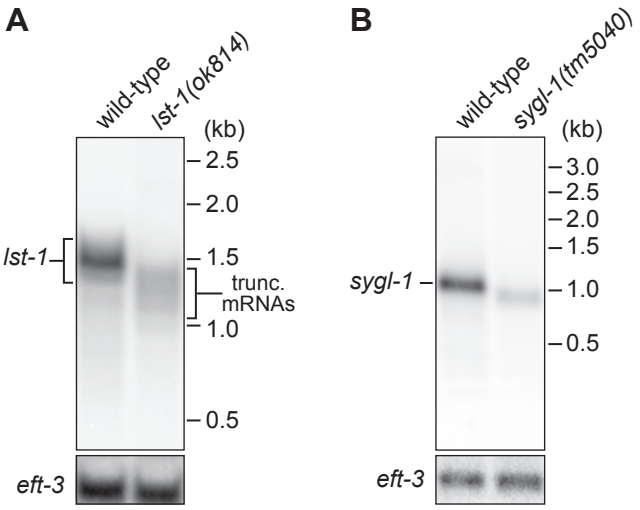

Fig. S2. Northern analysis of *lst-1* and *sygl-1* transcripts. See Fig. 1*C* for site of deletions and extent of exons targeted by probes. (***A***) Northern blot of *lst-1* mRNA in wild-type and *lst-1(ok814)* mutant. Wild-type animals produce a predominant ~1.5 kb mRNA, consistent in size to the shorter *lst-1S* isoform. RNA-seq data also indicate that the *lst-1S* is more abundant than the *lst-1L* isoform (26). *lst-1* single mutants lack that band and instead produce smaller, truncated mRNAs of ~1.0-1.5 kb in length. (***B***) Northern blot of *sygl-1* mRNA in wild-type and *sygl-1(tm5040)* mutant. Wild-type animals produce a single ~1.0 kb mRNA. *sygl-1(tm5040)* single mutants produce a truncated mRNA.

S3 Fig
Chapter 2

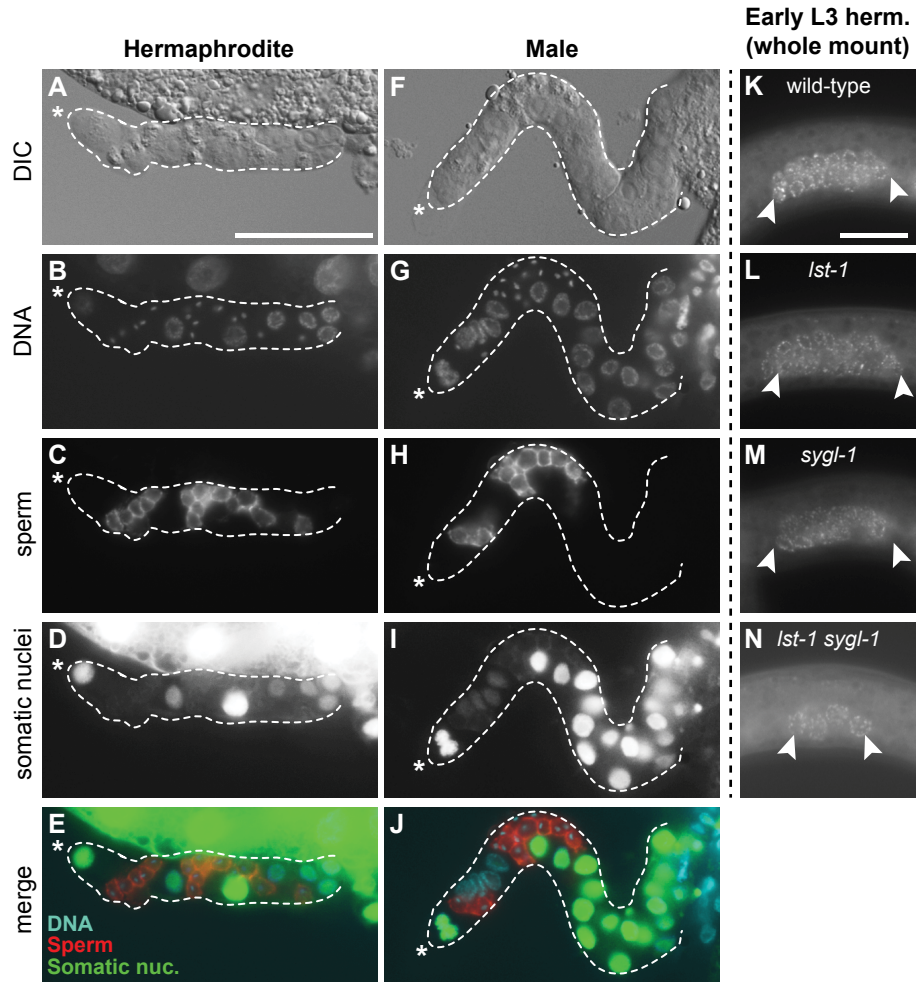

Fig. S3. *lst-1 sygl-1* double mutants do not maintain GSCs in either sex. (***A-J***) Gonads dissected from early L4 *lst-1 sygl-1* hermaphrodite (*A-E*) and *lst-1 sygl-1* male (*F-J*). Each hermaphrodite possesses two gonadal arms whereas males possess only one gonadal arm. The hermaphrodite arm shown in panels *A-E* is representative with an average of 14 ± 3 mature sperm derived from 3-4 premeiotic germ cells (n=9). The male gonad shown in panels *F-J* is representative with an average of 22 ± 2 sperm derived from 5-6 premeiotic germ cells (n=15). Asterisk marks distal end; dotted line demarcates entire germline tissue plus the DTC niche and a few additional somatic cells more proximally; arrows mark mature sperm. The scale bar in (*A*) applies to images in *B-J* and equals 50 µm. (*A, F*) Full extruded gonadal arm visualized with DIC; (*B, G*) same arm stained with DAPI to show all nuclei; (*C, H*) same arm stained with sperm-specific marker SP56; (*D, I*) same arm stained with a marker for somatic cells (complex integrated array harboring GFP driven by *sur-5* promoter); (*E, J*) Merge of *A-D*, and *F-I*, respectively. (*K-N*) Shown are representative images of early L3 hermaphrodite larvae prior to spermatogenesis whole mount stained using antibodies against PGL-1, which mark premeiotic germ cells (19). White arrowheads mark ends of the region containing PGL-1 positive cells. The scale bar in (*K*) also applies to *L-N* and equals 25 µm. (*A*) wild-type, (*B*) *lst-1(ok814)* homozygotes, (*C*) *sygl-1(tm5040)* homozygotes, and (*D*) *lst-1 sygl-1* homozygous double mutants. Germ cell numbers reported in Fig. 3*F*.

S4 Fig
Chapter 2

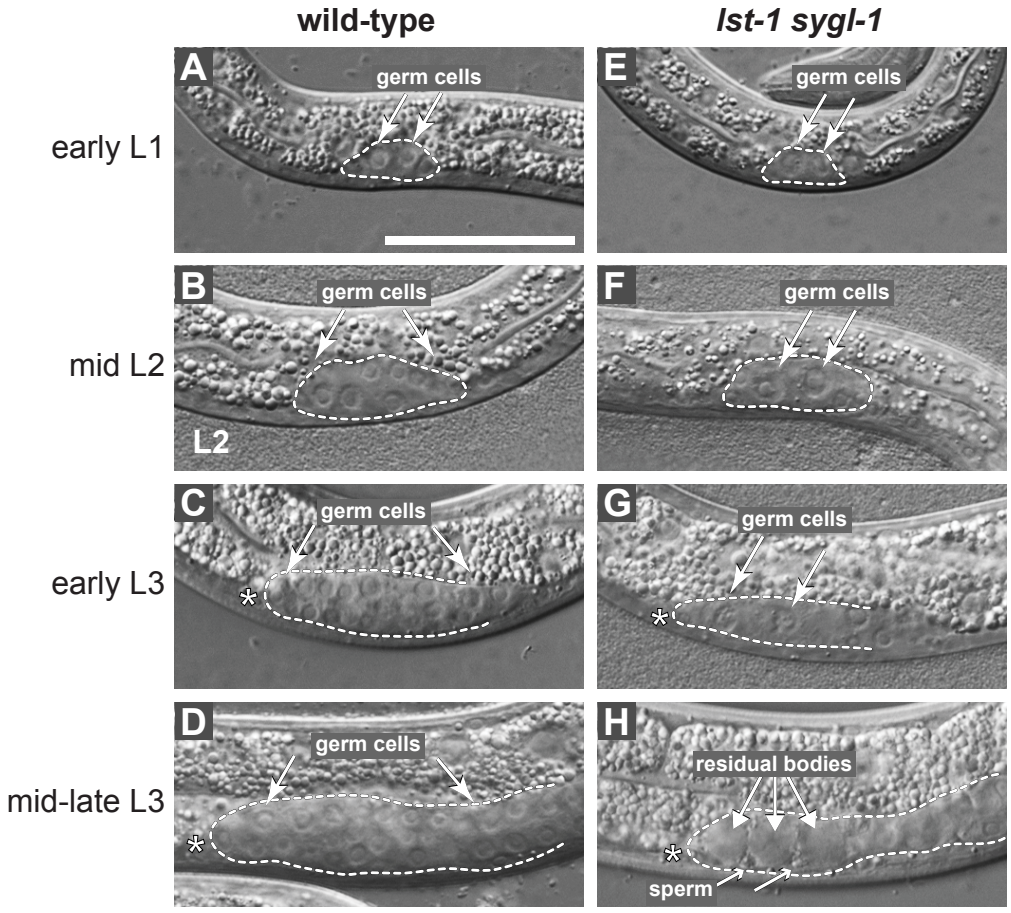

Fig. S4. Germ cells undergo spermatogenesis precociously in *lst-1 sygl-1* double mutants. (***A-H***) Nomarski micrographs of larval hermaphrodites from L1 (*A, E*) to L3 (*D, H*). Dotted line surrounds entire gonad in early L1 and mid-L2 images and surrounds one gonadal arm in L3 images. Scale bar equals 50 μm and applies to all panels. (*A-D*) Wild-type germ cells remain undifferentiated during first three larval stages. Arrows indicate extent of germline proliferation at individual stages. (*E-H*) Germ cells in *lst-1 sygl-1* double mutants are far fewer in number than wild-type and complete both spermatogenic meiotic divisions precociously – by mid-late L3 – to generate small compact sperm and large residual bodies which contain much of the cytoplasm of primary spermatocytes. Only three residual bodies are seen, which corresponds well in number with the ~3-4 premeiotic germ cells counted per *lst-1 sygl-1* gonadal arm (Fig. 2*F*; Fig. S3).

S5 Fig
Chapter 2

A

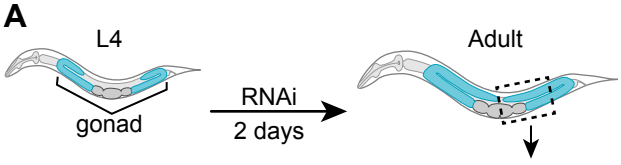

B

RNAi target	Length of mitotic zone in cell rows from DTC
empty	16.8 ± 1.0 (n=18)
lst-1 + *empty*	16.4 ± 1.0 (n=19)
sygl-1 + *empty*	10.0 ± 0.9 (n=18)
lst-1 + *sygl-1*	0 ± 0.0 (n=19)

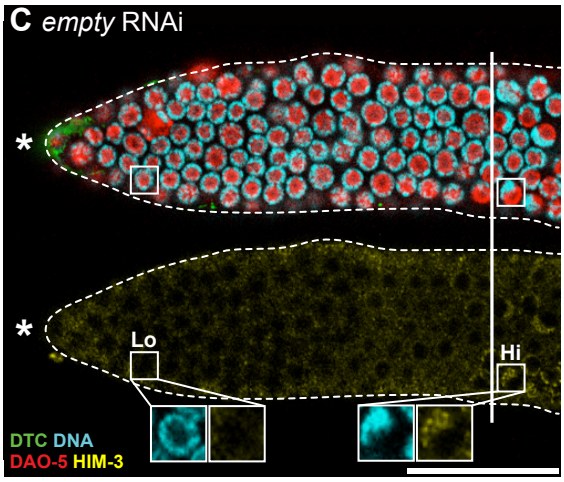

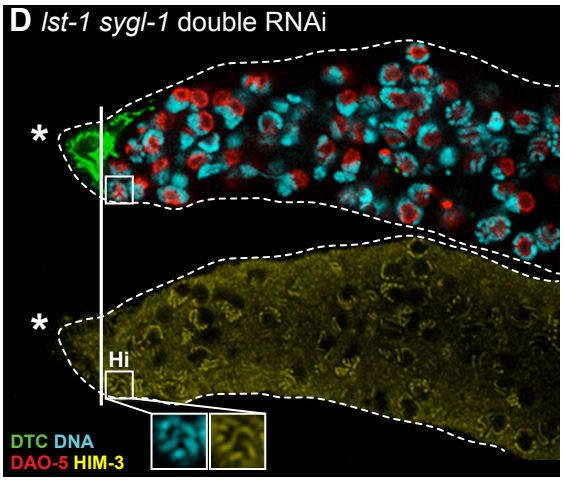

Fig. S5. *lst-1* and *sygl-1* function redundantly to promote GSC self-renewal in adults. (***A***) Experimental regimen. Wild-type late L4 larvae were treated with RNAi for 48 hours and scored as adults. RNAi used either empty vector alone, empty vector plus *lst-1,* empty vector plus *sygl-1*, or *lst-1* plus *sygl-1*. (***B***) Mitotic Zones were measured in number of germ cell diameters from distal end; the region was scored using morphology of DAPI-stained chromosomes to detect the first meiotic prophase nuclei and also by the extent of staining with anti-REC-8 antibodies, which corresponds well to the Mitotic Zone (27). Averages are given with the 95% confidence interval. RNAi depletion of only *lst-1* or *sygl-1* left the Mitotic Zone intact, but RNAi depletion of both *lst-1* and *sygl-1* abolished the Mitotic Zone. (***C-D***) *empty* RNAi germlines possess a Mitotic Zone, but *lst-1 sygl-1* double RNAi do not. Shown are representative confocal images of extruded gonads from animals treated either with *empty* RNAi or RNAi directed against both *lst-1* and *sygl-1* stained with antibodies against HIM-3 (yellow). A low level of nonchromosomal HIM-3 is typical of nuclei in the mitotic cell cycle (e.g., cell marked "Lo"), whereas a high level of *chromosomal* HIM-3 is typical of nuclei in meiotic prophase (e.g., cell marked "Hi"). Representative nuclei are shown in 2X magnified insets to more clearly visualize staining as nonchromosomal or chromosomal. Asterisk denotes distal end; dotted line delimits gonadal arm. Strain used for these images included a transgene with GFP expressed in the DTC at the distal end of the gonad. Antibodies against nucleolar marker DAO-5 helped distinguish germ cells in the mitotic cell cycle from those in early meiotic prophase: DAPI staining surrounds DAO-5 nucleolar staining in most germ cells in the mitotic cell cycle, whereas in early meiotic prophase where chromosomes have begun to pair (28), DAPI is asymmetrically localized relative to DAO-5 and typically forms a crescent. The scale bar in C equals 25 μm and also applies to D. (*C*) Confirmation that control RNAi germlines possess a Mitotic Zone. As germ cells progress proximally from the distal end (asterisk), the distal nuclei possess low nonchromosomal HIM-3 staining; the first nuclei with high chromosomal HIM-3 staining correspond to the onset of meiotic prophase as seen by DAPI (solid white line). (*D*) *lst-1 sygl-1*

double RNAi germlines lack a Mitotic Zone. Meiotic prophase nuclei and high chromosomal HIM-3 (see cell marked “Hi”) extend to the distal end (solid white line).

S6 Fig
Chapter 2

A

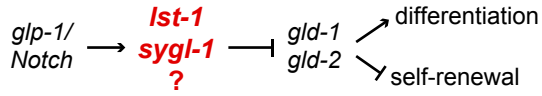

B *glp-1(oz112gf); empty vector(RNAi)*

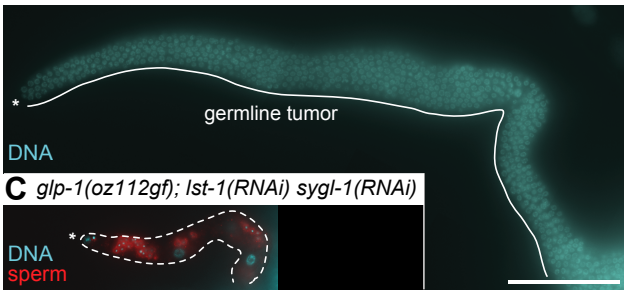

C *glp-1(oz112gf); lst-1(RNAi) sygl-1(RNAi)*

D *gld-2 gld-1* double mutant

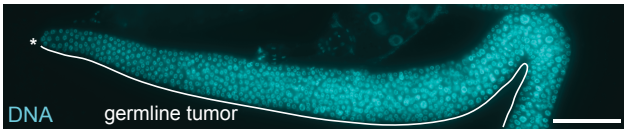

E *gld-2 gld-1 lst-1 sygl-1* quadruple mutant

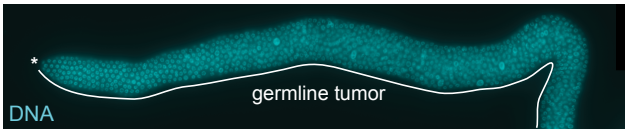

F

Genotype	% GL tumor (n)
glp-1(gf); empty RNAi	100 (n=37)
glp-1(gf); lst-1(RNAi) sygl-1(RNAi)	9 (n=58)
gld-2 gld-1 double mutant	100 (n=75)
gld-2 gld-1 lst-1 sygl-1 quadruple mutant	100 (n=95)

Fig. S6. Genetic epistasis experiments begin to place *lst-1* and *sygl-1* into GSC regulatory pathway. (***A***) Simplified genetic pathway governing GSC self-renewal or differentiation. If *lst-1* and *sygl-1* are critical GLP-1/Notch targets for GSC self-renewal, they are expected to behave genetically as downstream of *glp-1/Notch* signaling and upstream of *gld-2 gld-1*, which promote differentiation. Arrows denote activation, bars repression. (***B-E***) Representative images of gonads dissected from adult hermaphrodites. Asterisk marks distal end. DAPI staining (blue) shows nuclei. Scale bars equal 100 μm, with bar in (*B*) applying to (*B*) and (*C*), and bar in (*D*) applying to (*D*) and (*E*). (*B*) All *glp-1(oz112gf)* animals treated with control RNAi produced large germline tumors (Tum). (*C*) The vast majority of *glp-1(oz112gf)* animals treated with *lst-1 sygl-1* double RNAi had tiny germlines with only differentiated sperm (red); therefore, the *lst-1 sygl-1* Glp defect is epistatic to the *glp-1(oz112gf)* Tum defect. (*D*) All *gld-2 gld-1* double mutant germlines were Tum. (*E*) All *gld-2 gld-1 lst-1 sygl-1* quadruple mutant germlines were also Tum; therefore, the *gld-2 gld-1* Tum defect is epistatic to the *lst-1 sygl-1* Glp defect. (***F***) Summary of epistasis data.

S7 Fig
Chapter 2

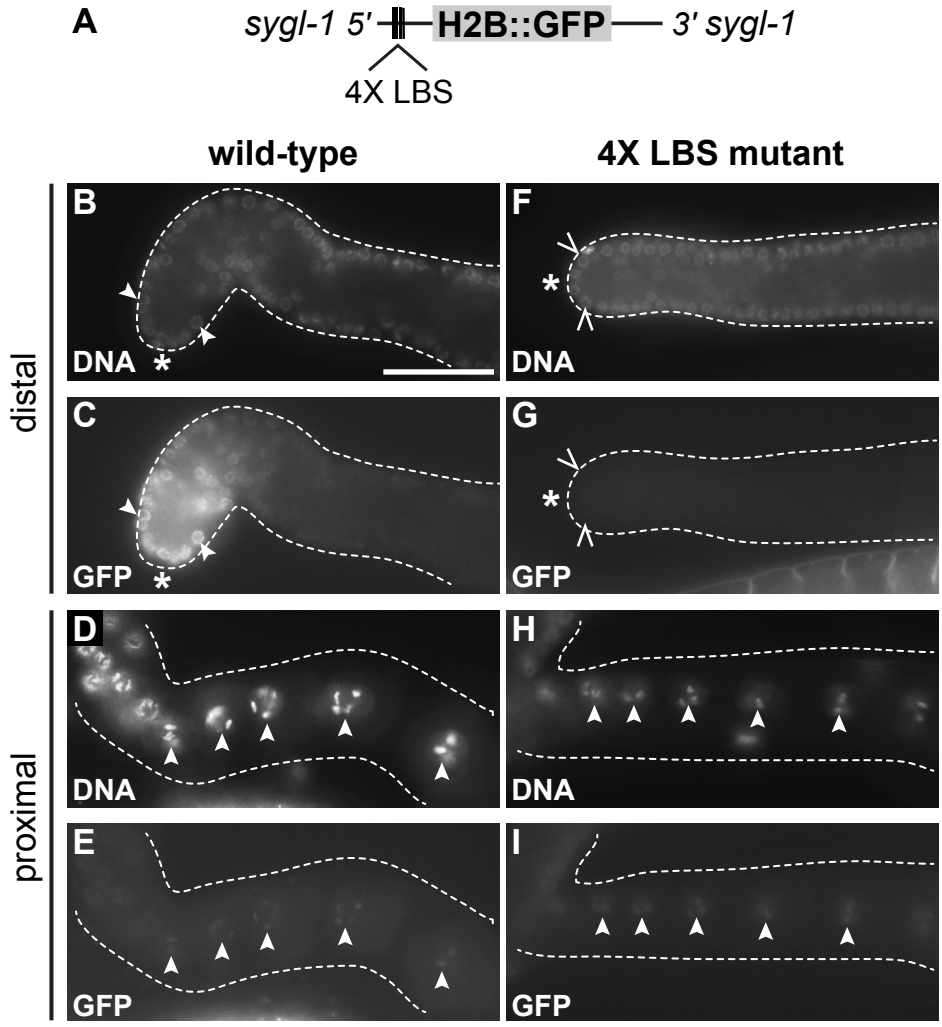

Fig. S7. *sygl-1* reporter transgenes are not silenced in the germline. (***A***) Diagram of reporter using wild-type *sygl-1* promoter to control H2B::GFP expression. The cluster of four LAG-1 binding sites (LBS) is indicated. (***B-I***) Shown are compound fluorescence images of dissected unfixed germlines expressing either the wild-type *sygl-1* reporter or the 4X LBS mutant version. Panels *B-E* show images of the same gonad, as do panels *F-I*. Samples were scored for presence of the nuclear H2B::GFP reporter and also stained with Hoechst 33342 to visualize DNA. Arrowheads mark examples of H2B::GFP positive nuclei; carets mark examples of H2B::GFP negative nuclei. Asterisk marks distal end of the germline; dotted lines show germline boundaries. Scale bar in (*B*) applies to all panels and equals 50 µm. (*B-E*) In the distal gonad, expression of the wild-type *sygl-1* reporter is limited to nuclei of the most distal germ cells (*C*); in the proximal gonad, expression of the wild-type *sygl-1* reporter is observed faintly in oocyte nuclei. All germlines with detectable GFP expressed the transgene in both distal and proximal nuclei (n=45). (*F-I*) The 4X LBS mutant *sygl-1* reporter was not expressed in distal-most germ cells (*G*), but was detectable in proximal oocyte nuclei (*I*). For this mutant promoter, expression was limited to oocytes in all germlines (n=46). Therefore, although transgene expression was absent from distal germ cells, it was detectable in oocytes and hence it was not silenced broadly in the germline**.**

Table S1. Genes common to predicted Notch targets and putative FBF-1 targets

Gene	Molecular function	Human homolog	*C. elegans* germline expressed?
sygl-1	novel	none	Yes (1,2)
lst-1	novel	none	Yes (1,2)
ima-3	importin alpha nuclear transport factor	importin subunit α-4	Yes (2,3)
lin-45	RAF protein kinase	*RAF*	Yes (1)
lst-4	sorting nexin	sorting nexin-33	Yes (1,2)
mau-2	chromatid cohesion factor	*MAU2*	Yes (1,2)
nhr-46	nuclear hormone receptor	Hepatocyte nuclear factor 4-alpha	Yes (1)
npp-13	nuclear pore complex protein	*NUP93*	Yes (1)
smg-6	Telomerase interacting protein	*EST1A*	Yes (1)
tag-341	Rho GTPase-activating protein	Rho GTPase-activating protein 29	Yes (1)
ulp-2	Ubiquitin-like protease	Sentrin-specific protease 6	Yes (1,2)
vha-7	vacuolar H ATPase subunit	lysosomal ATPase V0 subunit a1	Yes (1)
yif-1	protein transport	*YIF1A*	Unknown
F57G12.1	novel	none	Yes (1)
Y60A3A.8	novel	none	Unknown

[1]The Nematode Expression Pattern DataBase (NEXTDB). Available at http://nematode.lab.nig.ac.jp/db2/index.php

[2]Geles, K.G. and Adam, S.A. (2001). Germline and developmental roles of the nuclear transport factor importin α3 in *C. elegans*. Development 128, 1817-30.

[3]Reinke, V., Gil, I.S., Ward, S., Kazmer, K. (2004). Genome-wide germline-enriched and sex-biased profiles in *Caenorhabditis elegans*. *Development* 131, 311-23.

Table S2. Single and double RNAi to seek Glp phenotype

RNAi target gene	Single RNAi in wild type		Double RNAi with *sygl-1**		Single RNAi in *lst-1* mutant		Single RNAi in *sygl-1* mutant	
	fertile	**Glp**	**fertile**	**Glp**	**fertile**	**Glp**	**fertile**	**Glp**
Empty[+, ‡]	+	-	+	-	+	-	+	-
sygl-1[+]	+	-	na	na	-	**+**	na	na
lst-1[+]	+	-	-	**+**	na	na	-	+
ima-3[+]	-	-	-	-	-	-	nd	nd
lin-45[+]	+	-	+	-	+	-	nd	nd
lst-4[+]	+	-	+	-	+	-	nd	nd
mau-2[+]	+	-	+	-	+	-	nd	nd
nhr-46[+]	+	-	+	-	+	-	nd	nd
npp-13[+]	-	-	nd	nd	-	-	-	-
smg-6[‡]	+	-	nd	nd	+	-	+	-
tag-341[+]	+	-	+	-	+	-	nd	nd
ulp-2[‡]	+	-	nd	nd	+	-	+	-
vha-7 [+]	+	-	+	-	+	-	nd	nd
yif-1[+]	+	-	+	-	+	-	nd	nd
F57G12.1[+]	+	-	+	-	+	-	nd	nd
Y60A3A.8[‡]	+	-	nd	nd	+	-	+	-

Glp phenotype scored for any dramatic effect on germline proliferation

* used RNAi hypersensitive mutant *eri-1(mg366)*

+ L1 RNAi feeding, score treated animals as young adults

‡ L4 RNAi feeding, score next generation as young adults

na, not applicable; nd, no data

Table S3. Deletion mutants and RNAi confirm Glp effect

Genotype*	RNAi target(s)	% Glp	n
wild-type	empty vector	0	259
wild-type	*lst-1*	0	86
wild-type	*sygl-1*	0	154
wild-type	*lst-1* and *sygl-1*	89	112
lst-1 deletion	empty vector	0	167
lst-1 deletion	*sygl-1*	100	124
sygl-1 deletion	empty vector	0	61
sygl-1 deletion	*lst-1*	100	51
rrf-1	empty vector	0	47
rrf-1	*lst-1*	0	50
rrf-1	*sygl-1*	0	52
rrf-1	*lst-1* and *sygl-1*	98	65

Alleles: *lst-1(ok814), sygl-1(tm5040),* and *rrf-1(pk1417).*

Chapter 3

SYGL-1 and LST-1 link niche signaling to PUF RNA repression for stem cell maintenance

---

This chapter is published as:
Shin H*, Haupt KA*, Kershner AM, Kroll-Conner P, Wickens M, Kimble J. SYGL-1 and LST-1 link niche signaling to PUF RNA repression for stem cell maintenance in *Caenorhabditis elegans*. PLoS Genet. 2017;13(12):e1007121.* equal contribution

I conducted all experiments related to SYGL-1; K. Haupt conducted LST-1 related experiments in Figures 1, 3-5, Figures S1-S5; A Kershner provided preliminary LST-1 data for Figure 1G-H, Figure S1C-E, and Figure 5C, which were reproduced by K. Haupt and myself. I generated all other figures and wrote the paper, together with J. Kimble.

SYGL-1 and LST-1 link niche signaling to PUF RNA repression for stem cell maintenance in *Caenorhabditis elegans*

Heaji Shin[1¶], Kimberly A. Haupt[1¶], Aaron M. Kershner[2,#a], Peggy Kroll-Conner[2], Marvin Wickens[1], Judith Kimble[1,2*]

[1] Department of Biochemistry, University of Wisconsin-Madison, Madison, Wisconsin, United States of America

[2] Howard Hughes Medical Institute, University of Wisconsin-Madison, Madison, Wisconsin, United States of America

[#a] Current Address: Department of Biochemistry, Stanford University School of Medicine, Stanford, California, United States of America

* Corresponding author

Email: jekimble@wisc.edu (JK)

[¶]These authors contributed equally to this work

Short title: Molecular regulation of stem cell pool

Key words: stem cell niche, stem cell pool, SYGL-1, LST-1, PUF, FBF, *gld-1*, RNA regulation, germline stem cells, Notch signaling

Abstract

Central questions in regenerative biology include how stem cells are maintained and how they transition from self-renewal to differentiation. Germline stem cells (GSCs) in *Caenorhabditis elegans* provide a tractable *in vivo* model to address these questions. In this system, Notch signaling and PUF RNA binding proteins, FBF-1 and FBF-2 (collectively FBF), maintain a pool of GSCs in a naïve state. An open question has been how Notch signaling modulates FBF activity to promote stem cell self-renewal. Here we report that two Notch targets, SYGL-1 and LST-1, link niche signaling to FBF. We find that SYGL-1 and LST-1 proteins are cytoplasmic and normally restricted to the GSC pool region. Increasing the distribution of SYGL-1 expands the pool correspondingly, and vast overexpression of either SYGL-1 or LST-1 generates a germline tumor. Thus, SYGL-1 and LST-1 are each sufficient to drive “stemness” and their spatial restriction prevents tumor formation. Importantly, SYGL-1 and LST-1 can only drive tumor formation when FBF is present. Moreover, both proteins interact physically with FBF, and both are required to repress a signature FBF mRNA target. Together, our results support a model in which SYGL-1 and LST-1 form a repressive complex with FBF that is crucial for stem cell maintenance. We further propose that progression from a naïve stem cell state to a state primed for differentiation relies on loss of SYGL-1 and LST-1, which in turn relieves FBF target RNAs from repression. Broadly, our results provide new insights into the link between niche signaling and a downstream RNA regulatory network and how this circuitry governs the balance between self-renewal and differentiation.

Author Summary

Stem cells lie at the heart of metazoan development, regeneration, and tissue homeostasis, but the molecular basis of their regulation is poorly understood in their natural context within an animal. Here we investigate this problem in the nematode gonad, where germline stem cells are

maintained by Notch signaling from the niche and PUF RNA binding proteins in stem cells. Yet the link between Notch and PUF has been elusive. The two Notch target genes essential for GSC maintenance encode novel proteins with few clues to function. Here we report that these mysterious proteins are cytoplasmic and function post-transcriptionally as PUF partners to ensure RNA repression. We also show that the restricted spatial distribution of these newly identified regulators governs the size of the stem cell pool and prevents tumor formation. In sum, our results demonstrate how niche signaling is linked with downstream regulators to govern the stem cell fate and establish a stem cell pool.

Introduction

The balance between stem cell self-renewal and differentiation is pivotal for normal development, adult homeostasis, and regeneration. Indeed, aberrant stem cell regulation can cause disease, including human degenerative disorders and cancers [1]. Stem cell daughters can exist in a “naïve” multipotent state or a “primed” state that has been triggered to differentiate, typically via transit-amplification [2-4]. Stem cells that divide asymmetrically rely on oriented cell division to generate one naïve and one primed daughter [e.g. 5], but the mechanism underlying stem cells that divide stochastically to generate pools of naïve and primed daughters [e.g. 6, 7] remains largely unanswered. Challenges have included the complexity of their niches [8] and diversity of stem cell states (e.g. quiescent vs. proliferative) [9]. Thus, understanding how stem cell daughters are regulated to remain naïve or transition to a primed state can greatly benefit from a tractable model with well-defined niche and stem cells.

The *Caenorhabditis elegans* gonad provides a paradigm for analyzing regulation of a stem cell pool [10]. In this system, a single-celled mesenchymal niche maintains a pool of ~225 stochastically-dividing germ cells in the “progenitor zone” (**Fig 1A**) [10]. That progenitor zone itself consists of a distal pool of 30-70 naïve germline stem cells (GSCs) and a more proximal pool of GSC daughters that have been triggered to begin differentiation and hence have been

"primed" (**Fig 1A**) [11]. Central to GSC maintenance are two conserved regulators, Notch signaling and PUF (for Pumilio and FBF) RNA-binding proteins [12, 13]. GLP-1/Notch signaling from the niche is essential for GSC maintenance [14] and two nearly identical PUF proteins, FBF-1 and FBF-2 (collectively FBF), act as broad-spectrum repressors of differentiation RNAs to promote GSC self-renewal (**Fig 1B**) [15, 16]. FBF provides one regulatory hub in the stem cell regulatory network; other hubs rely on GLD translational regulators to drive differentiation [17]. However, key questions remain. Here we focus on how Notch signaling and FBF repression are coordinated to establish a naïve GSC pool and facilitate transition to the primed state.

Recently-identified GSC regulators are the *sygl-1* and *lst-1* genes, which are direct targets of niche signaling [18]. The *lst-1 sygl-1* double mutant exhibits the same severe GSC loss as a GLP-1/Notch mutant while single mutants maintain GSCs, revealing functional redundancy [18]. However, the molecular functions of SYGL-1 and LST-1 have been a mystery. LST-1 harbors a single Nanos-like zinc finger, suggesting a possible role in post-transcriptional regulation. Yet both proteins are composed largely of low-complexity regions; neither is recognizable beyond Caenorhabditids; and the two amino acid sequences bear little resemblance to each other despite their redundancy [18]. Despite the novelty of these proteins, their striking GSC loss phenotype coupled with the restriction of their mRNAs to a region corresponding to the GSC pool [18, 19] suggested that understanding their function and regulation would provide insights into regulation of a stem cell pool.

Here we investigate SYGL-1 and LST-1 proteins to understand their roles in stem cell regulation. We find that both are cytoplasmic proteins and spatially restricted to the GSC region. Intriguingly, modest SYGL-1 expansion increases size of the stem cell pool, and vast expansion of either SYGL-1 or LST-1 drives formation of a germline tumor. The SYGL-1 and LST-1–dependent tumors form in the absence of GLP-1/Notch signaling, reinforcing their key roles in stem cell maintenance. However, SYGL-1 and LST-1 no longer drive tumor formation in the

absence of FBF. Consistent with the idea that SYGL-1 and LST-1 drive stem cell self-renewal in a complex with FBF, SYGL-1 and LST-1 interact physically with FBF and are required for repression of an FBF target RNA. We suggest that SYGL-1 and LST-1 are FBF partners and function to ensure repression of FBF target RNAs within the stem cell pool.

Results

SYGL-1 and LST-1 are restricted to the GSC pool region

To visualize SYGL-1 and LST-1 proteins, we generated epitope-tagged versions of *sygl-1* and *lst-1*, including single-copy transgenes using MosSCI [20-22] and endogenous alleles using CRISPR-Cas9 [23, 24] (**Fig 1C and 1D**). Importantly, these epitope-tagged SYGL-1 and LST-1 proteins were functional: they maintain GSCs when tested in appropriate mutant backgrounds (**S1D and S1E Fig**). Therefore, they mimic their wild-type counterparts and we refer to them henceforth as SYGL-1 and LST-1. By immunostaining, both proteins were expressed in the cytoplasm of the distal-most germ cells within the progenitor zone**:** SYGL-1 was largely punctate while LST-1 was enriched in perinuclear granules (**Figs 1E-1H**, **S1A-S1C**)**.** Using the conventional metric for position along the gonadal axis, germ cell diameters (gcd) from the distal end (**Fig 1A**), we found SYGL-1 enriched from 1-~12 gcd, and LST-1 from 1-~5 gcd (**Fig 1K and 1L**, see legend for how we determined extents). These protein extents correspond well to the distributions of their respective wild-type mRNAs, assayed by single-molecule FISH [19], and were reproducible regardless of epitope tag. We counted the number of germ cells stained for each protein and found SYGL-1 in ~125 cells and LST-1 in ~45 germ cells (**Fig 1K and 1L**). Strikingly, high SYGL-1 and LST-1 levels were correlated with low GLD-1 expression (**Fig 1I and 1J**), consistent with their opposing functions (see Introduction). We conclude that SYGL-1 and LST-1 are restricted within the progenitor zone to the GSC region, consistent with their pivotal roles in GSC self-renewal.

Moderate expansion of SYGL-1 expands GSC pool size moderately

The spatial restriction of SYGL-1 and LST-1 proteins suggested that their distribution might govern size of the GSC pool. Previous studies reported that progenitor zones (PZ) were smaller in *sygl-1* and *lst-1* single mutants than in wild type [18, 25], but GSC pool size was not analyzed. We first confirmed the decreased PZ size in mutants used previously, *sygl-1(tm5040)* and *lst-1(ok814)*. We also generated additional mutants: *sygl-1(q828)* deletes the entire open reading frame plus all introns (**Fig 1C**) and *lst-1(q826)* harbors a premature stop codon (**Fig 1D**). PZ sizes were essentially the same for the various alleles of each gene (**S2A and S2B Fig**), as were other measures (e.g. brood size, fertility, embryonic lethality) (**S2C and S2D Fig**), suggesting that all are strong loss-of-function. We call them *sygl-1(0)* and *lst-1(0)* henceforth. Consistent with previous results [18, 25], the PZ size was affected differently for the two genes: the *sygl-1(0)* PZ was about half the size of wild type, while the *lst-1(0)* PZ was only marginally smaller than wild type (**S2A and S2B Fig**). We therefore focused on the SYGL-1 extent and its relationship to GSC pool size.

The onset of SYGL-1 expression relies on Notch signaling from the niche, which activates *sygl-1* transcription [18, 19], but we thought its distribution might be refined post-transcriptionally since genome-wide studies identified RNA regulatory proteins binding to the *sygl-1* 3'UTR [26, 27]. To test this idea, we replaced the *sygl-1* 3'UTR with a 3'UTR that supports expression throughout the germline, the tubulin *tbb-2* 3'UTR [28]. The transgene carrying this 3'UTR replacement was otherwise identical to the *sygl-1* transgene described above (**Fig 1C**), including insertion into the same chromosomal site and rescue of *lst-1 sygl-1* double mutants from sterility to fertility (**S3A Fig**). For simplicity, we refer in this section to the wild-type version as the "*sygl-1* 3'UTR" transgene, and to the replacement version as the "*tbb-2* 3'UTR" transgene (**Fig 2A**). The *tbb-2* 3'UTR transgene, assayed in the absence of endogenous SYGL-1, produced both an expanded distribution of SYGL-1 (~15 gcd or ~1.4-fold more extended than

normal) (**Fig 2B-2D**) and more abundant SYGL-1 (~2-fold more than normal) (**Fig 2E**). We conclude that the wild-type *sygl-1* 3'UTR restricts SYGL-1 distribution and lowers its abundance.

We first found that PZ size was 1.3-fold larger in *tbb-2* 3'UTR transgenic animals than in either *sygl-1* 3'UTR transgenic animals or wild type (**Fig 2F**). To test the idea that GSC pool size might also be enlarged, we used the *emb-30* assay [11]. Briefly, this assay arrests cell divisions with a temperature-sensitive allele of *emb-30* (*tn377*), which encodes a component of the anaphase promoting complex [29]. This arrest stops proximal movement of germ cells through the progenitor zone and resolves them into two discrete pools: cells in the distal GSC pool remain naïve and acquire an M-phase marker (PH3), while cells in the proximal pool are primed to differentiate and acquire a differentiation marker (GLD-1) [11] (**Fig 2G**). With this assay, we estimated GSC pool sizes in strains carrying *emb-30* and either the wild-type *sygl-1* locus (normal SYGL-1), the *sygl-1* null mutant (no SYGL-1) or the *tbb-2* 3'UTR transgene (expanded SYGL-1). GSC pools with wild-type SYGL-1 contained ~35 naïve cells; those with no SYGL-1 contained ~21, and those with expanded SYGL-1 had ~43 on average (**Fig 2H-2K**). Indeed, the 1.4-fold increase in SYGL-1 extent (from ~11 to ~15 gcd, on average) corresponds well with the estimated 1.3-fold increase in GSC number (from 35 to 43, on average) and PZ germ cell number (from 229 to 298, on average). Importantly, the extent of LST-1 expression along the gonadal axis (gcd) and number of LST-1–expressing cells in the distal gonad were essentially the same in *sygl-1(+)* and *sygl-1(0)* germlines as well as those harboring the *tbb-2* 3'UTR transgene (**S3B-S3F Fig**). The simplest explanation is that LST-1 expression is likely independent of SYGL-1: The smaller LST-1 expression domain establishes a smaller GSC pool size in *sygl-1* mutants, but that extent of SYGL-1 expression establishes GSC pool size in wild-type and *tbb-2* 3'UTR animals. We conclude that GSC pool size correlates with SYGL-1 extent and suggest that GSC pool size correlates with LST-1 extent in the absence of SYGL-1.

Ubiquitous germline expression of SYGL-1 or LST-1 generates a tumor

To extend the idea that distributions of SYGL-1 and LST-1 govern GSC pool size, we tested the effect of expressing SYGL-1 or LST-1 throughout the germline. To this end, we made single-copy transgenes driven with a *mex-5* germline promoter and the *tbb-2* 3'UTR, which supports ubiquitous expression throughout the germline [28] (**Fig 3A**). For brevity, we refer to the transgenes as *sygl-1(ubiq)* and *lst-1(ubiq)*, respectively (**Fig 3B and 3C**). Because ubiquitous germline expression of SYGL-1 or LST-1 might render animals sterile, we created transgenes on *sygl-1* or *lst-1* feeding RNAi, and scored effects after RNAi removal, waiting 2-3 generations to minimize transgenerational RNAi inheritance (**Fig 3A**). Strikingly, ubiquitous germline expression of either SYGL-1 or LST-1 created extensive germline tumors (**Fig 3E-3H**). The penetrance of tumor formation depended on both temperature and number of generations after removal from RNAi, but was close to 100% for both *sygl-1(ubiq)* and *lst-1(ubiq)* after two or three generations at 15°C (**S4A and S4B Fig**). About half of these tumors were proliferative throughout the gonad, while the other half included cells in the meiotic cell cycle, perhaps due to incomplete release from RNAi inheritance. Control animals harboring a GFP::H2B transgene driven with the same regulatory elements (**Fig 3D**) had no tumors (**Fig 3I and 3J**), demonstrating that the tumors are specific to SYGL-1 or LST-1.

We next used markers to determine the state of cells in *sygl-1(ubiq)* and *lst-1(ubiq)* tumors. REC-8 localizes to the nucleus of germ cells in the mitotic cycle [30] and REC-8 was nuclear throughout the tumor (**Figs 3E, 3G**, **S4I and S4J**); PH3 marks M-phase [31] and was seen in dividing cells throughout the tumor (**Fig 3F and 3H**); and PGL-1 marks germ cells [32] and also was found throughout the tumor (**S4C and S4D Fig**). Therefore, *sygl-1(ubiq)* and *lst-1(ubiq)* tumors are composed of germ cells that are mostly in the mitotic rather than the meiotic cell cycle. In addition, FBF-1 was abundant and GLD-1 was low throughout the tumors, consistent with germ cells being in an undifferentiated state (**S4F and S4G Fig**). As expected, all markers behaved like wild type in the GFP::H2B control (**Figs 3I, 3J, S4E**, **S4H**, **S4K**).

We also assessed *sygl-1(ubiq)* and *lst-1(ubiq)* tumors for features reported in other mutants with germline tumors. The *sygl-1(ubiq)* and *lst-1(ubiq)* tumors formed in both XX hermaphrodites (**Fig 3E and 3G**) and XO males (**S4I and S4J Fig**), in contrast to hermaphrodite-specific *gld-1* tumors [33]. They formed in animals making only sperm (males) or only oocytes (XX *fog-3* females [34]), in contrast to spermatogfenic-specific *puf-8* germline tumors [35]. Finally, they did not rely on Notch signaling (see below), in contrast to tumors arising from inappropriate soma/germline interactions or ectopic Notch activation [e.g. 36-39]. Thus, the most likely explanation of SYGL-1 and LST-1 tumors is that each regulator is sufficient to promote stemness in a germ-cell autonomous fashion and to do so in both sexes.

Placement of SYGL-1 and LST-1 in the GSC regulatory pathway

The *sygl-1(ubiq)* and *lst-1(ubiq)* strains provide new reagents to explore how SYGL-1 and LST-1 function within the GSC regulatory pathway. Previous analyses placed *sygl-1* and *lst-1* downstream of, or parallel to, GLP-1/Notch signaling and upstream of GLD differentiation regulators, but their relationship with FBF was unresolved [18, 25] **(Fig 1B)**.

We first asked whether *sygl-1(ubiq)* and *lst-1(ubiq)* can bypass GLP-1/Notch signaling. Whereas *glp-1(0)* mutants have no GSCs and make only a few sperm [14] (**Fig 4A**), *glp-1(0)* mutants develop germline tumors when either SYGL-1 or LST-1 is expressed ubiquitously (**Fig 4B and 4C**), confirming that *sygl-1* and *lst-1* function downstream of Notch signaling. We next asked if *sygl-1(ubiq)* and *lst-1(ubiq)* can drive germline tumors in double mutants lacking both *sygl-1* and *lst-1* endogenous loci. Whereas *lst-1 sygl-1* double mutants have no GSCs and only a few sperm (**Fig 4D**) [18], they become tumorous when either SYGL-1 or LST-1 is expressed ubiquitously (**Fig 4E and 4F**). Therefore, their tumor-forming activities are independent of each other, as expected.

Finally, we asked if *sygl-1(ubiq)* and *lst-1(ubiq)* can drive germline tumors in *fbf-1 fbf*-2 double mutants. Previous experiments relying on loss-of-function mutants suggested that *sygl-1*

and *lst-1* might function at the same position as *fbf-1* and *fbf-2* in the genetic pathway [25] (**Fig 1B**). Here, using gain-of-function *sygl-1(ubiq)* and *lst-1(ubiq)*, we sought to clarify the relationship between *sygl-1, lst-1* and *fbf*. Because the GSC loss phenotype of *fbf-1 fbf-2* is the most severe at 15°C [15, 40] and *sygl-1(ubiq)* and *lst-1(ubiq)* are the most penetrant at 15°C (**S4A and S4B Fig**), our initial analysis focused on 15°C. At this temperature, *fbf-1 fbf*-2 adults cannot maintain GSCs (**Fig 4G**) [15]; remarkably, they also cannot maintain GSCs even when either SYGL-1 or LST-1 is expressed ubiquitously (**Fig 4H and 4I**). We confirmed that *sygl-1(ubiq)* and *lst-1(ubiq)* were expressed in *fbf-1 fbf*-2 mutants (**S5A-S5C Fig**) and that they made functional proteins (**S5D Fig**). Therefore, the *fbf-1 fbf*-2 GSC loss is epistatic to *sygl-1(ubiq)* and *lst-1(ubiq)* tumors, which we interpret as *sygl-1* and *lst-1* acting either upstream or in parallel to FBF. In other words, SYGL-1 and LST-1 require FBF to drive self-renewal at this temperature.

Although *sygl-1* and *lst-1* require FBF for tumor formation at 15°C, they unlikely drive stemness exclusively via FBF for two reasons: GSC loss is more severe in *lst-1 sygl-1* double mutants than in *fbf-1 fbf-2* double mutants [15, 18], and GSC loss in *fbf-1 fbf-2* double mutants can be enhanced by removal of either *lst-1* or *sygl-1* [25; this work]. In an attempt to see their FBF-independent function, we tested *fbf-1 fbf-2 sygl-1(ubiq)* and *fbf-1 fbf-2 lst-1(ubiq)* animals for tumor formation at 25°C, because at this temperature, the FBF requirement is relieved in that *fbf-1 fbf-2* mutants can maintain a small GSC pool [40]. Again at 25°C, both *sygl-1(ubiq)* and *lst-1(ubiq)* failed to generate germline tumors in the absence of FBF: *fbf-1 fbf-2 sygl-1(ubiq)* maintained a progenitor zone comparable in size to *fbf-1 fbf-2* double mutants while *fbf-1 fbf-2 lst-1(ubiq)* were more variable, with only 10% maintaining a progenitor zone and differentiation extending to the distal end in the other 90% (**S5E-S5J Fig).** Nonetheless, from lines of evidence noted above, SYGL-1 and LST-1 must have an FBF-independent role in stem cell maintenance**.**

In summary, GLP-1/Notch signaling from the niche is dispensable for SYGL-1 and LST-1 tumors, and SYGL-1 and LST-1 do not need each other for their activity (**Fig 4J**). In contrast, SYGL-1 and LST-1 rely on FBF to form tumors (**Figs 4J and S5E-S5J**)**.** Therefore, our results

are consistent with a genetic model in which *sygl-1* and *lst-1* act downstream of Notch but upstream or parallel to *fbf* (**Fig 4K**).

SYGL-1 and LST-1 promote FBF activity rather than FBF expression

The reliance of SYGL-1 and LST-1 on FBF to promote tumor formation suggested two ideas for their molecular function. One possibility was that SYGL-1 and LST-1 regulate FBF expression. To test this notion, we compared FBF expression in germlines with and without SYGL-1 and LST-1, using a genetic background to circumvent the SYGL-1 and LST-1 requirement for GSC maintenance: *gld-2 gld-1* mutants make germline tumors independently of *sygl-1* and *lst-1* [18]. To detect FBF-1 and FBF-2, we used epitope-tagged transgenes, which are expressed and function biologically like their endogenous counterparts [27]. By staining, FBF-1 and FBF-2 proteins were expressed robustly both with and without SYGL-1 and LST-1 (**S6A-S6F Fig**), and Western blots confirmed the result (**S6G Fig**). We conclude that SYGL-1 and LST-1 are not required for FBF expression.

An alternate idea posits that SYGL-1 and LST-1 act together with FBF, perhaps by enhancing FBF activity in a molecular complex. To ask if SYGL-1 and LST-1 physically interact with FBF, we first turned to the yeast two-hybrid assay (**Fig 5A**). Briefly, SYGL-1 or LST-1 was fused to the Gal4 activation domain (AD), and the PUF repeats of FBF-1 or FBF-2 were fused with the LexA DNA binding domain (BD). Binding was assayed by monitoring growth on minimal media lacking histidine, as a measurement of *HIS3* gene expression level. We imposed a stringent threshold by adding a competitive inhibitor of the *HIS3* enzyme (50 mM 3-AT) to minimize false positives. Robust growth was observed when either SYGL-1-AD or LST-1-AD was co-transformed with either FBF-1-BD or FBF-2-BD but not in controls (**Fig 5B and 5C**). We conclude that SYGL-1 and LST-1 both interact with FBF-1 and FBF-2 in yeast.

We next set out to ask if SYGL-1 and LST-1 might associate with FBF in nematodes. Immunoprecipitation of SYGL-1 and LST-1 from nematodes had been technically difficult

because both proteins are normally expressed at low abundance and in only a subset of cells. To circumvent this problem, we attempted immunoprecipitation from *sygl-1(ubiq)* and *lst-1(ubiq)* tumorous animals. Immunoprecipitation was successful with SYGL-1 (**Fig 5D**), and subsequent biochemistry therefore focused on SYGL-1.

To ask if SYGL-1 associates with FBF in nematodes, we generated strains harboring a *sygl-1(ubiq)* transgene plus epitope-tagged 3xV5::FBF-2. Our experimental and control strains made germline tumors with 3xFLAG::SYGL-1 and 3xMYC::SYGL-1, respectively. The 3xV5::FBF-2 protein is functional and expressed (**S7A-S7D Fig**), as previously described [41]. We used FLAG antibodies to immunoprecipitate (IP) protein from both experimental and control strains; RNase A was added to all IPs to exclude RNA dependence of interactions. 3xFLAG::SYGL-1 co-immunoprecipitated with 3xV5::FBF-2 from the experimental but not the control strain, and this interaction was not dependent on RNA (**Fig 5D**). We conclude that SYGL-1 and FBF-2 associate with each other in nematodes and suggest that they form a complex.

FBF regulates many target mRNAs (see Introduction). If SYGL-1 works in a complex with FBF, then SYGL-1 protein might co-IP with FBF targets. To test this idea, we used the same strains described above and performed quantitative PCR of two established FBF targets, *gld-1* and *fem-3* mRNAs [15, 27, 42-44]. The experimental IP was enriched for both target mRNAs over the control IP, but it was not enriched for *eft-3* mRNA (**Fig 5E**), an mRNA not detected as a potential FBF target in genomic studies [27, 42]. We conclude that SYGL-1 associates specifically in nematodes with both FBF protein and with FBF target mRNAs.

SYGL-1 and LST-1 repress *gld-1* expression post-transcriptionally

The primary function of FBF in stem cell regulation is mRNA repression [16]. A crucial prediction of the idea that SYGL-1 and LST-1 work with FBF in a complex is that SYGL-1 and LST-1 should be required for repression of an FBF target mRNA. To test this idea, we examined *gld-1* mRNA, a well-established FBF target required for differentiation [15]. Previous experiments

detected a subtle increase in GLD-1 expression in GSCs of *sygl-1* and *lst-1* single mutants [25]. To explore this further, we again used *gld-2 gld-1* mutants to remove both *sygl-1* and *lst-1* without changing cell fate. This time, however, we used *gld-1(q361),* a missense mutant that abrogates GLD-1 protein function but produces detectable *gld-1* mRNA and GLD-1 protein [30, 45, 46] (**Fig 6A**). In this fashion, repression of *gld-1* mRNA was uncoupled from complications of GLD-1 function in the germline.

We first assayed expression of GLD-1(q361) protein. When either wild-type *sygl-1* or wild-type *lst-1* was present, GLD-1(q361) was expressed normally: barely detectable in distal-most germ cells and gradually increasing more proximally (**Fig 6B-6D**). However, when both *sygl-1* and *lst-1* were removed, GLD-1(q361) protein increased dramatically in the distal germline (**Fig 6E**), with quantitation revealing a three-fold increase on average (**Fig 6F**).

We next assayed expression of *gld-1(q361)* mRNA using single molecule fluorescence *in situ* hybridization (smFISH). Our probe was specific to *gld-1*: transcripts were patterned as described previously in wild type [41, 46] and cytoplasmic *gld-1* mRNAs were undetectable in *gld-1(q485)*, a deletion mutant that likely renders transcripts subject to non-sense mediated decay [45] (**S8 Fig**). Similar to the result with GLD-1 protein, *gld-1* mRNAs were barely detectable distally when either *sygl-1* or *lst-1* was present, but became easily detectable distally when both *sygl-1* and *lst-1* were removed (**Fig 6G-6J**). By contrast, nascent transcripts were seen in distal germ cell nuclei regardless of *sygl-1* and *lst-1* (**Fig 6K and 6L**). We conclude that SYGL-1 and LST-1 function post-transcriptionally to repress *gld-1* mRNA expression in the distal germline, a role that is strongly reminiscent of FBF activity. Collectively, our data support the idea that SYGL-1 and LST-1 partner with FBF to repress FBF target mRNAs in GSCs.

Discussion

The *sygl-1* and *lst-1* genes are targets of niche signaling and crucial for GSC self-renewal [18]. Here we investigate the functions of SYGL-1 and LST-1 proteins, which had been a mystery. Our results support three major conclusions: SYGL-1 and LST-1 are sufficient for stem cell maintenance and can be oncogenic when unregulated; the spatial restriction of SYGL-1 and LST-1 proteins governs GSC pool size; and SYGL-1 and LST-1 work with FBF to restrict its RNA repression to stem cells. Our discussion places these results in context with implications for stem cell biology more broadly.

SYGL-1 and LST-1 are sufficient for stem cell maintenance

We have found that ubiquitous expression of either SYGL-1 or LST-1 protein drives formation of extensive germline tumors, and that their tumor-forming activities do not require GLP-1/Notch signaling from the niche. The significance of this result is three-fold. First, SYGL-1 and LST-1 are not only required for GSC maintenance, albeit redundantly [18], but each on its own also drives stemness in the form of a tumor when ubiquitously expressed. This sufficiency underscores the importance of SYGL-1 and LST-1 as key stem cell regulators. Second, SYGL-1 and LST-1 are the primary targets of niche signaling for GSC maintenance: GLP-1/Notch signaling does not induce other regulators that must work with either SYGL-1 or LST-1 to maintain GSCs. Third, spatial restriction of SYGL-1 and LST-1 prevents tumor formation, making them prototypes for a new class of oncogenes.

Central to understanding the niche regulation of stem cells is the identification and characterization of key downstream effectors. Advances have been made in several model systems [e.g. 47-49], but examples of niche effectors with validated *in vivo* significance are rare. Perhaps the most striking parallels to SYGL-1 and LST-1 are *Ascl2* and *LgR5*, which encode niche signaling effectors in Wnt-regulated intestinal stem cells. Similar to SYGL-1 and LST-1, *Ascl2* and *LgR5* expression is limited to stem cells [50, 51], and ectopic expression promotes

hyperplasia [52]. However, in stark contrast to SYGL-1 and LST-1, *Ascl2* and *LgR5* functions are not independent of niche signaling: *LgR5* enhances Wnt signaling and *Ascl2* works with Wnt-dependent transcription factors to induce a stem cell transcriptional signature [53]. Therefore, SYGL-1 and LST-1 stand out as direct targets of niche signaling that promote self-renewal by an intrinsic signaling-independent mechanism.

Spatial restriction of SYGL-1 and LST-1 governs GSC pool size

Normally, SYGL-1 and LST-1 are spatially restricted to a region that correlates with estimates of the GSC pool (**Fig 7A**). We confirmed the biological significance of this spatial restriction in two ways. First, a moderate expansion of SYGL-1 expression led to a similar moderate expansion of pool size. Second, a major expansion of either SYGL-1 or LST-1 led to the formation of massive germline tumors. The simple conclusion is that the presence of either SYGL-1 or LST-1 promotes the stem cell fate, while their absence is critical for the transition towards differentiation. Logical corollaries are that spatial distributions of SYGL-1 and LST-1 govern the size of the GSC pool and that their loss facilitates the transition to a cell state primed for differentiation. A key question is how their spatial restriction is regulated. GLP-1/Notch signaling from the niche activates *sygl-1* and *lst-1* transcription in distal germ cells [18], but what regulates their disappearance? A partial answer is RNA regulation: the *sygl-1* 3'UTR restricts SYGL-1 protein expression compared to the *tbb-2* (tubulin) 3'UTR. In addition to RNA regulation, we suggest that SYGL-1 and LST-1 protein stabilities are also regulated. Despite the rapid kinetics of germ cell movement (~1 gcd per hour [54]), the distributions of *sygl-1* mRNA and protein are similar, as are those of *lst-1* mRNA and protein [19; this work]. Therefore, the SYGL-1 and LST-1 proteins must turn over as germ cells move proximally within the progenitor zone. Others have found that the proteolytic machinery is critical for progression from a stem cell state to a differentiated state in the progenitor zone [55, 56]. We suggest that SYGL-1 and LST-1 are likely targets of such proteolysis.

The *C. elegans* gonad therefore provides a new paradigm for how niche signaling can act through spatially restricted regulators to not only ensure the existence of stem cells but also to govern the size of a stem cell pool and facilitate the transition to a primed state. Spatial regulation is a common theme in animal development [57, 58] and extends to stem cell regulators. In addition to *Lgr5* and *Ascl2* (described above), the *Escargot*/Snail transcription factor follows a similar principle in intestinal stem cells in *Drosophila* and mouse models [59, 60]. More relevant to this work is the *Drosophila* PUF protein, Pumilio, which promotes GSC self-renewal [61, 62]. Pumilio is spatially restricted to GSCs and its ectopic expression generates germline tumors [63]. The clarifying advances of our work are an application of this theme to the maintenance of a stem cell pool, which is likely a broadly-used mechanism, and to a PUF protein partner rather than a PUF protein *per se* (see below).

SYGL-1 and LST-1 partner with FBF to repress mRNA in stem cells

When this work began, the molecular functions of SYGL-1 and LST-1 were unknown (see Introduction). A first clue from this work was their cytoplasmic localization, which is consistent with a role in post-transcriptional regulation but can be explained in other ways. A more significant clue was that SYGL-1 and LST-1 cannot drive germline tumors in the absence of the FBF RNA-binding protein. One explanation might have been that SYGL-1 and LST-1 promote FBF expression, but that possibility was not confirmed: FBF-1 and FBF-2 were expressed in the absence of SYGL-1 and LST-1. An alternative idea was that SYGL-1 and LST-1 might work with FBF to promote mRNA repression. In support of that explanation, SYGL-1 and LST-1 interact with FBF-1 and FBF-2 in yeast two-hybrid assays; SYGL-1 co-immunoprecipitates from nematodes with both FBF-2 protein and with FBF target mRNAs; and SYGL-1 and LST-1 post-transcriptionally repress expression of one of those FBF targets in GSCs. These multiple lines of evidence support the model that SYGL-1 and LST-1 partner with FBF to repress mRNAs in GSCs (**Fig 7B)**. We emphasize that SYGL-1 and LST-1 must also have FBF-independent

functions, because the *lst-1 sygl-1* phenotype is more severe than the *fbf-1 fbf-2* phenotype [15, 18], and because single *sygl-1* and *lst-1* mutants enhance the *fbf-1 fbf-2* phenotype [25; this work]. The *fog-1* gene, which encodes a cytoplasmic polyadenylation element binding (CPEB) related protein [64, 65], redundantly promotes GSC self-renewal with FBF in that *fog-1 fbf-1 fbf-2* triple mutants contain a GSC loss similar to that of *glp-1* null [66]. We speculate that the FBF-independent functions of SYGL-1 and LST-1 may involve regulation of FOG-1 protein or key FOG-1 mRNA targets. But of course, other possibilities exist. Regardless, this work shows conclusively that SYGL-1 and LST-1 have an FBF-dependent function and that they likely operate with FBF in a complex.

SYGL-1 and LST-1 stand out among PUF partners as the first to be essential for GSC maintenance, the first to be spatially restricted to the stem cell region, the first to affect size of a stem cell pool, the first to be tumorigenic when overexpressed, and the first to be essential for mRNA repression in GSCs. Previously identified FBF partners include NOS-3, a Nanos homolog which is expressed throughout the germline [67, 68], and CPEB/CPB-1, which is expressed and functions in spermatocytes [64, 69]. Two other FBF partners, GLD-2 and GLD-3, activate mRNAs and promote germ cell differentiation [70-72], a function opposite that of SYGL-1 and LST-1. The molecular mechanisms by which SYGL-1 and LST-1 repress RNAs await future studies. The simplest possibility is that they enhance FBF recruitment of the Not1 deadenylase complex, a conserved mode of PUF repression from yeast to humans [73-75]. Another idea is that SYGL-1 or LST-1 influences the sequence specificity and kinetics of FBF binding to target mRNAs, analogous to reports for other PUF partners such as CPB-1 for FBF [76] and Nanos or Brat for *Drosophila* Pumilio [77, 78]. A third thought is that SYGL-1 and LST-1 repress RNAs by recruiting them to sites of repression in RNP granules. The emerging view of low complexity proteins as RNA granule scaffolds [e.g. 79, 80] coupled with the punctate or granular appearance of SYGL-1 and LST-1 make this third possibility attractive, but it remains speculative. Given that several mechanisms remain plausible, we note that SYGL-1 and LST-1

may employ distinct biochemical mechanisms, despite their biological redundancy in GSC maintenance and their molecular redundancy in *gld-1* mRNA repression. A tantalizing future direction is to ask if similar counterparts of SYGL-1 or LST-1 exist in other vertebrate stem cell models to enhance the repressive activity of PUF proteins, Pum1 and Pum2.

Molecular model for governing the naïve state and size of a stem cell pool

Our findings together with previous studies support a model for how niche signaling is coordinated with intrinsic stem cell regulators to establish a GSC pool with stem cells in their naïve state and then facilitate the transition to a state primed for differentiation (**Fig 7C**). Essentially, Notch signaling localizes the GSC pool by activating expression of key intrinsic stem cell regulators, SYGL-1 and LST-1, which partner with FBF to repress differentiation mRNAs and thereby promote the naïve state (**Fig 7C, left)** [14, 15, 18, 19; this work]. Pool size is established roughly by Notch signaling, which activates *sygl-1* transcription in a steep gradient across the pool [18, 19]. However, *sygl-1* mRNAs are less graded and therefore transform the steep transcriptional gradient into a markedly less steep RNA gradient [19]. Here, we show that SYGL-1 protein abundance disappears in a pattern closely mirroring loss of its mRNAs. We propose that removal of these key FBF partners drives the transition from a naïve to a primed state (**Fig 7C, middle)**, and that loss of SYGL-1 and LST-1 triggers entry into a primed state by releasing *gld-1* and likely other RNAs from repression (**Fig 7C, right**). We note that FBF is present not only in the GSC pool but also in primed cells and cells beginning overt differentiation (entry into meiotic prophase) [15, 41, 81]. However, repression of FBF target mRNAs occurs in the distal germline [15, 40, 75, 82-84] and is strongest in the distal-most region or the naïve GSC pool [11]. This pattern suggests that FBF in primed cells is becoming less repressive as SYGL-1 and LST-1 are lost; indeed, FBF may be transitioning to an activating mode in this primed region [10, 75]. Two other FBF partners, GLD-2 and GLD-3, activate FBF-bound RNAs [75], suggesting the possibility of a partner exchange during the

transition in primed cells. One can imagine that SYGL-1 and LST-1 might be displaced by competition of other FBF partners or they might be removed by spatially regulated proteolysis. Although our model is surely oversimplified, it provides a heuristic framework for future explorations of stem cell pool regulation. For example, the model poises our thinking for analysis of both the mechanism and kinetics of transition from a naïve state to a primed state, which are likely to have profound consequences on pool regulation. Regardless, this model provides critical insights into how niche signaling is coordinated with downstream intrinsic effectors to govern the existence of a stem cell pool and its size.

Material and methods

Nematode strains and maintenance

Most strains were maintained and characterized at 20°C under standard conditions [85], except as follows: strains containing *emb-30(tn377ts)* were maintained at 15°C; strains harboring *sygl-1(ubiq)* tumor transgenes (*qSi235*, *qSi297*) were maintained on *sygl-1*(RNAi) feeding bacteria, and strains with *lst-1(ubiq)* tumor transgenes (*qSi267*) were maintained on *lst-1*(RNAi) (see RNAi section of Methods). The wild type was N2 Bristol strain. Alleles are as follows: LG*I*: *gld-2(q497*) [86], *gld-1(q485)* [33], *gld-1(q361)* [45], *fog-3(q520)* [34], *lst-1(ok814)* [87], *lst-1(q826)* (this work), *sygl-1(tm5040)* [18]. LG*II*: *fbf-2(q704*) [15], *fbf-2(q738)* [81], *fbf-1(ok91)* [15]. LG*III*: *glp-1(q46)* [14], *emb-30(tn377ts)* [29], *unc-119(ed3)* [88]. Balancers are as follows: LG*I*: *hT2[qIs48]* [89], LG*II*: *mIn1[mIs14 dpy-10(e128)]* [90], LG*III*: *hT2[qIs48]* [89]. Transgenes are as follows: LG*II*: *weSi2[P_{mex-5}::GFP::his-58::tbb-2 3'end, unc-119 (+)]* [91], *qSi22[P_{lst-1}::lst-1::1xHA::lst-1 3'end, unc-119 (+)]* (this work), *qSi49[P_{sygl-1}::3xFLAG::sygl-1::sygl-1 3'end, unc-119(+)]* (this work), *qSi69[P_{lst-1}::lst-1::3xFLAG::lst-1 3'end, unc-119 (+)]* (this work), *qSi75[P_{fbf-2}::3xFLAG::fbf-2::fbf-2 3'end, unc-119(+)]* [27], *qSi150[P_{sygl-1}::3xFLAG::sygl-1::tbb-2 3'end*, *unc-119(+)]* (this work), *qSi232[P_{fbf-1}::3xFLAG::fbf-1::fbf-1 3'end, unc-119(+)]* [27], *qSi235[P_{mex-}*

$_{5}$::3xFLAG::sygl-1::tbb-2 3'end, unc-119(+)] (this work), *qSi267[P$_{mex-5}$::lst-1::3xFLAG::tbb-2 3'end, unc-119(+)]* (this work), *qSi297[P$_{mex-5}$::3xMYC::sygl-1::tbb-2 3'end, unc-119(+)]* (this work). LG*IV*: *qSi93[P$_{lst-1}$::lst-1::1xHA::lst-1 3'end, unc-119 (+)]* (this work). Alleles generated using CRISPR-Cas9 are as follows: LG*I*: *lst-1(q1004)[lst-1::3xV5]* (this work), *lst-1(q1008)[lst-1::3xOLLAS]* (this work), *sygl-1(q828)* (this work), *sygl-1(q964)[3xMYC::sygl-1]* (this work), *sygl-1(q983)[3xOLLAS::sygl-1]* (this work), *sygl-1(q1015)[sygl-1::1xV5]* (this work). LG*II: fbf-2(q931)[3xV5::fbf-2]* (this work)*, fbf-2(q932)[3xV5::fbf-2]* (this work)*.* A complete list of strains used in this study is summarized in **S1 Table**.

Generation of *C. elegans* alleles and transgenes

Single-copy transgenes were generated using the Mos-1 mediated single-copy insertion method (MosSCI) [20-22]. Briefly, plasmids containing the gene of interest were constructed using the Gibson assembly method [92] and microinjected at 50 ng/μl along with transposase and co-injection markers to target the *ttTi5605* or *cxTi10816* sites. Several transgenes were generated and maintained on RNAi feeding bacteria. Those requiring *sygl-1*(RNAi) were *qSi235[P$_{mex-5}$::3xFLAG::sygl-1::tbb-2 3'end, unc-119(+)]* and *qSi297[P$_{mex-5}$::3xMYC::sygl-1::tbb-2 3'end*, *unc-119(+)].* That requiring *lst-1(RNAi)* was *qSi267[P$_{mex-5}$::lst-1::3xFLAG::tbb-2 3'end, unc-119(+)].* At least two independent lines for each construct were analyzed, and results of one representative line are reported. A complete list of generated alleles and plasmids used to generate MosSCI transgenes can be found in **S2 Table** and **S4 Table** respectively.

sygl-1(q828) was generated using CRISPR/Cas9 gene editing [93]. Briefly, three 25 ng/μl *sygl-1* sgRNAs, a 50 ng/μl repair template designed to substitute the *sygl-1* coding region with *Caenorhabditis briggsae unc-119,* and 50 ng/μl pDD162 encoding Cas-9 were microinjected into the *unc-119(ed3)* strain with co-injection markers, and progeny were screened for the Unc movement rescue. The substitution of the *sygl-1* gene with the *unc-119* gene resulted in deletion of the *sygl-1* coding region and was verified by sequencing.

The alleles *fbf-2(q931)*, *fbf-2(q932)*, *sygl-1(q964)*, *sygl-1(q983)*, *lst-1(q1004), lst-1(q1008),* and *sygl-1(q1015)* were generated by RNA protein complex (RNP) CRISPR [23, 24]. Briefly, injection mix containing gene-specific crRNAs (10 μM, IDT Alt-R™), *dpy-10* or *unc-58* co-CRISPR crRNAs (4 μM, IDT Alt-R™), tracrRNAs (14 μM, IDT Alt-R™), gene-specific repair oligo (4 μM) or repair plasmid (50 ng/μl), *dpy-10* or *unc-58* co-CRISPR repair oligo (1.4 μM), and Cas-9 protein (25 μM) was prepared. Strains were microinjected and the progeny were screened using PCR for edits. All CRISPR alleles were verified by sequencing and outcrossed 2-4 times with wild type prior to analysis. A complete list of reagents used to generate CRISPR alleles can be found in **S3-S5 Tables**.

To obtain *lst-1(q826)*, a *sygl-1* enhancer screen was performed with EMS mutagenesis as described [85], with minor modifications. Briefly, *sygl-1(tm5040)* hermaphrodites of the fourth larval stage (L4) were mutagenized with 25 mM Ethyl methanesulfonate (Sigma #M0880) for 4 hours at room temperature. F1 progeny were singled and maintained at 15°C, and F2 self-progeny were screened for germline proliferation defective (Glp) [14] mutants. Details of this mutagenesis screen are available upon request. The *lst-1* locus was sequenced from DNA extracted from Glp animals to identify the *lst-1(q826)* allele, which was outcrossed 10 times with wild type prior to analysis.

Reannotation of *sygl-1* and *lst-1* gene structures

The *sygl-1* and *lst-1* gene structures reported here are based on 5’ rapid amplification of cDNA ends (RACE), genome-wide mRNA sequencing data (WormBase release 255), and ribosome profiling data [94]. Specifically, the *sygl-1* 5’UTR, the *lst-1* 5’UTR, and the *lst-1* start codon have been re-annotated. Most importantly, our reported *lst-1* start codon removes 70 amino acids from the previously mis-annotated versions [18] and is consistent with evolutionary data from *C. briggsae*.

For 5' RACE, total RNA was extracted from young adult wild type (24 hours after L4 at 20°C) using TRIzol (Invitrogen #15596026). 1 μg of total RNA was converted to cDNA with SuperScript III (Invitrogen #18080051) using *sygl-1_RT_primer* (5'-AGCGACGAGTTGAAGAGACTC-3') or *lst_RT_primer* (5'-GGTGCGACATGTCTCGTGGATC-3'). cDNAs were purified (QIAquick PCR purification kit, Qiagen #28106), tailed with cytosines using Terminal Deoxynucleotidyl Transferase (Invitrogen #EP0161), and then PCR amplified using the following primers: for *sygl-1*, primary PCR used *Anchor_Primer* (5'-GGCCACGCGTCGACTAGTACGGGIIGGGIIGGGIIG-3') with *sygl-1_primary* (5'-TCGACGAGCGAGTCAGTCTC-3'); secondary PCR used *Universal_amplification_primer* (5'-GGCCACGCGTCGACTAGTAC-3') with *sygl-1_secondary* (5'-CGCCTCCGGTTGACGATGATG-3'); and tertiary PCR used *Universal_amplification_primer* with *sygl-1_tertiary* (5'-AGACGATGAGGTGGACATG-3'). An additional tertiary reaction was carried out to improve the signal to noise ratio. For *lst-1,* primary PCR used *Anchor_Primer* (5'-GGCCACGCGTCGACTAGTACGGGIIGGGIIGGGIIG-3') with *lst_primary* (5'-GAGTTGAAGCAGTTGCTTCGG-3') and secondary PCR used *Universal_amplification_primer* (5'-GGCCACGCGTCGACTAGTAC-3') with *lst_secondary* (5'-gtgttgcgacttcgagtagg-3'). All amplified products were analyzed by Sanger sequencing.

Phenotype analyses: brood counts, sterility and embryonic lethality

L4 hermaphrodites were placed onto individual plates at 20°C. At 6 to 12 hour intervals, the hermaphrodite was moved to a new plate and the embryos were counted for sterility and brood counts. Several days later, hatched progeny on each plate were counted to determine embryonic lethality.

Assessment of progenitor zone size

All characterization of progenitor zone (PZ) size was done in animals raised at 20°C until 24 hours after L4, except in **S5J Fig** where animals were raised at 25°C until 16-18 hrs after L4. To

visualize nuclear morphology, gonads were dissected, fixed, and stained with DAPI (see immunostaining and DAPI staining section below for dissection and fixation methods). To determine the PZ size, gonads were imaged using a confocal microscope with a z-stack depth of 0.4-0.5 μm. Next, the boundary between PZ and Transition Zone (TZ) was determined by conventional criteria [95]. Briefly, many germ cells in the TZ have entered meiotic prophase and hence have a crescent-shaped nuclear morphology. The PZ/TZ boundary was scored as the distal-most cell row with at least two crescent-shaped nuclei. Finally, the cells within the progenitor zone were counted manually using the cell-counter plug-in in FIJI/Image J, with each DAPI-stained nucleus scored as a single cell.

Germ cell number estimation in *fbf* gonads

To estimate the number of germ cells in *fbf-1 fbf-2* gonads reported in **S5D Fig**, compact nuclei typical of mature sperm in a gonadal arm were counted manually using the cell counter tab in Openlab 5.5.2 (PerkinElmer). Next, the number of sperm was converted to the number of germ cells (four sperm are made from one germ cell).

Estimation of SYGL-1 or LST-1 positive germ cells

To estimate the number of distal germ cells expressing SYGL-1 or LST-1, JK4996, JK5073, JK5205, JK5263, JK5893, JK5929 and JK6002 were raised at 20°C until adulthood (24 hours after L4), along with appropriate wild-type controls. Gonads were dissected, fixed, and stained with anti-FLAG, anti-OLLAS, anti-V5, or anti-HA (see immunostaining section below) and imaged using the confocal microscope. Next, the number of distal germ cells that contained positive V5 or OLLAS signal (SYGL-1) or positive HA, FLAG, or V5 signal (LST-1) above the background level was manually scored, using the cell-counter plugin in FIJI/Image J.

***emb-30* assay**

The assay was performed as described [11] with minor modifications. DG627, JK5233, JK5235 animals were raised at 15°C until 36 hours past mid-L4, then moved to plates pre-incubated at

25°C and maintained at 25°C for 12.5 hours. We chose 12.5 hours because germ cell counts became unreliable with longer times (nuclear morphology became increasingly compromised after incubations of 13 hours and longer). Next, gonads were dissected, fixed, and stained for anti-PH3, anti-GLD-1 and DAPI (see staining section below). To estimate the number of cells within the distal pool, we manually counted the number of M-phase arrested germ cells distal to the GLD-1 boundary (as assessed by DAPI morphology and PH3 staining) using the cell counter tab in Openlab 5.5.2 (PerkinElmer). Scoring was done blind to genotype. We excluded samples with abnormal, fragmented nuclei that made cell counting unreliable (22-49% per genotype). We note that not every nucleus distal to the GLD-1 boundary was arrested in M-phase in some gonads but these few nuclei were included in the "distal pool" counts.

RNAi

Feeding RNAi was performed as described [96] using *sygl-1* or *lst-1* clones from the Ahringer RNAi library [97]. Bacteria were grown overnight at 37°C in 2xYT media containing 25 μg/μl carbenicillin and 50 μg/μl tetracycline. Cultures were concentrated, seeded onto Nematode Growth Medium (NGM) plates containing 1mM IPTG, then induced overnight before plating worms.

***sygl-1(ubiq)* and *lst-1(ubiq)* germline tumor assays**

To induce *sygl-1(ubiq)* and *lst-1(ubiq)* germline tumors, L4 P0 animals were transferred from RNAi bacteria to OP50-seeded NGM plates, and subsequent generations were monitored using a dissecting scope for germline tumor formation. In some experiments, gravid adults were bleached between generations to synchronize populations. All experiments with *sygl-1(ubiq)* and *lst-1(ubiq)* were carried out at 15°C to maximize tumor penetrance, except those in **S4A and S4B Fig**, where tumor penetrance was tested with different temperature regimens, and in **S5E-S5J Fig**, where epistasis with *fbf-1 fbf-2* was assayed at 25°C. For most *sygl-1(ubiq)* tumors, data were obtained in the F3 generation after removal from RNAi, and for most

lst-1(ubiq) tumors, data were obtained in F2 after removal from RNAi. Two exceptions were: (1) For epistasis experiments requiring a balancer for strain maintenance (JK5401, JK5403, JK5538, JK5585; see **Fig 4B**, **4C**, **4E**, **4F**), tumors were scored in F1, because all F1 balancer-carrying animals were tumorous so additional generations could not be obtained. (2) For 25°C epistasis experiments with *fbf-1 fbf-2* (see **S5E-S5J Fig**), we scored in F8 (*sygl-1*) and F7 (*lst-1*) after removal from RNAi to maximize tumor penetrance.

Immunostaining and DAPI staining

Staining followed established protocols [98] with minor modifications. Briefly, staged animals were dissected in PBStw (PBS + 0.1% (v/v) Tween-20) with 0.25 mM levamisole to extrude gonads. Tissues were fixed in 2% (w/v) paraformaldehyde diluted in 100 mM K_2HPO_4 (pH 7.2) for 10 minutes when using anti-FBF-1 and anti-PGL-1 antibodies. For all other antibodies, tissues were fixed in 3%(w/v) paraformaldehyde diluted in 100 mM K_2HPO_4 (pH 7.2) for 30 minutes. Post fixation, all samples were permeabilized with ice-cold methanol or PBStw + 0.2% (v/v) Triton-X for 5-10 minutes. Next, they were blocked with either 30% (v/v) goat serum diluted in PBStw (for anti-FLAG) or 0.5% (w/v) bovine serum albumin diluted in PBStw (all other antibodies) for 1 hour. For primary antibodies, samples were incubated overnight at the following dilutions in the blocking solution: Mouse anti-FLAG (1:1000, M2 clone, Sigma #F3165), Rabbit anti-GLD-1 (1:100, Gift from E. Goodwin), Rat anti-HA (1:100, 3F10 clone, Roche #11867423001), Rabbit anti-REC-8 (1:100, [30]), Rat anti-FBF-1 (1:5, [15]), Mouse anti-SP56 (1:200, [99]), Mouse anti-PH3 (1:200, Cell Signaling #9706), Rabbit anti-PGL-1 (1:100 [32]), Mouse anti-V5 (1:1000, Bio-Rad #MCA1360), Rat anti-OLLAS (1:2000, L2 clone, Novus Biologicals #NBP1-96713). For secondary antibodies, samples were incubated for 1 hour at room temperature at the following dilutions: Donkey Alexa 555 anti-mouse (1:1000, Invitrogen #A31570), Goat Alexa 555 anti-rabbit (1:1000, Invitrogen #A21429), Goat Alexa 488 anti-rabbit (1:1000, Invitrogen #A11034), Donkey Alexa 488 anti-rat (1:500, Invitrogen #A21208), Donkey

Alexa 647 anti-mouse (1:500, Invitrogen #A31571). To visualize DNA, DAPI was included at a final concentration of 0.5-1 ng/μl during the last 10 minutes of secondary antibody incubation. Vectashield (Vector Laboratories #H-1000) was used as mounting medium.

In situ hybridization

Single molecule FISH (smFISH) was performed as described [19, 41, 100]. Custom Stellaris® FISH probes were designed by utilizing the Stellaris® FISH probe designer (Biosearch Technologies, Inc) available online at www.biosearch.com/stellarisdesigner. The *gld-1* probe set contains 48 unique probes labeled with CAL Fluor® Red 610 and was used at a final concentration of 0.25 μM.

Microscopy

For the compound microscopy data shown in **Fig 4,** images were taken using a Zeiss Axioskop with Hamamatsu CCD or ORCA cMOS camera equipped with 63x 1.4NA Plan Apochromat oil immersion objective. Carl Zeiss filter sets 49, 38, and 43HE were used for the visualization of DAPI, Alexa 488, and Alexa 555 respectively. An X-Cite 120Q lamp (Lumen Dynamics) was used as the fluorescence light source. Openlab 5.5.2 (PerkinElmer) and Micromanager [101, 102] were used as acquisition software. For all other figures, a Leica TCS SP8 confocal microscope driven by LAS software version 3.3.1 or X was used. This laser scanning confocal microscope was equipped with Photomultiplier (PMT) and Hybrid detectors (HyD). For all images, a 63x 1.4NA HC Plan Apochromat oil immersion objective was used with 100-200% zoom for immunostaining, and 300% zoom for single molecule FISH, using the standard scanner with 400Hz scanning speed. For figure preparation, contrast was linearly adjusted in Adobe Photoshop identically across all samples. In some cases, images were merged using the stitching plugin in FIJI/Image J [103] to generate whole gonad images.

Fluorescence quantitation

All images used for quantitation were acquired using the sequential scan mode on the Leica TCS SP8, under the same conditions across all samples. Next, average intensity of multiple z-slices was projected onto a single plane. To eliminate signal intensities outside of the gonad (i.e. intestine), a separate binary mask was created by thresholding Nomarski images of the gonad taken at the same time; the binary mask was then multiplied to other channels such that only signals within the gonad would be considered for quantitation. Next, intensity at a given distance "x" from the distal tip of the gonad was averaged over five-micron intervals ("moving average"). For simplicity, distance from the distal end was converted to conventional germ cell diameters, using a conversion ratio of 4.55 μm for one germ cell diameter [19]. A custom MATLAB script was used to process steps described above.

Yeast two hybrid

Modified yeast two-hybrid assays were performed as described [104]. Briefly, *sygl-1* cDNA encoding full-length SYGL-1 (a.a. 1-206) or *lst-1* cDNA encoding full-length LST-1 (a.a. 1-328) was cloned into the *Nco* I and *Xho* I sites in pACT2 (Gal4 activation domain plasmid) to generate pJK1580 and pJK2015, respectively. Regions encoding FBF-1 (a.a. 121-614) and FBF-2 (a.a. 121-632) were cloned into the *Eco*R I and *Sal* I sites in pBTm116 (LexA binding domain plasmid) to generate pJK2019 [67] and pJK2017, respectively. Plasmids were co-transformed into a L40-*ura* strain using the Te-LiAc method [105]. *His3* reporter activity was assayed on synthetic defined medium (SD) supplemented with –Leu –Trp –His containing 50 mM 3-Amino-1,2,4-triazole (Sigma #A8056), or –Leu –Trp plates as controls for 4 days at 30°C.

Immunoprecipitations and Western Blots

JK5366, JK5574, JK5783, and JK5844 animals were raised at 15°C until they developed germline tumors as young adults (12 hours after L4) (see tumor assay above). Animals were washed twice with M9 buffer [3 g/L KH2PO4, 6 g/L NaHPO4, 5 g/L NaCl, and 1 mM MgSO4]

and cross-linked with 1% (w/v) formaldehyde for 10 minutes at room temperature (RT). Pellets were resuspended in 1 ml lysis buffer [50 mM HEPES pH 7.5, 150 mM NaCl, 1 mM EDTA, 1% (v/v) Triton-X, cOmplete Protease inhibitor cocktail (Roche)], frozen in liquid nitrogen, and pulverized with mortar and pestle for 10 minutes. Lysates were cleared twice by centrifugation (12,000g, 10 minutes), and the total protein concentration was measured by Direct Detect Spectrophotometer (Millipore). To prepare antibody conjugated beads, 30 μg anti-FLAG (M2 clone, Sigma #F3165) was incubated with 4.5 mg protein G Dynabeads® (Novex, Life Technologies, #10003D) for 30 minutes at RT. Next, 20 mg lysates were incubated with the antibody-bead mixture for 4 hours at 4°C, with the presence of RNase A at 10 μg/ml. RNA degradation was confirmed by isolating total RNA from post-IP lysates using TRIzol LS (Invitrogen #10296028) and analyzing on agarose gels. Beads were pelleted, washed four times with lysis buffer, and then two times with wash buffer [50 mM HEPES pH 7.5, 0.5 M NaCl, 1 mM EDTA, 1% (v/v) Triton X-100]. Samples then were eluted with elution buffer [1% (w/v) SDS, 250 mM NaCl, 1 mM EDTA, 10 mM TRIS pH 8] for 10 minutes at 65°C, and analyzed using SDS-PAGE on an 8% or 12% acrylamide gel.

To probe FBF abundance in **S6G Fig**, N2, JK5181, JK5182, JK5600, JK5602, JK5603, and JK5604 animals were raised at 20°C to young adulthood (12 hours after L4 stage). 40 animals were boiled in 2x Laemmli buffer and then analyzed by SDS-PAGE on a 4-20% gradient gel (Lonza #58527).

For primary antibodies, blots were incubated overnight at 4°C at the following dilutions: Mouse anti-FLAG (1:1000, M2 clone, Sigma #F3165), Mouse anti-V5 (1:1000, Bio-Rad #MCA1360), Mouse anti-actin (1:40,000, C4 clone, Millipore #MAB1501), Mouse anti-α-tubulin (1:20,000, Sigma #T5168). For secondary antibody, blots were incubated for 1 hour at RT with Donkey HRP-conjugated anti-mouse (1:10,000, Jackson ImmunoResearch). Immunoblots were developed using SuperSignal™ West Pico/Femto Sensitivity substrate (Thermo Scientific

#34080, #34095) and imaged using an ImageQuant LAS4000 (GE Healthcare). FIJI/Image J was used to calculate blot intensity. For final figure preparations, contrast of the blot was linearly adjusted in Adobe Photoshop.

RNA immunoprecipitation (IP) and quantitative PCR

JK5366 and JK5574 were raised at 15°C until they developed germline tumors as young adults (see tumor assay above). Immunoprecipitation was done as above except that formaldehyde cross-linking and RNase treatment of lysates were omitted. Instead, lysis buffer contained 1 U/µl SUPERase·In™ RNase inhibitor (Ambion #AM2694). Successful IP was confirmed by analyzing 10% of elution by Western blot, and RNA was eluted from the rest of the beads with 0.5 ml TRIzol (Invitrogen #15596026). RNA was purified by RNeasy Micro kit (Qiagen #74004) including DNase I treatment on column. Purified RNA was checked for integrity, and converted to cDNA with Superscript III first strand synthesis kit (Invitrogen #18080051) using random-hexamers as primers. Quantitative PCR was carried out using a Roche Lightcycler 480 with TaqMan gene expression assays (Applied Biosystems). Enrichment was calculated by $\Delta\Delta C_T$ method [106]. Taqman probes used are as follows: *gld-1,* Ce02409901_g1; *eft-3*, Ce02448437_gH; *rps-25*, Ce02464216_g1; *fem-3*, Ce02457444_g1.

Statistical Analysis

Statistical tests are indicated in figure legends with sample sizes. In most cases, one-way ANOVA and *post-hoc* Tukey multiple comparison tests were performed to calculate p-values. In cases where equal variance assumption of ANOVA was not established at $p<0.01$ (Levine's test), Welch's one-way ANOVA (modified ANOVA with heteroskedastic data) and *post-hoc* Games-Howell multiple comparison tests were performed to calculate p-values. All statistics were performed in R.

Acknowledgments

We thank the past and present members of the Kimble and Wickens laboratories for helpful discussions, especially Sarah Crittenden and Hannah Seidel for insightful suggestions. We are grateful to Brian Kraemer for preliminary data, Jadwiga Forster for technical assistance, and Laura Vanderploeg and Anne Helsley-Marchbanks for assistance with figure and manuscript preparation. We thank Susan Strome (University of California at Santa Cruz) for PGL-1 and SP56 antibodies. Some strains used in the study were provided by the *Caenorhabditis* Genetics Center, supported by NIH Office of Research Infrastructure Programs (P40 OD010440).

References

1. He S, Nakada D, Morrison SJ. Mechanisms of stem cell self-renewal. Annu Rev Cell Dev Biol. 2009;25:377-406. Epub 2009/07/07. doi: 10.1146/annurev.cellbio.042308.113248. PubMed PMID: 19575646.

2. Greco V, Guo S. Compartmentalized organization: a common and required feature of stem cell niches? Development. 2010;137(10):1586-94. Epub 2010/05/01. doi: 10.1242/dev.041103. PubMed PMID: 20430743; PubMed Central PMCID: PMC2860245.

3. Nichols J, Smith A. Naive and primed pluripotent states. Cell Stem Cell. 2009;4(6):487-92. Epub 2009/06/06. doi: 10.1016/j.stem.2009.05.015. PubMed PMID: 19497275.

4. Wu J, Izpisua Belmonte JC. Dynamic pluripotent stem cell states and their applications. Cell Stem Cell. 2015;17(5):509-25. doi: 10.1016/j.stem.2015.10.009. PubMed PMID: 26544113.

5. de Cuevas M, Matunis EL. The stem cell niche: lessons from the *Drosophila* testis. Development. 2011;138(14):2861-9. doi: 10.1242/dev.056242. PubMed PMID: 21693509; PubMed Central PMCID: PMC3119301.

6. Morrison SJ, Kimble J. Asymmetric and symmetric stem-cell divisions in development and cancer. Nature. 2006;441(7097):1068-74. PubMed PMID: 16810241.

7. Simons BD, Clevers H. Strategies for homeostatic stem cell self-renewal in adult tissues. Cell. 2011;145(6):851-62. Epub 2011/06/15. doi: 10.1016/j.cell.2011.05.033. PubMed PMID: 21663791.

8. Lander AD, Kimble J, Clevers H, Fuchs E, Montarras D, Buckingham M, *et al*. What does the concept of the stem cell niche really mean today? BMC Biology. 2012;10:19. doi: 10.1186/1741-7007-10-19. PubMed PMID: 22405133; PubMed Central PMCID: PMC3298504.

9. Li L, Clevers H. Coexistence of quiescent and active adult stem cells in mammals. Science. 2010;327(5965):542-5. Epub 2010/01/30. doi: 10.1126/science.1180794. PubMed PMID: 20110496.

10. Kimble J, Crittenden SL. Controls of germline stem cells, entry into meiosis, and the sperm/oocyte decision in *Caenorhabditis elegans*. Annu Rev Cell Dev Biol. 2007;23:405-33. doi: 10.1146/annurev.cellbio.23.090506.123326. PubMed PMID: 17506698.

11. Cinquin O, Crittenden SL, Morgan DE, Kimble J. Progression from a stem cell-like state to early differentiation in the *C. elegans* germ line. Proc Natl Acad Sci USA. 2010;107(5):2048-53. Epub 2010/01/19. doi: 10.1073/pnas.0912704107. PubMed PMID: 20080700; PubMed Central PMCID: PMC2836686.

12. Wickens M, Bernstein DS, Kimble J, Parker R. A PUF family portrait: 3'UTR regulation as a way of life. Trends Genet. 2002;18(3):150-7. PubMed PMID: 11858839.

13. Bray SJ. Notch signalling in context. Nat Rev Mol Cell Biol. 2016;17(11):722-35. doi: 10.1038/nrm.2016.94. PubMed PMID: 27507209.

14. Austin J, Kimble J. *glp-1* is required in the germ line for regulation of the decision between mitosis and meiosis in *C. elegans*. Cell. 1987;51:589-99. PubMed PMID: 3677168.

15. Crittenden SL, Bernstein DS, Bachorik JL, Thompson BE, Gallegos M, Petcherski AG, *et al*. A conserved RNA-binding protein controls germline stem cells in *Caenorhabditis elegans*. Nature. 2002;417:660-3. doi: 10.1038/nature754. PubMed PMID: 12050669.

16. Kershner A, Crittenden SL, Friend K, Sorensen EB, Porter DF, Kimble J. Germline stem cells and their regulation in the nematode *Caenorhabditis elegans*. Adv Exp Med Biol. 2013;786:29-46. doi: 10.1007/978-94-007-6621-1_3. PubMed PMID: 23696350.

17. Hansen D, Schedl T. Stem cell proliferation versus meiotic fate decision in *Caenorhabditis elegans*. Adv Exp Med Biol. 2013;757:71-99. Epub 2012/08/09. doi: 10.1007/978-1-4614-4015-4_4. PubMed PMID: 22872475; PubMed Central PMCID: PMC3786863.

18. Kershner AM, Shin H, Hansen TJ, Kimble J. Discovery of two GLP-1/Notch target genes that account for the role of GLP-1/Notch signaling in stem cell maintenance. Proc Natl Acad Sci

U S A. 2014;111(10):3739-44. doi: 10.1073/pnas.1401861111. PubMed PMID: 24567412; PubMed Central PMCID: PMC3956202.

19. Lee C, Sorensen EB, Lynch TR, Kimble J. *C. elegans* GLP-1/Notch activates transcription in a probability gradient across the germline stem cell pool. Elife. 2016;5:e18370. doi: 10.7554/eLife.18370. PubMed PMID: 27705743; PubMed Central PMCID: PMC5094854.

20. Frøkjær-Jensen C, Davis MW, Hopkins CE, Newman BJ, Thummel JM, Olesen SP, *et al*. Single-copy insertion of transgenes in *Caenorhabditis elegans*. Nat Genet. 2008;40(11):1375-83. Epub 2008/10/28. doi: 10.1038/ng.248. PubMed PMID: 18953339; PubMed Central PMCID: PMC2749959.

21. Frøkjær-Jensen C, Davis MW, Ailion M, Jorgensen EM. Improved *Mos1*-mediated transgenesis in *C. elegans*. Nat Methods. 2012;9(2):117-8. doi: 10.1038/nmeth.1865. PubMed PMID: 22290181; PubMed Central PMCID: PMC3725292.

22. Frøkjær-Jensen C, Davis MW, Sarov M, Taylor J, Flibotte S, LaBella M, *et al*. Random and targeted transgene insertion in *Caenorhabditis elegans* using a modified *Mos1* transposon. Nat Methods. 2014;11(5):529-34. doi: 10.1038/nmeth.2889. PubMed PMID: 24820376; PubMed Central PMCID: PMC4126194.

23. Paix A, Folkmann A, Rasoloson D, Seydoux G. High efficiency, homology-directed genome editing in *Caenorhabditis elegans* using CRISPR-Cas9 ribonucleoprotein complexes. Genetics. 2015;201(1):47-54. doi: 10.1534/genetics.115.179382. PubMed PMID: 26187122; PubMed Central PMCID: PMC4566275.

24. Arribere JA, Bell RT, Fu BX, Artiles KL, Hartman PS, Fire AZ. Efficient marker-free recovery of custom genetic modifications with CRISPR/Cas9 in *Caenorhabditis elegans*. Genetics. 2014;198(3):837-46. doi: 10.1534/genetics.114.169730. PubMed PMID: 25161212; PubMed Central PMCID: PMC4224173.

25. Brenner JL, Schedl T. Germline Stem Cell Differentiation Entails Regional Control of Cell Fate Regulator GLD-1 in *Caenorhabditis elegans*. Genetics. 2016;202(3):1085-103. doi:

10.1534/genetics.115.185678. PubMed PMID: 26757772; PubMed Central PMCID: PMC4788111.

26. Jungkamp AC, Stoeckius M, Mecenas D, Grun D, Mastrobuoni G, Kempa S, *et al*. *In vivo* and transcriptome-wide identification of RNA binding protein target sites. Mol Cell. 2011;44(5):828-40. Epub 2011/12/14. doi: 10.1016/j.molcel.2011.11.009. PubMed PMID: 22152485; PubMed Central PMCID: PMC3253457.

27. Prasad A, Porter DF, Kroll-Conner PL, Mohanty I, Ryan AR, Crittenden SL, *et al.* The PUF binding landscape in metazoan germ cells. RNA. 2016;22(7):1026-43. doi: 10.1261/rna.055871.116. PubMed PMID: 27165521; PubMed Central PMCID: PMC4911911.

28. Merritt C, Rasoloson D, Ko D, Seydoux G. 3' UTRs are the primary regulators of gene expression in the *C. elegans* germline. Curr Biol. 2008;18(19):1476-82. Epub 2008/09/27. doi: 10.1016/j.cub.2008.08.013. PubMed PMID: 18818082; PubMed Central PMCID: PMC2585380.

29. Furuta T, Tuck S, Kirchner J, Koch B, Auty R, Kitagawa R, *et al*. EMB-30: An APC4 homologue required for metaphase-to-anaphase transitions during meiosis and mitosis in *Caenorhabditis elegans*. Mol Biol Cell. 2000;11(4):1401-19. PubMed PMID: 10749938.

30. Hansen D, Hubbard EJA, Schedl T. Multi-pathway control of the proliferation versus meiotic development decision in the *Caenorhabditis elegans* germline. Dev Biol. 2004;268(2):342-57. PubMed PMID: 15063172.

31. Hans F, Dimitrov S. Histone H3 phosphorylation and cell division. Oncogene. 2001;20(24):3021-7. doi: 10.1038/sj.onc.1204326. PubMed PMID: 11420717.

32. Kawasaki I, Shim Y-H, Kirchner J, Kaminker J, Wood WB, Strome S. PGL-1, a predicted RNA-binding component of germ granules, is essential for fertility in *C. elegans*. Cell. 1998;94(5):635-45. PubMed PMID: 9741628.

33. Francis R, Barton MK, Kimble J, Schedl T. *gld-1*, a tumor suppressor gene required for oocyte development in *Caenorhabditis elegans*. Genetics. 1995;139(2):579-606. PubMed PMID: 7713419.

34. Ellis RE, Kimble J. The *fog-3* gene and regulation of cell fate in the germ line of *Caenorhabditis elegans*. Genetics. 1995;139:561-77. PubMed PMID: 7713418.

35. Subramaniam K, Seydoux G. Dedifferentiation of primary spermatocytes into germ cell tumors in *C. elegans* lacking the Pumilio-like protein PUF-8. Curr Biol. 2003;13(2):134-9. PubMed PMID: 12546787.

36. McGovern M, Voutev R, Maciejowski J, Corsi AK, Hubbard EJ. A "latent niche" mechanism for tumor initiation. Proc Natl Acad Sci USA. 2009;106(28):11617-22. Epub 2009/07/01. doi: 10.1073/pnas.0903768106. PubMed PMID: 19564624; PubMed Central PMCID: PMC2710656.

37. Pepper AS-R, Killian DJ, Hubbard EJA. Genetic analysis of *Caenorhabditis elegans glp-1* mutants suggests receptor interaction or competition. Genetics. 2003;163(1):115-32. PubMed PMID: 12586701.

38. Berry LW, Westlund B, Schedl T. Germ-line tumor formation caused by activation of *glp-1*, a *Caenorhabditis elegans* member of the *Notch* family of receptors. Development. 1997;124(4):925-36. PubMed PMID: 9043073.

39. Vaid S, Ariz M, Chaturbedi A, Kumar GA, Subramaniam K. PUF-8 negatively regulates RAS/MAPK signalling to promote differentiation of *C. elegans* germ cells. Development. 2013;140(8):1645-54. Epub 2013/03/15. doi: 10.1242/dev.088013. PubMed PMID: 23487310; PubMed Central PMCID: PMC3621483.

40. Merritt C, Seydoux G. The Puf RNA-binding proteins FBF-1 and FBF-2 inhibit the expression of synaptonemal complex proteins in germline stem cells. Development. 2010;137(11):1787-98. doi: 10.1242/dev.050799. PubMed PMID: 20431119; PubMed Central PMCID: PMC2867315.

41. Voronina E, Paix A, Seydoux G. The P granule component PGL-1 promotes the localization and silencing activity of the PUF protein FBF-2 in germline stem cells. Development.

2012;139(20):3732-40. doi: 10.1242/dev.083980. PubMed PMID: 22991439; PubMed Central PMCID: PMC3445306.

42. Kershner AM, Kimble J. Genome-wide analysis of mRNA targets for *Caenorhabditis elegans* FBF, a conserved stem cell regulator. Proc Natl Acad Sci USA. 2010;107(8):3936-41. Epub 2010/02/08. doi: 10.1073/pnas.1000495107. PubMed PMID: 20142496; PubMed Central PMCID: PMC2840422.

43. Ahringer J, Kimble J. Control of the sperm-oocyte switch in *Caenorhabditis elegans* hermaphrodites by the *fem-3* 3′ untranslated region. Nature. 1991;349(6307):346-8. PubMed PMID: 1702880.

44. Zhang B, Gallegos M, Puoti A, Durkin E, Fields S, Kimble J, *et al*. A conserved RNA-binding protein that regulates sexual fates in the *C. elegans* hermaphrodite germ line. Nature. 1997;390(6659):477-84. PubMed PMID: 9393998.

45. Jones AR, Schedl T. Mutations in *gld-1*, a female germ cell-specific tumor suppressor gene in *Caenorhabditis elegans*, affect a conserved domain also found in Src-associated protein Sam68. Genes Dev. 1995;9(12):1491-504. PubMed PMID: 7601353.

46. Jones AR, Francis R, Schedl T. GLD-1, a cytoplasmic protein essential for oocyte differentiation, shows stage- and sex-specific expression during *Caenorhabditis elegans* germline development. Dev Biol. 1996;180(1):165-83. PubMed PMID: 8948583.

47. Stine RR, Greenspan LJ, Ramachandran KV, Matunis EL. Coordinate regulation of stem cell competition by Slit-Robo and JAK-STAT signaling in the *Drosophila* testis. PLoS Genet. 2014;10(11):e1004713. doi: 10.1371/journal.pgen.1004713. PubMed PMID: 25375180; PubMed Central PMCID: PMC4222695.

48. Leatherman JL, Dinardo S. Zfh-1 controls somatic stem cell self-renewal in the *Drosophila* testis and nonautonomously influences germline stem cell self-renewal. Cell Stem Cell. 2008;3(1):44-54. doi: 10.1016/j.stem.2008.05.001. PubMed PMID: 18593558; PubMed Central PMCID: PMC2601693.

49. VanDussen KL, Carulli AJ, Keeley TM, Patel SR, Puthoff BJ, Magness ST, *et al*. Notch signaling modulates proliferation and differentiation of intestinal crypt base columnar stem cells. Development. 2012;139(3):488-97. Epub 2011/12/23. doi: 10.1242/dev.070763. PubMed PMID: 22190634; PubMed Central PMCID: PMC3252352.

50. Van der Flier LG, Sabates-Bellver J, Oving I, Haegebarth A, De Palo M, Anti M, *et al*. The intestinal Wnt/TCF signature. Gastroenterology. 2007;132(2):628-32. doi: 10.1053/j.gastro.2006.08.039. PubMed PMID: 17320548.

51. Itzkovitz S, Lyubimova A, Blat IC, Maynard M, van Es J, Lees J, *et al.* Single-molecule transcript counting of stem-cell markers in the mouse intestine. Nat Cell Biol. 2011;14(1):106-14. Epub 2011/11/29. doi: 10.1038/ncb2384. PubMed PMID: 22119784; PubMed Central PMCID: PMC3292866.

52. van der Flier LG, van Gijn ME, Hatzis P, Kujala P, Haegebarth A, Stange DE, *et al.* Transcription factor *achaete scute-like 2* controls intestinal stem cell fate. Cell. 2009;136(5):903-12. doi: 10.1016/j.cell.2009.01.031. PubMed PMID: 19269367.

53. Schuijers J, Junker JP, Mokry M, Hatzis P, Koo BK, Sasselli V, *et al.* Ascl2 acts as an R-spondin/Wnt-responsive switch to control stemness in intestinal crypts. Cell Stem Cell. 2015;16(2):158-70. doi: 10.1016/j.stem.2014.12.006. PubMed PMID: 25620640.

54. Rosu S, Cohen-Fix O. Live-imaging analysis of germ cell proliferation in the *C. elegans* adult supports a stochastic model for stem cell proliferation. Dev Biol. 2017;423(2):93-100. doi: 10.1016/j.ydbio.2017.02.008. PubMed PMID: 28215939; PubMed Central PMCID: PMC5382985.

55. Macdonald LD, Knox A, Hansen D. Proteasomal regulation of the proliferation vs. meiotic entry decision in the *Caenorhabditis elegans* germ line. Genetics. 2008;180(2):905-20. doi: 10.1534/genetics.108.091553. PubMed PMID: 18791239; PubMed Central PMCID: PMC2567390.

56. Gupta P, Leahul L, Wang X, Wang C, Bakos B, Jasper K, *et al*. Proteasome regulation of the chromodomain protein MRG-1 controls the balance between proliferative fate and differentiation in the *C. elegans* germ line. Development. 2015;142(2):291-302. doi: 10.1242/dev.115147. PubMed PMID: 25564623.

57. Wolpert L. Positional Information and Pattern Formation. Curr Top Dev Biol. 2016;117:597-608. doi: 10.1016/bs.ctdb.2015.11.008. PubMed PMID: 26970003.

58. Ingham PW, Martinez Arias A. Boundaries and fields in early embryos. Cell. 1992;68:221-35.

59. Korzelius J, Naumann SK, Loza-Coll MA, Chan JS, Dutta D, Oberheim J, *et al*. *Escargot* maintains stemness and suppresses differentiation in *Drosophila* intestinal stem cells. EMBO J. 2014;33(24):2967-82. doi: 10.15252/embj.201489072. PubMed PMID: 25298397; PubMed Central PMCID: PMC4282643.

60. Horvay K, Jarde T, Casagranda F, Perreau VM, Haigh K, Nefzger CM, *et al.* Snai1 regulates cell lineage allocation and stem cell maintenance in the mouse intestinal epithelium. EMBO J. 2015;34(10):1319-35. doi: 10.15252/embj.201490881. PubMed PMID: 25759216; PubMed Central PMCID: PMC4491994.

61. Forbes A, Lehmann R. Nanos and Pumilio have critical roles in the development and function of *Drosophila* germline stem cells. Development. 1998;125(4):679-90. PubMed PMID: 9435288.

62. Slaidina M, Lehmann R. Translational control in germline stem cell development. J Cell Biol. 2014;207(1):13-21. Epub 2014/10/15. doi: 10.1083/jcb.201407102. PubMed PMID: 25313405; PubMed Central PMCID: PMC4195835.

63. Carreira-Rosario A, Bhargava V, Hillebrand J, Kollipara RK, Ramaswami M, Buszczak M. Repression of Pumilio Protein Expression by Rbfox1 Promotes Germ Cell Differentiation. Dev Cell. 2016;36(5):562-71. doi: 10.1016/j.devcel.2016.02.010. PubMed PMID: 26954550; PubMed Central PMCID: PMC4785839.

64. Luitjens C, Gallegos M, Kraemer B, Kimble J, Wickens M. CPEB proteins control two key steps in spermatogenesis in *C. elegans*. Genes Dev. 2000;14(20):2596-609. PubMed PMID: 11040214.

65. Jin S-W, Kimble J, Ellis RE. Regulation of cell fate in *Caenorhabditis elegans* by a novel cytoplasmic polyadenylation element binding protein. Dev Biol. 2001;229(2):537-53. doi: doi:10.1006/dbio.2000.9993. PubMed PMID: 11150246.

66. Thompson BE, Bernstein DS, Bachorik JL, Petcherski AG, Wickens M, Kimble J. Dose-dependent control of proliferation and sperm specification by FOG-1/CPEB. Development. 2005;132(15):3471-81. doi: 10.1242/dev.01921. PubMed PMID: 16000383; PubMed Central PMCID: PMC1350643.

67. Kraemer B, Crittenden S, Gallegos M, Moulder G, Barstead R, Kimble J, *et al*. NANOS-3 and FBF proteins physically interact to control the sperm-oocyte switch in *Caenorhabditis elegans*. Curr Biol. 1999;9(18):1009-18. PubMed PMID: 10508609.

68. Arur S, Ohmachi M, Berkseth M, Nayak S, Hansen D, Zarkower D, *et al.* MPK-1 ERK controls membrane organization in *C. elegans* oogenesis via a sex-determination module. Dev Cell. 2011;20(5):677-88. Epub 2011/05/17. doi: 10.1016/j.devcel.2011.04.009. PubMed PMID: 21571224; PubMed Central PMCID: PMC3098718.

69. Campbell ZT, Menichelli E, Friend K, Wu J, Kimble J, Williamson JR, *et al*. Identification of a conserved interface between PUF and CPEB proteins. J Biol Chem. 2012;287(22):18854-62. Epub 2012 Apr 11. doi: 10.1074/jbc.M112.352815. PubMed PMID: 22496444; PubMed Central PMCID: PMC3365739.

70. Wang L, Eckmann CR, Kadyk LC, Wickens M, Kimble J. A regulatory cytoplasmic poly(A) polymerase in *Caenorhabditis elegans*. Nature. 2002;419(6904):312-6. PubMed PMID: 12239571.

71. Wu J, Campbell ZT, Menichelli E, Wickens M, Williamson JR. A protein • protein interaction platform involved in recruitment of GLD-3 to the FBF • *fem-3* mRNA complex. J Mol

Biol. 2013;425(4):738-54. doi: 10.1016/j.jmb.2012.11.013. PubMed PMID: 23159559; PubMed Central PMCID: PMC3568228.

72. Eckmann CR, Kraemer B, Wickens M, Kimble J. GLD-3, a Bicaudal-C homolog that inhibits FBF to control germline sex determination in *C. elegans*. Dev Cell. 2002;3(5):697-710. PubMed PMID: 12431376.

73. Goldstrohm AC, Hook BA, Seay DJ, Wickens M. PUF proteins bind Pop2p to regulate messenger mRNAs. Nat Struct Mol Biol. 2006;13(6):533-9. PubMed PMID: 16715093.

74. Goldstrohm AC, Seay DJ, Hook BA, Wickens M. PUF protein-mediated deadenylation is catalyzed by Ccr4p. J Biol Chem. 2007;282(1):109-14. doi: 10.1074/jbc.M609413200. PubMed PMID: 17090538.

75. Suh N, Crittenden SL, Goldstrohm AC, Hook B, Thompson B, Wickens M, *et al*. FBF and its dual control of *gld-1* expression in the *Caenorhabditis elegans* germline. Genetics. 2009;181(4):1249-60. Epub 2009/02/18. doi: 10.1534/genetics.108.099440. PubMed PMID: 19221201; PubMed Central PMCID: PMC2666496.

76. Campbell ZT, Bhimsaria D, Valley CT, Rodriguez-Martinez JA, Menichelli E, Williamson JR, *et al.* Cooperativity in RNA-protein interactions: global analysis of RNA binding specificity. Cell Rep. 2012;1(5):570-81. doi: 10.1016/j.celrep.2012.04.003. PubMed PMID: 22708079; PubMed Central PMCID: PMC3375920.

77. Weidmann CA, Qiu C, Arvola RM, Lou TF, Killingsworth J, Campbell ZT, *et al*. Drosophila Nanos acts as a molecular clamp that modulates the RNA-binding and repression activities of Pumilio. Elife. 2016;5. doi: 10.7554/eLife.17096. PubMed PMID: 27482653; PubMed Central PMCID: PMC4995099.

78. Loedige I, Stotz M, Qamar S, Kramer K, Hennig J, Schubert T, *et al.* The NHL domain of BRAT is an RNA-binding domain that directly contacts the hunchback mRNA for regulation. Genes Dev. 2014;28(7):749-64. doi: 10.1101/gad.236513.113. PubMed PMID: 24696456; PubMed Central PMCID: PMC4015489.

79. Wang JT, Smith J, Chen BC, Schmidt H, Rasoloson D, Paix A, *et al*. Regulation of RNA granule dynamics by phosphorylation of serine-rich, intrinsically disordered proteins in *C. elegans*. Elife. 2014;3:e04591. Epub 2014/12/24. doi: 10.7554/eLife.04591. PubMed PMID: 25535836; PubMed Central PMCID: PMC4296509.

80. Smith J, Calidas D, Schmidt H, Lu T, Rasoloson D, Seydoux G. Spatial patterning of P granules by RNA-induced phase separation of the intrinsically-disordered protein MEG-3. Elife. 2016;5:e21337. doi: 10.7554/eLife.21337. PubMed PMID: 27914198; PubMed Central PMCID: PMC5262379.

81. Lamont LB, Crittenden SL, Bernstein D, Wickens M, Kimble J. FBF-1 and FBF-2 regulate the size of the mitotic region in the *C. elegans* germline. Dev Cell. 2004;7(5):697-707. PubMed PMID: 15525531.

82. Eckmann CR, Crittenden SL, Suh N, Kimble J. GLD-3 and control of the mitosis/meiosis decision in the germline of *Caenorhabditis elegans*. Genetics. 2004;168:147-60. doi: 10.1534/genetics.104.029264. PubMed PMID: 15454534; PubMed Central PMCID: PMC1448115.

83. Lee M-H, Hook B, Lamont LB, Wickens M, Kimble J. LIP-1 phosphatase controls the extent of germline proliferation in *Caenorhabditis elegans*. EMBO J. 2006;25(1):88-96. PubMed PMID: 16319922; PubMed Central PMCID: PMC1351240.

84. Lee MH, Hook B, Pan G, Kershner AM, Merritt C, Seydoux G, *et al*. Conserved regulation of MAP kinase expression by PUF RNA-binding proteins. PLoS Genet. 2007;3(12):e233. doi: 10.1371/journal.pgen.0030233. PubMed PMID: 18166083; PubMed Central PMCID: PMC2323325.

85. Brenner S. The genetics of *Caenorhabditis elegans*. Genetics. 1974;77(1):71-94. PubMed PMID: 4366476.

86. Kadyk LC, Kimble J. Genetic regulation of entry into meiosis in *Caenorhabditis elegans*. Development. 1998;125(10):1803-13. PubMed PMID: 9550713.

87. Singh K, Chao MY, Somers GA, Komatsu H, Corkins ME, Larkins-Ford J, *et al*. *C. elegans* Notch signaling regulates adult chemosensory response and larval molting quiescence. Curr Biol. 2011;21(10):825-34. Epub 2011/05/10. doi: 10.1016/j.cub.2011.04.010. PubMed PMID: 21549604; PubMed Central PMCID: PMC3100419.

88. Maduro M, Pilgrim D. Identification and cloning of *unc-119*, a gene expressed in the *Caenorhabditis elegans* nervous system. Genetics. 1995;141(3):977-88. PubMed PMID: 8582641.

89. Siegfried K, Kimble J. POP-1 controls axis formation during early gonadogenesis in *C. elegans*. Development. 2002;129(2):443-53. doi: DEV3556. PubMed PMID: 11807036.

90. Edgley ML, Riddle DL. LG II balancer chromosomes in *Caenorhabditis elegans*: mT1(II;III) and the mIn1 set of dominantly and recessively marked inversions. Mol Genet Genomics. 2001;266(3):385-95. Epub 2001/11/20. doi: 10.1007/s004380100523. PubMed PMID: 11713668.

91. Zeiser E, Frøkjær-Jensen C, Jorgensen E, Ahringer J. MosSCI and gateway compatible plasmid toolkit for constitutive and inducible expression of transgenes in the *C. elegans* germline. PLoS One. 2011;6(5):e20082. doi: 10.1371/journal.pone.0020082. PubMed PMID: 21637852; PubMed Central PMCID: PMC3102689.

92. Gibson DG, Young L, Chuang RY, Venter JC, Hutchison CA, 3rd, Smith HO. Enzymatic assembly of DNA molecules up to several hundred kilobases. Nat Methods. 2009;6(5):343-5. doi: 10.1038/nmeth.1318. PubMed PMID: 19363495.

93. Dickinson DJ, Ward JD, Reiner DJ, Goldstein B. Engineering the *Caenorhabditis elegans* genome using Cas9-triggered homologous recombination. Nat Methods. 2013;10(10):1028-34. doi: 10.1038/nmeth.2641. PubMed PMID: 23995389; PubMed Central PMCID: PMC3905680.

94. Stadler M, Fire A. Wobble base-pairing slows *in vivo* translation elongation in metazoans. RNA. 2011;17(12):2063-73. doi: 10.1261/rna.02890211. PubMed PMID: 22045228; PubMed Central PMCID: PMC3222120.

95. Crittenden SL, Leonhard KA, Byrd DT, Kimble J. Cellular analyses of the mitotic region in the *Caenorhabditis elegans* adult germ line. Mol Biol Cell. 2006;17(7):3051-61. PubMed PMID: 16672375; PubMed Central PMCID: PMC1552046.

96. Timmons L, Fire A. Specific interference by ingested dsRNA. Nature. 1998;395(6705):854. doi: 10.1038/27579. PubMed PMID: 9804418.

97. Fraser AG, Kamath RS, Zipperlen P, Martinez-Campos M, Sohrmann M, Ahringer J. Functional genomic analysis of *C. elegans* chromosome I by systematic RNA interference. Nature. 2000;408:325-30.

98. Crittenden SL, Seidel HS, Kimble J. Analysis of the *C. elegans* germline stem cell pool. Methods Mol Biol. 2017;1463:1-33. doi: 10.1007/978-1-4939-4017-2_1. PubMed PMID: 27734344.

99. Ward S, Roberts TM, Strome S, Pavalko FM, Hogan E. Monoclonal antibodies that recognize a polypeptide antigenic determinant shared by multiple *Caenorhabditis elegans* sperm-specific proteins. J Cell Biol. 1986;102(5):1778-86. PubMed PMID: 2422180.

100. Raj A, van den Bogaard P, Rifkin SA, van Oudenaarden A, Tyagi S. Imaging individual mRNA molecules using multiple singly labeled probes. Nat Methods. 2008;5(10):877-9. Epub 2008/09/23. doi: 10.1038/nmeth.1253. PubMed PMID: 18806792; PubMed Central PMCID: PMC3126653.

101. Edelstein A, Amodaj N, Hoover K, Vale R, Stuurman N. Computer control of microscopes using μManager. Curr Protoc Mol Biol. 2010;Chapter 14:Unit14 20. Epub 2010/10/05. doi: 10.1002/0471142727.mb1420s92. PubMed PMID: 20890901; PubMed Central PMCID: PMC3065365.

102. Edelstein AD, Tsuchida MA, Amodaj N, Pinkard H, Vale RD, Stuurman N. Advanced methods of microscope control using μManager software. J Biol Methods. 2014;1(2). Epub 2015/01/22. doi: 10.14440/jbm.2014.36. PubMed PMID: 25606571; PubMed Central PMCID: PMC4297649.

103. Preibisch S, Saalfeld S, Tomancak P. Globally optimal stitching of tiled 3D microscopic image acquisitions. Bioinformatics. 2009;25(11):1463-5. doi: 10.1093/bioinformatics/btp184. PubMed PMID: 19346324; PubMed Central PMCID: PMC2682522.

104. Bartel PL, Fields S, editors. The Yeast Two-Hybrid System. New York: Oxford University Press; 1997.

105. Gietz RD, Schiestl RH. High-efficiency yeast transformation using the LiAc/SS carrier DNA/PEG method. Nat Protoc. 2007;2(1):31-4. doi: 10.1038/nprot.2007.13. PubMed PMID: 17401334.

106. Schmittgen TD, Livak KJ. Analyzing real-time PCR data by the comparative C(T) method. Nat Protoc. 2008;3(6):1101-8. PubMed PMID: 18546601.

Fig 1
Chapter 3

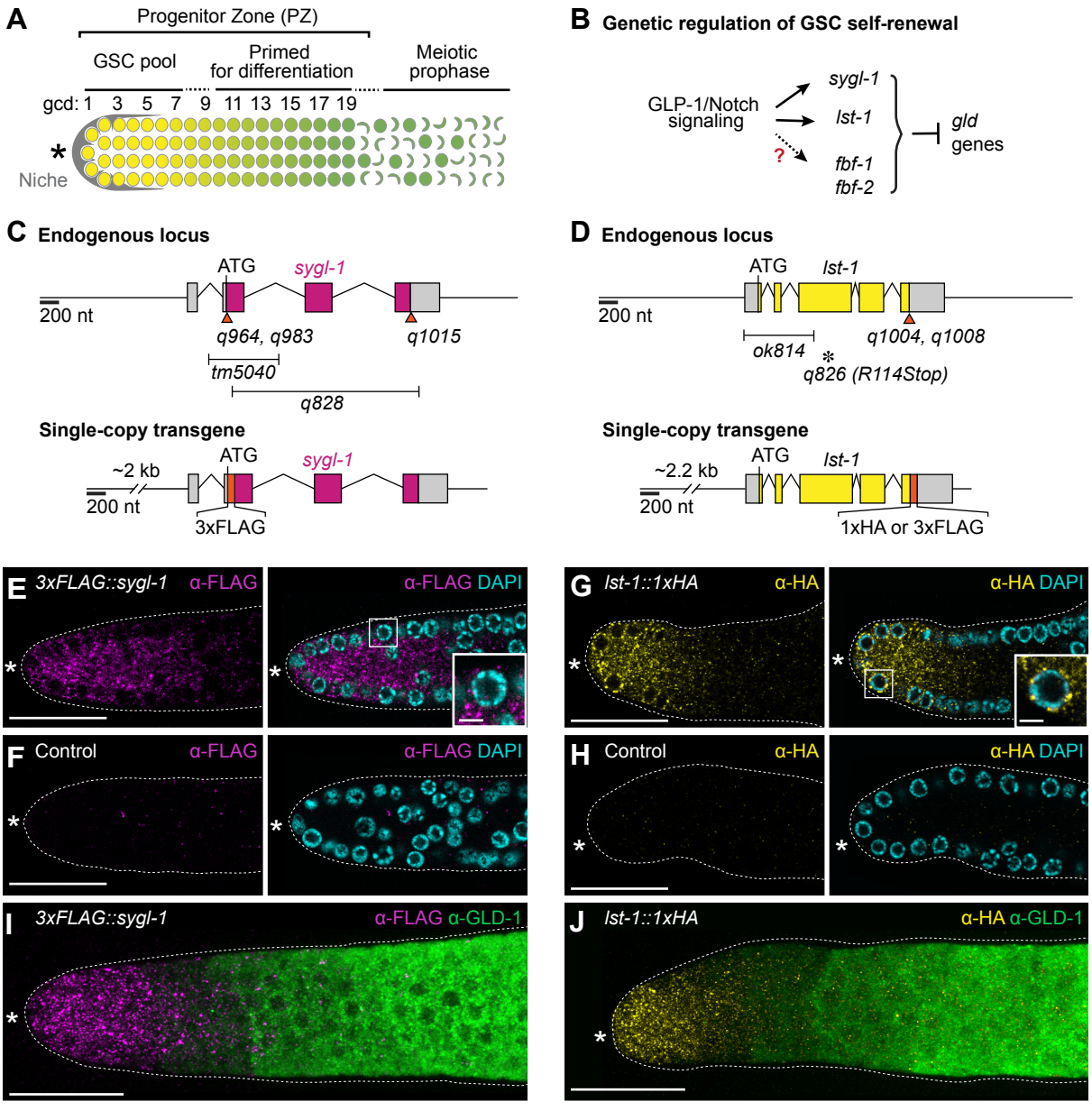

K Extent of SYGL-1 expression

Protein assayed	Approximate extent (gcd)	n	# of cells mean ± SD	n
3xFLAG::SYGL-1[1]	11	33	nd	–
3xOLLAS::SYGL-1[2]	12	22	**118 ± 20**	25
SYGL-1::1xV5[2]	13	30	**134 ± 14**	15

[1] Epitope-tagged single-copy transgenes
[2] Epitope-tagged endogenous loci

L Extent of LST-1 expression

Protein assayed	Approximate extent (gcd)	n	# of cells mean ± SD	n
LST-1::1xHA[1]	5	20	**48 ± 9**	20
LST-1::3xFLAG[1]	6	27	**41 ± 13**	20
LST-1::3xV5[2]	5	25	**47 ± 9**	25

[1] Epitope-tagged single-copy transgenes
[2] Epitope-tagged endogenous loci

Figure legends

Fig 1. SYGL-1 and LST-1 proteins are spatially restricted to the GSC pool region. (**A**) Schematic of adult distal gonad. The progenitor zone (PZ) includes a distal pool of germline stem cells (GSC) and a proximal pool of cells primed to differentiate [11]. The conventional metric for axis position is number of germ cell diameters from the distal end (gcd). Somatic niche for GSCs (gray); naïve stem cell state (yellow circles); early meiotic prophase (green crescents); primed transiting state (yellow to green gradient). Asterisk marks distal end. (**B**) Genetic pathway of GSC regulation. (**C and D**) Schematics of *sygl-1 and lst-1* loci (top) and transgenes (bottom). Epitope tagged endogenous alleles are: *sygl-1(q964)[3xMYC::sygl-1]*, *sygl-1(q983)[3xOLLAS::sygl-1]* and *sygl-1(q1015)[sygl-1::1xV5]*; *lst-1(q1004)[lst-1::3xV5]* and *lst-1(q1008)[lst-1::3xOLLAS]*. Colored boxes, *sygl-1* or *lst-1* exons; gray boxes, untranslated regions; orange boxes and triangles, epitopes. Bars below schematic, deletions; asterisk, nonsense mutation. See Methods for updated gene structures. (**E-J**) SYGL-1 and LST-1 proteins in dissected adult gonads. (E-H) Representative slice or (I-J) maximum intensity z-projections of distal gonad stained with α-FLAG (SYGL-1, magenta), α-HA (LST-1, yellow), α-GLD-1 (green), and DAPI (cyan). Dashed line, gonadal outline; asterisk, distal end. Scale bar is 20 μm in all images, except 5 μm in (E) and (G) insets. (E) *sygl-1(q828); qSi49[*$P_{sygl\text{-}1}$*::3xFLAG::sygl-1::sygl-1 3'end].* (F) *sygl-1(q828).* (G) *lst-1(ok814); qSi22[*$P_{lst\text{-}1}$*::lst-1::1xHA::lst-1 3'end].* (H) *lst-1(ok814)*. See **S1A-S1C Fig** for whole gonad images. (K and L) Extent of SYGL-1 and LST-1 expression along the gonadal axis, estimated with functional epitope-tagged proteins. Expression is robust distally and graded proximally. Proximal boundaries were estimated by eye as the point at which staining becomes barely detected. nd, not determined. See **S1D and S1E Fig** for data supporting functionality of epitope-tagged proteins and see **S2 Fig** for characterization of *sygl-1* or *lst-1* mutants.

Fig 2
Chapter 3

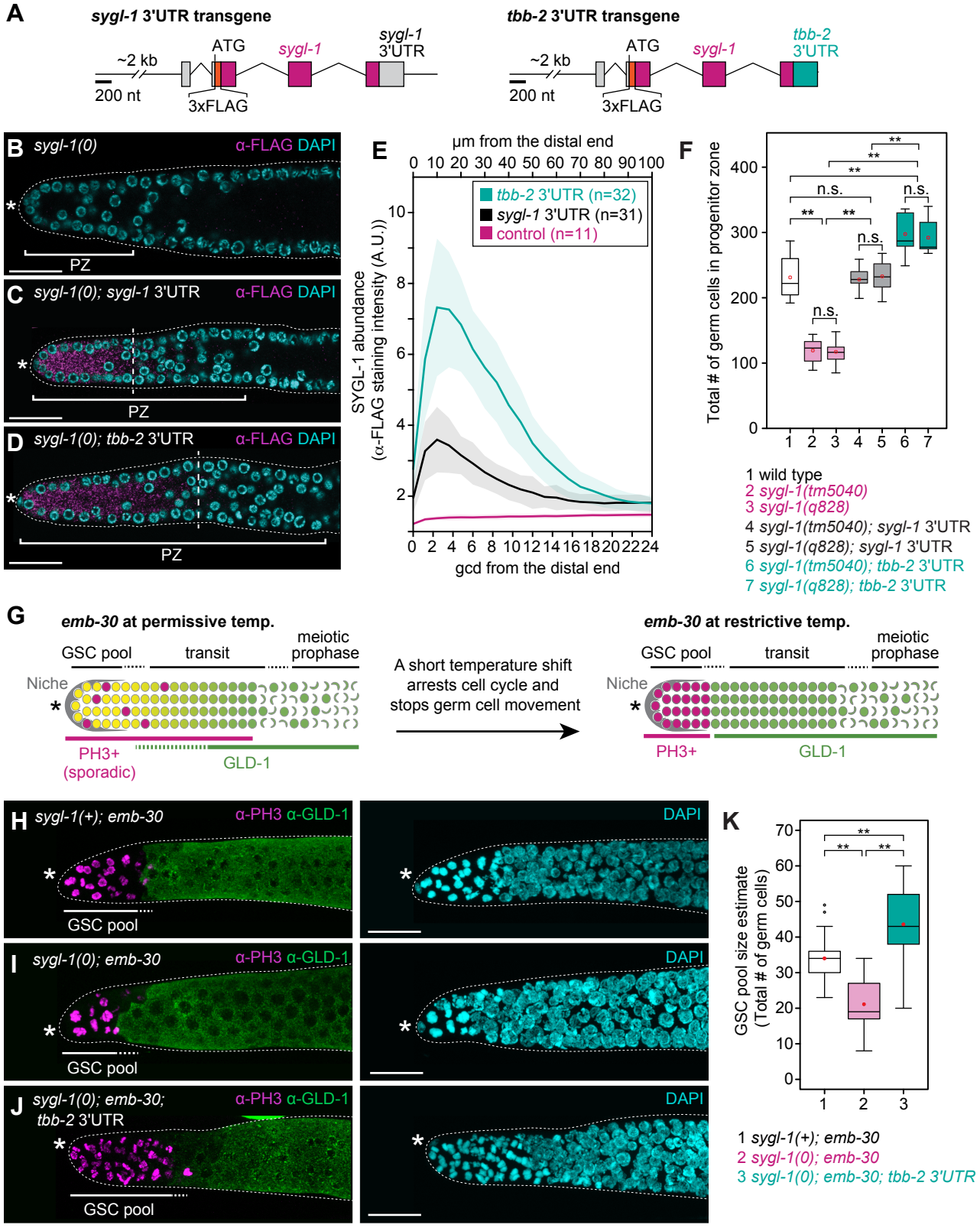

Fig 2. Extent of SYGL-1 expression domain correlates with size of GSC pool. (**A**) Schematics of transgenes. Conventions as in **Fig 1C**. Left, *sygl-1* 3'UTR transgene. Right, *tbb-2* 3'UTR transgene replaces *sygl-1* 3'UTR with *tbb-2* (β-tubulin) 3'UTR. See **S3 Fig** for data supporting functionality of *tbb-2* 3'UTR transgene. (**B-D**) Extents of SYGL-1 protein in dissected adult gonads stained with α-FLAG (SYGL-1, magenta) and DAPI (cyan). Conventions as in **Fig 1E-1J**; scale bar is 20 μm. (B) *sygl-1(q828).* (C) *sygl-1(q828); qSi49[*$P_{sygl\text{-}1}$*::3xFLAG::sygl-1::sygl-1 3'end].* (D) *sygl-1(q828); qSi150[*$P_{sygl\text{-}1}$*::3xFLAG::sygl-1::tbb-2 3'end].* (**E**) Quantitation of SYGL-1 abundance, based on intensity of α-FLAG staining. Average intensity values were plotted against distance in microns along the gonadal axis (x-axis, top), which were converted to the conventional metric of germ cell diameters from distal end (x-axis, bottom) (see Methods). Lines, average intensity in arbitrary units (A.U.); shaded areas, standard deviation; n, number of gonadal arms. (**F**) Progenitor zone sizes. Averages and standard deviations for each genotype are as follows: (1) 231 ± 33 (n=12); (2) 119 ± 17 (n=22); (3) 117 ± 16 (n=20); (4) 229 ± 16 (n=15); (5) 234 ± 23 (n=12); (6) 298 ± 34 (n=13); (7) 292 ± 25 (n=12). Bottom and top boundaries of each box, first and third quartiles; middle lines, median; red dots, mean; whiskers, minimum and maximum values. Asterisks indicate a statistically significant difference by Welch's ANOVA with Games-Howell *post hoc* test. **p<0.001, n.s.= non-significant. (**G**) *emb-30* assay to measure GSC pool size. An *emb-30* temperature-sensitive mutant stops germ cell movement by cell cycle arrest [29]. At permissive temperature (15°C), the distal gonad appears normal, with scattered PH3-positive M-phase cells and graded GLD-1, a differentiation marker. A shift to restrictive temperature (25°C) reveals a distal pool of naïve stem-like germ cells arrested in M-phase and a proximal pool of germ cells primed to differentiate and hence expressing GLD-1 [11]. (**H-J**) GSC pool size correlates with SYGL-1 expression. Maximum intensity z-projected images of dissected gonads stained with α-PH3 (magenta), α-GLD-1 (green) and DAPI (cyan). Conventions as in **Fig 1E-1J**; scale bar is 20 μm. (H) Control: *emb-*

30(tn377ts). (I) *sygl-1(tm5040); emb-30(tn377ts).* (J) *sygl-1(tm5040); qSi150[P$_{sygl-1}$::3xFLAG::sygl-1::tbb-2 3'end]; emb-30(tn377ts)*. (K) GSC pool size estimates. Box plot conventions as in **Fig 2F**. Averages and standard deviations for each genotype are as follows: (1) 35 $\pm$ 7; (2) 21 $\pm$ 7; (3) 43 $\pm$ 11; n>28 gonadal arm per genotype. Asterisks indicate a statistically significant difference by 1-way ANOVA with Tukey HSD *post hoc* test. ** p<0.001. Genotypes as in **Fig 2H-2J**.

Fig 3
Chapter 3

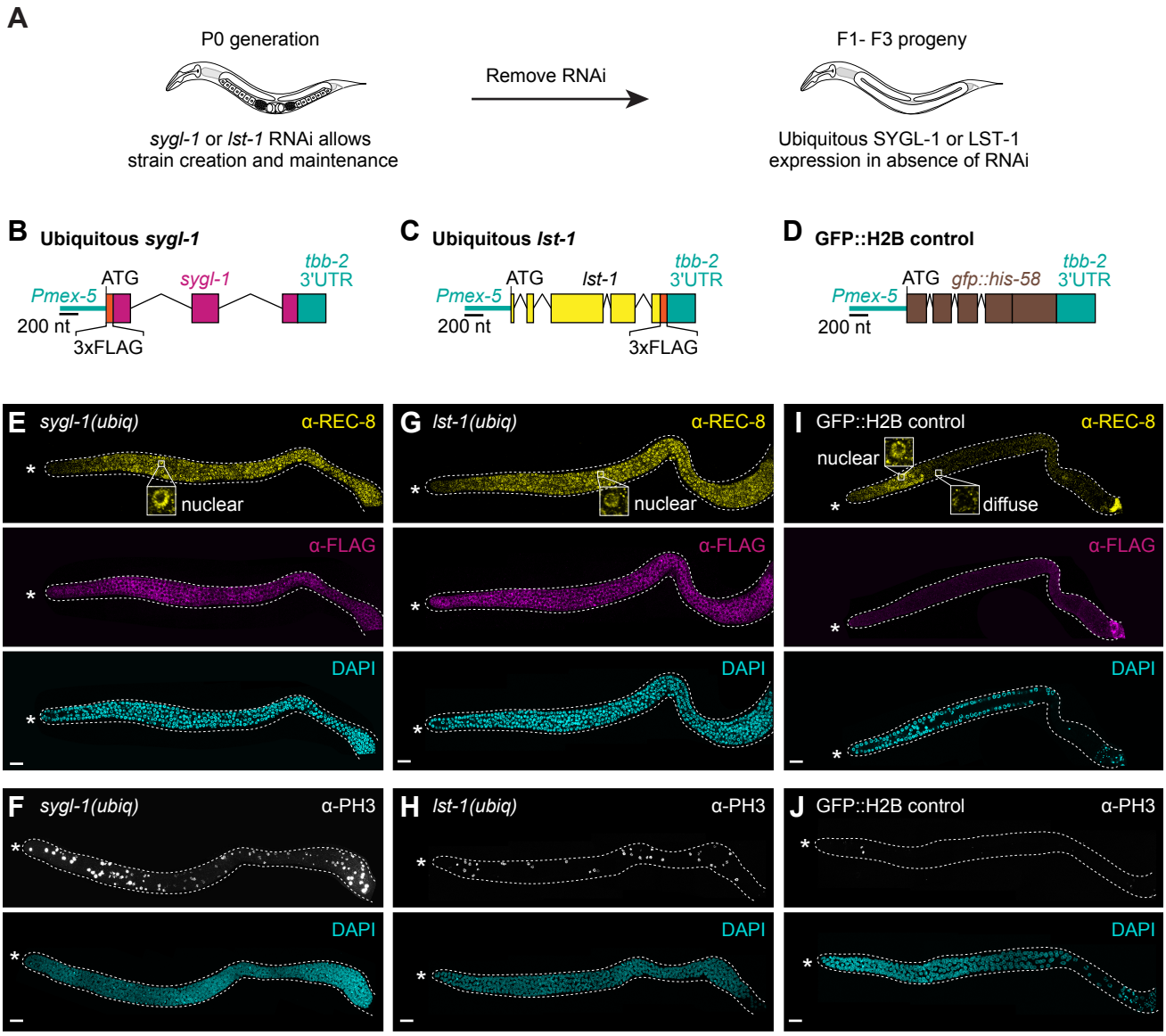

Fig 3. Ubiquitous germline expression of SYGL-1 or LST-1 drives tumor formation.

(**A**) Protocol to induce ubiquitous germline expression of SYGL-1 or LST-1. See text for explanation and **S4A and S4B Fig** for tumor penetrance over generations. (**B-D**) Schematics of transgenes. The *mex-5* promoter and *tbb-2* 3'UTR were used to promote ubiquitous germline expression. (**E-J**) Young adult gonads stained with mitotic marker α-REC-8 (yellow), α-FLAG (SYGL-1 or LST-1, magenta), M-phase marker α-PH3 (white), and DAPI (cyan). Images are either single slice (E, G, I) or maximum intensity z-projections (F, H, J). Conventions as in **Fig 1E-1J**; scale bar is 20 μm. (E and F) Genotype for ubiquitous SYGL-1: *sygl-1(tm5040); qSi235[P_{mex-5}::3xFLAG::sygl-1::tbb-2 3'end]*. (G and H) Genotype for ubiquitous LST-1: *lst-1(ok814); qSi267[P_{mex-5}::lst-1::3xFLAG::tbb-2 3'end]*. (I and J) Genotype for ubiquitous GFP::H2B control, *weSi2[P_{mex-5}::GFP::his-58::tbb-2 3'end]* [91]. See **S4C-S4K Fig** for further characterization.

Fig 4
Chapter 3

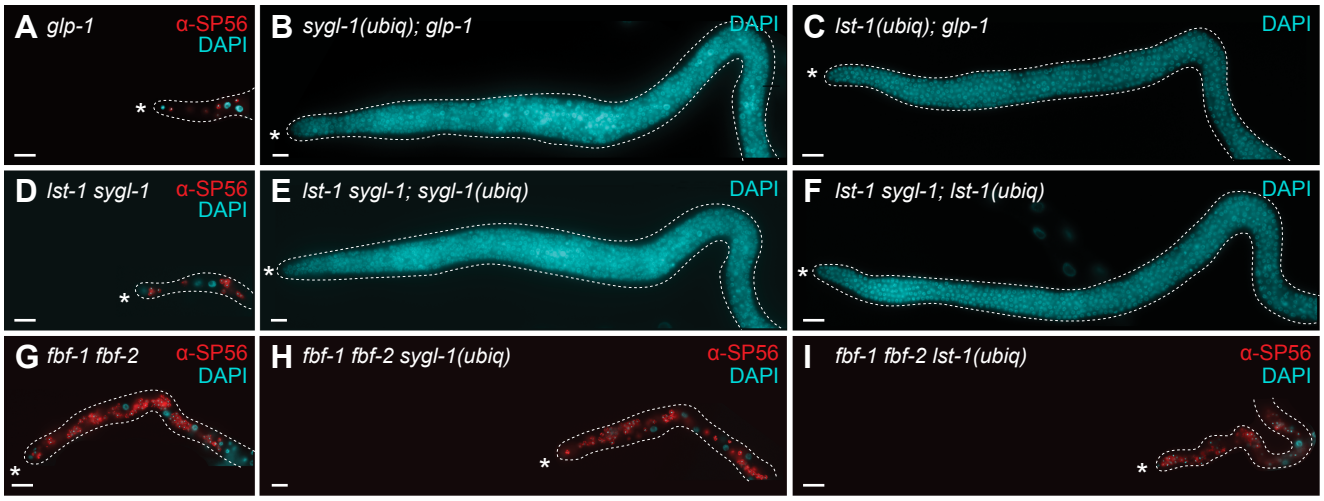

J

Genetic background	Ubiquitous *sygl-1*[1]	Ubiquitous *lst-1*[2]	% animals with tumors	n	Total # germ cells mean ± s.d.[3]	n
glp-1	–	–	0	50	2-4[4]	
	+	–	95	113	Tumor	
	–	+	92	85	Tumor	
lst-1 sygl-1	–	–	0	50	2-4[5]	
	+	–	97	35	Tumor	
	–	+	88	33	Tumor	
fbf-1 fbf-2	–	–	0	> 50	26 ± 12	27
	+	–	0	>100	26 ± 8	17
	–	+	0	>100	21 ± 10	20

K

GLP-1/Notch signaling → *sygl-1* *lst-1* → *fbf-1* *fbf-2* ⊣ *gld* genes

[1] *qSi235[Pmex-5::3xFLAG::sygl-1::tbb-2* 3'end*]*
[2] *qSi267[Pmex-5::lst-1::3xFLAG::tbb-2* 3'end*]*
[3] per gonadal arm, 15°C
[4] *Austin and Kimble (1987)*
[5] *Kershner et al (2014)*

Fig 4. SYGL-1 and LST-1 tumor formation relies on FBF. (**A-I**) Epistasis tests using *sygl-1(ubiq)* or *lst-1(ubiq)* transgenes. All images are dissected young adult gonads stained with sperm marker SP56 (red) and DAPI (cyan). (A-C) Epistasis with *glp-1*. (A) GSC defect in *glp-1(q46)* null: the few GSCs in L1 larvae differentiate as sperm [14]. (B and C) Germline tumor in *sygl-1(ubiq); glp-1(q46)* null and *lst-1(ubiq); glp-1(q46)* null. (D-F) Epistasis with *lst-1 sygl-1.* (D) GSC defect in *lst-1(ok814) sygl-1(tm5040)* double mutant is indistinguishable from that of *glp-1* null [18]. (E and F) Germline tumor in *lst-1(ok814) sygl-1(tm5040); sygl-1(ubiq)* and in *lst-1(ok814) sygl-1(tm5040); lst-1(ubiq)*. (G-I) Epistasis test with *fbf-1 fbf-2*. GSC defect in *fbf-1(ok91) fbf-2(q704)* double mutant: GSCs made in larvae but not maintained past late L4 when all differentiate as sperm at 15°C and 20°C [15]. At 25°C, a small number of GSCs is maintained in adults [40]. (H and I) GSC defect similar to that of *fbf-1 fbf-2* double mutant in *fbf-1(ok91) fbf-2(q704) sygl-1(ubiq)* and *fbf-1(ok91) fbf-2(q704) lst-1(ubiq).* See **S5 Fig** for confirmation that SYGL-1 and LST-1 are expressed and functional in these strains, and for characterization of these strains at 25°C. Conventions as in **Fig 1E-1J**; scale bar is 20 μm. In all strains, *sygl-1(ubiq)* is *qSi235[P_{mex-5}::3xFLAG::sygl-1::tbb-2 3'end]* and *lst-1(ubiq)* is *qSi267[P_{mex-5}:: lst-1::3xFLAG::tbb-2 3'end]*. (**J**) Summary of epistasis results. (**K**) Revised genetic model for GSC regulation. See text for further explanation.

Fig 5
Chapter 3

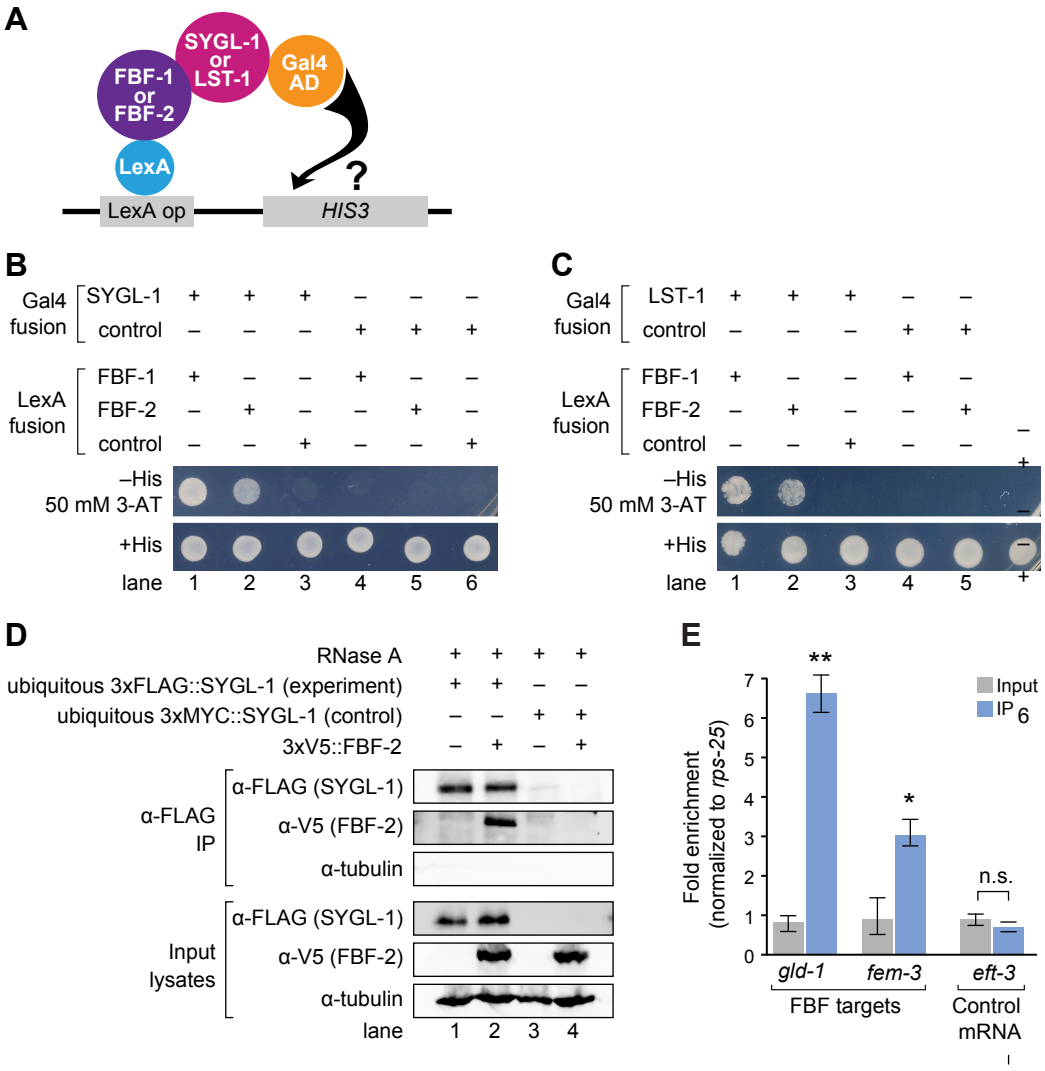

Fig 5. SYGL-1 and LST-1 interact physically with FBF. (**A**) Yeast two hybrid assay. Full length SYGL-1 or LST-1 was fused to Gal4 activation domain (AD); PUF repeats of FBF-1(121-614) or FBF-2(121-632) were fused to LexA binding domain (BD). Interaction activates transcription of *HIS3* gene. (**B and C**) Yeast growth assays tested interaction between SYGL-1 and FBF (B) or LST-1 and FBF (C). Yeast strains were monitored for growth on synthetic defined media (SD), either lacking histidine or with histidine as a control. A *HIS3* competitive inhibitor (3-AT) improved stringency. (**D**) SYGL-1 and FBF-2 co-immunoprecipitation (IP). Western blots probed with α-FLAG to detect SYGL-1, α-V5 to detect FBF-2, and anti-α-tubulin as a loading control. 2% of input lysates and 20% of IP elutes were loaded. Exposure times of input and IP lanes are different, so band intensities are not comparable. RNA degradation by RNase A was confirmed. Genotypes for each lane: (1) *sygl-1(tm5040); qSi235[P_{mex-5}::3xFLAG::sygl-1::tbb-2 3'end];* (2) *sygl-1(tm5040); fbf-2(q931)[3xV5::fbf-2] qSi235[P_{mex-5}::3xFLAG::sygl-1::tbb-2 3'end];* (3) *sygl-1(tm5040); qSi297[P_{mex-5}::3xMYC::sygl-1::tbb-2 3'end];* (4) *sygl-1(tm5040); fbf-2(q932)[3xV5::fbf-2] qSi297[P_{mex-5}::3xMYC::sygl-1::tbb-2 3'end]*. See **S7 Fig** for data supporting functionality of epitope-tagged FBF-2. (**E**) Quantitative PCR of two signature FBF target mRNAs and a control mRNA after α-FLAG IP, using either *3xFLAG::sygl-1(ubiq)* for the experiment or *3xMYC::sygl-1*(*ubiq*) as the control. Abundance of mRNAs in input (gray bars) and IPs (blue bars) was calculated with the $\Delta\Delta C_T$ method, using *rps-25* for normalization. Error bar indicates standard error. Asterisks indicate a statistically significant difference by 1-way ANOVA with Tukey HSD *post hoc* test. * $p<0.05$, ** $p<0.01$.

Fig 6
Chapter 3

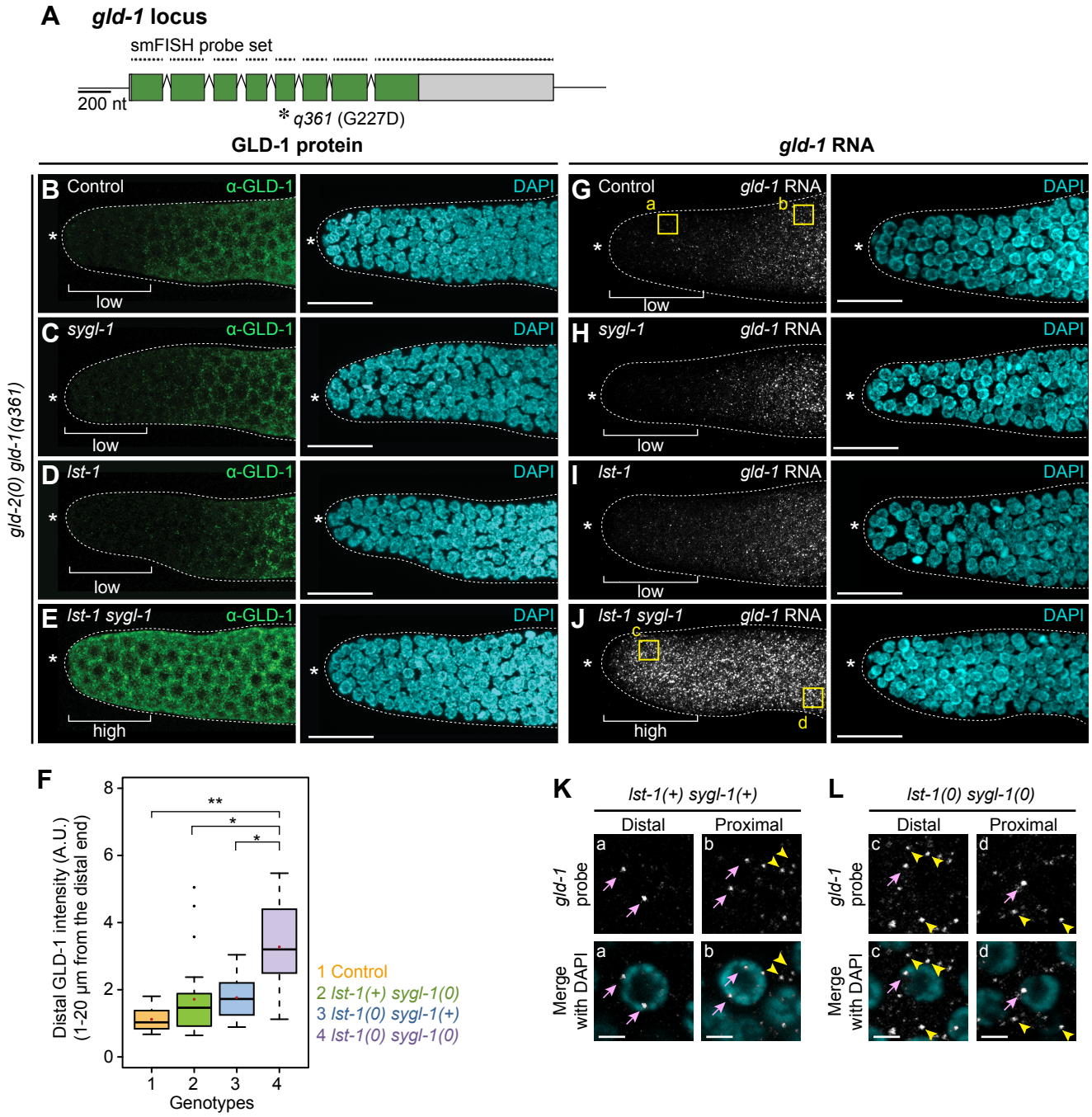

Fig 6. SYGL-1 and LST-1 repress *gld-1* expression post-transcriptionally in GSC pool. (**A**) Schematic of *gld-1(q361),* a missense allele with a null phenotype [45] that generates mRNA and protein normally [30]. The smFISH probe set spanned the locus. See text for details. (**B-E**) GLD-1(q361) protein in distal gonads, stained with α-GLD-1 (green) and DAPI (cyan). Genotypes are: (B) *gld-2(q497) gld-1(q361)*; (C) *sygl-1(q828) gld-2(q497) gld-1(q361)*; (D) *lst-1(ok814) gld-2(q497) gld-1(q361)*; (E) *lst-1(ok814) sygl-1(q828) gld-2(q497) gld-1(q361)*. (**F**) Quantitation of GLD-1(q361). α-GLD-1 intensities in 0-20 μm (1-~5 gcd) from the distal end were averaged and plotted. Box plot conventions as in **Fig 2F**, genotypes as in **Fig 6B-6E**. Asterisks indicate a statistically significant difference by 1-way Welch's ANOVA with Games Howell *post hoc* test. ** $p<0.001$, * $p< 0.05$. Number of gonads examined: Control, n=23; *sygl-1,* n=26; *lst-1*, n=24; *lst-1 sygl-1,* n=38. (**G-J**) *gld-1(q361)* transcripts in distal gonads, probed using smFISH (white) and DAPI (cyan). Genotypes as in **Fig 6B-6E**. All gonads (100%) had mRNA distributions as shown: control, n=32; *sygl-1,* n=35; *lst-1*, n=41; *lst-1 sygl-1,* n=38. (K and L) Pink arrows, nascent transcripts in nucleus. Yellow arrowheads, mature mRNAs in cytoplasm. Top, *gld-1* RNA; bottom, RNA merged with DAPI. (**K**) Magnifications from boxed areas in (G). In the presence of wild-type *sygl-1* and *lst-1*, distal germ cells possess nuclear transcripts, but little cytoplasmic mRNA, whereas proximal germ cells have both. (**L**) Magnifications from boxed areas in (J). Without *sygl-1* and *lst-1*, both distal and proximal germ cells contain nuclear and cytoplasmic *gld-1* transcripts**.** See **S8 Fig** for confirmation of *gld-1* probe specificity. All images are maximum intensity z-projections, except (K) and (L) show a single z-slice. Conventions as in **Fig 1E-1J**; scale bar is 20 μm in all images, except 2 μm in (K) and (L). n, number of gonadal arms.

Fig 7
Chapter 3

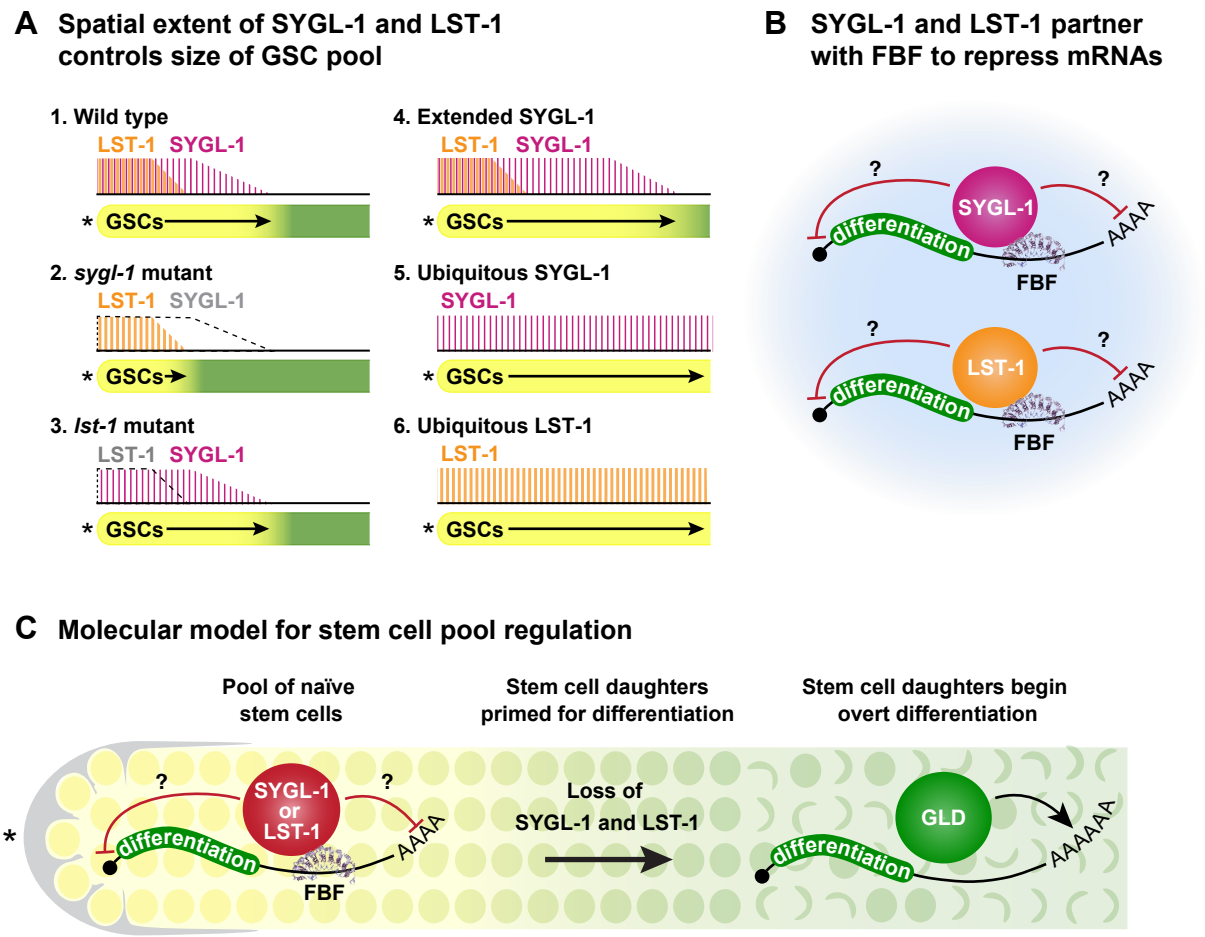

Fig 7. Models for stem cell pool regulation. (**A**) In each schematic, wild-type or manipulated extents of SYGL-1 (magenta) and LST-1 (orange) are shown above and GSC pool sizes are shown below. Wild type: GSC pool size corresponds to SYGL-1 rather than LST-1 extent; *sygl-1* mutant: pool size smaller than wild type and likely determined by smaller LST-1 extent; *lst-1* mutant: pool size not determined experimentally but likely similar to wild type, because progenitor zone is nearly the same size as normal; Extended SYGL-1 expression: moderate increase in SYGL-1 extent expands GSC pool (*tbb-2* 3'UTR transgene); Ubiquitous SYGL-1 expression: major expansion of SYGL-1 forms a massive tumor; Ubiquitous LST-1 expression: major expansion of LST-1 forms a massive tumor. (**B**) FBF forms a complex with SYGL-1 or LST-1 to repress differentiation RNAs. Red bars indicate repression; large pale blue circle represents an RNP granule. See text for explanation. (**C**) Loss of SYGL-1 and LST-1 triggers the switch from a naïve state to one primed-for-differentiation. See text for explanation.

S1 Fig
Chapter 3

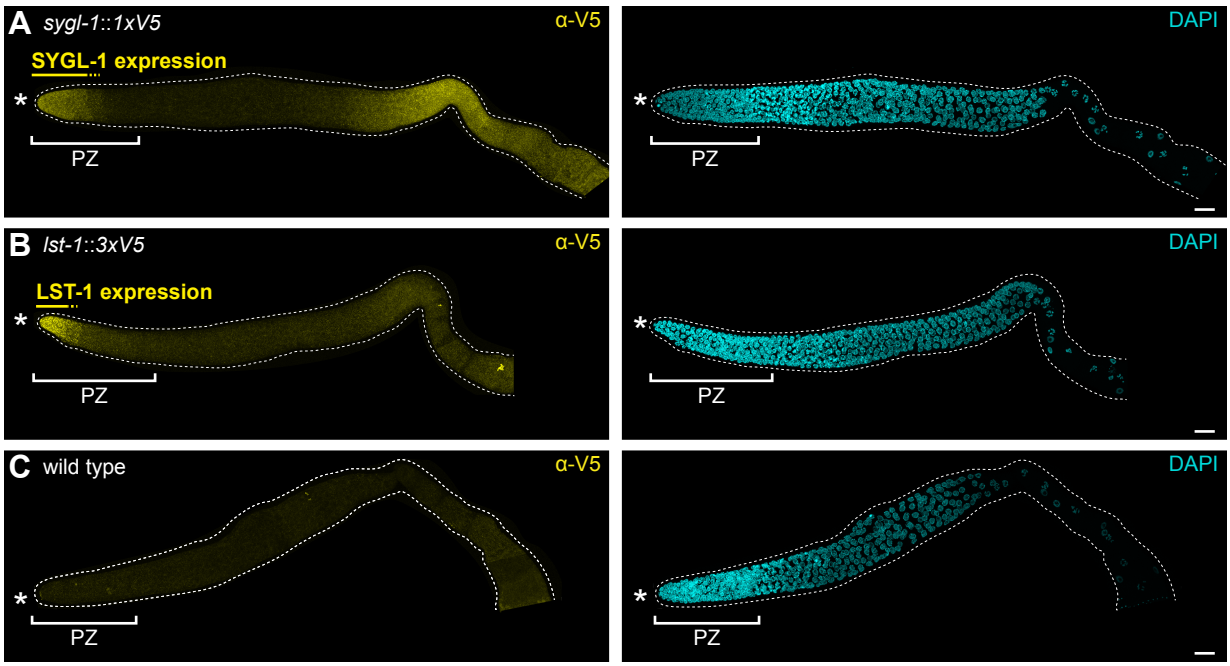

D **Epitope-tagged SYGL-1 and LST-1 transgenic proteins are functional**

lst-1 sygl-1 genotypes	Transgene	% Fertile	% Sterile	n
lst-1(ok814) sygl-1(tm5040)	–	0	100	>100
lst-1(ok814) sygl-1(q828)	–	0	100	>100
lst-1(q826) sygl-1(tm5040)	–	0	100	>100
lst-1(q826) sygl-1(q828)	–	0	100	>100
lst-1(ok814) sygl-1(tm5040)	*qSi49 [Psygl-1::3xFLAG::sygl-1::sygl-1* 3'UTR*]*	91	9	108
lst-1(ok814) sygl-1(q828)	*qSi49 [Psygl-1::3xFLAG::sygl-1::sygl-1* 3'UTR*]*	100	0	40
lst-1(ok814) sygl-1(tm5040)	*qSi22 [Plst-1::lst-1::1xHA::lst-1* 3'UTR*]*	99	1	104
lst-1(q826) sygl-1(tm5040)	*qSi22 [Plst-1::lst-1::1xHA::lst-1* 3'UTR*]*	100	0	102
lst-1(q826) sygl-1(q828)	*qSi69 [Plst-1::lst-1::3xFLAG::lst-1* 3'UTR*]*	95	5	102
lst-1(ok814) sygl-1(tm5040)	*qSi93 [Plst-1::lst-1::1xHA::lst-1* 3'UTR]	97	3	68

E **Endogenous epitope-tagged SYGL-1 and LST-1 are functional**

lst-1 sygl-1 genotypes	Identity of tag at endogenous locus	% Fertile	% Sterile	n
lst-1(ok814) sygl-1(+)	–	91	9	91
lst-1(+) sygl-1(tm5040)	–	98	2	128
lst-1(ok814) sygl-1(tm5040)	–	0	100	>100
lst-1(ok814) sygl-1(q964)	3xMYC::*sygl-1*	96	4	124
lst-1(ok814) sygl-1(q983)	3xOLLAS::*sygl-1*	100	0	113
lst-1(ok814) sygl-1(q1015)	*sygl-1::1xV5*	95	5	98
lst-1(q1004) sygl-1(tm5040)	*lst-1*::3xV5	97	3	99
lst-1(q1008) sygl-1(tm5040)	*lst-1*::3xOLLAS	100	0	70

S1 Fig. Characterization of *sygl-1* and *lst-1* epitope-tagged alleles. (**A-C**) SYGL-1 and LST-1 in dissected gonads. Representative z-projection images of staining with α-V5, using *sygl-1*::*1xV5* and *lst-1*::*3xV5* epitope tagged alleles. Conventions are as in **Fig 1E-1J**; scale bar is 20 μm. Genotypes are (A) *sygl-1(q1015)[sygl-1::1xV5],* (B) *lst-1(q1004)[lst-1::3xV5],* (C) wild type. In addition to distal expression within the progenitor zone (PZ), SYGL-1 and LST-1 are present in the proximal gonad, consistent with their mRNA expression [18, 19]. (**D and E**) Functionality of epitope-tagged SYGL-1 or LST-1 transgenic proteins (D) or endogenous alleles (E). Because *lst-1 sygl-1* double mutants are 100% sterile but single mutants are fertile [18], functionality of epitope-tagged transgenes or endogenous alleles was tested by scoring fertility in the appropriate mutant background.

S2 Fig
Chapter 3

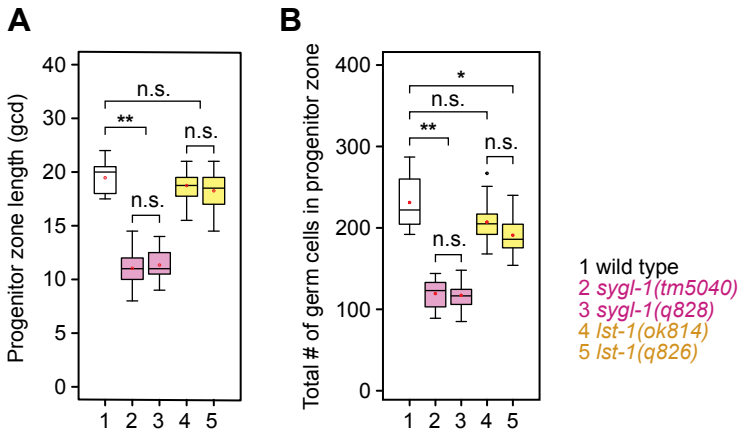

C **Brood size and embryonic lethality of *sygl-1* and *lst-1* mutants**

Genotype	Mean brood size ± SD	n	Mean % embryos hatched ± SD	n
wild type	189 ± 27	11	95 ± 5	1,360
sygl-1(tm5040)	237 ± 55	12	97 ± 3	2,851
sygl-1(q828)	225 ± 46	9	98 ± 2	1,854
lst-1(ok814)	191 ± 61	9	91 ± 8	1,725
lst-1(q826)	217 ± 72	11	97 ± 14	2,392

D **Fertility of *sygl-1* and *lst-1* mutants**

Genotype	% Fertile	% Masculinized sterile	% Other sterile	n
wild type	100	0	0	>100
sygl-1(tm5040)	98	0	2	128
sygl-1(q828)	100	0	0	130
lst-1(ok814)	91	9	0	91
lst-1(q826)	96	4	0	94

S2 Fig. Characterization of *sygl-1* and *lst-1* single mutants. (**A and B**) Progenitor zone (PZ) size in *sygl-1* and *lst-1* mutants. (A) PZ length measured in number of germ cell diameters (gcd) from distal end. The averages and standard deviations are as follows: wild type, 19 ± 2 (n=13); *sygl-1(tm5040),* 11 ± 1 (n=104); *sygl-1(q828),* 11 ± 1 (n=49)*; lst-1(ok814),* 19 ± 2 (n=20)*; lst-1(q826),* 18 ± 2 (n=23). (B) Total number of cells in PZ. The averages and standard deviations are as follows: wild type, 231 ± 33 (n=12); *sygl-1(tm5040),* 119 ± 17 (n=22); *sygl-1(q828),* 117 ± 16 (n=20)*; lst-1(ok814),* 207 ± 24 (n=20)*; lst-1(q826),* 192 ± 21 (n=23). Box plot convention as in **Fig 2F**. Asterisks indicate a statistically significant difference by 1-way ANOVA with Tukey HSD *post hoc* test: ** $p<0.001$, * $p<0.05$, n.s.= non-significant. (**C and D**) Characterization of brood size, embryonic lethality, and fertility of *sygl-1* and *lst-1* mutants.

S3 Fig
Chapter 3

A **SYGL-1 functionality from *tbb-2* 3'UTR transgene**

lst-1 sygl-1 genotypes	Transgene	% Fertile	n
lst-1(ok814) sygl-1(tm5040)	–	0	>100
lst-1(ok814) sygl-1(q828)	–	0	>100
lst-1(ok814) sygl-1(tm5040)	*qSi150[Psygl-1::3xFLAG::sygl-1::tbb-2 3'UTR]*	90	50
lst-1(ok814) sygl-1(q828)	*qSi150[Psygl-1::3xFLAG::sygl-1::tbb-2 3'UTR]*	95	38

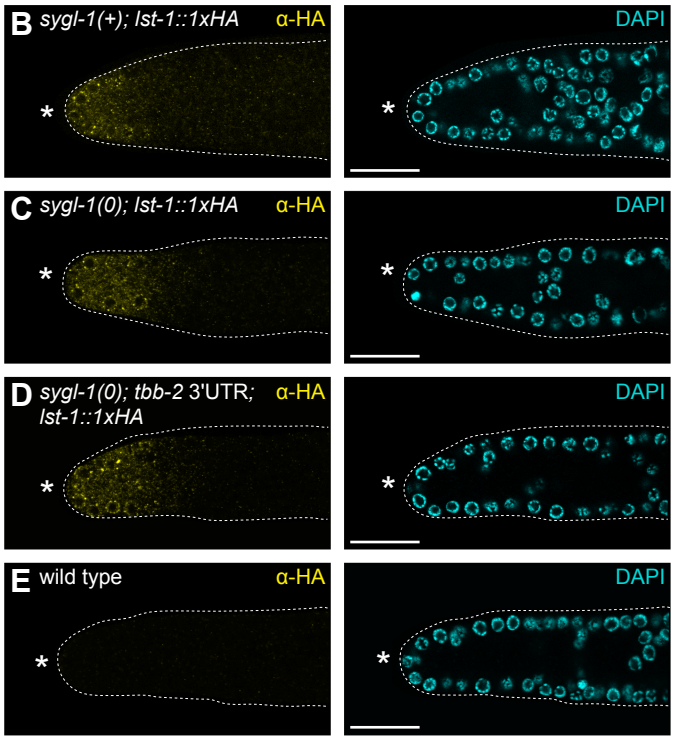

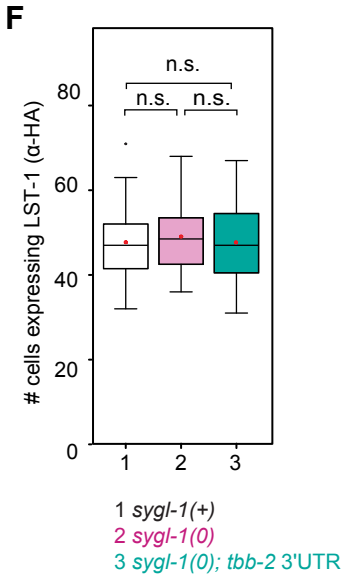

S3 Fig. Characterization of *tbb-2* 3'UTR transgene. (**A**) Functionality of SYGL-1 protein encoded by the *tbb-2* 3'UTR transgene. (**B-F**) LST-1 expression in animals expressing varying abundance of SYGL-1. Assays are done with transgenic HA-tagged LST-1, which functions as endogenous LST-1 (**S1D Fig**). (B-E) Images of distal gonad stained with α-HA (LST-1, yellow) and DAPI (cyan), each a single z-slice. Conventions as in **Fig 1E-1J**; scale bar is 20 μm. Genotypes are: (B) *lst-1(ok814); qSi93[P_{lst-1}::lst-1::1xHA::lst-1 3'end]*. (C) *lst-1(ok814) sygl-1(tm5040); qSi93[P_{lst-1}::lst-1::1xHA::lst-1 3'end]*. (D) *lst-1(ok814) sygl-1(tm5040); qSi150[P_{sygl-1}::3xFLAG::sygl-1::tbb-2 3'end]; qSi93[P_{lst-1}::lst-1::1xHA::lst-1 3'end]*. (E) wild type. (F) Total number of LST-1 expressing cells. Averages and standard deviations for each genotype are: (1) 48 ± 9 cells [5 ± 1 gcd] (n=20); (2) 49 ± 9 cells [6 ± 1 gcd] (n=20); (3) 48 ± 10 cells [5 ± 1 gcd] (n=20). n.s.= non-significant by 1-way ANOVA with Tukey HSD *post hoc* test.

S4 Fig
Chapter 3

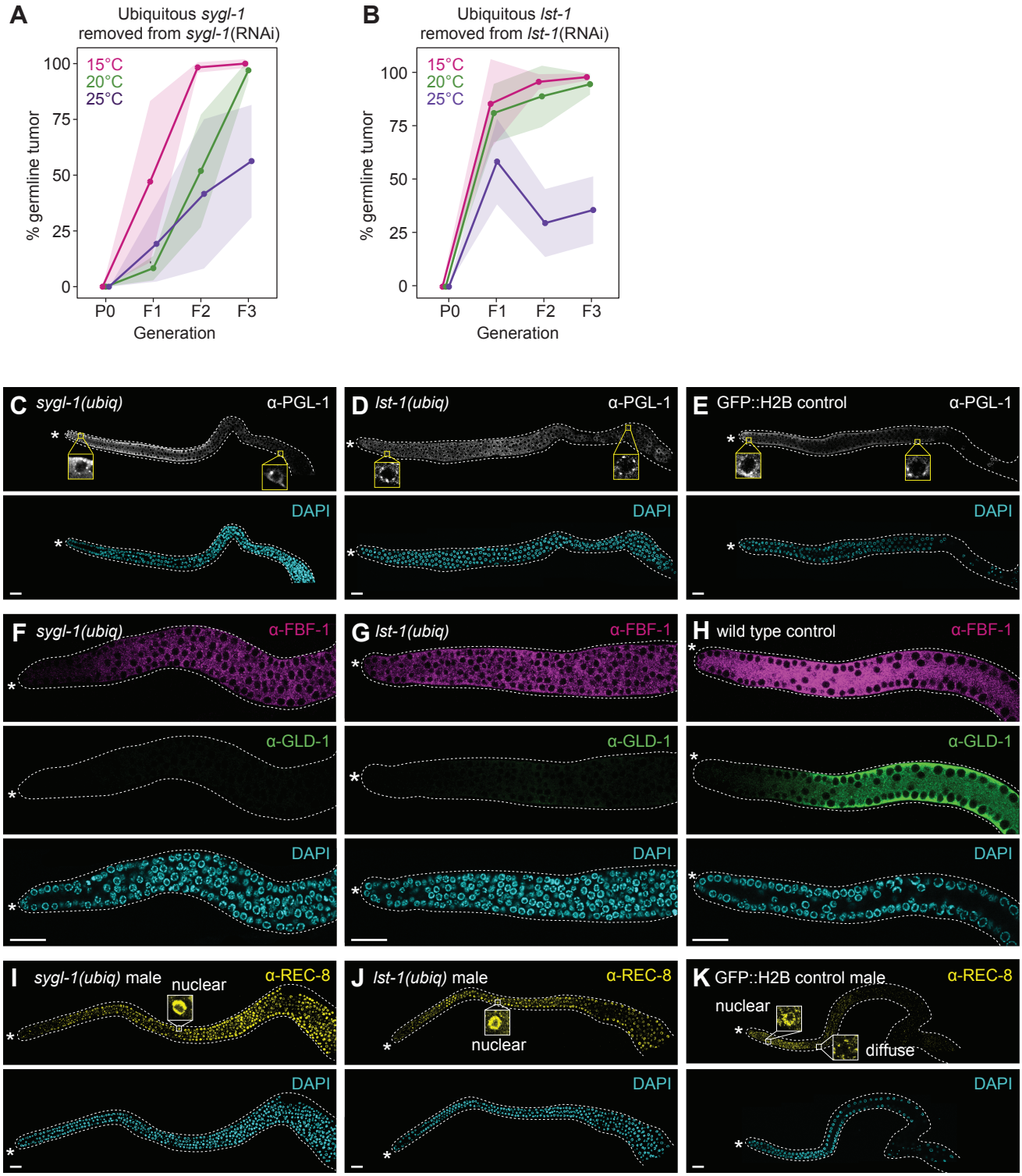

S4 Fig. Characterization of *sygl-1(ubiq)* and *lst-1(ubiq)* tumors. (**A and B**) Penetrance of germline tumors in consecutive generations after removal from RNAi and at indicated temperatures, 15°C (pink), 20°C (green), 25°C (purple). Germline tumors scored by dissecting microscope after removal from *sygl-1* RNAi (A) or *lst-1* RNAi (B). Dots, mean values from at least 5 independent experiments; shaded areas, standard deviations. (**C-H**) Images of dissected young adult gonads stained with α-PGL-1 (white), α-FBF-1 (magenta), α-GLD-1 (green), and DAPI (cyan), each a single z-slice. (**I-K**) Images of dissected young male gonads stained with α-REC-8 (yellow), and DAPI (cyan). Conventions as in **Fig 1E-1J**; genotypes as detailed in **Fig 3E-3J**; scale bar is 20 μm.

S5 Fig
Chapter 3

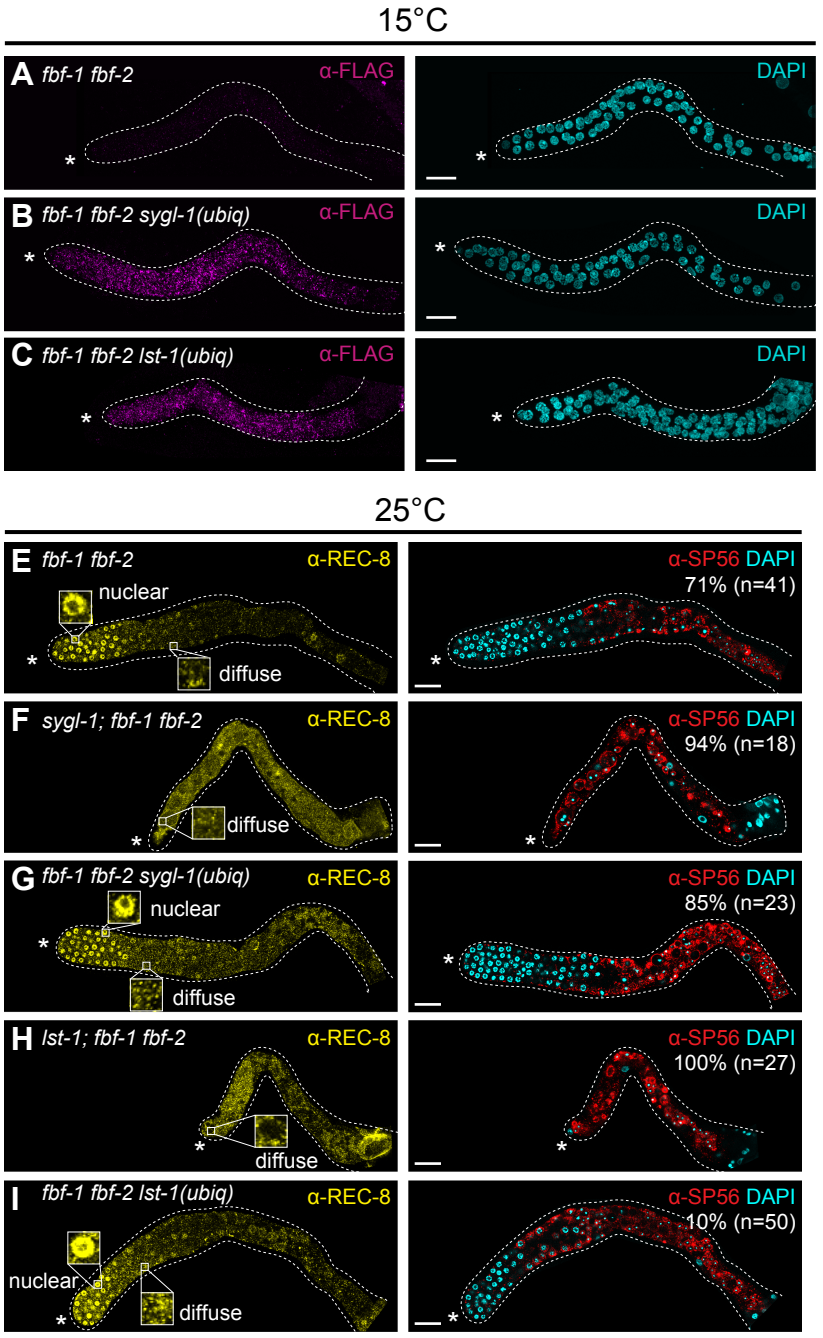

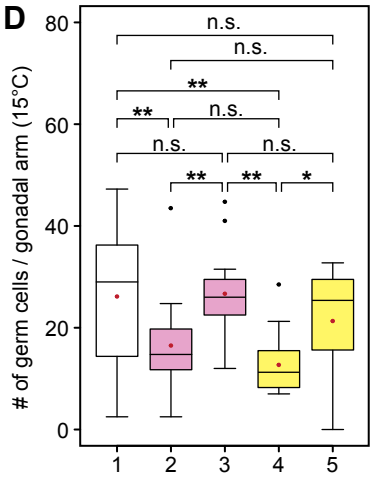

1 *fbf-1 fbf-2*
2 *sygl-1; fbf-1 fbf-2*
3 *sygl-1; fbf-1 fbf-2 sygl-1(ubiq)*
4 *lst-1; fbf-1 fbf-2*
5 *lst-1; fbf-1 fbf-2 lst-1(ubiq)*

J

Genetic background	% distal proliferation	% distal differentiation[3]	PZ size (cell rows)	n
fbf-1 fbf-2	71	29	6 ± 5	41
sygl-1; fbf-1 fbf-2	6	94	0 ± 1**	18
sygl-1; fbf-1 fbf-2 sygl-1(ubiq)[1]	85	15	8 ± 4 n.s.	23
lst-1; fbf-1 fbf-2	0	100	0 ± 0**	27
lst-1; fbf-1 fbf-2 lst-1(ubiq)[2]	10	90	3 ± 2 n.s.	50

** p<0.01
n.s. non-significant

[1] *qSi235[Pmex-5::3xFLAG::sygl-1::tbb-2* 3'end*]*
[2] *qSi267[Pmex-5::lst-1::3xFLAG::tbb-2* 3'end*]*
[3] Meiotic cells, primary spermatocytes, or mature sperm

S5 Fig. Characterization of SYGL-1 and LST-1 in *fbf-1 fbf-2 sygl-1(ubiq)* and *fbf-1 fbf-2 lst-1(ubiq)* strains. (**A-C**) Dissected third larval stage (L3) gonads grown at 15°C before sperm differentiation, stained with α-FLAG (magenta) and DAPI (cyan). Shown are maximum z-projection images. Conventions and genotypes are as in **Fig 4G-4I**; scale bar is 20 μm. (**D**) Total germ cell number per gonadal arm, in each genotype. Total number of sperm in each gonad was converted to the number of germ cells for simplicity (see Methods). Loss of either *sygl-1* or *lst-1* enhances the GSC defect of *fbf-1 fbf-2,* as previously reported [25]. That loss is rescued by *sygl-1(ubiq)* or *lst-1(ubiq),* confirming expression and functionality of SYGL-1 and LST-1 at 15°C. Box plot conventions as in **Fig 2F**. Averages and standard deviations for each genotype are as follows: (1) *fbf-1(ok91) fbf-2(q704)*, 26 ± 12, (n=27); (2) *sygl-1(tm5040); fbf-1(ok91) fbf-2(q704),* 17 ± 8 (n=22); (3) *sygl-1(tm5040); fbf-1(ok91) fbf-2(q704) qSi235[P_{mex-5}::3xFLAG::sygl-1::tbb-2 3'end],* 27 ± 8 (n=17); (4) *lst-1(ok814); fbf-1(ok91) fbf-2(q704),* 13 ± 8 (n=18); (5) *lst-1(ok814); fbf-1(ok91) fbf-2(q704) qSi267[P_{mex-5}:: lst-1::3xFLAG::tbb-2 3'end],* 21 ± 10 (n=20). Asterisks indicate a statistically significant difference by 1-way ANOVA with Tukey HSD *post hoc* test. ** p<0.001, * p<0.01, n.s.= non-significant. (**E-I**) Dissected young adult gonads raised at 25°C, stained with mitotic marker α-REC-8 (yellow), sperm marker α-SP56 (red), and DAPI (cyan). REC-8 localizes to the nucleus of mitotic germ cells but is diffuse in meiotic germ cells [30]. Conventions and genotypes are as in **Fig 4G-4I**; images are a single z-slice, scale bar is 20 μm. Germlines in *fbf-1 fbf-2* mutant adults can proliferate at 25°C, as previously reported [40]. Loss of either *sygl-1* or *lst-1* enhances the GSC defects of *fbf-1 fbf-2* [25; this work]. That loss is rescued by *sygl-1(ubiq)* or *lst-1(ubiq),* confirming expression and functionality of SYGL-1(ubiq) and LST-1(ubiq) at 25°C. Regardless, SYGL-1(ubiq) and LST-1(ubiq) do not generate germline tumors. (J) Summary of epistasis test with *fbf-1 fbf-2* at 25°C. Asterisks indicate a statistically significant difference by 1-way ANOVA with Tukey HSD *post hoc* test. ** p<0.01, n.s.= non-significant.

S6 Fig
Chapter 3

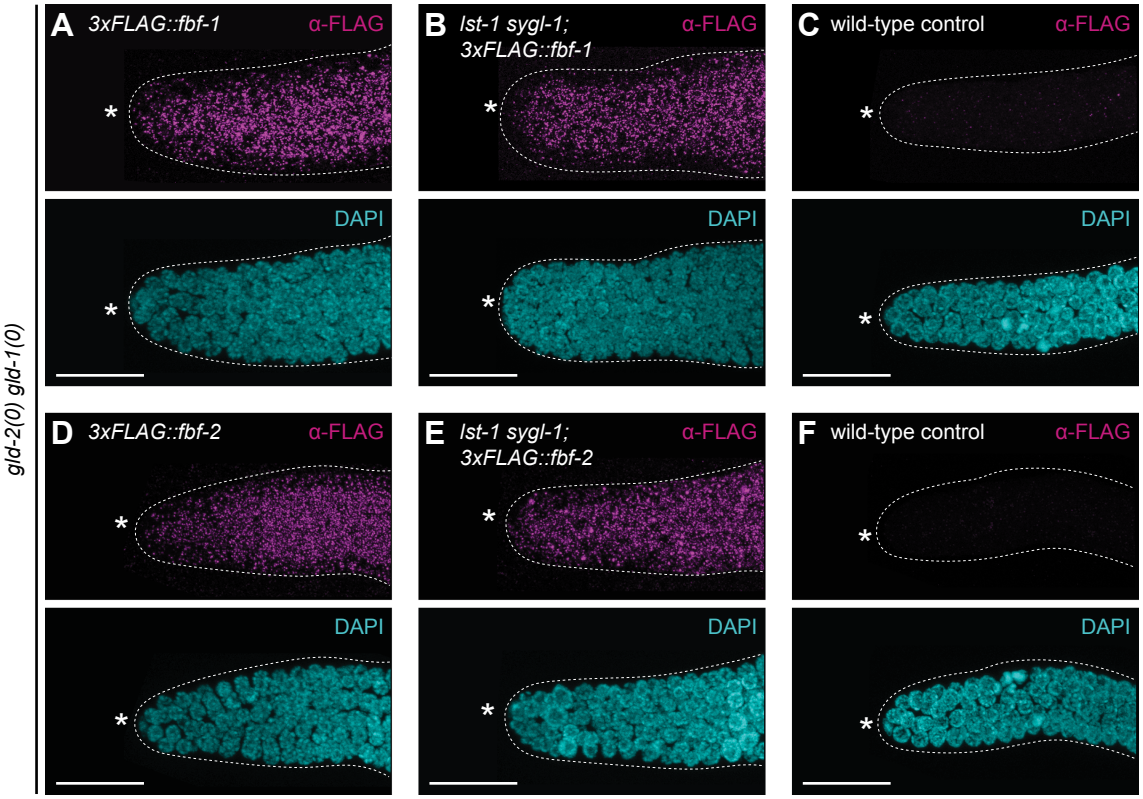

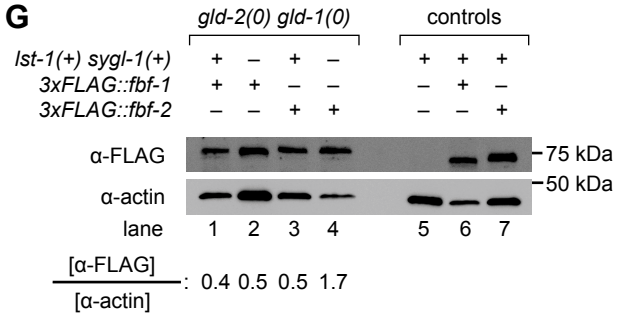

S6 Fig. *sygl-1* and *lst-1* are not required for FBF expression. (**A-F**) Dissected young adult gonads stained with α-FLAG (FBF-1 or FBF-2, magenta) and DAPI (cyan). FBF-1 (A-C) or FBF-2 (D-F) was measured with and without *sygl-1* and *lst-1*. All experiments were done in *gld-2 gld-1* tumorous germlines to compare cells in the same state. Genotypes: (A) *gld-2(q497) gld-1(q485); fbf-1(ok91) qSi232[P_{fbf-1}::3xFLAG::fbf-1::fbf-1 3'end]*. (B) *lst-1(ok814) sygl-1(tm5040) gld-2(q497) gld-1(q485); fbf-1(ok91) qSi232[P_{fbf-1}::3xFLAG::fbf-1::fbf-1 3'end]*. (C) wild type. (D) *gld-2(q497) gld-1(q485); fbf-2(q738) qSi75[P_{fbf-2}::3xFLAG::fbf-2::fbf-2 3'end]*. (E) *lst-1(ok814) sygl-1(tm5040) gld-2(q497) gld-1(q485); fbf-2(q738) qSi75[P_{fbf-2}::3xFLAG::fbf-2::fbf-2 3'end]*. (F) wild type. All images are maximum intensity z-projections. Conventions as in **Fig 1E-1J**; scale bar is 20 μm. (**G**) Western blots. Blot was probed with α-FLAG (FBF-1 or FBF-2) or α-actin, and the ratio between α-FLAG and α-actin was calculated. FBF-1 was expressed at similar abundance with and without SYGL-1 and LST-1, whereas a minor increase of FBF-2 was observed without SYGL-1 and LST-1. This minor effect may reflect indirect regulation between *sygl-1, lst-1* and *fbf-2,* perhaps a by-product of their role in the genetic circuity. Genotypes: (1) *gld-2(q497) gld-1(q485); fbf-1(ok91) qSi232[P_{fbf-1}::3xFLAG::fbf-1::fbf-1 3'end].* (2) *lst-1(ok814) sygl-1(tm5040) gld-2(q497) gld-1(q485); fbf-1(ok91) qSi232[P_{fbf-1}::3xFLAG::fbf-1::fbf-1 3'end]*. (3) *gld-2(q497) gld-1(q485); fbf-2(q738) qSi75[P_{fbf-2}::3xFLAG::fbf-2::fbf-2 3'end].* (4) *lst-1(ok814) sygl-1(tm5040) gld-2(q497) gld-1(q485); fbf-2(q738) qSi75[P_{fbf-2}::3xFLAG::fbf-2::fbf-2 3'end].* (5) wild type. (6) *fbf-1(ok91) qSi232[P_{fbf-1}::3xFLAG::fbf-1::fbf-1 3'end].* (7) *fbf-2(q738) qSi75[P_{fbf-2}::3xFLAG::fbf-2::fbf-2 3'end].*

S7 Fig
Chapter 3

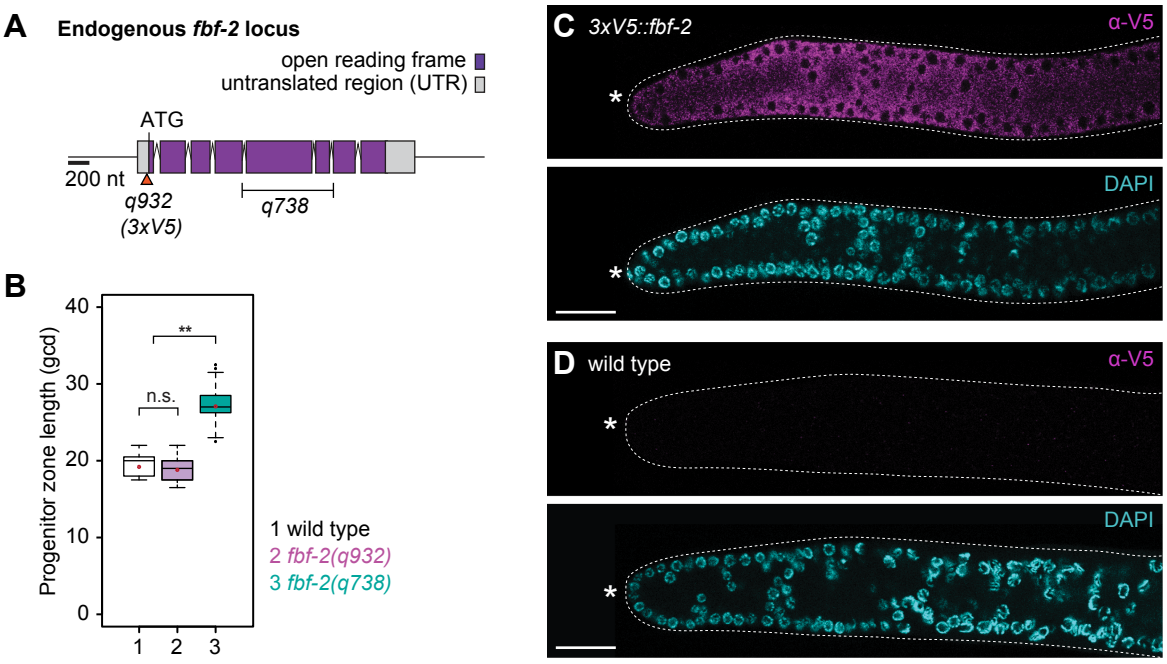

S7 Fig. 3xV5::FBF-2 is a functional protein. (**A**) Schematic of *fbf-2* endogenous locus. Conventions as in **Fig 1C**. 3xV5 epitope tag was inserted at the N-terminus of *fbf-2* to generate *fbf-2(q932).* The *fbf-2(q738)* deletion is a loss-of-function allele [81]. (**B**) Progenitor zone (PZ) lengths were measured in germ cell diameters from the distal end (gcd). The *fbf-2(q738)* deletion mutant has an increased PZ size, as previously reported [81]. The PZ length of *fbf-2(q932)* is indistinguishable from wild type; 3xV5::FBF-2 is therefore functional. Box plot conventions as in **Fig 2F**. Averages and standard deviations for each genotype are as follows: (1) wild type, 19 ± 2 (n=13); (2) *fbf-2(q932)*, 19 ± 2 (n=25); (3) *fbf-2(q738),* 27 ± 2 (n=35). Asterisks indicate a statistically significant difference by 1-way ANOVA with Tukey HSD *post hoc* test. ** $p<0.001$, n.s.= non-significant. (**C and D**) Images of distal gonads stained with α-V5 (FBF-2, magenta) and DAPI (cyan), each a single z-slice. Genotypes: *fbf-2(q932)* (C), wild type (D). Conventions as in **Fig 1E-1J**; scale bar is 20 μm.

S8 Fig
Chapter 3

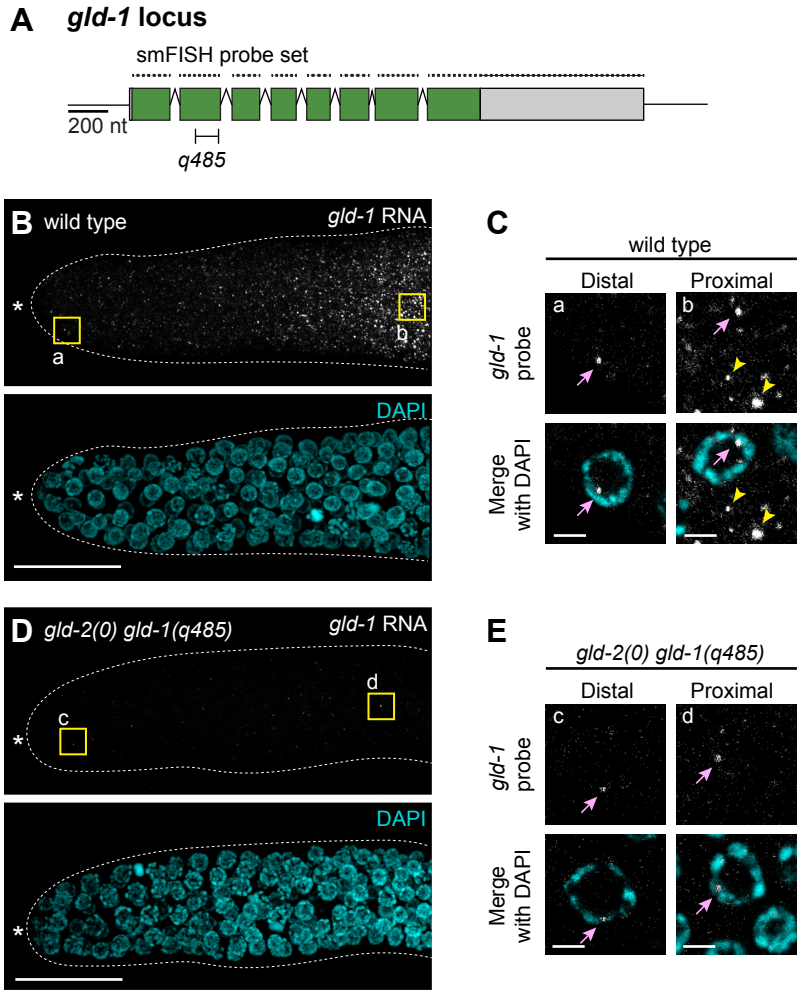

S8 Fig. *gld-1* smFISH probe set is specific to *gld-1* mRNA. (**A**) The *gld-1(q485)* deletion causes a frameshift and thus a null phenotype [45]. (**B-E**) Dissected gonads probed for *gld-1* smFISH probe (white) and DAPI (cyan). (B and C) wild type; (D and E) *gld-2(q497) gld-1(q485)*. (C and E) Boxed areas in B and D were magnified in C and E respectively to reveal *gld-1* nascent transcripts in the nucleus (pink arrows) and *gld-1* mature mRNAs in the cytoplasm (yellow arrowheads). Top, *gld-1* RNAs; Bottom, RNAs merged with DAPI. Images are maximum intensity z-projection (B and D), or a single slice (C and E). Conventions as in **Fig 1E-1J**; scale bar is 20μm (B and D) or 2 μm (C and E).

Table S1. Nematode strains used in this study

Name	Genotype	Reference
N2	wild type	*Brenner, 1974*
DG627	*emb-30(tn377ts) III*	*Furata et al, 2000*
EG4322	*ttTi5605 II; unc-119(ed3) III*	*Frøkjær-Jensen et al, 2008*
EG6699	*ttTi5605 II; unc-119(ed3) III*	*Frøkjær-Jensen et al, 2012*
EG6703	*unc-119(ed3) III; cxTi10816 IV; oxEx1582*	*Frøkjær-Jensen et al, 2012*
HT1593	*unc-119(ed3) III*	*Maduro and Pilgrim, 1995*
JA1515	*weSi2[P_{mex-5}::GFP::his-58::tbb-2 3'end] II; unc-119(ed3) III*	*Zeiser et al, 2011*
JK4299	*gld-2(q497) gld-1(q361) I/ hT2[qIs48](I;III)*	*This work*
JK4356	*lst-1(ok814) I*	*Singh et al, 2011*
JK4361	*lst-1(ok814) I; fbf-1(ok91) fbf-2(q704)/ mIn1[mIs14 dpy-10(e128)] II*	*This work*
JK4774	*lst-1(ok814) sygl-1(tm5040) I/ hT2[qIs48](I;III)*	*Kershner et al, 2014*
JK4836	*lst-1(ok814) I; qSi22[P_{lst-1}::lst-1::1xHA::lst-1 3'end] II*	*This work*
JK4852	*lst-1(ok814) sygl-1(tm5040) I; qSi22[P_{lst-1}::lst-1::1xHA::lst-1 3'end] II*	*This work*
JK4862	*glp-1(q46) III/ hT2[qIs48](I;III)*	*Kershner et al, 2014*
JK4942	*sygl-1(tm5040) I; qSi49[P_{sygl-1}::3xFLAG::sygl-1::sygl-1 3'end] II; unc-119(ed3) III*	*This work*
JK4950	*lst-1(ok814) I; ttTi5605 II; unc-119(ed3) III*	*This work*
JK4966	*sygl-1(tm5040) I; ttTi5605 II; unc-119(ed3) III*	*This work*
JK4996	*lst-1(ok814) I; qSi69[P_{lst-1}::lst-1::3xFLAG::lst-1 3'end] II; unc-119(ed3) III*	*This work*
JK5064	*sygl-1(tm5040) I; fbf-1(ok91) fbf-2(q704)/ mIn1[mIs14 dpy-10(e128)] II*	*This work*

JK5073	*lst-1(ok814) sygl-1(tm5040) I; qSi93[P$_{lst-1}$::lst-1::1xHA::lst-1 3'end] IV*	*This work*
JK5195	*sygl-1(tm5040) I; qSi150[P$_{sygl-1}$::3xFLAG::sygl-1::tbb-2 3'end] II; unc-119(ed3) III*	*This work*
JK5205	*lst-1(ok814) I; qSi93[P$_{lst-1}$::lst-1::1xHA::lst-1 3'end] IV*	*This work*
JK5233	*sygl-1(tm5040) I/ hT2[qIs48](I;III); qSi150[P$_{sygl-1}$::3xFLAG::sygl-1::tbb-2 3'end] II; emb-30(tn377ts) III/ hT2[qIs48](I;III)*	*This work*
JK5235	*sygl-1(tm5040) I/ hT2[qIs48](I;III); emb-30(tn377ts) III/ hT2[qIs48](I;III)*	*This work*
JK5263	*lst-1(ok814) sygl-1(tm5040) I/ hT2[qIs48](I;III); qSi150[P$_{sygl-1}$::3xFLAG::sygl-1::tbb-2 3'end] II; qSi93[P$_{lst-1}$::lst-1::1xHA::lst-1 3'end] IV*	*This work*
JK5277	*lst-1(q826) I/ hT2[qIs48](I;III)*	*This work*
JK5315	*lst-1(q826) sygl-1(tm5040) I/ hT2[qIs48](I;III)*	*This work*
JK5366	*sygl-1(tm5040) I; qSi235[P$_{mex-5}$::3xFLAG::sygl-1::tbb-2 3'end] II; unc-119(ed3) III*	*This work*
JK5401	*sygl-1(tm5040) I/ hT2[qIs48](I;III); qSi235[P$_{mex-5}$::3xFLAG::sygl-1::tbb-2 3'end] II; glp-1(q46) III/ hT2[qIs48](I;III)*	*This work*
JK5403	*lst-1(ok814) sygl-1(tm5040) I/ hT2[qIs48](I;III); qSi235[P$_{mex-5}$::3xFLAG::sygl-1::tbb-2 3'end] II*	*This work*
JK5411	*sygl-1(tm5040) I; fbf-1(ok91) fbf-2(q704) qSi235[P$_{mex-5}$::3xFLAG::sygl-1::tbb-2 3'end]/ mIn1[mIs14 dpy-10(e128)] II*	*This work*
JK5485	*lst-1(ok814) I; qSi267[P$_{mex-5}$::lst-1::3xFLAG::tbb-2 3'end] II; unc-119(ed3) III*	*This work*
JK5499	*sygl-1(q828) I; qSi49[P$_{sygl-1}$::3xFLAG::sygl-1::sygl-1 3'end] II*	*This work*
JK5500	*sygl-1(q828) I; qSi150[P$_{sygl-1}$::3xFLAG::sygl-1::tbb-2 3'end] II*	*This work*
JK5537	*lst-1(ok814) I; fbf-1(ok91) fbf-2(q704) qSi267[P$_{mex-5}$::lst-1::3xFLAG::tbb-2 3'end]/ mIn1[mIs14 dpy-10(e128)] II*	*This work*
JK5538	*lst-1(ok814) I/ hT2[qIs48](I;III); qSi267[P$_{mex-5}$::lst-1::3xFLAG::tbb-2 3'end] II; glp-1(q46) III/ hT2[qIs48](I;III)*	*This work*
JK5574	*sygl-1(tm5040) I; qSi297[P$_{mex-5}$::3xMYC::sygl-1::tbb-2 3'end] II; unc-119(ed3) III*	*This work*
JK5585	*lst-1(ok814) sygl-1(tm5040) I/ hT2[qIs48](I;III); qSi267[P$_{mex-5}$::lst-1::3xFLAG::tbb-2 3'end] II*	*This work*
JK5590	*lst-1(ok814) sygl-1(q828) I/ hT2[qIs48](I;III)*	*This work*
JK5600	*gld-2(q497) gld-1(q485) I/ hT2[qIs48](I;III); fbf-1(ok91) qSi232[P$_{fbf-1}$::3xFLAG::fbf-1::fbf-1 3'end] II*	*This work*
JK5602	*gld-2(q497) gld-1(q485) I/ hT2[qIs48](I;III); fbf-2(q738) qSi75[P$_{fbf-2}$::3xFLAG::fbf-2::fbf-2 3'end] II*	*This work*

JK5603	*gld-2(q497) gld-1(q485) lst-1(ok814) sygl-1(tm5040) I/ hT2[qIs48](I;III); fbf-1(ok91) qSi232[P$_{fbf-1}$::3xFLAG::fbf-1::fbf-1 3'end] II*	*This work*
JK5604	*gld-2(q497) gld-1(q485) lst-1(ok814) sygl-1(tm5040) I/ hT2[qIs48](I;III); fbf-2(q738) qSi75[P$_{fbf-2}$::3xFLAG::fbf-2::fbf-2 3'end] II*	*This work*
JK5621	*sygl-1(tm5040) I*	*This work*
JK5622	*sygl-1(q828) I*	*This work*
JK5623	*lst-1(ok814) sygl-1(tm5040) I; qSi49[P$_{sygl-1}$::3xFLAG::sygl-1::sygl-1 3'end] II*	*This work*
JK5624	*lst-1(ok814) sygl-1(q828) I; qSi49[P$_{sygl-1}$::3xFLAG::sygl-1::sygl-1 3'end] II*	*This work*
JK5625	*lst-1(ok814) sygl-1(q828) I; qSi150[P$_{sygl-1}$::3xFLAG::sygl-1::tbb-2 3'end] II*	*This work*
JK5656	*lst-1(ok814) sygl-1(tm5040) I; qSi150[P$_{sygl-1}$::3xFLAG::sygl-1::tbb-2 3'end] II*	*This work*
JK5760	*lst-1(ok814) sygl-1(q828) gld-2(q497) gld-1(q361) I/ hT2[qIs48](I;III)*	*This work*
JK5761	*sygl-1(q828) gld-2(q497) gld-1(q361) I/ hT2[qIs48](I;III)*	*This work*
JK5762	*lst-1(ok814) gld-2(q497) gld-1(q361) I/ hT2[qIs48](I;III)*	*This work*
JK5783	*sygl-1(tm5040) I; fbf-2(q931)[3xV5::fbf-2] qSi235[P$_{mex-5}$::3xFLAG::sygl-1::tbb-2 3'end] II*	*This work*
JK5842	*fbf-2(q932)[3xV5::fbf-2] II*	*This work*
JK5844	*sygl-1(tm5040) I; fbf-2(q932)[3xV5::fbf-2] qSi297[P$_{mex-5}$::3xMYC::sygl-1::tbb-2 3'end] II*	*This work*
JK5850	*sygl-1(q964)[3xMYC::sygl-1] I*	*This work*
JK5867	*lst-1(q826) sygl-1(q828) I/ hT2[qIs48](I;III)*	*This work*
JK5893	*sygl-1(q983)[3xOLLAS::sygl-1] I*	*This work*
JK5929	*lst-1(q1004)[lst-1::3xV5] I*	*This work*
JK5930	*lst-1(ok814) sygl-1(q964)[3xMYC::sygl-1] I*	*This work*
JK5934	*lst-1(q826) sygl-1(q828) I; qSi69[P$_{lst-1}$::lst-1::3xFLAG::lst-1 3'end] II*	*This work*
JK5937	*fog-3(q520) I/ hT2[qIs48](I;III); qSi235[P$_{mex-5}$::3xFLAG::sygl-1::tbb-2 3'end] II*	*This work*
JK5938	*fog-3(q520) I/ hT2[qIs48](I;III); qSi267[P$_{mex-5}$::lst-1::3xFLAG::tbb-2 3'end] II*	*This work*

JK5948	*lst-1(q1004)[lst-1::3xV5] sygl-1(tm5040) I*	*This work*
JK5968	*lst-1(ok814) sygl-1(q983)[3xOLLAS::sygl-1] I*	*This work*
JK5964	*lst-1(q1008)[lst-1::3xOLLAS] I*	*This work*
JK6002	*sygl-1(q1015)[sygl-1::1xV5] I*	*This work*
JK6008	*lst-1(ok814) sygl-1(q1015)[sygl-1::1xV5] I*	*This work*
JK6027	*lst-1(q1008)[lst-1::3xOLLAS] sygl-1(tm5040) I*	*This work*

Table S2. MosSCI transgenes generated in this study

Allele	Insert Description	Injected plasmid	Parent strain	Integration locus
qSi22	P_{lst-1}*::lst-1::1xHA::lst-1* 3'end	pJK1631	EG4322	*ttTi5605*
qSi49	P_{sygl-1}*::3xFLAG::sygl-1::sygl-1* 3'end	pJK1658	EG6699	*ttTi5605*
qSi69	P_{lst-1}*::lst-1::3xFLAG::lst-1* 3'end	pJK1692	JK4950	*ttTi5605*
qSi93	P_{lst-1}*::lst-1::1xHA::lst-1 3'end*	pJK1734	EG6703	*cxTi10816*
qSi150	P_{sygl-1}*::3xFLAG::sygl-1::tbb-2* 3'end	pJK1798	JK4966	*ttTi5605*
qSi235	P_{mex-5}*::3xFLAG::sygl-1::tbb-2* 3'end	pJK1873	JK4966	*ttTi5605*
qSi267	P_{mex-5}*::lst-1::3xFLAG::tbb-2* 3'end	pJK1898	JK4950	*ttTi5605*
qSi297	P_{mex-5}*::3xMYC::sygl-1::tbb-2* 3'end	pJK1897	JK4966	*ttTi5605*

Table S3. CRISPR alleles generated in this study

Allele	Description	Guide	Repair template	Parent strain	Method
q828	*sygl-1* null mutant	pJK1875 pJK1879 pJK1800	pJK1799	HT1593	Plasmid injection; Dickinson *et al* 2013
q931	*3xV5::fbf-2*	*fbf-2* crRNA N-term	*3xV5 fbf-2* oligo	JK5366	RNP co-CRISPR; Arribere *et al*, 2014, Paix *et al*, 2015
q932	*3xV5::fbf-2*	*fbf-2* crRNA N-term	*3xV5 fbf-2* oligo	JK5574	
q964	*3xMYC::sygl-1*	*sygl-1* crRNA N-term	pJK1926	wild type	
q983	*3xOLLAS::sygl-1*	*sygl-1* crRNA N-term	*3xOLLAS sygl-1* oligo	wild type	
q1004	*lst-1::3xV5*	*lst-1* crRNA C-term	*lst-1 3xV5* oligo	wild type	
q1008	*lst-1::3xOLLAS*	*lst-1* crRNA C-term	*lst-1 3xOLLAS* oligo	wild type	
q1015	*sygl-1::1xV5*	*sygl-1* crRNA C-term	*sygl-1 1xV5* oligo	JK5921[a]	

[a] Aoki ST and Kimble J (in preparation)

Table S4. Plasmids used to generate CRISPR and MosSCI transgenes

Plasmid	Insert Description	Cloning sites	Vector Backbone
pJK1631	P_{lst-1} (~2.6kb)*::lst-1::1xHA::lst-1* 3'end (~0.6kb)	*Bss*H II	pCFJ151
pJK1658	P_{sygl-1} (~2kb)*::3xFLAG::sygl-1::sygl-1* 3'end (~0.8kb)	*Spe* I	pCFJ151
pJK1692	P_{lst-1} (~2.6kb)*::lst-1::3xFLAG::lst-1* 3'end (~0.6kb)	*Spe* I	pCFJ151
pJK1734	P_{lst-1} (~2.6kb)*::lst-1::1xHA::lst-1* 3'end (~0.6kb)	*Xba* I *Bss*H II	pCFJ151
pJK1798	P_{sygl-1} (~2kb)*::3xFLAG::sygl-1::tbb-2* 3'end (~0.3kb)	*Spe* I	pCFJ151
pJK1799	*sygl-1* upstream homology (~1.6kb)*::loxP::* $P_{unc-119}$*::Cbr_unc-119::unc-119* 3'UTR*::loxP*:: *sygl-1* downstream homology (~1.6 kb)	*Xma* I	pUC19
pJK1873	P_{mex-5} (~0.5kb)*::3xFLAG::sygl-1::tbb-2* 3'end (~0.3kb)	*Spe* I	pCFJ151
pJK1875	Sequence targeting *sygl-1* loci (5'-agatttcgactaacaactc-3') joined with sgRNA scaffold from pDD162 [a]	*Xma* I	pUC19
pJK1879	Sequence targeting *sygl-1* loci (5'-tttattttcgcaagcacgg-3') joined with sgRNA scaffold from pDD162 [a]	*Xma* I	pUC19
pJK1800	Sequence targeting *sygl-1* loci (5'-gtaactgtggagaccaaat-3') joined with sgRNA scaffold from pDD162 [a]	*Xma* I	pUC19
pJK1898	P_{mex-5} (~0.5kb)*::lst-1::3xFLAG::tbb-2* 3'end (~0.3kb)	*Spe* I	pCFJ151
pJK1897	P_{mex-5} (~0.5kb)*::3xMYC::sygl-1::tbb-2* 3'end (~0.3kb)	*Spe* I	pCFJ151
pJK1926	P_{sygl-1} (~2kb)*::3xMYC::sygl-1::sygl-1* 3'end (~0.8kb)	*Spe* I	pCFJ151

[a] Dickinson *et al* (2013)

Table S5. Sequences of crRNA and repair oligos used to generate CRISPR alleles

Name	Sequence[1,2,3]
sygl-1 crRNA N-term	5'-AUGGAAUGGCAUUAUGCACGGUUUUAGAGCUAUGCU-3'
sygl-1 crRNA C-term	5'-CUACUGCAAAUAAUAGCUGUGUUUUAGAGCUAUGC-3'
lst-1 crRNA C-term	5'-UCCAGUCUAAGCAAUAAAAUGUUUUAGAGCUAUGCU-3'
fbf-2 crRNA N-term	5'-UCGUUCUGCGCAUCUUUGAUGUUUUAGAGCUAUGCU-3'
3xOLLAS sygl-1 oligo	5'-gtgatccatgtagagttttggataatggaatggCTTTCCCATAAGGCGTGGTCCGA GCTCGTTGGCGAATCCAGACTGCTTTCCCATGAGGCGTGGTCCGAG CTCGTTGGCGAATCCAGACTGCTTTCCCATAAGGCGTGGTCCAAGC TCGTTAGCGAATCCGGAcattatgcacgtggcgtgatgacaatggttcgatg-3'
sygl-1 1xV5 oligo	5'-gaacaacaacacttcactgatgatgggctc**T**aacagctattatttgcagGGTAAGCCTAT CCCTAACCCTCTCCTCGGTCTAGATAGTACTGGAGGATCCtagagcgta cttgctcttttaaattttctaatcc-3'
lst-1 3xV5 oligo	5'-caaatgggacacgctcgaaatgttccagtcGGTAAGCCTATCCCTAACCCTCTC CTCGGTCTAGATAGTACTGGAAAGCCAATCCCAAACCCACTCCTCG GACTTGATAGCACCGGTAAGCCTATCCCTAACCCACTCCTCGGACTT GATAGCACCtaagcaataaaattggtttaaatatcaattaatttatattttac-3'
lst-1 3xOLLAS oligo	5'-tataaattaattgatatttaaaccaattttattgcttaCTTTCCCATAAGGCGTGGTCCG AGCTCGTTGGCGAATCCAGACTGCTTTCCCATGAGGCGTGGTCCGA GCTCGTTGGCGAATCCAGACTGCTTTCCCATAAGGCGTGGTCCAAG CTCGTTAGCGAATCCGGAgactggaacatttcgagcgtgtcccatttg-3'
3xV5 fbf-2 oligo	5'-tcattctaataaaattatcaactaatcgacatgGGTAAGCCTATCCCTAACCCTCT CCTCGGTCTAGATAGTACTGGAAAGCCAATCCCAAACCCACTCCTC GGACTTGATAGCACCGGTAAGCCTATCCCTAACCCACTCCTCGGAC TTGATAGCACCga**T**caatcaaagatgcgcagaacgaatcagttcagaaaagt-3'

1. Upper case letters indicate inserted sequences
2. Lower case letters indicate homology arms

Bold letters indicate mutations incorporated

Chapter 4

Conclusions and Future Directions

The goal of my thesis was to understand the molecular basis of stem cell self-renewal. To this end, I investigated the regulation of *C. elegans* germline stem cells (GSCs), which provide a tractable paradigm of stem cells maintained in a stochastically dividing population. Specifically, my work focused on the identification and characterization of two novel downstream targets of GLP-1/Notch signaling from the niche, *sygl-1* and *lst-1*. Investigation of SYGL-1 and LST-1 revealed two important aspects of stem cell self-renewal in the *C. elegans* germline. Here I summarize key findings, address future directions, and offer some speculations.

4.1. Conclusions

A. SYGL-1 and LST-1 are major effectors of Notch signaling from the niche

A long-standing concept in the stem cell field is that signaling from the niche determines stem cell self-renewal. Yet, how niche signaling promotes the stem cell state has not been understood in great depth. My thesis work reveals the key downstream targets of niche signaling that govern the stem cell state. In the *C. elegans* germline, *sygl-1* and *lst-1* are key Notch signaling targets that are not only required, but sufficient for GSC self-renewal [1, 2]. SYGL-1 and LST-1 are cell-autonomous regulators that are expressed in a subset of cells in the progenitor zone; their highly restricted expression governs stem cell pool size [1, 2]. In addition, *sygl-1* and *lst-1* work redundantly to maintain the stem cell state; their functional redundancy underscores the biological robustness [1]. Collectively, SYGL-1 and LST-1 are the pivotal effectors of niche signaling that are responsible for GSC maintenance and demonstrate that niche signaling can drive stem cell self-renewal by activating key downstream effectors.

B. *sygl-1* and *lst-1* are molecular links between Notch signaling and PUF RNA repression

Another long-standing question in the stem cell field is how extrinsic signaling from the niche is connected to intrinsic stem cell regulators. In the *C. elegans* germline, Notch signaling from the niche and PUF family of RNA binding proteins drive the stem cell state [3, 4], yet the link between the two was largely unknown. The discovery of *sygl-1* and *lst-1* provide this molecular link and demonstrate how niche signaling modulates cell-intrinsic RNA regulatory network. SYGL-1 and LST-1 encode novel proteins that are distinct from each other, largely composed of low-complexity sequences [1]. Both proteins require FBF for their stem cell function, physically interact with FBF, and are required for the repression of a well-established FBF target mRNA at the post-transcriptional level [2]. From these lines of evidence, I propose that both proteins are involved in mRNA repression, as trans-acting PUF regulatory proteins. Therefore, spatial restriction of SYGL-1 and LST-1 likely limit FBF RNA repression activity to the distal-most germ cells, and the regulation of this molecular complex likely maintains a balanced GSC pool size.

4.2. Remaining research questions

Several questions remain unsolved despite the identification of SYGL-1 and LST-1 as critical stem cell regulators. Three key questions remain to be addressed. First, what restricts SYGL-1 and LST-1 to the distal-most pool of cells? Studying the mechanism(s) of their spatial restriction will provide regulatory insights into stem cell fate decision, as extents of both proteins govern the stem cell pool size. Second, how do SYGL-1 and LST-1 repress mRNA? Understanding their mechanism of mRNA repression will likely reveal novel insights into RNA regulation, as both encode novel proteins. Finally, how does stem cell pool, represented by positive SYGL-1 or LST-1 cells, respond to various physiological and environmental inputs? As

stem cell pool responds to tissue damage, understanding the kinetics of stem cell pool under different stress conditions will have profound consequence in regenerative biology. Here I suggest some future directions and offer some speculations.

4.2.1. What controls SYGL-1 and LST-1 spatial restriction?

A. Develop a quantitative assay to determine *sygl-1* and *lst-1* expression levels

One major future direction is to understand the molecular mechanism underlying SYGL-1 and LST-1 spatial restriction. Answers to this question will offer insights into the size regulation of the GSC pool in normal conditions, and will provide the basis for future exploration of the GSC pool upon tissue damage and stress. Two types of experiments would be informative. The first is to elucidate *cis*-regulatory regions responsible for the spatial restriction; the other is to identify *trans*-acting factors that control the *cis*-regulatory regions. Various biochemical or molecular techniques will be needed, because multiple regulatory mechanisms are likely involved. Here I describe one possible genetic and cell biological approach, focusing on *sygl-1*.

To probe *sygl-1* regulation at multiple levels, one critical step is to establish a quantitative assay to measure *sygl-1* mRNA and protein. Key reagents have been described [2, 5] but could be improved to measure *sygl-1* mRNA and protein in a high-throughput manner. To this end, one could develop a fluorescently-tagged *sygl-1* allele for live-cell imaging purposes and couple this with rapid *in situ* hybridization methods (e.g. TurboFISH [6]), to directly visualize mRNA and protein in the same gonad. Recent advancements in genome editing [7], high sensitivity small molecular tags [8-10], and semi-automated quantitation [5, 11] could be employed to quantitate *sygl-1* mRNA and protein in a high-throughput scale with improved precision.

B. Structure–Function studies to identify *cis*-regulatory regions

The key next step is to identify *cis*-regulatory regions involved in *sygl-1* spatial restriction, using the quantitative method developed above. Multiple regulatory mechanisms are likely involved including DNA, mRNA, and protein, but a candidate approach focusing on *sygl-1* 3'untranslated region (UTR) may be the starting point because *sygl-1* 3' UTR is implicated in *sygl-1* spatial restriction [2]. This region harbors potential binding sites for miRNA and RNA binding proteins (e.g. FBF [12], GLD-1 [13], and Poly C binding protein [14]), which can be explored further *in vitro*, or *in vivo*. At the protein level, multiple *in silico* tools (e.g. SLiM [15]) can be utilized to investigate the role of potential short interaction motifs and phosphorylation sites within SYGL-1. In a complementary approach, systemic mapping experiments could identify regions involved in spatial restriction, both at the mRNA and protein levels. For this approach, truncation boundaries guided by conservation (e.g.[16]) could be useful, as critical residues are likely conserved in other Caenorhabditis. Next, potential regions could be mutated *in vivo* to assay functional and molecular outcomes. A critical mutation or truncation will likely change *sygl-1* mRNA or protein levels, accompanied by phenotypic changes in the GSC pool.

C. A genetic screen to identify *trans*-regulatory factors

Next, *trans*-acting factors that restrict *sygl-1* expression need to be identified to fully understand the molecular basis of the spatial restriction. The nature of the *cis*-regulatory elements identified above will inevitably guide future experiments, but here I describe one approach—genetic screens to identify factors that change *sygl-1* spatial distribution in the distal gonad. A fluorescently tagged *sygl-1* allele coupled with high-throughput quantitation will prove essential for the screen. *C. elegans* is a great model system for this unbiased genetic approach: life cycle is short [17], RNAi feeding library covers 87% of the genome [18], and gene mapping tools are well established [19, 20]. Since this is an unbiased approach, a genetic screen may identify novel regulators involved in stem cell fate decision. However, one potential caveat is

that factors identified in the genetic screen may be indirect regulators of *sygl-1*, or pervasive redundancy in the biological system may hinder identifying novel regulators.

D. Broad implications and speculations

Spatial control is a broad principle underlying cell fate control, cell cycle regulation, and pattern formation [21]. Therefore, regulatory insights learned from *sygl-1* spatial restriction will likely have broad implications in animal development, especially in tissues sharing common cytoplasm. Spatial control is seen both in multi-nucleate and single-nucleated cells [21], but the underlying patterning strategies may be common. For example, spatial patterning in multi-nucleate cells have uncovered elaborate transcriptional factors and RNA binding proteins (e.g. *Drosophila* embryo patterning [22]; *A. gossypii* cell cycle regulation [23]) whose regulatory theme permeates broad animal development. Therefore, studying the spatial regulation of *sygl-1* may reveal regulatory insights broadly applicable to animal development, and may also reveal insights into Notch target regulation in stem cells.

4.2.2. How do SYGL-1 and LST-1 regulate PUF activity?

A. Identification of the binding interface between FBF and SYGL-1/LST-1

The second major future direction is to understand the molecular mechanism of SYGL-1 and LST-1 in stem cell self-renewal. I have proposed that their physical binding to the PUF protein FBF is central to solving this mechanism; the remaining question is to address how they regulate FBF activity. Addressing this regulatory relationship would provide mechanistic insights into the regulation of PUF proteins and the mechanism of RNA repression within stem cells.

The first step is to map the interaction region between SYGL-1/FBF, or LST-1/FBF. Identification of the binding interface between SYGL-1/FBF, or LST-1/FBF would allow us to test the *in vivo* significance of this binding. Key questions are as follows: Do SYGL-1 and LST-1

interact with FBF in the same region? How is this region similar to, or different from the binding interface for other PUF regulatory protein partners? Since NOS-3 and GLD-3 are previously identified binding partners of FBF [24-26] whose biological functions are opposite to SYGL-1 and LST-1 [27, 28], answers to these questions may generate molecular insights into the cell fate transition. For example, SYGL-1 and LST-1 may compete with NOS-3 or GLD-3 for FBF binding to drive FBF into its repressive mode for stem cell self-renewal; NOS-3 or GLD-3 may compete with SYGL-1 or LST-1 for FBF binding to drive FBF into its activating mode to promote differentiation.

To this end, *in vitro* mapping experiments may be a tractable starting point. As demonstrated in Chapter 3, yeast two hybrid assays are a fast and robust way to map the binding region between SYGL-1/FBF, and LST-1/FBF. For SYGL-1 and LST-1, several truncations could be generated and tested, prioritizing the conserved regions identified through homology. On the FBF side, several published point mutants or truncations can be tested [26, 29], or chimeric PUF proteins that combine FBF and non-interacting PUF could be utilized to make an educated guess on the binding interface [30]. As a parallel approach, *in vitro* pull-down or circular dichroism experiments can be done with recombinant SYGL-1, LST-1, and FBF to understand the binding kinetics. Attempts to purify full-length recombinant SYGL-1 and LST-1 have not been successful to date, but efforts to purify truncated versions using different expression strategies may be fruitful (e.g. co-expression with FBF, or using insect cells). Successful purification of recombinant proteins will permit us to determine the structure of FBF/SYGL-1 or FBF/LST-1 with X-ray crystallography, which will reveal an atomic resolution of the interaction.

Next, functional significance of the binding must be queried *in vivo*. To this end, interaction residues identified in yeast two hybrid assays, or in X-ray structure could be mutated *in vivo*. Loss-of-function phenotypes (i.e. decreased GSC pool size) can occur if the identified residues are indeed important and mediate interaction *in vivo;* gain-of-function phenotypes (i.e.

increased GSC pool size) may occur if the identified residues are mutated to increase the binding affinity. Together, *in vitro* and *in vivo* structure-function studies will prove useful to explore the SYGL-1/FBF and LST-1/FBF relationships to the next level.

B. Functional significance of SYGL-1/FBF or LST-1/FBF complex

Another outstanding question is how SYGL-1 and LST-1 work with FBF to repress mRNA. Here I discuss two potential models to approach this problem, which are not mutually exclusive.

Model 1: Ribonucleoprotein (RNP) granules assembly

One hypothesis is that SYGL-1 and LST-1 recruit FBF to functional sites of RNA repression. Indeed, LST-1 localizes to perinuclear granules and SYGL-1 localizes to cytoplasmic puncta [2], and these cellular foci may represent sites of mRNA repression. Thus, understanding the nature of these foci remains a critical next step. To date, several cellular compartments have been implicated in RNA repression [31] but the mechanism of RNA repression in these compartments remains largely unknown.

In the *C. elegans* germline, P-granules are arguably the best understood sites of RNA regulation; several RNA binding proteins and translational initiation factors localize to P-granules [31, 32]. Indeed, a significant fraction of FBF-2 also localizes to P-granules [33], but it is unknown whether these perinuclear granules are required for FBF mediated RNA repression. One possibility is that P-granules are a storage place to sequester mRNA and RNA binding proteins. Alternatively, P-granules may represent functional sites of mRNA repression. Thus, one tractable experiment to begin to investigate this hypothesis is to ask whether SYGL-1 or LST-1 cellular foci overlap with P-granule markers, and if so, identify regions in SYGL-1 or LST-1 involved in granule assembly.

Two experimental approaches are possible to test this idea. The first approach is to visualize SYGL-1/FBF and LST-1/FBF molecular complex *in vivo,* and ask where these

interactions occur in the GSC pool. To this end, molecular visualization methods could be developed (e.g. proximity ligation assay [34], FRET [35]). The second approach is to track *gld-1* mRNA, a well-established target of FBF, to visualize sites of FBF repression. Recent advancements in RNA visualization techniques allow tracking mRNAs from synthesis to decay through live-cell imaging [36]; these methods are also actively developed in *C. elegans* and now possible (Appendix D). Once these sites of mRNA decay are established, one can ask if SYGL-1 or LST-1 localize to such sites, or recruit FBF to such sites for mRNA repression.

Model 2: 3' end mRNA regulation

Another hypothesis is that SYGL-1 and LST-1 are directly involved in 3'end regulation. Two observations support this model: The first is SYGL-1 and LST-1 can physically associate with FBF [2]. The second is that SYGL-1 can repress expression of a tethered transcript *in vivo* (Appendix A). Still, this model remains to be vigorously tested. Critical next steps include the identification of the molecular machinery that work with either SYGL-1 or LST-1 to repress mRNA, and elucidating the nature of target mRNAs being regulated.

A conserved molecular mechanism of PUF proteins is recruiting the deadenylase complex to repress target mRNAs [37]. To date, mechanism of FBF repression of target mRNAs have been linked to two molecular complexes. The first is the CCR-4/NOT deadenylation complex [38], and the other is the CSR-1/EFT-3 Argonuate/translation elongation factor complex that can attenuate translation elongation [39]. Regardless, neither has been demonstrated *in vivo* in the context of stem cell maintenance. Furthermore, a double depletion of deadenylase and Argonuate (i.e. *ccf-1; csr-1* mutant) does not recapitulate the Fbf or Glp stem cell loss phenotypes, suggesting that additional mechanisms underlie FBF stem cell maintenance (Kimble lab, unpublished observations).

Therefore, I hypothesize that SYGL-1 and LST-1 mediated mRNA repression may involve these two candidate molecular complexes, but likely involve additional regulators. To identify these complexes, proteins that co-purify with either SYGL-1 or LST-1 could be identified

by immunoprecipitation followed by mass-spectrometry. The *sygl-1* or *lst-1* germline tumors [2], or *glp-1(gf)* tumors may be useful to get enough quantity of proteins. Alternatively, a suppressor genetic screen could be performed using *sygl-1* or *lst-1* germline tumors to identify factors required for SYGL-1 and LST-1 stem cell activity. Candidate molecules identified in these approaches must be further tested *in vivo* to ask whether they are indeed required for mRNA repression.

Finally, what is the identity of regulated mRNAs? SYGL-1 or LST-1 may directly associate with mRNAs, or regulate them via FBF. One possibility is that SYGL-1 and LST-1 regulate FBF associated target mRNAs, but they may preferentially associate with some targets to regulate stem cell self-renewal. To this end, cross-linking immunoprecipitation (CLIP) or mRNA tagging approaches can be used to identify SYGL-1 or LST-1 associated mRNAs [40]; Alternatively, *in vitro* methods such as SELEX (Systemic Evolution of Ligands by Exponential Enrichment) could be utilized to ask if SYGL-1 and LST-1 can change the kinetics and binding of FBF to FBF binding elements [41]. Next logical questions would be to identify binding elements (if any), measure binding kinetics, and understand the mechanism of target selection.

C. Broad implications and speculations

Post-transcriptional regulation is critical for many aspects of biology including stem cell self-renewal. SYGL-1 and LST-1 are low-complexity proteins that are critical for stem cell self-renewal. Emerging views on intrinsically disordered proteins reveal that a liquid-like phase transition is a driving force for RNP granule assembly [42, 43]; One speculative idea is that low complexity regions of SYGL-1 and LST-1 mediate RNA repression, by increasing the local concentration of proteins involved in this process. Thus, understanding how SYGL-1 and LST-1 can regulate PUF proteins may unravel mechanistic insights into RNP granule formation and RNA regulation.

Given that multiple mechanisms remain plausible for SYGL-1 and LST-1 molecular functions, SYGL-1 and LST-1 act similarly or differently at the molecular level. Regardless, I favor this idea that SYGL-1 and LST-1 represent two novel mechanisms of mRNA regulation based on two following observations: First, SYGL-1 and LST-1 encode molecularly distinct proteins. Second, they perform non-redundant functions in sex-determination despite their redundancy in stem cell self-renewal (Appendix C), suggesting that these two gene products are not identical. Perhaps, two molecularly distinct proteins have evolved to function redundantly to work with PUF proteins to provide biological robustness in stem cell maintenance.

4.2.3. How is stem cell pool controlled under different physiological conditions?

A. SYGL-1 and LST-1 as molecular markers to investigate GSC pool

The last major future direction is to utilize SYGL-1 or LST-1 as molecular markers of stem cells to understand the behavior of GSC pool during normal development and regeneration. To date, methods to investigate the *C. elegans* GSCs have been limited to using several differentiation markers, or using a cell-cycle defective mutant to resolve the stem cell pool within mitotic progenitors [44, 45]. The discovery of SYGL-1 and LST-1 will provide additional molecular readouts to examine the GSC pool, as a counterpart to well-established markers available for differentiating germ cells [46].

One important task is to characterize the kinetics of GSC pool during multiple stages of development. Previous analyses examined all cells within progenitor zone and revealed similar proliferative kinetics during development [44], yet it remains unknown whether the GSC pool size remains constant during development. Specific questions include whether the GSC pool can expand during tissue growth, and shrink in response to stress or aging. Further, similar analyses could be done on male GSCs to understand sexually dimorphic GSCs. Previous

analyses identified different cell cycle speed between the two sexes [47], yet it remains unknown whether germline sex affects the GSC pool size *per se*.

Last but not least, another important task is to examine the GSC pool during stress and regeneration using SYGL-1 and LST-1 as stem cell markers. Stem cells survive under different physiological or environmental conditions, such as malnutrition, stress, and pathogenesis [48]. *C. elegans* GSCs are also maintained during such conditions as starvation [49, 50], but the molecular mechanism of this tissue plasticity remains largely unknown. Such analyses will be fundamental to understand the stem cell homeostasis during development and aging. For example, one can investigate whether different physiological stimuli directly stabilize SYGL-1 and LST-1 during extreme stress to maintain the GSC pool [51], and increase SYGL-1 and LST-1 abundance to expand the stem cell pool size during tissue growth and regeneration.

B. Broad implications and speculations

Addressing how stem cells are maintained under diverse physiological conditions is fundamental to understanding tissue development, regeneration, and aging. *C. elegans* GSCs are an excellent model to approach these questions. I propose that SYGL-1 and LST-1 can serve as key molecular readouts of GSC pool, and speculate that multiple physiological conditions can regulate SYGL-1 and LST-1 stability to control the stem cell pool size during development and regeneration. Lessons learned from this system will likely have broadly applicable lessons as similar principles likely govern metazoan stem cells.

References

1. Kershner AM, Shin H, Hansen TJ, Kimble J. Discovery of two GLP-1/Notch target genes that account for the role of GLP-1/Notch signaling in stem cell maintenance. Proc Natl Acad Sci U S A. 2014;111(*10*):3739-44. doi: 10.1073/pnas.1401861111. PubMed PMID: 24567412; PubMed Central PMCID: PMC3956202.

2. Shin H, Haupt KA, Kershner AM, Kroll-Conner P, Wickens M, Kimble J. SYGL-1 and LST-1 link niche signaling to PUF RNA repression for stem cell maintenance in *Caenorhabditis elegans*. PLoS Genet. 2017;13(12):e1007121. Epub 2017/12/13. doi: 10.1371/journal.pgen.1007121. PubMed PMID: 29232700.

3. Austin J, Kimble J. *glp-1* is required in the germ line for regulation of the decision between mitosis and meiosis in *C. elegans*. Cell. 1987;51(4):589-99. PubMed PMID: 3677168.

4. Crittenden SL, Bernstein DS, Bachorik JL, Thompson BE, Gallegos M, Petcherski AG, *et al*. A conserved RNA-binding protein controls germline stem cells in *Caenorhabditis elegans*. Nature. 2002;417(6889):660-3. doi: 10.1038/nature754. PubMed PMID: 12050669.

5. Lee C, Sorensen EB, Lynch TR, Kimble J. *C. elegans* GLP-1/Notch activates transcription in a probability gradient across the germline stem cell pool. Elife. 2016;5. doi: 10.7554/eLife.18370. PubMed PMID: 27705743; PubMed Central PMCID: PMC5094854.

6. Shaffer SM, Wu MT, Levesque MJ, Raj A. Turbo FISH: a method for rapid single molecule RNA FISH. PLoS One. 2013;8(9):e75120. Epub 2013/09/26. doi: 10.1371/journal.pone.0075120. PubMed PMID: 24066168; PubMed Central PMCID: PMC3774626.

7. Paix A, Folkmann A, Seydoux G. Precision genome editing using CRISPR-Cas9 and linear repair templates in *C. elegans*. Methods. 2017;121-122:86-93. Epub 2017/04/11. doi: 10.1016/j.ymeth.2017.03.023. PubMed PMID: 28392263.

8. Thorn K. Genetically encoded fluorescent tags. Mol Biol Cell. 2017;28(7):848-57. Epub 2017/04/01. doi: 10.1091/mbc.E16-07-0504. PubMed PMID: 28360214; PubMed Central PMCID: PMC5385933.

9. Kamiyama D, Sekine S, Barsi-Rhyne B, Hu J, Chen B, Gilbert LA, *et al*. Versatile protein tagging in cells with split fluorescent protein. Nat Commun. 2016;7:11046. Epub 2016/03/19. doi: 10.1038/ncomms11046. PubMed PMID: 26988139; PubMed Central PMCID: PMC4802074.

10. Lotze J, Reinhardt U, Seitz O, Beck-Sickinger AG. Peptide-tags for site-specific protein labelling in vitro and *in vivo*. Mol Biosyst. 2016;12(6):1731-45. Epub 2016/03/11. doi: 10.1039/c6mb00023a. PubMed PMID: 26960991.

11. Mueller F, Senecal A, Tantale K, Marie-Nelly H, Ly N, Collin O, *et al.* FISH-quant: automatic counting of transcripts in 3D FISH images. Nat Methods. 2013;10(4):277-8. Epub 2013/03/30. doi: 10.1038/nmeth.2406. PubMed PMID: 23538861.

12. Prasad A, Porter DF, Kroll-Conner PL, Mohanty I, Ryan AR, Crittenden SL, *et al.* The PUF binding landscape in metazoan germ cells. RNA. 2016. doi: 10.1261/rna.055871.116. PubMed PMID: 27165521.

13. Jungkamp AC, Stoeckius M, Mecenas D, Grun D, Mastrobuoni G, Kempa S, *et al*. *In vivo* and transcriptome-wide identification of RNA binding protein target sites. Mol Cell. 2011;44(5):828-40. doi: 10.1016/j.molcel.2011.11.009. PubMed PMID: 22152485; PubMed Central PMCID: PMC3253457.

14. Stoeckius M, Grun D, Kirchner M, Ayoub S, Torti F, Piano F, *et al*. Global characterization of the oocyte-to-embryo transition in *Caenorhabditis elegans* uncovers a novel mRNA clearance mechanism. EMBO J. 2014;33(16):1751-66. Epub 2014/06/25. doi: 10.15252/embj.201488769. PubMed PMID: 24957527; PubMed Central PMCID: PMC4195759.

15. Dinkel H, Van Roey K, Michael S, Kumar M, Uyar B, Altenberg B, *et al*. ELM 2016--data update and new functionality of the eukaryotic linear motif resource. Nucleic Acids Res.

2016;44(D1):D294-300. Epub 2015/11/29. doi: 10.1093/nar/gkv1291. PubMed PMID: 26615199; PubMed Central PMCID: PMC4702912.

16. Notredame C, Higgins DG, Heringa J. T-Coffee: A novel method for fast and accurate multiple sequence alignment. J Mol Biol. 2000;302(1):205-17. Epub 2000/08/31. doi: 10.1006/jmbi.2000.4042. PubMed PMID: 10964570.

17. Brenner S. The genetics of *Caenorhabditis elegans*. Genetics. 1974;77(1):71-94. PubMed PMID: 4366476.

18. Fraser AG, Kamath RS, Zipperlen P, Martinez-Campos M, Sohrmann M, Ahringer J. Functional genomic analysis of *C. elegans* chromosome I by systematic RNA interference. Nature. 2000;408(6810):325-30. Epub 2000/12/01. doi: 10.1038/35042517. PubMed PMID: 11099033.

19. Minevich G, Park DS, Blankenberg D, Poole RJ, Hobert O. CloudMap: a cloud-based pipeline for analysis of mutant genome sequences. Genetics. 2012;192(4):1249-69. Epub 2012/10/12. doi: 10.1534/genetics.112.144204. PubMed PMID: 23051646; PubMed Central PMCID: PMC3512137.

20. Hobert O. The impact of whole genome sequencing on model system genetics: get ready for the ride. Genetics. 2010;184(2):317-9. Epub 2010/01/28. doi: 10.1534/genetics.109.112938. PubMed PMID: 20103786; PubMed Central PMCID: PMC2828713.

21. Wolpert L. Positional Information and Pattern Formation. Curr Top Dev Biol. 2016;117:597-608. doi: 10.1016/bs.ctdb.2015.11.008. PubMed PMID: 26970003.

22. Mannervik M. Control of *Drosophila* embryo patterning by transcriptional co-regulators. Exp Cell Res. 2014;321(1):47-57. Epub 2013/10/26. doi: 10.1016/j.yexcr.2013.10.010. PubMed PMID: 24157250.

23. Lee C, Zhang H, Baker AE, Occhipinti P, Borsuk ME, Gladfelter AS. Protein aggregation behavior regulates cyclin transcript localization and cell-cycle control. Dev Cell. 2013;25(6):572-

84. Epub 2013/06/19. doi: 10.1016/j.devcel.2013.05.007. PubMed PMID: 23769973; PubMed Central PMCID: PMC4113091.

24. Kraemer B, Crittenden S, Gallegos M, Moulder G, Barstead R, Kimble J, *et al*. NANOS-3 and FBF proteins physically interact to control the sperm-oocyte switch in *Caenorhabditis elegans*. Curr Biol. 1999;9(18):1009-18. PubMed PMID: 10508609.

25. Wu J, Campbell ZT, Menichelli E, Wickens M, Williamson JR. A protein.protein interaction platform involved in recruitment of GLD-3 to the FBF.*fem-3* mRNA complex. J Mol Biol. 2013;425(4):738-54. Epub 2012/11/20. doi: 10.1016/j.jmb.2012.11.013. PubMed PMID: 23159559; PubMed Central PMCID: PMC3568228.

26. Eckmann CR, Kraemer B, Wickens M, Kimble J. GLD-3, a bicaudal-C homolog that inhibits FBF to control germline sex determination in *C. elegans*. Dev Cell. 2002;3(5):697-710. PubMed PMID: 12431376.

27. Hansen D, Wilson-Berry L, Dang T, Schedl T. Control of the proliferation versus meiotic development decision in the *C. elegans* germline through regulation of GLD-1 protein accumulation. Development. 2004;131(1):93-104. Epub 2003/12/09. doi: 10.1242/dev.00916. PubMed PMID: 14660440.

28. Eckmann CR, Crittenden SL, Suh N, Kimble J. GLD-3 and control of the mitosis/meiosis decision in the germline of *Caenorhabditis elegans*. Genetics. 2004;168(1):147-60. doi: 10.1534/genetics.104.029264. PubMed PMID: 15454534; PubMed Central PMCID: PMC1448115.

29. Campbell ZT, Menichelli E, Friend K, Wu J, Kimble J, Williamson JR, *et al.* Identification of a conserved interface between PUF and CPEB proteins. J Biol Chem. 2012;287(22):18854-62. Epub 2012/04/13. doi: 10.1074/jbc.M112.352815. PubMed PMID: 22496444; PubMed Central PMCID: PMC3365739.

30. Opperman L, Hook B, DeFino M, Bernstein DS, Wickens M. A single spacer nucleotide determines the specificities of two mRNA regulatory proteins. Nat Struct Mol Biol. 2005;12(11):945-51. Epub 2005/10/26. doi: 10.1038/nsmb1010. PubMed PMID: 16244662.

31. Voronina E, Seydoux G, Sassone-Corsi P, Nagamori I. RNA granules in germ cells. Cold Spring Harb Perspect Biol. 2011;3(12). Epub 2011/07/20. doi: 10.1101/cshperspect.a002774. PubMed PMID: 21768607; PubMed Central PMCID: PMC3225947.

32. Voronina E. The diverse functions of germline P-granules in *Caenorhabditis elegans*. Mol Reprod Dev. 2013;80(8):624-31. Epub 2012/11/15. doi: 10.1002/mrd.22136. PubMed PMID: 23150384.

33. Voronina E, Paix A, Seydoux G. The P granule component PGL-1 promotes the localization and silencing activity of the PUF protein FBF-2 in germline stem cells. Development. 2012;139(20):3732-40. doi: 10.1242/dev.083980. PubMed PMID: 22991439; PubMed Central PMCID: PMC3445306.

34. Fredriksson S, Gullberg M, Jarvius J, Olsson C, Pietras K, Gustafsdottir SM, *et al*. Protein detection using proximity-dependent DNA ligation assays. Nat Biotechnol. 2002;20(5):473-7. Epub 2002/05/01. doi: 10.1038/nbt0502-473. PubMed PMID: 11981560.

35. Roy R, Hohng S, Ha T. A practical guide to single-molecule FRET. Nat Methods. 2008;5(6):507-16. Epub 2008/05/31. doi: 10.1038/nmeth.1208. PubMed PMID: 18511918; PubMed Central PMCID: PMC3769523.

36. Eliscovich C, Singer RH. RNP transport in cell biology: the long and winding road. Curr Opin Cell Biol. 2017;45:38-46. Epub 2017/03/05. doi: 10.1016/j.ceb.2017.02.008. PubMed PMID: 28258033; PubMed Central PMCID: PMC5482755.

37. Goldstrohm AC, Hook BA, Seay DJ, Wickens M. PUF proteins bind Pop2p to regulate messenger RNAs. Nat Struct Mol Biol. 2006;13(6):533-9. doi: 10.1038/nsmb1100. PubMed PMID: 16715093.

38. Suh N, Crittenden SL, Goldstrohm A, Hook B, Thompson B, Wickens M, *et al.* FBF and its dual control of *gld-1* expression in the *Caenorhabditis elegans* germline. Genetics. 2009;181(4):1249-60. doi: 10.1534/genetics.108.099440. PubMed PMID: 19221201; PubMed Central PMCID: PMC2666496.

39. Friend K, Campbell ZT, Cooke A, Kroll-Conner P, Wickens MP, Kimble J. A conserved PUF-Ago-eEF1A complex attenuates translation elongation. Nat Struct Mol Biol. 2012;19(2):176-83. doi: 10.1038/nsmb.2214. PubMed PMID: 22231398; PubMed Central PMCID: PMC3293257.

40. Van Nostrand EL, Pratt GA, Shishkin AA, Gelboin-Burkhart C, Fang MY, Sundararaman B, *et al*. Robust transcriptome-wide discovery of RNA-binding protein binding sites with enhanced CLIP (eCLIP). Nat Methods. 2016;13(6):508-14. Epub 2016/03/29. doi: 10.1038/nmeth.3810. PubMed PMID: 27018577; PubMed Central PMCID: PMC4887338.

41. Campbell ZT, Bhimsaria D, Valley CT, Rodriguez-Martinez JA, Menichelli E, Williamson JR, *et al*. Cooperativity in RNA-protein interactions: global analysis of RNA binding specificity. Cell Rep. 2012;1(5):570-81. doi: 10.1016/j.celrep.2012.04.003. PubMed PMID: 22708079; PubMed Central PMCID: PMC3375920.

42. Jarvelin AI, Noerenberg M, Davis I, Castello A. The new (dis)order in RNA regulation. Cell Commun Signal. 2016;14:9. Epub 2016/04/07. doi: 10.1186/s12964-016-0132-3. PubMed PMID: 27048167; PubMed Central PMCID: PMC4822317.

43. Protter DS, Parker R. Principles and Properties of Stress Granules. Trends Cell Biol. 2016;26(9):668-79. Epub 2016/06/13. doi: 10.1016/j.tcb.2016.05.004. PubMed PMID: 27289443; PubMed Central PMCID: PMC4993645.

44. Crittenden SL, Leonhard KA, Byrd DT, Kimble J. Cellular analyses of the mitotic region in the *Caenorhabditis elegans* adult germ line. Mol Biol Cell. 2006;17(7):3051-61. doi: 10.1091/mbc.E06-03-0170. PubMed PMID: 16672375; PubMed Central PMCID: PMC1552046.

45. Cinquin O, Crittenden SL, Morgan DE, Kimble J. Progression from a stem cell-like state to early differentiation in the *C. elegans* germ line. Proc Natl Acad Sci U S A. 2010;107(5):2048-53. doi: 10.1073/pnas.0912704107. PubMed PMID: 20080700; PubMed Central PMCID: PMC2836686.

46. Jones AR, Francis R, Schedl T. GLD-1, a cytoplasmic protein essential for oocyte differentiation, shows stage- and sex-specific expression during *Caenorhabditis elegans* germline development. Dev Biol. 1996;180(1):165-83. doi: 10.1006/dbio.1996.0293. PubMed PMID: 8948583.

47. Morgan DE, Crittenden SL, Kimble J. The *C. elegans* adult male germline: stem cells and sexual dimorphism. Dev Biol. 2010;346(2):204-14. doi: 10.1016/j.ydbio.2010.07.022. PubMed PMID: 20659446; PubMed Central PMCID: PMC2945412.

48. Wabik A, Jones PH. Switching roles: the functional plasticity of adult tissue stem cells. EMBO J. 2015;34(9):1164-79. Epub 2015/03/31. doi: 10.15252/embj.201490386. PubMed PMID: 25812989; PubMed Central PMCID: PMC4426478.

49. Angelo G, Van Gilst MR. Starvation protects germline stem cells and extends reproductive longevity in *C. elegans*. Science. 2009;326(5955):954-8. doi: 10.1126/science.1178343. PubMed PMID: 19713489.

50. Seidel HS, Kimble J. The oogenic germline starvation response in *C. elegans*. PLoS One. 2011;6(12):e28074. doi: 10.1371/journal.pone.0028074. PubMed PMID: 22164230; PubMed Central PMCID: PMC3229504.

51. Seidel HS, Kimble J. Cell-cycle quiescence maintains *Caenorhabditis elegans* germline stem cells independent of GLP-1/Notch. Elife. 2015;4. doi: 10.7554/eLife.10832. PubMed PMID: 26551561; PubMed Central PMCID: PMC4718729.

Appendix A.

SYGL-1 in mRNA regulation

I generated all data and wrote this appendix. Aaron Kershner, Scott Aoki, Jon Doenier contributed to the design of the experiments described.

Introduction

RNA regulation is critical for multiple processes in biology, with broad implications in development and diseases [1]. Every point in the life of an mRNA is regulated: mRNAs are synthesized, transported, relay the genetic information to be translated into proteins, and finally undergo decay [2]. The mRNA level is precisely controlled to accommodate environmental changes and physiological requirements. Thus, understanding the regulatory mechanisms of mRNA processing provides fundamental insights into biology.

One critical step of the mRNA regulation involves the 3' untranslated region (UTR). 3'UTR refers to an untranslated end region of an mRNA transcript that immediately follows the stop codon. This region often contains the regulatory information required for transcript localization and stability: For example, 3'UTR contains miRNA binding sites, polyadenylation elements, and localization elements, which can together control the location, stability, and the translation efficiency of the transcript [3]. Central to understanding the role of 3'UTR in mRNA biology is to elucidate the *cis*-acting elements within the transcript, and trans-acting RNA binding proteins that execute these regulatory roles.

PUF (Pumilio and FBF) proteins are a conserved family of RNA binding proteins that are exemplary 3'UTR regulators [4]. Broadly conserved in metazoan, PUF proteins recognize distinct RNA sequence motifs called PUF binding elements (PBE), mostly found in the 3'UTR [4]. PUF proteins control many aspects of mRNA expression depending on the cellular and developmental context [5]. For example, PUF proteins can control the stability of target mRNA by recruiting CCR4/NOT deadenylation complex to destabilize the targets [6], promote the expression of the transcript [7-10], or change the transcript localization to accommodate local translation requirements within the cell [11]. Since PUF regulation of mRNA can have multiple biological outcomes, one theme is that PUF can work with diverse protein binding partners to combinatorically control diverse mRNA fate outcomes.

In this appendix, I focus on the physical interaction of one such PUF protein and one such PUF-binding partner, FBF and SYGL-1. FBF is a founding member of the PUF protein family first identified in *C. elegans* [4]; SYGL-1 is a critical niche signaling target that maintains the *C. elegans* germline stem cells (GSCs) [12], whose expression domain controls the stem cell pool size [13]. Multiple lines of evidence support the model that SYGL-1 stem cell activity is dependent on two nearly identical PUF proteins, *fbf-1* and *fbf-2* (collectively FBF): SYGL-1 driven germline tumors require FBF for tumor formation; SYGL-1 physically interacts with FBF in yeast two hybrid and co-immunoprecipitation assays; SYGL-1 controls the stability of an FBF target mRNA *gld-1* within stem cells [13]. Emerging model is that SYGL-1 work with FBF to control mRNA stability. Thus, understanding the relationship between SYGL-1 and FBF may provide novel aspects of mRNA regulation in the context of stem cell self-renewal.

Here I describe my efforts to test the significance of SYGL-1 and FBF interaction. First, I show that N-terminal half of SYGL-1 protein can interact with FBF in the yeast two hybrid assay. Next, I tether SYGL-1 protein to the 3' UTR of a reporter transcript using the bacteriophage λN tethering system [14], and show that tethering SYGL-1 to the 3'UTR of a reporter is sufficient to repress the reporter expression *in vivo*. Collectively, the data presented in this appendix support the model that SYGL-1 controls mRNA stability. Further, reagents provided in this appendix may provide useful in future explorations of SYGL-1 in post-transcriptional regulation.

Results and Discussion

SYGL-1 N-terminal half can interact with FBF in yeast two hybrid

To map the binding interface between SYGL-1 and FBF, I performed a directed yeast two hybrid assay using multiple truncations of SYGL-1. To this end, either full-length SYGL-1, or truncated versions of SYGL-1 were fused to the Gal4 activation domain (AD), and the PUF repeats of FBF-1 (a.a.121-614) were fused with the LexA DNA binding domain (BD) (**Figure**

1A). Several truncations of SYGL-1 were designed based on sequence alignments among SYGL-1 homologs, to ask which conserved regions are required for FBF interaction (**Figure 1B**). Yeast strains were co-transformed with both AD and BD plasmids, and the interaction was assayed by monitoring growth on minimal media lacking histidine, as a measurement of *HIS3* gene expression level. A competitive inhibitor of *HIS3* enzyme (50 mM 3-AT) was added to impose a stringent threshold and to minimize false positives.

Robust growth was observed when either full length, or N-terminal half of SYGL-1 was co-transformed with FBF-1 BD, but not when the C-terminal half of SYGL-1 was co-transformed with FBF-1 (**Figure 1C, Top three rows**). This result demonstrated that N-terminal half of SYGL-1 is required for FBF-1 interaction. To further investigate which conserved regions are required for FBF interaction, three additional truncations spanning the SYGL-1 N-terminal half were tested: SYGL-1 (a. a. 34-103), SYGL-1 (a. a. 1-72), and SYGL-1 (a. a. 73-103) each contain at least one conserved stretch identified by homology (**Figure 1B**, [15]). All three additional truncations interacted with FBF by growth assay, albeit at a lower level than the full length, or N-terminal half (a.a. 1-103) SYGL-1 (**Figure 1C, Bottom three rows**). Collectively, these results suggest that multiple conserved stretches within the SYGL-1 N-terminal region may mediate the physical interaction with FBF-1.

SYGL-1 can repress the expression of a tethered transcript

To further explore the idea that SYGL-1 represses mRNA expression, I tethered SYGL-1 to the 3' UTR of a reporter transcript and asked if the reporter expression can change upon SYGL-1 recruitment. This assay took advantage of the lambda N (λN) tethering system, which utilizes the interaction between bacteriophage λN peptide and *boxb* RNA hairpin (**Figure 2A**) [16]. This tethering system is widely used to tether protein to RNA for affinity purification and visualization purposes, including the *C. elegans* [e.g. 17]. Moreover, additional reagents that

contain *boxb* hairpins in the 3'UTR of a germline expressing GFP reporter are actively being developed in the Kimble laboratory (Aoki *et al*, in preparation).

Briefly, λN peptide was inserted at the endogenously V5 tagged *sygl-1* allele (see methods). Next, strains expressing either SYGL-1::V5::λN (experiment) or SYGL-1::V5 (control) were crossed with a GFP::H2B reporter strain containing three *boxb* hairpins in the 3' UTR (**Figure 2B**). To assay the effects of SYGL-1 recruitment to the tethered mRNA, the nuclear GFP expression was measured at the distal end of the gonad. Specifically, the nuclear GFP levels were determined to see if SYGL-1 can repress GFP expression. Interestingly, the nuclear GFP level in the distal-most cells was dramatically reduced in strains expressing λN containing SYGL-1 (SYGL-1::V5::λN) (**Figure 2C, left**), but not in control animals (SYGL-1::V5) (**Figure 2C, middle**); The extents of GFP repression observed in the experimental strain correlated well with the extents of SYGL-1 expression within GSCs. Both versions of SYGL-1 with and without λN encode functional proteins, as all could maintain GSCs in the absence of *lst-1* whereas *lst-1 sygl-1* double mutants cannot maintain GSCs (**Figure 2D**). Collectively, these results demonstrate that SYGL-1 can repress the expression of a tethered transcript.

Conclusions and Future Directions

Here I have described two preliminary observations that support the notion of SYGL-1 as an mRNA regulator. First, I have shown that N-terminal half of SYGL-1 is sufficient to interact with FBF-1 in the yeast two hybrid assay. Second, I have shown that SYGL-1 can repress the expression of a tethered reporter transcript, when recruited to the 3' UTR of the reporter. Here I put these results in context and suggest some future experiments.

Identifying the binding interface between SYGL-1 and FBF provides an opportunity to test the significance of SYGL-1 and FBF interaction, as discussed in Chapter 4. For example, SYGL-1 might change the specificity or kinetics of FBF binding to target mRNAs. One possibility

is to test these ideas by developing reagents that will allow *in vitro* binding assays: SYGL-1 N-terminal half could be attempted for purification since this region is sufficient to bind FBF in two hybrid assays. Next, EMSA (Electrophoretic Mobility Shift Assay) could be performed to ask whether the presence of SYGL-1 can enhance the binding affinity of FBF and FBF binding elements (FBEs), using either *fem-3* or *gld-1* RNAs encoding FBEs. Alternatively, purified SYGL-1 could be directly tested for RNA binding using EMSA, starting with poly uracil (U) containing RNA stretches. Results from these assay will address the molecular significance of FBF and SYGL-1 interaction.

How does SYGL-1 repress mRNAs? SYGL-1 can repress the expression of at least one target mRNA, *gld-1,* in stem cells [13]. Consistent with this observation, the result of the tethering assay suggests that SYGL-1 may be directly involved in mRNA regulation, as tethering SYGL-1 to the 3'UTR of a reporter transcript can repress its expression. Still, the result of this tethering assay should be taken with caution. First, the reporter is an artificial setup devoid of endogenous context, and the question whether SYGL-1 can directly repress mRNA awaits future experiments using relevant mRNA targets *in vivo*. Second, high affinity of λN-*boxb* interaction may cause artifacts in the system. Recently, a commonly used tethering technique based on similar principles, bacteriophage MS2 – MCP tagging system, was reported to accumulate unexpected mRNA aggregates due to inefficient 3' end decay [18-20]. To address these possibilities, the effects of λN on tagged proteins, or the effects of λN itself on tagged transcripts need to be vigorously tested *in vivo*. One immediate next step is to visualize GFP transcripts by single molecular FISH to ask if the repression happens at the transcription, or post-transcriptional level.

Regardless, the tethering assay provides new methods to explore the role of SYGL-1 in mRNA regulation. A plausible model is that FBF can associate with target mRNAs using FBF binding elements, and SYGL-1 can act as a scaffold in this molecular complex to recruit protein

machineries required for repression. One possibility is to use this tethering assay to identify factors required for repression, using candidate or genome-wide RNAi screens. For example, multiple deadenylation machineries (ex. *ccf-1*, *ccr-4*) or cap binding proteins (ex. *ife-1, ife-3*) could be depleted to ask their requirements in SYGL-1 mediated repression. Therefore, reagents presented in this appendix may prove useful to address the molecular mechanism of SYGL-1 in future studies, and may reveal novel aspects of mRNA regulation by PUF proteins.

Material and Methods

Nematode strains and maintenance

Most strains were maintained and characterized at 20°C under standard conditions [21]. The wild type was N2 Bristol strain. Alleles are as follows: LG*I*: *sygl-1(q1005), sygl-1(q1006), sygl-1(q1007), sygl-1(q1008)* (this work), *lst-1(ok814)* [22]. LG*II*: *qSi375 [$_{Pmex-5}$::GFP::his-58::3xboxb::tbb-2 3'end]* (S. Aoki and J. Kimble, in preparation).

Nematode strains used in the study

N2: wild type

JK5921: *qSi375[P$_{mex-5}$::GFP:: his-58::3xboxb::tbb-2 3'end] II*

JK6002: *sygl-1(q1005)[sygl-1:1xV5] I*

JK6003: *sygl-1(q1006)[sygl-1:1xV5] I*

JK6004: *sygl-1(q1007)[sygl-1::1xV5::λN] I*

JK6005: *sygl-1(q1008)[sygl-1::1xV5::λN] I*

JK6006: *sygl-1(q1005)[sygl-1:1xV5] I; qSi375[P$_{mex-5}$:GFP:: his-58::3xboxb::tbb-2 3'end] II*

JK6007: *sygl-1(q1007)[sygl-1:1xV5: λN] I;; qSi375[P$_{mex-5}$:GFP:: his-58::3xboxb::tbb-2 3'end] II*

JK6008: *lst-1(ok814) sygl-1(q1005)[sygl-1:1xV5::λN] I*

JK6009: *lst-1(ok814) sygl-1(q1007)[sygl-1::1xV5::λN] I*

Generation of *C. elegans* alleles

The alleles *sygl-1(q1005), sygl-1(q1006), sygl-1(q1007),* and *sygl-1(q1008)* were generated by RNA protein complex (RNP) CRISPR, using *unc-58* co-CRISPR to mark edited broods [23]. Briefly, CRISPR reagents were ordered from IDT Alt-R™ to prepare an injection mix containing 10 μM crRNAs targeting *sygl-1* stop codon (CTACTGCAAATAATAGCTGT), 4 μM *unc-58* co-CRISPR crRNAs, 14 μM tracrRNA, 4 μM 1xV5::GGS linker oligo (5'-gaacaacaacacttcactgatgat-gggctcTaacagctattatttgcagGGTAAGCCTATCCCTAACCCTCTCCTCGGTCTAGATAGTACTGG AGGATCCtagagcgtacttgctcttttaaattttctaatcc-3'), or 1xV5::GGS linker::λN oligo (5'-gaacaacaaca-cttcactgatgatgggctcTaacagctattatttgcagGGTAAGCCTATCCCTAACCCTCTCCTCGGTCTAGAT AGTACTGGAGGATCCGGAAACGCCCGTACCCGTCGTCGTGAGCGTCGTGCCGAGAAGCA AGCCCAATGGAAGGCCGCCAACtagagcgtacttgctcttttaaattttctaatcc-3'), 1.4 μM co-CRISPR *unc-58* repair oligo, and 25 μM Cas-9 protein. JK5921 strains were microinjected and the progeny were screened using PCR for edits. All CRISPR alleles were verified by sequencing and outcrossed 2-4 times with wild type prior to analysis.

Assessment of sterility

JK6008 and JK6009 hermaphrodites of forth larval stage (L4) were placed onto individual plates at 20°C. After 3 days, plates were counted for the presence or progeny. Plates with hatched progeny were counted as fertile.

Immunostaining and DAPI staining

Staining followed established protocols [24]. Briefly, staged animals were dissected in PBStw (PBS + 0.1% (v/v) Tween-20) with 0.25 mM levamisole to extrude gonads. Tissues were fixed in 2% (w/v) paraformaldehyde diluted in 100 mM K_2HPO_4 (pH 7.2) for 10 minutes. Post fixation, all samples were permeabilized with PBStw + 0.2% (v/v) Triton-X for 10 minutes, blocked with

0.5% (w/v) bovine serum albumin for 1 hour. For primary antibodies, samples were incubated overnight at the following dilutions in the blocking solution: Mouse anti-V5 (1:1000, Bio-Rad #MCA1360), Rabbit anti-GFP (1:1000, Invitrogen #A11122). For secondary antibodies, samples were incubated for 1 hour at room temperature at the following dilutions: Donkey Alexa 555 anti-mouse (1:1000, Invitrogen #A31570), Goat Alexa 488 anti-rabbit (1:1000, Invitrogen #A11034). To visualize DNA, DAPI was included at a final concentration of 0.5-1 ng/μl during the last 10 minutes of secondary antibody incubation. Vectashield (Vector Laboratories #H-1000) was used as mounting medium.

Yeast two hybrid

Modified yeast two-hybrid assays were performed as described [25]. Briefly, *sygl-1* cDNA encoding full-length or truncated SYGL-1 was cloned into the Nco I and Xho I sites in pACT2 (Gal4 activation domain plasmid) to generate pJK1580 (a.a. 1-206) [13], pJK1581(a.a. 1-103), pJK1582 (a.a.103-206), pJK2024 (a.a. 1-72), pJK2025 (a.a. 7-103), and pJK2016 (a.a. 34-103). pJK2019 encoding FBF-1 (a.a. 121-614) [26] was used. Plasmids were co-transformed into a L40-ura strain using the Te-LiAc method [27]. *HIS3* reporter activity was assayed on synthetic defined medium (SD) supplemented with – Leu – Trp – His containing 50 mM 3-Amino-1,2,4-triazole (Sigma #A8056), or – Leu – Trp plates as controls for 4 days at 30°C.

Acknowledgements

I am grateful to Aaron Kershner for generating pJK1580, pJK1581, pJK1582 plasmids that were used in the yeast two hybrid assay, and for the discussion on this appendix. I thank Jonathan Doeiner and Scott Aoki for conceiving the tethering assay and sharing early versions of the reagents.

References

1. Cooper TA, Wan L, Dreyfuss G. RNA and disease. Cell. 2009;136(4):777-93. Epub 2009/02/26. doi: 10.1016/j.cell.2009.02.011. PubMed PMID: 19239895; PubMed Central PMCID: PMC2866189.

2. Morris KV, Mattick JS. The rise of regulatory RNA. Nat Rev Genet. 2014;15(6):423-37. Epub 2014/04/30. doi: 10.1038/nrg3722. PubMed PMID: 24776770; PubMed Central PMCID: PMC4314111.

3. Matoulkova E, Michalova E, Vojtesek B, Hrstka R. The role of the 3' untranslated region in post-transcriptional regulation of protein expression in mammalian cells. RNA Biol. 2012;9(5):563-76. Epub 2012/05/23. doi: 10.4161/rna.20231. PubMed PMID: 22614827.

4. Wickens M, Bernstein DS, Kimble J, Parker R. A PUF family portrait: 3'UTR regulation as a way of life. Trends Genet. 2002;18(3):150-7. PubMed PMID: 11858839.

5. Quenault T, Lithgow T, Traven A. PUF proteins: repression, activation and mRNA localization. Trends Cell Biol. 2011;21(2):104-12. doi: 10.1016/j.tcb.2010.09.013. PubMed PMID: 21115348.

6. Goldstrohm AC, Hook BA, Seay DJ, Wickens M. PUF proteins bind Pop2p to regulate messenger RNAs. Nat Struct Mol Biol. 2006;13(6):533-9. doi: 10.1038/nsmb1100. PubMed PMID: 16715093.

7. Moore FL, Jaruzelska J, Fox MS, Urano J, Firpo MT, Turek PJ, *et al.* Human Pumilio-2 is expressed in embryonic stem cells and germ cells and interacts with DAZ (Deleted in AZoospermia) and DAZ-like proteins. Proc Natl Acad Sci U S A. 2003;100(2):538-43. doi: 10.1073/pnas.0234478100. PubMed PMID: 12511597; PubMed Central PMCID: PMC141031.

8. Suh N, Crittenden SL, Goldstrohm A, Hook B, Thompson B, Wickens M, *et al.* FBF and its dual control of *gld-1* expression in the *Caenorhabditis elegans* germline. Genetics. 2009;181(4):1249-60. doi: 10.1534/genetics.108.099440. PubMed PMID: 19221201; PubMed Central PMCID: PMC2666496.

9. Zhang M, Chen D, Xia J, Han W, Cui X, Neuenkirchen N, *et al*. Post-transcriptional regulation of mouse neurogenesis by Pumilio proteins. Genes Dev. 2017. Epub 2017/08/11. doi: 10.1101/gad.298752.117. PubMed PMID: 28794184; PubMed Central PMCID: PMC5580656.

10. Kaye JA, Rose NC, Goldsworthy B, Goga A, L'Etoile ND. A 3'UTR pumilio-binding element directs translational activation in olfactory sensory neurons. Neuron. 2009;61(1):57-70. doi: 10.1016/j.neuron.2008.11.012. PubMed PMID: 19146813; PubMed Central PMCID: PMC4274156.

11. Lee CD, Tu BP. Glucose-Regulated Phosphorylation of the PUF Protein Puf3 Regulates the Translational Fate of Its Bound mRNAs and Association with RNA Granules. Cell Rep. 2015;11(10):1638-50. Epub 2015/06/09. doi: 10.1016/j.celrep.2015.05.014. PubMed PMID: 26051939; PubMed Central PMCID: PMC4472502.

12. Kershner AM, Shin H, Hansen TJ, Kimble J. Discovery of two GLP-1/Notch target genes that account for the role of GLP-1/Notch signaling in stem cell maintenance. Proc Natl Acad Sci U S A. 2014;111(10):3739-44. doi: 10.1073/pnas.1401861111. PubMed PMID: 24567412; PubMed Central PMCID: PMC3956202.

13. Shin H, Haupt KA, Kershner AM, Kroll-Conner P, Wickens M, Kimble J. SYGL-1 and LST-1 link niche signaling to PUF RNA repression for stem cell maintenance in *Caenorhabditis elegans.* PLoS Genet. 2017;13(12):e1007121. Epub 2017/12/13. doi: 10.1371/journal.pgen.1007121. PubMed PMID: 29232700.

14. Baron-Benhamou J, Gehring NH, Kulozik AE, Hentze MW. Using the lambdaN peptide to tether proteins to RNAs. Methods Mol Biol. 2004;257:135-54. Epub 2004/02/11. doi: 10.1385/1-59259-750-5:135. PubMed PMID: 14770003.

15. Notredame C, Higgins DG, Heringa J. T-Coffee: A novel method for fast and accurate multiple sequence alignment. J Mol Biol. 2000;302(1):205-17. Epub 2000/08/31. doi: 10.1006/jmbi.2000.4042. PubMed PMID: 10964570.

16. Franklin NC. Conservation of genome form but not sequence in the transcription antitermination determinants of bacteriophages lambda, phi 21 and P22. J Mol Biol. 1985;181(1):75-84. Epub 1985/01/05. PubMed PMID: 3157001.

17. Wedeles CJ, Wu MZ, Claycomb JM. Protection of germline gene expression by the *C. elegans* Argonaute CSR-1. Dev Cell. 2013;27(6):664-71. Epub 2013/12/24. doi: 10.1016/j.devcel.2013.11.016. PubMed PMID: 24360783.

18. Garcia JF, Parker R. MS2 coat proteins bound to yeast mRNAs block 5' to 3' degradation and trap mRNA decay products: implications for the localization of mRNAs by MS2-MCP system. RNA. 2015;21(8):1393-5. Epub 2015/06/21. doi: 10.1261/rna.051797.115. PubMed PMID: 26092944; PubMed Central PMCID: PMC4509929.

19. Garcia JF, Parker R. Ubiquitous accumulation of 3' mRNA decay fragments in *Saccharomyces cerevisiae* mRNAs with chromosomally integrated MS2 arrays. RNA. 2016;22(5):657-9. Epub 2016/04/20. doi: 10.1261/rna.056325.116. PubMed PMID: 27090788; PubMed Central PMCID: PMC4836640.

20. Heinrich S, Sidler CL, Azzalin CM, Weis K. Stem-loop RNA labeling can affect nuclear and cytoplasmic mRNA processing. RNA. 2017;23(2):134-41. Epub 2017/01/18. doi: 10.1261/rna.057786.116. PubMed PMID: 28096443; PubMed Central PMCID: PMC5238788.

21. Brenner S. The genetics of *Caenorhabditis elegans*. Genetics. 1974;77(1):71-94. PubMed PMID: 4366476.

22. Singh K, Chao MY, Somers GA, Komatsu H, Corkins ME, Larkins-Ford J, *et al*. *C. elegans* Notch signaling regulates adult chemosensory response and larval molting quiescence. Curr Biol. 2011;21(10):825-34. doi: 10.1016/j.cub.2011.04.010. PubMed PMID: 21549604; PubMed Central PMCID: PMC3100419.

23. Arribere JA, Bell RT, Fu BX, Artiles KL, Hartman PS, Fire AZ. Efficient marker-free recovery of custom genetic modifications with CRISPR/Cas9 in *Caenorhabditis elegans.*

Genetics. 2014;198(3):837-46. doi: 10.1534/genetics.114.169730. PubMed PMID: 25161212; PubMed Central PMCID: PMC4224173.

24. Crittenden SL, Seidel HS, Kimble J. Analysis of the *C. elegans* germline stem cell pool. Methods Mol Biol. 2017;1463:1-33. doi: 10.1007/978-1-4939-4017-2_1. PubMed PMID: 27734344.

25. Bartel PL, Fields S. The yeast two-hybrid system. New York: Oxford University Press; 1997. xi, 344 p. p.

26. Kraemer B, Crittenden S, Gallegos M, Moulder G, Barstead R, Kimble J, *et al*. NANOS-3 and FBF proteins physically interact to control the sperm-oocyte switch in *Caenorhabditis elegans.* Curr Biol. 1999;9(18):1009-18. PubMed PMID: 10508609.

27. Gietz RD, Schiestl RH. High-efficiency yeast transformation using the LiAc/SS carrier DNA/PEG method. Nat Protoc. 2007;2(1):31-4. doi: 10.1038/nprot.2007.13. PubMed PMID: 17401334.

Fig 1
Appendix A

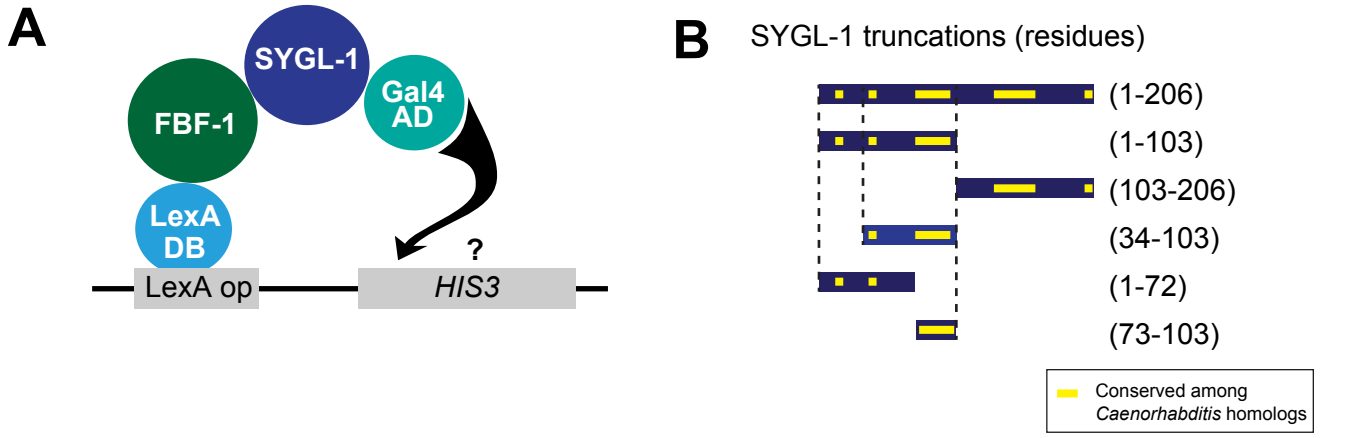

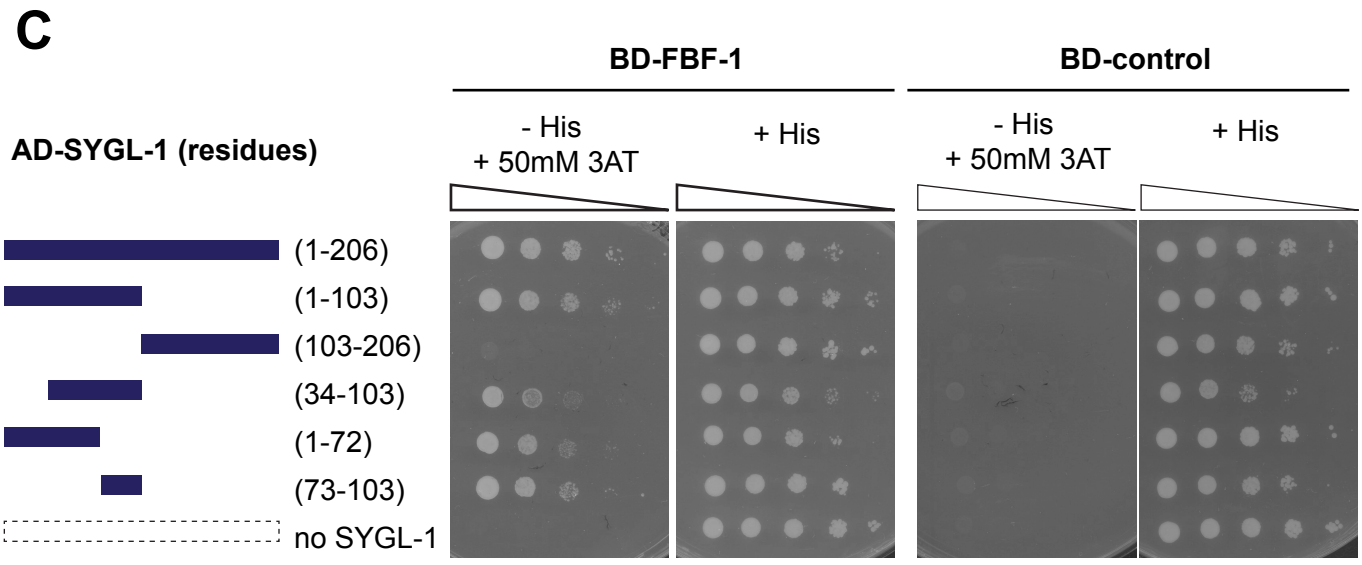

Figure 1. SYGL-1 N-terminal half is sufficient for FBF-1 interaction in yeast.

(**A**) Yeast two hybrid assay. Full length or truncated SYGL-1 was fused to Gal4 activation domain (AD); PUF repeats of FBF-1 (a.a. 121-614) were fused to LexA binding domain (BD). Interaction activates transcription of *HIS3* gene. (**B**) Schematic of SYGL-1 full length or truncations. Numbers, amino acid residues. Yellow, stretches of conservation among Caenorhabditis SYGL-1 homologs, predicted by T-coffee [15]. (**C**) Growth assay testing interaction between SYGL-1–AD and FBF-1–BD. Left, SYGL-1 full length or truncations used. Right, yeast strains were monitored for growth on synthetic defined media (SD), either lacking histidine or with histidine as a control. A *HIS3* competitive inhibitor (3-AT) improved stringency. SYGL-1 N-terminus (a.a.1-103) was sufficient to bind FBF-1 (a.a.121-614). This interaction likely involves multiple conserved regions within SYGL-1 N-terminal half region, as smaller SYGL-1 truncations (ex. a.a. 34-103, a.a. 1-72, a.a. 73-103) also show interaction.

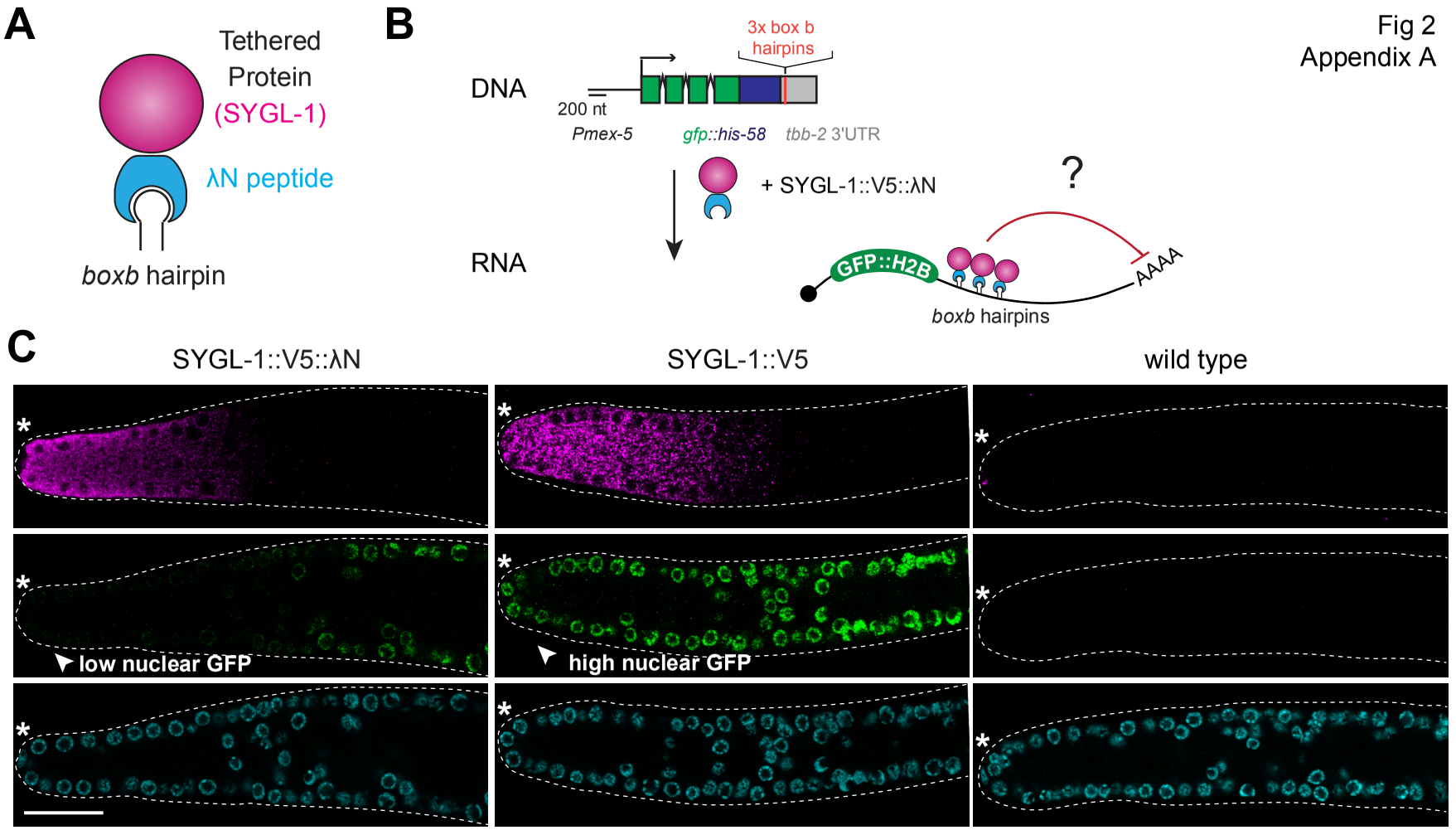

D **Fertility of *sygl-1* alleles in *lst-1 sygl-1* background**

Genotype	% Fertile	% Sterile	n	Reference
lst-1(ok814) sygl-1(tm5040)	0	100	>100	Kershner *et al*, 2014
lst-1(ok814) sygl-1(q1015)[sygl-1::1xV5]	95	5	60	This work
lst-1(ok814) sygl-1(q1017) [sygl-1::1xV5::λN]	94	6	81	This work

Figure 2. SYGL-1 can repress the expression of the tethered transcript.

(**A**) Lambda N (λN) – *boxb* system. λN specifically recognizes the *box b* hairpin [16]. Protein of interest (e.g. SYGL-1) can be fused with λN to tether protein to *boxb* containing RNA. (**B**) Schematic of the tethering assay. A transgenic reporter strain expresses GFP ubiquitously in the germ cell nucleus. This reporter construct contains three copies of *boxb* hairpins in its 3'UTR (Aoki *et al*, in preparation). SYGL-1 protein is fused with λN to recruit SYGL-1 to *boxb* containing transcripts. Effects of protein-RNA tethering is assayed by measuring nuclear GFP expression level. Colored boxes, exons. Grey box, untranslated regions. (**C**) Representative slices of dissected adult gonads stained with anti-V5, anti-GFP, and DAPI to measure V5 (SYGL-1), GFP expression, and nuclear morphology. Left, an experimental gonad containing λN containing SYGL-1. Middle, a control gonad containing no λN. Right, a wild-type gonad used as staining controls. n > 20 in all conditions. Scale bar, 20 microns. Asterisk, distal end. (**D**) Functionality of epitope-tagged *sygl-1* alleles. *sygl-1(q1015)* and *sygl-1(q1017*) were tested for fertility in *lst-1(0)* background, because *sygl-1* and *lst-1* double mutants are synthetic sterile [12]. Fertility in *lst-1(0)* background indicates that tested *sygl-1* alleles are functional.

Appendix B.

Screen to identify genetic enhancers of *sygl-1* and *lst-1* phenotype

---

Aaron Kershner, Kimberly Haupt, Peggy Kroll-Conner, and I equally contributed to this appendix in isolating new alleles. Aaron Kershner, Sarah Robinson and I characterized the molecular nature of new isolated alleles. I wrote this appendix. The result of this screen will be submitted for publication (Robinson *et al*, in preparation).

Introduction

One unbiased approach to identify genes involved in a biological process is to perform a forward genetic screen and isolate animals that are defective in that process. Such methods have been successful in the model organism *C. elegans* [1]. Traditionally, forward genetic screens identify novel genes and novel alleles of genes involved in the pathway, which enhance the understanding of genetic and molecular circuitry governing biological processes.

In this appendix, I describe our efforts to identify novel genes that promote germline stem cell (GSC) self-renewal in *C. elegans*. Previous genetic screens using wild-type isolates successfully discovered the GLP-1/Notch receptor [2], which encodes the signaling receptor involved in stem cell self-renewal. Further, modified genetic screens using either weak *glp-1* alleles or gain-of-function *glp-1* alleles also identified additional genes [3, 4]; For example, RNA dependent RNA polymerase [5], E3 ligases [6] brought additional regulatory insights into germ cell proliferation, or stem cell self-renewal. Yet, no downstream effectors of GLP-1/Notch have been identified in this approach, suggesting that such genes await further discovery.

Here we have used *sygl-1* or *lst-1* single mutants to perform a modified genetic screen to identify novel genes promoting GSC self-renewal. The discovery of *sygl-1* and *lst-1* as critical but redundant GSC regulators led us to hypothesize that previous genetic screens were not successful in identifying GLP-1/Notch targets due to biological redundancy. Since *lst-1 sygl-1* double mutants but not single mutants show germline proliferation defective (Glp) phenotype identical to *glp-1*/Notch null [7], our approach took advantage of the fertility of *sygl-1* or *lst-1* single mutants: We mutagenized *sygl-1* or *lst-1* single mutants and isolated animals that exhibit Glp sterility. Next, we tested if the Glp sterility is dependent on *sygl-1* or *lst-1*. By design, this approach will isolate additional alleles of *glp-1*, or any novel genes that promote GSC self-renewal either dependent or independent of *sygl-1* or *lst-1*. We reasoned that any novel mutation that results in a synthetic Glp phenotype with either *sygl-1* or *lst-1* will likely work with SYGL-1 or LST-1 to promote GSC self-renewal.

Results and Discussion

We performed a mutagenesis screen using *sygl-1* or *lst-1* single mutants. Briefly, *sygl-1* or *lst-1* single loss-of-function mutants were mutagenized with Ethyl methanesulfonate (EMS), and the progeny of mutagenized animals were screened for the germline proliferation defective (Glp) phenotype [2]. We hypothesized that the mutation of interest would segregate in a recessive manner. Thus, our primary screen was to isolate F1 that contain 25% Glp phenotype in the F2 generation (**Figure 1A**). Since any *glp-1* mutation results in Glp sterile by definition, we expected to isolate multiple *glp-1* alleles as a positive control. In addition, we expected to get novel *sygl-1* or *lst-1* alleles, perhaps at a lesser frequency than *glp-1*, because the small size of *sygl-1* and *lst-1* genes render deleterious mutations to occur less frequently. Most importantly, we expected to identify novel genes required for GSC self-renewal: this novel allele may exhibit a Glp-like phenotype on its own, or in a synthetic manner with either *sygl-1* or *lst-1*.

We screened a total of 26,043 haploid gametes and identified a total of 12 alleles (**Figure 1B**). We isolated 9 *glp-1* alleles, as expected, confirming that the screen was executed as designed. During the course of the screen, we introduced two additional copies of *glp-1* transgene in the parental strain to avoid isolating *glp-1* alleles. This strategy helped us to isolate two *lst-1* alleles, and one novel allele that does not map to *sygl-1, lst-1,* or *glp-1.* No *sygl-1* allele was isolated, possibly because the screen was not saturated enough to identify genes of such small size.

We next investigated the molecular nature of the isolated alleles (**Figure 3**). Nine alleles that failed to complement the *glp-1(q175)* null allele were mapped to various locations in the *glp-1* gene, including one *glp-1(q823)* allele that failed to map to within the open reading frame or nearby regulatory regions (A. Kershner, S. Robinson, and H. Shin, unpublished data). Two alleles that failed to complement the *lst-1(ok814)* loss-of-function mutant were mapped to the *lst-1* gene (A. Kershner, H. Shin, unpublished data). One novel allele, *q831*, was further mapped to the right arm of linkage group I (A. Kershner, unpublished data). SNP mapping and whole

genome-sequencing revealed that *q831* maps to the *pole-1* locus, which encodes a homolog of DNA Polymerase epsilon (A. Kershner and S. Robinson, unpublished data).

The *pole-1* phenotype was pleiotropic: animals were uncoordinated and vulval defects were seen in addition to germline proliferation defects, consistent with the idea that *pole-1* is involved in multiple biological processes (A. Kershner, unpublished data). Often, germ cells of *pole-1* mutants were enlarged and appeared to be arrested in the cell cycle, but a significant portion of animals showed premature differentiation, which is a hallmark of Glp phenotype (A. Kershner, unpublished data). The Glp defect of *pole-1* was not dependent on either *sygl-1* or *lst-1*, demonstrating that *pole-1* likely promotes GSC self-renewal in a *sygl-1* or *lst-1* independent manner.

How does *pole-1* promote GSC self-renewal? Because DNA polymerases are critically involved in all biological processes, it is surprising that a mutation of a polymerase subunit can make viable animals. One possibility is that *q831* encodes a weak allele rather than a null allele. In this scenario, a defective polymerase may slow down DNA replication, delaying progression through the cell cycle. This defective cell cycle may activate cell-cycle checkpoints and cause premature differentiation. Indeed, examples have been reported in other systems where aberrant activation of cell cycle checkpoints can trigger premature differentiation [8-11]. Thus, one possible interpretation of *q831* having a Glp sterile phenotype is that aberrant DNA replication can cause premature differentiation, but of course, other possibilities exist. One tractable question is to ask whether this Polymerase epsilon subunit is required for proliferation, in a germ cell intrinsic manner. To this end, genetic epistasis experiments with germ cell tumors (i.e. *glp-1* [12], *sygl-1* or *lst-1* [13], *gld-1 gld-2* [14], *gld-3 nos-3* [15]) may be informative to see if *pole-1* regulate genes in the *glp-1* pathway.

Conclusions and Future Directions

Using a forward genetics approach, we have identified multiple *glp-1* and *lst-1* alleles. These alleles may prove useful in studying GLP-1 and LST-1 function. In addition, we identified a DNA polymerase epsilon subunit (*pole-1*) as a novel regulator of self-renewal. Studying how *pole-1* promotes stem cell self-renewal provide opportunities to investigate two closely related but separable cell fate and cell cycle decisions. In particular, premature germ cell differentiation of *pole-1* mutant raises a hypothesis that S-phase of the cell cycle may be particularly susceptible to differentiation signals.

Despite our extensive efforts to identify novel genes that promote GSC self-renewal downstream of GLP-1/Notch signaling, we were unable to find such genes in our genetic screen. What could be the reason? Successful isolation of *glp-1* and *lst-1* alleles demonstrate that the design of the screen was executed as planned. One possibility is saturation: The screen was not saturated, as evidenced by the failure to identify mutations of small genes such as *sygl-1*. In this case, saturating the screen may identify potential gene of interest. Another possibility is that such a gene, if it exists, may have pleiotropic effects resulting in embryo or larval lethality. In this case, the design of the screen needs to be revisited.

Therefore, modified methods are required to identify novel regulators of GSC self-renewal using this approach. One possibility is to saturate the screen, and use combinations of mutagens (e.g. Ethyl methanesulfonate (EMS) and N-ethyl-N-nitrosourea (ENU)) to obtain diverse profiles of mutations, as used in other forward *C. elegans* genetics screen [16]. Alternatively, redesigning the screen to utilize strains that allow high-throughput screening may be beneficial. For example, *sygl-1* or *lst-1* tumors [13] can be mutagenized and be screened for mutations that cause suppression of tumor. This method may be easier, as positive selection using animal fertility will facilitate screening a large number of progeny.

Material and Methods

Nematode strain maintenance

Strains were maintained at 15°C as described in [17]. Alleles and balancers are as follows: LG I: *lst-1(ok814)* [18], *sygl-1(tm5040)* [7]. LG *II: qSi44[Pglp-1::glp-1::6xmyc::6xHIS::glp-1 3'end]* (E. Sorensen, unpublished). Balancers are as follows: LG*I*: *hT2[qIs48]* [19], *hIn1[unc-54(h1040)]* [20].

Nematode strains used in the study

N2: wild type

JK4356: *lst-1(ok814) I*

JK4899: *sygl-1(tm5040) I*

JK5135: *sygl-1(tm5040) I; qSi44[Pglp-1::glp-1::6xmyc::6xHIS::glp-1 3'end] II*

JK5203: *lst-1(ok814) I; qSi44[Pglp-1::glp-1::6xmyc::6xHIS::glp-1 3'end] II*

EMS screen

A modified Ethyl methanesulfonate (EMS) screen was performed as described [17]. Briefly, *sygl-1(tm5040)* or *lst-1 (ok814)* hermaphrodites of the fourth larval stage (L4) were mutagenized with 25 mM EMS (Sigma M0880) for 4 hours at room temperature. F1 progeny were singled and let self at 15°C, and F2 self-progeny were screened for germline proliferation defective (Glp) mutants [2]. Isolated mutants are as follows:

JK5120: *glp-1(q817) III/hT2[qIs48](I;III)*

JK5121: *glp-1(q818) III/hT2[qIs48](I;III)*

JK5131: *glp-1(q819) III/hT2[qIs48](I;III)*

JK5132: *glp-1(q820) III/hT2[qIs48](I;III)*

JK5133: *glp-1(q821) III/hT2[qIs48](I;III)*

JK5134: *glp-1(q822) III/hT2[qIs48](I;III)*

JK5141: *glp-1(q823) III/hT2[qIs48](I;III)*

JK5142: *glp-1(q824) III/hT2[qIs48](I;III)*

JK5143: *glp-1(q825) III/hT2[qIs48](I;III)*

JK5211: *lst-1(q826) I/ hT2[qIs48](I;III)*

JK5241: *lst-1(q827) I/ hT2[qIs48](I;III)*

JK5250: *pole-1(q831) / hIn1[unc-54(h1040)] I*

Mapping of isolated alleles

Isolated alleles were first tested for their dependence on *sygl-1* or *lst-1* for their Glp (germline proliferation defective) phenotype [2]. For alleles caused Glp regardless of *sygl-1* or *lst-1*, a quick genetic mapping was performed to test if the isolated alleles map close to the endogenous *glp-1* locus. For alleles that cause Glp only in a synergistic fashion with *sygl-1*, a quick genetic mapping was performed to test whether they encode *lst-1* alleles. All *glp-1* and *lst-1* alleles were confirmed by complementation tests with *glp-1(q175)* or *lst-1(ok814)* loss-of-function alleles, and their molecular nature was analyzed by Sanger sequencing. A novel allele, *q831*, was further mapped to *pole-1* using SNP mapping [21], and whole genome sequencing using Illumina Hiseq paired-end sequencing (UW Biotechnology Center). Modified CloupMap [22] was used for whole genome sequencing analyses.

Acknowledgements

Performance of this genetic screen was a collaborative effort. I thank Judith Kimble, Aaron Kershner, Peggy Kroll-Conner, and Kimberly Haupt for the conceptual design and execution of the screen. Aaron Kershner and I isolated and mapped new *lst-1* and *glp-1* alleles. Sarah Robinson sequenced new *glp-1* alleles. Aaron Kershner isolated the novel mutation *q831* and performed genetic and genomic mapping experiments, with the help of Sarah Robinson.

References

1. Jorgensen EM, Mango SE. The art and design of genetic screens: *Caenorhabditis elegans*. Nat Rev Genet. 2002;3(5):356-69. Epub 2002/05/04. doi: 10.1038/nrg794. PubMed PMID: 11988761.

2. Austin J, Kimble J. *glp-1* is required in the germ line for regulation of the decision between mitosis and meiosis in *C. elegans*. Cell. 1987;51(4):589-99. PubMed PMID: 3677168.

3. Kimble J, Crittenden SL. Germline proliferation and its control. WormBook. 2005:1-14. Epub 2007/12/01. doi: 10.1895/wormbook.1.13.1. PubMed PMID: 18050413; PubMed Central PMCID: PMC4781503.

4. Rastogi S, Borgo B, Pazdernik N, Fox P, Mardis ER, Kohara Y, *et al*. *Caenorhabditis elegans glp-4* Encodes a Valyl Aminoacyl tRNA Synthetase. G3 (Bethesda). 2015;5(12):2719-28. Epub 2015/10/16. doi: 10.1534/g3.115.021899. PubMed PMID: 26464357; PubMed Central PMCID: PMC4683644.

5. Qiao L, Lissemore JL, Shu P, Smardon A, Gelber MB, Maine EM. Enhancers of *glp-1*, a gene required for cell-signaling in *Caenorhabditis elegans*, define a set of genes required for germline development. Genetics. 1995;141(2):551-69. Epub 1995/10/01. PubMed PMID: 8647392; PubMed Central PMCID: PMC1206755.

6. Safdar K, Gu A, Xu X, Au V, Taylor J, Flibotte S, *et al*. UBR-5, a Conserved HECT-Type E3 Ubiquitin Ligase, Negatively Regulates Notch-Type Signaling in *Caenorhabditis elegans*. G3 (Bethesda). 2016;6(7):2125-34. Epub 2016/05/18. doi: 10.1534/g3.116.027805. PubMed PMID: 27185398; PubMed Central PMCID: PMC4938665.

7. Kershner AM, Shin H, Hansen TJ, Kimble J. Discovery of two GLP-1/Notch target genes that account for the role of GLP-1/Notch signaling in stem cell maintenance. Proc Natl Acad Sci U S A. 2014;111(10):3739-44. doi: 10.1073/pnas.1401861111. PubMed PMID: 24567412; PubMed Central PMCID: PMC3956202.

8. Chen D, Wang Q, Huang H, Xia L, Jiang X, Kan L, *et al*. Effete-mediated degradation of Cyclin A is essential for the maintenance of germline stem cells in *Drosophila*. Development. 2009;136(24):4133-42. Epub 2009/11/13. doi: 10.1242/dev.039032. PubMed PMID: 19906849.

9. Ables ET, Drummond-Barbosa D. Cyclin E controls *Drosophila* female germline stem cell maintenance independently of its role in proliferation by modulating responsiveness to niche signals. Development. 2013;140(3):530-40. Epub 2013/01/08. doi: 10.1242/dev.088583. PubMed PMID: 23293285; PubMed Central PMCID: PMC3561789.

10. Wang Z, Lin H. The division of *Drosophila* germline stem cells and their precursors requires a specific cyclin. Curr Biol. 2005;15(4):328-33. Epub 2005/02/23. doi: 10.1016/j.cub.2005.02.016. PubMed PMID: 15723793.

11. Jenik PD, Jurkuta RE, Barton MK. Interactions between the cell cycle and embryonic patterning in *Arabidopsis* uncovered by a mutation in DNA polymerase epsilon. Plant Cell. 2005;17(12):3362-77. Epub 2005/11/10. doi: 10.1105/tpc.105.036889. PubMed PMID: 16278345; PubMed Central PMCID: PMC1315375.

12. Berry LW, Westlund B, Schedl T. Germ-line tumor formation caused by activation of *glp-1*, a *Caenorhabditis elegans* member of the Notch family of receptors. Development. 1997;124(4):925-36. PubMed PMID: 9043073.

13. Shin H, Haupt KA, Kershner AM, Kroll-Conner P, Wickens M, Kimble J. SYGL-1 and LST-1 link niche signaling to PUF RNA repression for stem cell maintenance in *Caenorhabditis elegans*. PLoS Genet. 2017;13(12):e1007121. Epub 2017/12/13. doi: 10.1371/journal.pgen.1007121. PubMed PMID: 29232700.

14. Kadyk LC, Kimble J. Genetic regulation of entry into meiosis in *Caenorhabditis elegans*. Development. 1998;125(10):1803-13. PubMed PMID: 9550713.

15. Eckmann CR, Crittenden SL, Suh N, Kimble J. GLD-3 and control of the mitosis/meiosis decision in the germline of *Caenorhabditis elegans*. Genetics. 2004;168(1):147-60. doi:

10.1534/genetics.104.029264. PubMed PMID: 15454534; PubMed Central PMCID: PMC1448115.

16. Thompson O, Edgley M, Strasbourger P, Flibotte S, Ewing B, Adair R, *et al*. The million mutation project: a new approach to genetics in *Caenorhabditis elegans*. Genome Res. 2013;23(10):1749-62. Epub 2013/06/27. doi: 10.1101/gr.157651.113. PubMed PMID: 23800452; PubMed Central PMCID: PMC3787271.

17. Brenner S. The genetics of *Caenorhabditis elegans*. Genetics. 1974;77(1):71-94. PubMed PMID: 4366476.

18. Singh K, Chao MY, Somers GA, Komatsu H, Corkins ME, Larkins-Ford J, *et al*. *C. elegans* Notch signaling regulates adult chemosensory response and larval molting quiescence. Curr Biol. 2011;21(10):825-34. doi: 10.1016/j.cub.2011.04.010. PubMed PMID: 21549604; PubMed Central PMCID: PMC3100419.

19. Siegfried KR, Kimble J. POP-1 controls axis formation during early gonadogenesis in *C. elegans.* Development. 2002;129(2):443-53. Epub 2002/01/25. PubMed PMID: 11807036.

20. Lee J, Jongeward GD, Sternberg PW. *unc-101*, a gene required for many aspects of *Caenorhabditis elegans* development and behavior, encodes a clathrin-associated protein. Genes Dev. 1994;8(1):60-73. Epub 1994/01/01. PubMed PMID: 8288128.

21. Fay D, Bender A. Genetic mapping and manipulation: chapter 4--SNPs: introduction and two-point mapping. WormBook. 2006:1-7. Epub 2007/12/01. doi: 10.1895/wormbook.1.93.1. PubMed PMID: 18050460.

22 Minevich G, Park DS, Blankenberg D, Poole RJ, Hobert O. CloudMap: a cloud-based pipeline for analysis of mutant genome sequences. Genetics. 2012;192(4):1249-69. Epub 2012/10/12. doi: 10.1534/genetics.112.144204. PubMed PMID: 23051646; PubMed Central PMCID: PMC3512137.

Fig 1
Appendix B

A

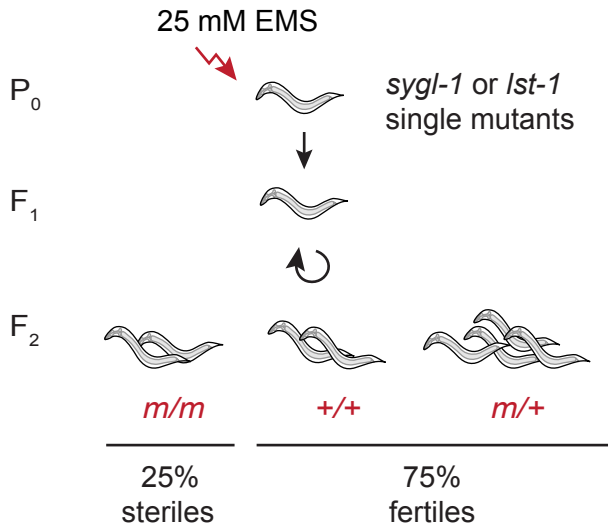

B

Classification	Genotype	Haploid gametes screened	# Isolated Glp mutants
lst-1 enhancer screen	*lst-1(ok814)*	8,749	6
	lst-1(ok814); qSi44[glp-1::6xMYC6xHIS][1]	7,922	0
sygl-1 enhancer screen	*sygl-1(tm5040)*	5,504	4
	sygl-1(tm5040)qSi44[glp-1::6xMYC6xHIS][1]	3,868	2

C

Alleles	Gene	Descriptions
q817	*glp-1*	P111S (missense)
q818	*glp-1*	98Qstop (nonsense)
q819	*glp-1*	H1000Y (missense)
q820	*glp-1*	N992K (missense)
q821	*glp-1*	R499stop (nonsense)
q822	*glp-1*	Y176stop (nonsense)
q823	*likely glp-1*	not mapped
q824	*glp-1*	Intronic mutation
q825	*glp-1*	5' splice site mutation
q826	*lst-1*	R114stop (nonsense)
q827	*lst-1*	5' splice site mutation
q831	*pole-1*	W1899stop (nonsense)

D

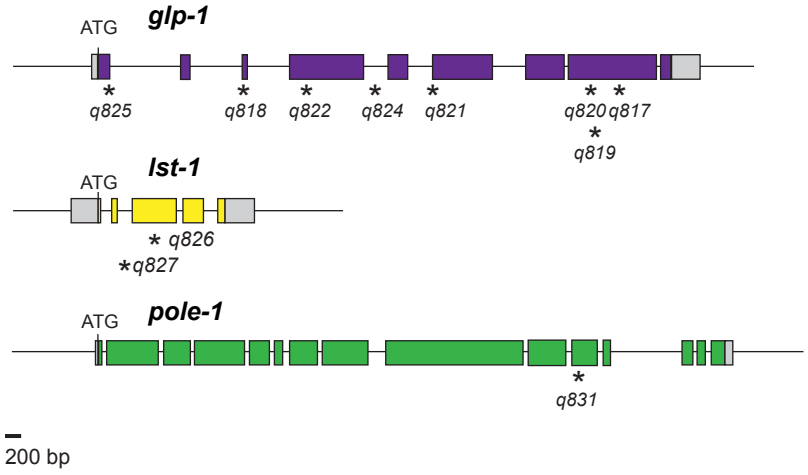

Figure 1. Summary of *sygl-1* and *lst-1* enhancer screen.

(**A**) Schematic of the *sygl-1* or *lst-1* enhancer screen. P0 animals were mutagenized, F1 animals were singled, and F2 progeny were screened for the germline proliferation defective (Glp) phenotype [2]. F1 progeny that show 25% Glp phenotype in the F2 generation were isolated. (**B**) Summary of the enhancer screen. 26,043 haploid gametes were screened yielding 12 new alleles. A single copy *glp-1* transgene, *qSi44 [Pglp-1::glp-1::6xmyc::6xHIS::glp-1 3'end],* was included in the second half of the screen to avoid getting additional *glp-1* alleles. (**C**) Summary of isolated alleles and mapping results. A total of nine *glp-1* mutations, two *lst-1* mutations, and one allele of novel gene were isolated. (**D**) Mapping of isolated *glp-1, lst-1,* and *pole-1* alleles. Colored boxes, exons; gray boxes, untranslated regions. Asterisk, mutations. One allele, *q823,* is not shown, as the mutation was not identified within the coding region or nearby regulatory region spanning ~2kb upstream and ~1kb downstream. Regardless, *q823* likely encodes a *glp-1* allele as it fails to complement the *glp-1(q175*) null allele.

Appendix C. *sygl-1* and *puf-8* redundantly promote oogenesis by repressing the MAP kinase pathway

---

I generated all data and wrote this appendix.

Introduction

PUF (Pumilio and FBF) proteins are a family of RNA binding proteins that govern multiple biological processes, including germline stem cell maintenance, memory formation, and sex determination [1, 2]. Despite their conservation, different species contain different number of PUF proteins, suggesting specialized functions in different organisms. For example, *S. cerevisiae* has 6 PUF homologs, *D. melanogaster* has 1 Pumilio homolog, *M. musculus* and *H. sapiens* have two PUM homologs [1]. In contrast, *C. elegans* contains a divergent family of 11 PUF proteins [1], making this model an excellent candidate to understand PUF functions in light of development and evolution. The central question is to ask how structurally similar proteins have evolved to control similar or different biological processes.

In this appendix, I focus on PUF-8, a *C. elegans* PUF protein that is most similar to vertebrate PUF homologs [1]. PUF-8 controls multiple aspects of germ cell development, including germ cell proliferation [3], differentiation [4, 5], sex determination [6-8], and and de-differentiation [9]. Most relevant here is its role in nematode sex-determination. *C. elegans* is a hermaphroditic organism that produces sperm in larva, and later switches to produce oocyte as adults [10] (**Figure 1A**). Sex-determination in this organism relies on elaborate regulatory network control ling conserved signaling pathways, transcription, RNA regulation, and protein turnover [11]. Loss-of-function or gain-of-function mutations of such key regulators either masculinize or feminize animals, demonstrating cell fate plasticity [11].

One critical signaling pathway that controls this switch from spermatogenesis to oogenesis is the MAPK (mitogen-activated protein kinase) pathway. MAPK signaling governs multiple processes in germ cell development including stem cell proliferation and germ cell differentiation [12]; Most relevant here is its role in promoting sperm fate [13], as multiple genetic backgrounds that lead to MAPK overexpression cause germ cell masculinization. For example, double mutants that lack either *fbf-1* or *puf-8* PUF homologs, combined with a loss of a MAPK phosphatase *lip-1* masculinize animals [6, 14]: FBF-1 and PUF-8 repress MAPK

expression at the mRNA level [4, 13], whereas LIP-1, a dual-specificity MAPK phosphatase, inactivates MAPK by dephosphorylation [15]. Although exact molecular mechanisms by which MAPK drives the sperm fate is not well understood, it is thought that MAPK controls the terminal RNA regulators of the sex-determination pathway (ex. FOG-1, FOG-3) by phosphorylation [16].

Here I focus on *sygl-1* and *lst-1* stem cell regulators and investigate their genetic relationship with *puf-8*. In Chapter 3, I demonstrated that these two Notch signaling targets redundantly promote FBF activity to drive germline stem cell (GSC) self-renewal. To ask if similar genetic redundancy exists in relation to another PUF protein *puf-8*, I analyzed germline sex phenotypes of animals depleted with either *sygl-1* and *puf-8*, or *lst-1* and *puf-8*. I found that *sygl-1* and *puf-8* redundantly promote oogenesis. I further demonstrate that MAPK overexpression underlies the *sygl-1 puf-8* double mutant oogenesis defects. Intriguingly, *sygl-1*, but not *lst-1*, cause synthetic oogenesis defects when combined with *puf-8*. Therefore, *sygl-1* and *lst-1* act in a non-redundant fashion in sex determination, unlike their redundant function in stem cell self-renewal. I propose that these observations provide clues to delineate *sygl-1* and *lst-1* biological redundancy.

Results and Discussion

sygl-1 and *puf-8* redundantly promote oogenesis

To investigate whether *sygl-1* or *lst-1* can regulate additional PUF proteins, I focused on *puf-8*. I hypothesized that genetic interaction with *puf-8* was likely because PUF-8 is detected in mitotic germ cells [5], which partially overlaps with SYGL-1 or LST-1 expression in the distal-most germ cells. To this end, I depleted *puf-8* in *sygl-1* or *lst-1* single mutants by RNA interference (RNAi), and asked whether synthetic phenotypic changes occur in these animals. Interestingly, *sygl-1* and *lst-1* mutants responded differently: 100% of *sygl-1* single mutants were sterile, whereas 100% of *lst-1* single mutants were fertile in the absence of *puf-8* (n> 50). This

defect was specific to *puf-8* knockdown, as control RNAi did not result in any sterility (**Figure 1B**).

To confirm this result, I generated *sygl-1; puf-8* double mutant and examined the gonad. Immunostaining with sperm marker (SP56) and oocyte marker (RME-2) revealed that 100% of *sygl-1; puf-8* double mutants are sterile due to masculinization (**Figure 1C, top)**; However, weak oocyte marker expression was observed in ~15% animals despite the lack of functional oocytes (**Figure 1C, bottom)** (n=30). This intersexual molecular signature is highly similar to previously reported masculinized mutants with overexpressed MAPK (see below) [6]. I conclude that *sygl-1* and *puf-8* redundantly promote oogenesis, and *puf-8* promote oogenesis synergistically with *sygl-1,* but not with *lst-1*.

sygl-1; puf-8 **masculinization is suppressed by MAPK depletion**

Previously, multiple genetic backgrounds containing *puf-8* were reported to masculinize the germline, but the molecular mechanisms were different. For example, *puf-8 fbf-1* double mutants are masculinized due to ectopic FOG-2 expression, a key regulator in sex-determination pathway [8]. In contrast, *puf-8; lip-1* and *fbf-1; lip-1* double mutants are masculinized due to ectopic overexpression of MAPK [6, 7]: a small molecule inhibitor of MAPK, or *mpk-1* depletion by RNAi can reprogram germ cells of these mutants to switch from spermatogenesis to oogenesis, demonstrating that decreasing the dose of MAPK can reprogram the germ cell sexual fate in a highly plastic manner [6, 7].

To ask if MAPK overexpression is the underlying cause of *sygl-1; puf-8* double mutant masculinization, I depleted *mpk-1* in these animals using an RNAi construct that targets germline enriched *mpk-1b* isoform [13]. Surprisingly, decreasing *mpk-1* expression rescued *sygl-1; puf-8* masculinization defects: 86% of *sygl-1 puf-8* mutants treated with *mpk-1*(RNAi) produced oocytes and produced viable progeny (n=42), whereas 100% animals treated with

control RNAi resulted in masculinized sterility (n=38) (**Figure 1D**). These results demonstrate that *sygl-1* and *puf-8* redundantly repress the MAPK pathway to promote oogenesis.

How do *sygl-1* and *puf-8* repress MAPK? As PUF-8 associates with the core MAPK pathway genes such as *let-60, lin-45*, and *mpk-1* by immunoprecipitation (IP) experiments [3, 4], one likely hypothesis is that PUF-8 represses these transcripts at the mRNA level (**Figure 1E**). However, it is not clear how SYGL-1 represses MAPK either directly or indirectly. As FBF is a conserved MAPK repressor [13] and SYGL-1 work with FBF to promote stem cell self-renewal [17], one plausible model is that SYGL-1 can work with FBF to repress transcripts encoding the core MAPK pathway (**Figure 1E**). Alternatively, SYGL-1 may repress MAPK independent of FBF. Three experiments are critical to address this molecular mechanism. The first is to ask whether MPK repression in the germline requires the distal-most, Notch-dependent SYGL-1 positive cells, or proximal, Notch-independent SYGL-1 positive cells, as SYGL-1 proteins are enriched in two distinct regions in the germline including the distal-most GSC pool and the proximal loop and oocytes [17]. Next, *mpk-1* single molecular FISH or MPK-1 staining in *sygl-1* mutants may reveal molecular clues to this repression. Finally, asking if SYGL-1 can IP *let-60, lin-45*, *lip-1,* and *mpk-1* transcripts will address whether SYGL-1 can repress these genes at the mRNA level.

Conclusion and Future Directions

Here I have shown that *sygl-1* and *puf-8* redundantly promote *C. elegans* oogenesis, by repressing the MAPK pathway. While the molecular basis of this repression remains to be explored in the future, these observations uncover a role of SYGL-1 in nematode sex-determination. Interestingly, I find that two redundant genes in GSC self-renewal, *sygl-1* and *lst-1*, act differently in *puf-8* mutants.

As discussed above, future experiments need to address how SYGL-1 and PUF-8 repress the MAPK pathway. Key experiments will address which cells in the germline are

required for proper MAPK repression to promote oogenesis, and how repression happens at the transcription, mRNA regulation, or at the protein level. I suggest that understanding the molecular basis of this repression may uncover conserved gene regulatory circuits that control broad animal development.

Material and Methods

Nematode strain maintenance

Strains were maintained at 20°C as described in [18]. Alleles and balancers are as follows: LG I: *lst-1(ok814)* [19], *sygl-1(tm5040)* [20]. LG *II: puf-8 (q725*) [8]. Balancers are as follows: LG*II*: *mIn1[mIs14 dpy-10(e128)]* [21].

Nematode strains used in this study

N2: wild type

JK4356: *lst-1(ok814) I*

JK4899: *sygl-1(tm5040) I*

JK5508: *sygl-1(tm5040) I; puf-8(q725)/ mIn1[mIs14 dpy-10(e128)] II*

RNAi

Feeding RNAi was performed as described [22] using *puf-8* clone from the Ahringer RNAi library [23] or *mpk-1b* clone from [13]. Control was the L4440 backbone plasmid. Bacteria were grown overnight at 37°C in 2xYT media containing 25 µg/µl carbenicillin and 50 µg/µl tetracycline. Cultures were concentrated, seeded onto Nematode Growth Medium (NGM) plates containing 1mM IPTG, then induced overnight. Animals of fourth larval stage (L4) were plated and the next generation was scored for phenotypic analysis.

Immunostaining and DAPI staining

Staining followed established protocols [24]. Briefly, staged animals were dissected in PBStw (PBS + 0.1% (v/v) Tween-20) with 0.25 mM levamisole to extrude gonads. Tissues were fixed in 3% (w/v) paraformaldehyde diluted in 100 mM K_2HPO_4 (pH 7.2) for 30 minutes. Post fixation, all samples were permeabilized with ice-cold methanol for 30 minutes, blocked with 0.5% (w/v) bovine serum albumin for 1 hour. For primary antibodies, samples were incubated overnight at the following dilutions in the blocking solution: Mouse SP56 (1:200, [25], Rabbit RME-2 (1:50, [26]). For secondary antibodies, samples were incubated for 1 hour at room temperature at the following dilutions: Donkey Alexa 555 anti-mouse (1:1000, Invitrogen #A31570), Goat Alexa 488 anti-rabbit (1:1000, Invitrogen #A11034). To visualize DNA, DAPI was included at a final concentration of 0.5-1 ng/μl during the last 10 minutes of secondary antibody incubation. Vectashield (Vector Laboratories #H-1000) was used as mounting medium.

Microscopy

Zeiss Axioskop with Hamamatsu CCD or ORCA cMOS camera equipped with 63x 1.4NA Plan Apochromat oil immersion objective was used. Carl Zeiss filter sets 49, 38, and 43HE were used for the visualization of DAPI, Alexa 488, and Alexa 555 respectively. An X-Cite 120Q lamp (Lumen Dynamics) was used as the fluorescence light source. Openlab 5.5.2 (PerkinElmer) and Micromanager [27, 28] were used as acquisition software.

References

1. Wickens M, Bernstein DS, Kimble J, Parker R. A PUF family portrait: 3'UTR regulation as a way of life. Trends Genet. 2002;18(3):150-7. PubMed PMID: 11858839.

2. Quenault T, Lithgow T, Traven A. PUF proteins: repression, activation and mRNA localization. Trends Cell Biol. 2011;21(2):104-12. doi: 10.1016/j.tcb.2010.09.013. PubMed PMID: 21115348.

3. Ariz M, Mainpal R, Subramaniam K. C. elegans RNA-binding proteins PUF-8 and MEX-3 function redundantly to promote germline stem cell mitosis. Dev Biol. 2009;326(2):295-304. doi: 10.1016/j.ydbio.2008.11.024. PubMed PMID: 19100255; PubMed Central PMCID: PMC2680957.

4. Vaid S, Ariz M, Chaturbedi A, Kumar GA, Subramaniam K. PUF-8 negatively regulates RAS/MAPK signalling to promote differentiation of *C. elegans* germ cells. Development. 2013;140(8):1645-54. doi: 10.1242/dev.088013. PubMed PMID: 23487310; PubMed Central PMCID: PMC3621483.

5. Racher H, Hansen D. PUF-8, a Pumilio homolog, inhibits the proliferative fate in the *Caenorhabditis elegans* germline. G3 (Bethesda). 2012;2(10):1197-205. doi: 10.1534/g3.112.003350. PubMed PMID: 23050230; PubMed Central PMCID: PMC3464112.

6. Sorokin EP, Gasch AP, Kimble J. Competence for chemical reprogramming of sexual fate correlates with an intersexual molecular signature in *Caenorhabditis elegans*. Genetics. 2014;198(2):561-75. Epub 2014/08/26. doi: 10.1534/genetics.114.169409. PubMed PMID: 25146970; PubMed Central PMCID: PMC4196613.

7. Morgan DE, Crittenden SL, Kimble J. The *C. elegans* adult male germline: stem cells and sexual dimorphism. Dev Biol. 2010;346(2):204-14. doi: 10.1016/j.ydbio.2010.07.022. PubMed PMID: 20659446; PubMed Central PMCID: PMC2945412.

8. Bachorik JL, Kimble J. Redundant control of the *Caenorhabditis elegans* sperm/oocyte switch by PUF-8 and FBF-1, two distinct PUF RNA-binding proteins. Proc Natl Acad Sci U S A.

2005;102(31):10893-7. doi: 10.1073/pnas.0504593102. PubMed PMID: 16037210; PubMed Central PMCID: PMC1182444.

9. Subramaniam K, Seydoux G. Dedifferentiation of primary spermatocytes into germ cell tumors in *C. elegans* lacking the pumilio-like protein PUF-8. Curr Biol. 2003;13(2):134-9. PubMed PMID: 12546787.

10. Hubbard EJ, Greenstein D. Introduction to the germ line. WormBook. 2005:1-4. Epub 2007/12/01. doi: 10.1895/wormbook.1.18.1. PubMed PMID: 18050415; PubMed Central PMCID: PMC4781435.

11. Ellis RE. Sex determination in the *Caenorhabditis elegans* germ line. Curr Top Dev Biol. 2008;83:41-64. Epub 2009/01/03. doi: 10.1016/S0070-2153(08)00402-X. PubMed PMID: 19118663.

12. Lee MH, Ohmachi M, Arur S, Nayak S, Francis R, Church D, *et al*. Multiple functions and dynamic activation of MPK-1 extracellular signal-regulated kinase signaling in *Caenorhabditis elegans* germline development. Genetics. 2007;177(4):2039-62. Epub 2007/12/13. doi: 10.1534/genetics.107.081356. PubMed PMID: 18073423; PubMed Central PMCID: PMC2219468.

13. Lee MH, Hook B, Pan G, Kershner AM, Merritt C, Seydoux G, *et al*. Conserved regulation of MAP kinase expression by PUF RNA-binding proteins. PLoS Genet. 2007;3(12):e233. doi: 10.1371/journal.pgen.0030233. PubMed PMID: 18166083; PubMed Central PMCID: PMC2323325.

14. Morgan CT, Lee MH, Kimble J. Chemical reprogramming of *Caenorhabditis elegans* germ cell fate. Nat Chem Biol. 2010;6(2):102-4. Epub 2010/01/19. doi: 10.1038/nchembio.282. PubMed PMID: 20081824; PubMed Central PMCID: PMC2808631.

15. Berset T, Hoier EF, Battu G, Canevascini S, Hajnal A. Notch inhibition of RAS signaling through MAP kinase phosphatase LIP-1 during *C. elegans* vulval development. Science.

2001;291(5506):1055-8. Epub 2001/02/13. doi: 10.1126/science.1055642. PubMed PMID: 11161219.

16. Datla US, Scovill NC, Brokamp AJ, Kim E, Asch AS, Lee MH. Role of PUF-8/PUF protein in stem cell control, sperm-oocyte decision and cell fate reprogramming. J Cell Physiol. 2014;229(10):1306-11. Epub 2014/03/19. doi: 10.1002/jcp.24618. PubMed PMID: 24638209.

17. Shin H, Haupt KA, Kershner AM, Kroll-Conner P, Wickens M, Kimble J. SYGL-1 and LST-1 link niche signaling to PUF RNA repression for stem cell maintenance in *Caenorhabditis elegans*. PLoS Genet. 2017;13(12):e1007121. Epub 2017/12/13. doi: 10.1371/journal.pgen.1007121. PubMed PMID: 29232700.

18. Brenner S. The genetics of *Caenorhabditis elegans*. Genetics. 1974;77(1):71-94. PubMed PMID: 4366476.

19. Singh K, Chao MY, Somers GA, Komatsu H, Corkins ME, Larkins-Ford J, *et al*. *C. elegans* Notch signaling regulates adult chemosensory response and larval molting quiescence. Curr Biol. 2011;21(10):825-34. doi: 10.1016/j.cub.2011.04.010. PubMed PMID: 21549604; PubMed Central PMCID: PMC3100419.

20. Kershner AM, Shin H, Hansen TJ, Kimble J. Discovery of two GLP-1/Notch target genes that account for the role of GLP-1/Notch signaling in stem cell maintenance. Proc Natl Acad Sci U S A. 2014;111(10):3739-44. doi: 10.1073/pnas.1401861111. PubMed PMID: 24567412; PubMed Central PMCID: PMC3956202.

21. Edgley ML, Riddle DL. LG II balancer chromosomes in *Caenorhabditis elegans*: *mT1(II;III)* and the *mIn1* set of dominantly and recessively marked inversions. Mol Genet Genomics. 2001;266(3):385-95. Epub 2001/11/20. doi: 10.1007/s004380100523. PubMed PMID: 11713668.

22. Timmons L, Fire A. Specific interference by ingested dsRNA. Nature. 1998;395(6705):854. doi: 10.1038/27579. PubMed PMID: 9804418.

23. Fraser AG, Kamath RS, Zipperlen P, Martinez-Campos M, Sohrmann M, Ahringer J. Functional genomic analysis of C. elegans chromosome I by systematic RNA interference. Nature. 2000;408(6810):325-30. Epub 2000/12/01. doi: 10.1038/35042517. PubMed PMID: 11099033.

24. Crittenden SL, Seidel HS, Kimble J. Analysis of the *C. elegans* germline stem cell pool. Methods Mol Biol. 2017;1463:1-33. doi: 10.1007/978-1-4939-4017-2_1. PubMed PMID: 27734344.

25. Ward S, Roberts TM, Strome S, Pavalko FM, Hogan E. Monoclonal antibodies that recognize a polypeptide antigenic determinant shared by multiple *Caenorhabditis elegans* sperm-specific proteins. J Cell Biol. 1986;102(5):1778-86. Epub 1986/05/01. PubMed PMID: 2422180; PubMed Central PMCID: PMC2114204.

26. Grant B, Hirsh D. Receptor-mediated endocytosis in the *Caenorhabditis elegans* oocyte. Mol Biol Cell. 1999;10(12):4311-26. Epub 1999/12/10. PubMed PMID: 10588660; PubMed Central PMCID: PMC25760.

27. Edelstein AD, Tsuchida MA, Amodaj N, Pinkard H, Vale RD, Stuurman N. Advanced methods of microscope control using μManager software. J Biol Methods. 2014;1(2). Epub 2015/01/22. doi: 10.14440/jbm.2014.36. PubMed PMID: 25606571; PubMed Central PMCID: PMC4297649.

28. Edelstein A, Amodaj N, Hoover K, Vale R, Stuurman N. Computer control of microscopes using μManager. Curr Protoc Mol Biol. 2010;Chapter 14:Unit14 20. Epub 2010/10/05. doi: 10.1002/0471142727.mb1420s92. PubMed PMID: 20890901; PubMed Central PMCID: PMC3065365.

Fig 1
Appendix C

A ***C. elegans* development**

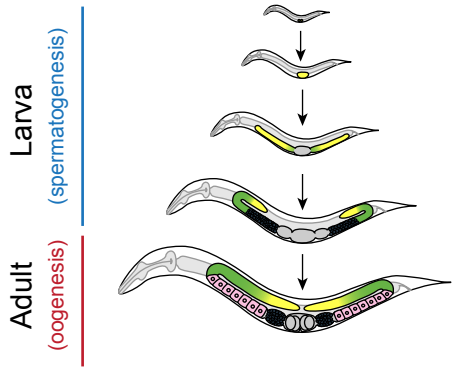

B

Allele	*puf-8* RNAi[1]	control RNAi[1]
sygl-1(tm5040)	Sterile (100%)[2]	Fertile (100%)[2]
lst-1(ok814)	Fertile (100%)[2]	Fertile (100%)[2]

[1] L4 feeding
[2] n > 50

C

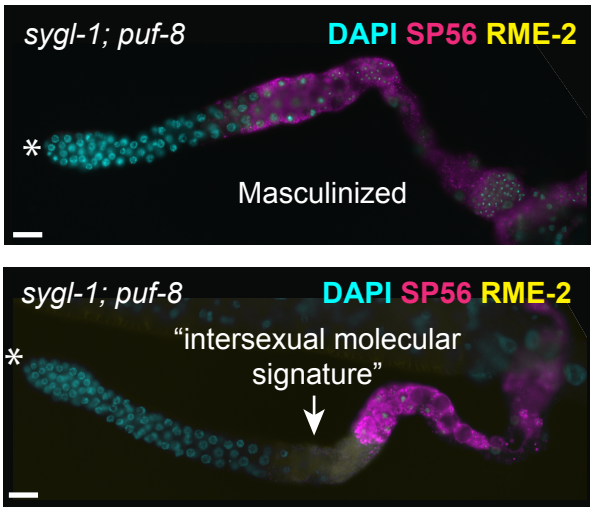

D

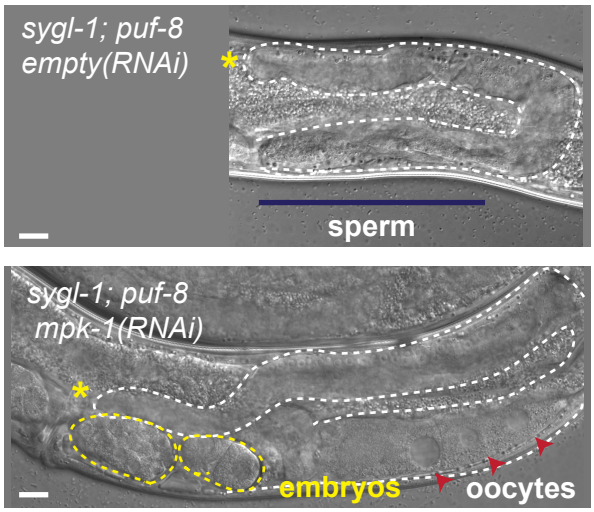

E **Model**

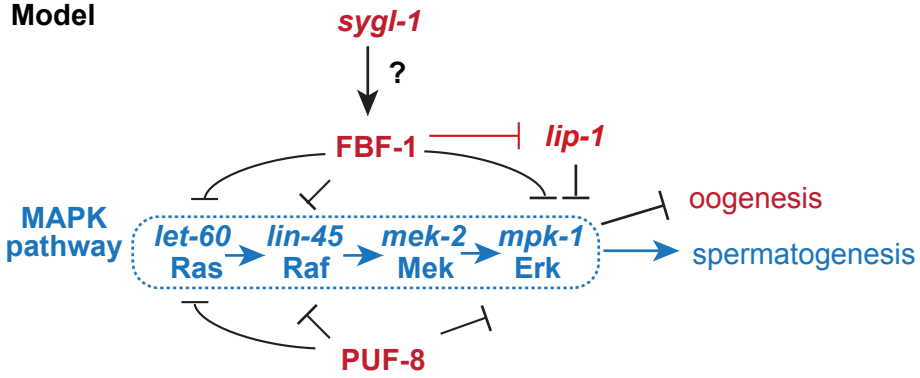

Figure 1. *sygl-1* and *puf-8* redundantly promotes oogenesis by repressing MAP kinase. (**A**) Schematics of the *C. elegans* development. *C. elegans* hermaphrodites (XO) produce sperm as larva, but switches to oogenesis as adults. (**B**) Summary of *puf-8* knockdown in *sygl-1* or *lst-1* single mutants. *sygl-1; puf-8 (RNAi)* were 100% sterile, whereas *lst-1; puf-8 (RNAi)* were fertile. (**C**) Dissected *sygl-1; puf-8* gonads stained with sperm (SP56) and oocyte (RME-2) markers. DAPI was added to visualize DNA. Essentially all *sygl-1; puf-8* animals were masculinized. The majority of gonads (~85%) exclusively expressed the sperm marker (top), but some gonads (~15%) also expressed the oocyte marker (bottom) showing "intersexual molecular signature" [6]. Scale bar is 20 microns. (**D**) MAPK suppression restores the fertility of *sygl-1; puf-8* animals. *sygl-1; puf-8* animals treated with *mpk-1b(RNAi)* generates functional oocytes and viable embryos (bottom). In contrast, controls treated with *empty* (RNAi) are sterile due to masculinization (top). White dotted lines, outline of the gonad. Yellow dotted lines, embryos. Arrowheads, oocytes. Asterisk, distal end. Scale bar, 20 microns. (**E**) Molecular model for MAPK regulation in sperm-oocyte switch. FBF-1 and PUF-8 likely repress multiple genes in the MAPK pathway (e.g. *let-60, lin-45, mpk-1*) through 3'UTR mediated regulation [16]. SYGL-1 may work with FBF to repress mRNA transcripts, which encode the core MAPK pathway.

Appendix D. Development of a live-cell Notch transcriptional reporter

---

This is an ongoing project in collaboration with ChangHwan Lee in the Kimble laboratory. I performed experiments described in this appendix, which will be submitted for publication (Lee *et al,* in preparation).

Introduction

Life is constantly in motion, and so are molecules in cells. Observing molecules in motion offers spatial and temporal information and reveals dynamic nature of cellular events. Recent developments in mRNA visualization techniques allow tracking of single or multiple mRNAs using live-cell microscopy. In these methods, mRNAs are tethered to fluorescent molecules or protein tags to track movements [1]. One such tethering method is the bacteriophage MS2/MCP, a system that utilizes a high-affinity interaction between MS2 RNA sequence and MS2 Coat proteins (MCP) [2]. Briefly, an mRNA of interest can be modified to include multiple MS2 sequences at various regions within the transcript, including untranslated regions (UTR); co-expression of MCP fused with a fluorescent protein (MCP-FP) allows tracking individual mRNA through live-cell imaging (**Figure 1A**) [2, 3]. To date, this approach has successfully been utilized to visualize mRNAs in unicellular and multicellular organisms, and has greatly contributed to understanding fundamental biological processes such as memory formation [e.g. 4].

Here we have utilized MS2/MCP tethering system to visualize Notch-dependent transcription within stem cells, in the *C. elegans* germline. We have focused on *sygl-1*, a key transcriptional target of GLP-1/Notch signaling critical for the stem cell maintenance [5] (**Figure 1B**). Preliminary results reveal that *sygl-1* active transcription sites (ATS) could be visualized in distal-most germ cells, in real time. *sygl-1* ATS appears graded, highly robust in the distal-most germ cells but less frequent as cells move proximally, similar to results revealed by single-molecule FISH to the endogenous *sygl-1* gene in fixed gonad [6]. Reagents described in this appendix successfully visualize *sygl-1* transcription events *in vivo*, and provide a toolkit to analyze the dynamics of Notch transcription in stem cells. Similar approaches could be utilized to study transcription dynamics in other cell lineages, which may reveal insights into transcriptional control in development.

Results and Discussion

To visualize *sygl-1* transcription in real time, we developed a live-cell reporter using MS2 –MCP system. This reporter system consists of two parts: a *sygl-1* transgene that contains 24 copies of MS2 stem loops at the 5'UTR (hereafter 24xMS2::3xFLAG::*sygl-1*), and the MS2 coating protein (MCP) tagged with a super-folder GFP (sfGFP) protein that is ubiquitously expressed in the germline (hereafter MCP::sfGFP). To label germ cell nuclei, mCherry tagged histone (hereafter H2B::mCherry) was co-expressed with MCP::sfGFP in an operon (**Figure 1C**). Transgenic animals containing each construct were generated by Mos-1 mediated single-copy methods [7, 8]; Next, animals harboring each construct were crossed together to visualize *sygl-1* transcription sites. We expected that active transcription sites (ATS) would be visible in bright foci in germ cell nuclei in this setup, as ATS contains multiple mRNAs and therefore yield improved signal to noise ratio. However, we did not expect to visualize cytoplasmic mRNAs because MCP::sfGFP is brightly expressed in the cytoplasm.

As expected, robust nuclear foci were visible in the distal-most germ cells (**Figure 1D**), corresponding to the region of *sygl-1* mRNA expression [5, 6]. The *sygl-1* transcription sites were abundant in the distal-most cells, as previously observed in fixed cells using single-molecule FISH [6]. Additional *sygl-1* nuclear foci were detected in the proximal loop region (data not shown); these proximal transcription foci likely produce Notch-independent *sygl-1* transcripts [5, 6]. We conclude that 24xMS2::3xFLAG::*sygl-1* and MCP::sfGFP successfully visualize *sygl-1* transcription events in the germline, demonstrating the possibility that these reagents can be utilized to study transcription dynamics *in vivo*.

We next characterized 24xMS2::3xFLAG::*sygl-1*, to ask if this transgenic construct can generate functional SYGL-1 protein. Our specific question was to ask whether 24xMS2::3xFLAG::*sygl-1* can produce functional SYGL-1, as 24x MS2 loops in the *sygl-1* 5'UTR may inhibit SYGL-1 translation due to secondary RNA structure. First, we assayed the amount of 3xFLAG::SYGL-1 generated in the distal gonad. Immunostaining with anti-FLAG

antibody revealed that no signal was detectable above the background level (**Figure 1E)**, suggesting that 24xMS2 sequences within the 5'UTR likely inhibit SYGL-1 translation. To probe this further, we tested the function of 24xMS2::3xFLAG::*sygl-1*. Our functional assay utilized the genetic redundancy with *lst-1*, as *sygl-1* null mutants cause synthetically sterility with *lst-1* mutant [5]. Therefore, the presence of 24xMS2::3xFLAG::*sygl-1* transgene will rescue *lst-1 sygl-1* sterile phenotype if the transgenic copy makes enough functional SYGL-1. We found that 100% of 24xMS2::3xFLAG::*sygl-1* transgenic animals were sterile on *lst-1*(RNAi) (n=48), consistent with the idea that 24xMS2::3xFLAG::*sygl-1* transgene cannot make functional SYGL-1 proteins. In contrast, control animals that did not have 24xMS2 loops but have tagged transgenic copy of *sygl-1* (3xFLAG::*sygl-1)* were 100% fertile (n=34). Importantly, these RNAi experiments were done in a *sygl-1* null background such that transgenic copies are the sole source of *sygl-1*. Together, these results demonstrate that 24xMS2::3xFLAG::*sygl-1* can be used to visualize *sygl-1* transcription events, but the presence of 24xMS2 loops inhibits SYGL-1 translation.

Conclusion and Future directions

Here we have developed a live-cell, *in vivo* molecular reporter of Notch signaling using the *sygl-1* gene. Analyses of this reporter will provide spatial and temporal insights into Notch dependent transcription within germline stem cells. Characterization of transcription bursts (size, frequency) and investigating the regulatory input that control these events are key next steps. Insights from these analyses can be utilized to investigate Notch dependent transcription in soma (e.g. embryo [9], vulva [10]), or to study other canonical signaling pathways (e.g. Wnt, MAPK) in *C. elegans*.

Material and Methods

Nematode strain maintenance

Strains were maintained at 20°C as described in [11]. Alleles and balancers are as follows: LG I: *sygl-1(tm5040)* [5], *sygl-1(q828)* [12]. LG *II: ttTi5605* [8], *qSi49[Psygl-1::3xFLAG::sygl-1::sygl-1 3'UTR]* [12]. LG *III*: *glp-1(q224)* [13]. LG *V*: *oxTi365* [7].

Nematode strains used in this study

N2: wild type

EG6699: *ttTi5605 II; unc-119(ed3) III*

EG8082: *unc-119(ed3) III; oxTi365 V*

JK5499: *sygl-1(q828) I; qSi49[Psygl-1::3xFLAG::sygl-1::sygl-1 3'end] II*

JK5863: *qSi368 [Psygl-1:: 24xMS2 loops::3xFLAG::sygl-1::sygl-1 3'end] II; unc-119(ed3) III; qsi371[Pmex-5::MS2 Coat Protein::linker::sfGFP::tbb-2 3'end::gpd-2 intergenic sequence::H2B::mCherry::unc-54 3'end] V*

JK5896: *qSi369 [Psygl-1:: 24xMS2 loops::3xFLAG::sygl-1::sygl-1 3'end] II; unc-119(ed3) III; qsi370[Pmex-5::MS2 Coat Protein::linker::sfGFP::tbb-2 3'end::gpd-2 intergenic sequence::H2B::mCherry::unc-54 3'end] V*

JK5943: *qSi369[Psygl-1:: 24xMS2 loops::3xFLAG::sygl-1::sygl-1 3'end] II; glp-1(q224) III*; *qSi370[Pmex-5::MS2 Coat Protein::linker::sfGFP::tbb-2 3'end::gpd-2 intergenic sequence::H2B::mCherry::unc-54 3'end] V*

JK5932: *sygl-1(q828) I; qSi369[Psygl-1:: 24xMS2 loops::3xFLAG::sygl-1::sygl-1 3'end] II; qSi370[Pmex-5::MS2 Coat Protein::linker::sfGFP::tbb-2 3'end::gpd-2 intergenic sequence::H2B::mCherry::unc-54 3'end] V*

Transgenic *C. elegans*

Single-copy transgenes were generated using the Mos-1 mediated single-copy insertion method (MosSCI) [7, 8]. Briefly, pJK2014 *[Psygl-1:: 24xMS2 loops::3xFLAG::sygl-1::sygl-1 3'end]* was generated in two steps. First, pJK1658 [*Psygl-1::3xFLAG::sygl-1::sygl-1 3'end*] [12] was modified to include the NotI and PmeI restriction sites in front of the *sygl-1* start codon, to generate an intermediate plasmid. Next, this intermediate plasmid and pCR4-24MS2 (Addgene #31865) were both digested with NotI and PmeI restriction enzymes, and ligated together to insert 24xMS2 sequences in front of the *sygl-1* start codon. 50 ng/μl pJK2014 was injected into EG6699 along with transposase and co-injection markers to generate *qSi368* and *qSi369.*

Next, pJK2020 [*Pmex-5::MS2 Coat Protein::linker::sfGFP::tbb-2 3'end::gpd-2 intergenic sequence::H2B::mCherry::unc-54 3'end]* was constructed by using the Gibson assembly method, using pMS2-GFP (Addgene #27121) and pDONR-sfGFP (Gift from Andy Golden and Harold Smith) as templates. The *mex-5* promoter and *tbb-2* unc-*54* 3 'end sequences used are as described in [14], and *gpd-2* intergenic sequence was used to make an SL2 trans-spliced operon, as described in [15]. 50 ng/μl pJK2020 was injected into EG8082 along with transposase and co-injection markers to generate *qSi370* and *qSi371*.

***lst-1* RNAi**

Feeding RNAi was performed as described [16] using the *lst-1* clone from the Ahringer RNAi library [17]. Control was the L4440 backbone plasmid. Bacteria were grown overnight at 37°C in 2xYT media containing 25 μg/μl carbenicillin and 50 μg/μl tetracycline. Cultures were concentrated, seeded onto Nematode Growth Medium (NGM) plates containing 1mM IPTG, then induced overnight. JK5499, JK5932 animals of fourth larval stage (L4) were plated, and the next generation was scored for sterility as adults.

Immunostaining and DAPI staining, and Microscopy

Staining followed established protocols [18]. Briefly, N2, JK5499, JK5896 were staged to 24 hours after the forth larval stage, and were dissected in PBStw (PBS + 0.1% (v/v) Tween-20) with 0.25 mM levamisole to extrude gonads. Tissues were fixed in 3% (w/v) paraformaldehyde diluted in 100 mM K_2HPO_4 (pH 7.2) for 30 minutes. Post fixation, all samples were permeabilized with ice-cold methanol for 10 minutes, blocked with 30% (v/v) goat serum for 1 hour. For primary antibody, samples were incubated with mouse anti-FLAG (1:1000, Sigma #F1804) for overnight at 4°C. For secondary antibody, samples were incubated with donkey Alexa 555 anti-mouse (1:1000, Invitrogen #A31570) for 1 hour at room temperature. To visualize DNA, DAPI was included at a final concentration of 0.5 ng/μl during the last 10 minutes of secondary antibody incubation. Vectashield (Vector Laboratories #H-1000) was used as mounting medium. For microscopy, Zeiss Axioskop with ORCA cMOS camera equipped with 63x 1.4NA Plan Apochromat oil immersion objective was used. Carl Zeiss filter sets 49, 38, and 43HE were used for the visualization of DAPI, Alexa 488, and Alexa 555 respectively. An X-Cite 120Q lamp (Lumen Dynamics) was used as the fluorescence light source. For confocal microscopy, Leica TCS SP8 confocal microscope driven by LAS software version X was used using the resonance scanner. μmanager [21,22] were used as acquisition software.

Acknowledgements

I thank ChangHwan Lee for the conceptual design of the study, and the opportunity for collaboration.

References

1. Mannack LV, Eising S, Rentmeister A. Current techniques for visualizing RNA in cells. F1000Res. 2016;5. Epub 2016/05/10. doi: 10.12688/f1000research.8151.1. PubMed PMID: 27158473; PubMed Central PMCID: PMC4850879.

2. Bertrand E, Chartrand P, Schaefer M, Shenoy SM, Singer RH, Long RM. Localization of ASH1 mRNA particles in living yeast. Mol Cell. 1998;2(4):437-45. Epub 1998/11/11. PubMed PMID: 9809065.

3. Buxbaum AR, Haimovich G, Singer RH. In the right place at the right time: visualizing and understanding mRNA localization. Nat Rev Mol Cell Biol. 2015;16(2):95-109. Epub 2015/01/01. doi: 10.1038/nrm3918. PubMed PMID: 25549890; PubMed Central PMCID: PMC4484810.

4. Park HY, Lim H, Yoon YJ, Follenzi A, Nwokafor C, Lopez-Jones M, *et al*. Visualization of dynamics of single endogenous mRNA labeled in live mouse. Science. 2014;343(6169):422-4. Epub 2014/01/25. doi: 10.1126/science.1239200. PubMed PMID: 24458643; PubMed Central PMCID: PMC4111226.

5. Kershner AM, Shin H, Hansen TJ, Kimble J. Discovery of two GLP-1/Notch target genes that account for the role of GLP-1/Notch signaling in stem cell maintenance. Proc Natl Acad Sci U S A. 2014;111(10):3739-44. doi: 10.1073/pnas.1401861111. PubMed PMID: 24567412; PubMed Central PMCID: PMC3956202.

6. Lee C, Sorensen EB, Lynch TR, Kimble J. C. *elegans* GLP-1/Notch activates transcription in a probability gradient across the germline stem cell pool. Elife. 2016;5. doi: 10.7554/eLife.18370. PubMed PMID: 27705743; PubMed Central PMCID: PMC5094854.

7. Frokjaer-Jensen C, Davis MW, Sarov M, Taylor J, Flibotte S, LaBella M, *et al*. Random and targeted transgene insertion in *Caenorhabditis elegans* using a modified Mos1 transposon.

Nat Methods. 2014;11(5):529-34. Epub 2014/05/14. doi: 10.1038/nmeth.2889. PubMed PMID: 24820376; PubMed Central PMCID: PMC4126194.

8. Frokjaer-Jensen C, Davis MW, Hopkins CE, Newman BJ, Thummel JM, Olesen SP, *et al*. Single-copy insertion of transgenes in *Caenorhabditis elegans*. Nat Genet. 2008;40(11):1375-83. doi: 10.1038/ng.248. PubMed PMID: 18953339; PubMed Central PMCID: PMC2749959.

9. Priess JR. Notch signaling in the *C. elegans* embryo. WormBook. 2005:1-16. Epub 2007/12/01. doi: 10.1895/wormbook.1.4.1. PubMed PMID: 18050407; PubMed Central PMCID: PMC4780919.

10. Greenwald I. LIN-12/Notch signaling in *C. elegans*. WormBook. 2005:1-16. Epub 2007/12/01. doi: 10.1895/wormbook.1.10.1. PubMed PMID: 18050403; PubMed Central PMCID: PMC4781465.

11. Brenner S. The genetics of *Caenorhabditis elegans*. Genetics. 1974;77(1):71-94. PubMed PMID: 4366476.

12. Shin H, Haupt KA, Kershner AM, Kroll-Conner P, Wickens M, Kimble J. SYGL-1 and LST-1 link niche signaling to PUF RNA repression for stem cell maintenance in *Caenorhabditis elegans*. PLoS Genet. 2017;13(12):e1007121. Epub 2017/12/13. doi: 10.1371/journal.pgen.1007121. PubMed PMID: 29232700.

13. Kodoyianni V, Maine EM, Kimble J. Molecular basis of loss-of-function mutations in the *glp-1* gene of *Caenorhabditis elegans*. Mol Biol Cell. 1992;3(11):1199-213. Epub 1992/11/01. PubMed PMID: 1457827; PubMed Central PMCID: PMC275687.

14. Merritt C, Seydoux G. The Puf RNA-binding proteins FBF-1 and FBF-2 inhibit the expression of synaptonemal complex proteins in germline stem cells. Development. 2010;137(11):1787-98. doi: 10.1242/dev.050799. PubMed PMID: 20431119; PubMed Central PMCID: PMC2867315.

15. Huang T, Kuersten S, Deshpande AM, Spieth J, MacMorris M, Blumenthal T. Intercistronic region required for polycistronic pre-mRNA processing in *Caenorhabditis elegans*. Mol Cell Biol. 2001;21(4):1111-20. Epub 2001/02/07. doi: 10.1128/MCB.21.4.1111-1120.2001. PubMed PMID: 11158298; PubMed Central PMCID: PMC99565.

16. Timmons L, Fire A. Specific interference by ingested dsRNA. Nature. 1998;395(6705):854. doi: 10.1038/27579. PubMed PMID: 9804418.

17. Fraser AG, Kamath RS, Zipperlen P, Martinez-Campos M, Sohrmann M, Ahringer J. Functional genomic analysis of *C. elegans* chromosome I by systematic RNA interference. Nature. 2000;408(6810):325-30. Epub 2000/12/01. doi: 10.1038/35042517. PubMed PMID: 11099033.

18. Crittenden SL, Seidel HS, Kimble J. Analysis of the *C. elegans* germline stem cell pool. Methods Mol Biol. 2017;1463:1-33. doi: 10.1007/978-1-4939-4017-2_1. PubMed PMID: 27734344.

19. Cinquin O, Crittenden SL, Morgan DE, Kimble J. Progression from a stem cell-like state to early differentiation in the *C. elegans* germ line. Proc Natl Acad Sci U S A. 2010;107(5):2048-53. doi: 10.1073/pnas.0912704107. PubMed PMID: 20080700; PubMed Central PMCID: PMC2836686.

20. Merritt C, Rasoloson D, Ko D, Seydoux G. 3' UTRs are the primary regulators of gene expression in the *C. elegans* germline. Curr Biol. 2008;18(19):1476-82. doi: 10.1016/j.cub.2008.08.013. PubMed PMID: 18818082; PubMed Central PMCID: PMC25853

21. Edelstein AD, Tsuchida MA, Amodaj N, Pinkard H, Vale RD, Stuurman N. Advanced methods of microscope control using μManager software. J Biol Methods. 2014;1(2). Epub 2015/01/22. doi: 10.14440/jbm.2014.36. PubMed PMID: 25606571; PubMed Central PMCID: PMC4297649.

22. Edelstein A, Amodaj N, Hoover K, Vale R, Stuurman N. Computer control of microscopes using μManager. Curr Protoc Mol Biol. 2010;Chapter 14:Unit14 20. Epub

2010/10/05. doi: 10.1002/0471142727.mb1420s92. PubMed PMID: 20890901; PubMed Central PMCID: PMC3065365.

Fig 1
Appendix D

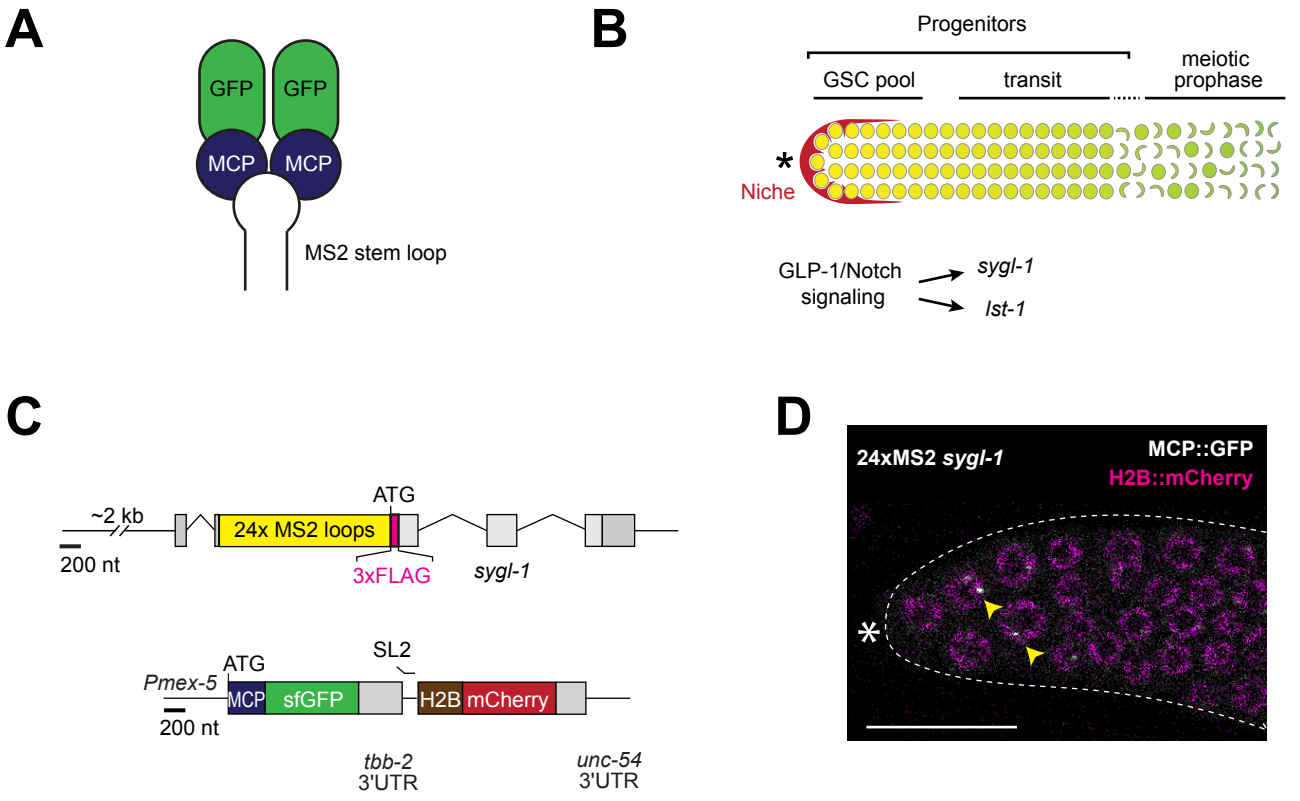

Figure 1. A live-cell Notch transcriptional reporter in the germline stem cell pool.

(**A**) Schematic of the MS2/MCP system for live-cell imaging. The MS2 coat protein binds MS2 stem loop as a dimer. GFP is fused to MCP for visualization. (**B**) Schematic of the *C. elegans* adult distal gonad. The progenitor zone (PZ) includes a distal pool of germline stem cells (GSC) and a proximal pool of cells primed to differentiate [19]. Notch signaling from the niche activates *sygl-1* and *lst-1* genes [5]. Somatic niche for GSCs (gray); naïve stem cell state (yellow circles); early meiotic prophase (green crescents); primed transiting state (yellow to green gradient). Asterisk marks the distal end. (**C**) Schematics of constructs used to generate MS2 and MCP transgenes. Top, 24 copies of MS2 stem loops were inserted in the *sygl-1* 5'UTR. Bottom, MCP was fused to superfolder GFP (MCP::sfGFP), and was co-expressed with histone tagged mCherry (H2B::mCherry) in an operon, using the *mex-5* promoter and *tbb-2* or *unc-54* 3' UTRs that support ubiquitous germline expression [20]. Colored boxes, exons; gray boxes, untranslated regions. (**D**) Nuclear *sygl-1* transcription sites in adult distal gonad detected by live-cell imaging. Yellow arrows, bright nuclear foci. A transgenic strain (JK5896) expressing 24xMS2::3xFLAG::*sygl-1*, MCP::sfGFP, and H2B::mCherry was used. Asterisk marks the distal end. Scale bar is 20 microns. (**E**) Dissected gonads stained with anti-FLAG or DAPI, to visualize SYGL-1 protein and nuclear morphology. Asterisk marks the distal end. No detectable staining was observed in 24xMS2::3xFLAG::*sygl-1* (JK5896) gonads. 3xFLAG::*sygl-1* (JK5499) was used as a positive control for staining, wild type was used as a negative control for staining. n > 20 for all conditions. Scale bar is 20 microns.